EXPERIMENTAL INVESTIGATION OF LARGE SPRING-SUPPORTED THRUST BEARINGS USED IN HYDROELECTRIC GENERATORS

by

John Haojiang Yuan

A thesis
presented to the University of Waterloo
in the fulfillment of the
thesis requirement for the degree of

Doctor of Philosophy

in

Mechanical Engineering

Waterloo, Ontario, Canada, 2000

EXPERIMENTAL INVESTIGATION OF LARGE SPRING-SUPPORTED THRUST BEARINGS USED IN HYDROELECTRIC GENERATORS

John Haojiang Yuan

The University of Waterloo requires the signatures of all persons using or photocopying this thesis. Please sign below, and give address and date.

Abstract

Large spring-supported thrust berings are key components in hydroelectric generators and have not been considered in much detail in the academic literature. The present thesis describes the application of a comprehensive commercial software package (GENMAT) to provide numerical predictions of spring-supported thrust bearing performance. A minor study of the accuracy of the pad deflection model in the software package was performed with a finite element analysis but the issues of accuracy were not resolved. GE Hydro's unique test facility for large thrust bearings was commissioned and extensive experimental measurements of film thicknesses, pad temperatures and film pressures were collected and compared with numerical predictions of GENMAT.

The agreement was good for the temperatures and the shape of the pad but somewhat erratic for film thickness and poor for pressures. The film thicknesses had been measured with eddy current displacement probes and their output voltage relationships to target diatance, temperature, pressure and target material were characterized in subsequent labotory experiments. Although probe calibration was implicated in the accuracy of the film thickness measurements, other unknown factors also contributed. An argument was made for accepting GENMAT predictions of film thickness for a given case, provided the temperatures and pad shapes showed good agreement. The neglect of rotor crowning was suggested as an explanation for the poor agreement of the pressures.

A combination of theoretical and experimental investigation was performed on a large number of cases. It was found that minimum film thicknesses were always about 15 - 20 μm despite considerable variation in geometry, lubricant viscosity , loads and rotor speeds. Temperature was influenced more readily by these variations, thus suggesting that energy efficiency which depended to a large extent on lubricant temperatures could be improved while maintaining adequate film thickness. Recommendations were made for more extensive application of the GENMAT package to the design of better spring-supported thrust bearings.

Acknowledgements

I would like to express my sincere appreciation to my supervisor, Dr. John B. Medley, for his profound knowledge in this discipline; for his guidance, encouragement and patience. I also would like to thank his family for their kindness and understanding.

Also I would like to express my sincere thanks to Mr. James H. Ferguson of *GE Hydro, Peterborough*, for his guidance and encouragement to the great and exciting engineering world through this well conceived project, and for his strong support in every aspect.

The experiments was performed at *GE Hydro's Lachine Plant* in *Quebec*. Mr. Bernard Cantin provided day-to-day support. Mr. Geoffery Turner, Mr. Ozzie Gallant in *Peterborough*, and Mr. Bill Nolan, Mr. Danny Kardash at *Lachine* provided technical assistance and maintained the apparatus. Mr. Ernst Huber and Paul Renkema provided technical support for laboratory studies at the *University of Waterloo*. Mr. Dave Mizgala, Mr. Mario Boutin, Ms. Jennifer Youngberg and Mr. Louis Houle assisted in experimental work by running the apparatus and collecting data.

The computational work was performed using the GENMAT computer software, which was developed by Dr Criss Ettles (202 Van Wies Point Road, Glenmont, NY 12077, U.S.A.); his help and encouragement weregreatly appreciated.

I would like to acknowledge my indebtedness to my fellow graduate students, colleagues and friends in *Waterloo, Peterborough and Montreal* for their friendship, humour and their in making my life so colourful. In particular, I would like to thank Ms. Wendy Cipera, Mr. Xin Wang, for their friendship.

Last but not least, I would like to express my sincere gratitude to my country *China*, hoping that I will help in her development, and to all professors who contributed by any means to my education in *China* and in *Canada*.

This research was funded by *National Science and Engineering Research Council (NSERC)* and *GE Hydro*.

To my beloved wife, Hongbing

for her love, understanding and sacrifices; and for her support in every way.

Without her, my life would not be complete.

To my father and mother, and my family

for their inspiration and support, and the mostly, for their unconditional love.

Without them, I would not be able to carry on this far.

To all those who love and support me so greatly in Canada, USA and China.

Table of Contents

List of Figures

List of Tables

List of Symbols

Roman Letters

A	Area of the control volume interface
BL	(Thrust) Block
C_1	Intercept of the voltage-dstance curve
D	Plate factor in Section 3.1.4; distance in Section 7.9.2, m
d_s	Distance from probe tip to surface, μm
E	Elastic modulus, Pa
F_j	Function in Section 2.2.1
h	Film thickness, m; distance in Section 7.4.3
ID	Inner diameter, m
J, K, L	Indices relating grid position. JT, KT, LT, LTP: maximum values
K_0, K_1	Constants
k_0, k_p	Thermal conductivity, W/mK
l	Distance in calculating Renold number
l_1, l_2, l_3, l_4	Distance from the spring centre to nodes 1, 2, 3, 4
M	Constant in Section 2.2.1
M_T	Thermal moment
m	Slope in volts/μm
N	Constant in Section 2.2.1
OD	Outer dismeter, m

P, p, p'	Pressure, Pa
Pn	Probe number
P_n	Proportion of spring stiffness
q	Heat flux, W/m^2
RR	Rotating ring
RTD	Resistance thermal detector
Re	Renolds number
$r.\theta.z$	Cylindrical coordinates
T, T_0, T_p, t	Temperature, °C
t	Distance from grid node to interface
t_h	Pad thickness, m
U	Vilocity in x-direction, m/s, constant at boundary
u_θ, u_r	Displacement, m
u,v,w	Lubricant velocities in the r, θ, and z directions, m/s
V, v	Probe output, volts
w	Pad deflection in Section 3.1.4, m
x,y,z	Coordinates

Greek Letters

β	Constant in Section 2.2.1
ϕ	Diameter, m
γ	Constant in Section 2.2.1
η, η_0	Viscosity of lubricant
ν	Poisson's ratio
ρ, ρ_0	Density, kg/m^3
∇^2, ∇^4	Mathematical operators in Section 3.1.4

Chapter 1

Introduction

GE Hydro (a division of General Electric Canada) uses spring-supported, sector pad thrust bearings (Figure 1.1) in its hydroelectric generators. The thrust bearing is part of a complex bearing assembly (Figure 1.2) that supports and locates a large vertical rotating shaft that connects the generator rotor to the hydraulic turbine (Figure 1.3). The entire vertical load is carried by the stationary thrust bearing pads, including the weight of the generator rotor, hydraulic turbine and hydraulic thrust while allowing the rotation necessary for generation of electricity.

1.1 Thrust Bearing Geometry and Physics

The large spring-supported thrust bearing, which is a key component of the hydroelectric generator, is the subject of the present research program. A typical example of this class of thrust bearing has been in service since 1971 in Churchill Falls, Labrador. It has 24 stationary sector pads configured with an inside diameter of 2.48 m and an outside diameter of 3.3 m. The thickness of each thrust bearing pad is 39.6 mm with an additional 2 mm layer of soft metal called Babbitt on the top of each pad. Each pad is

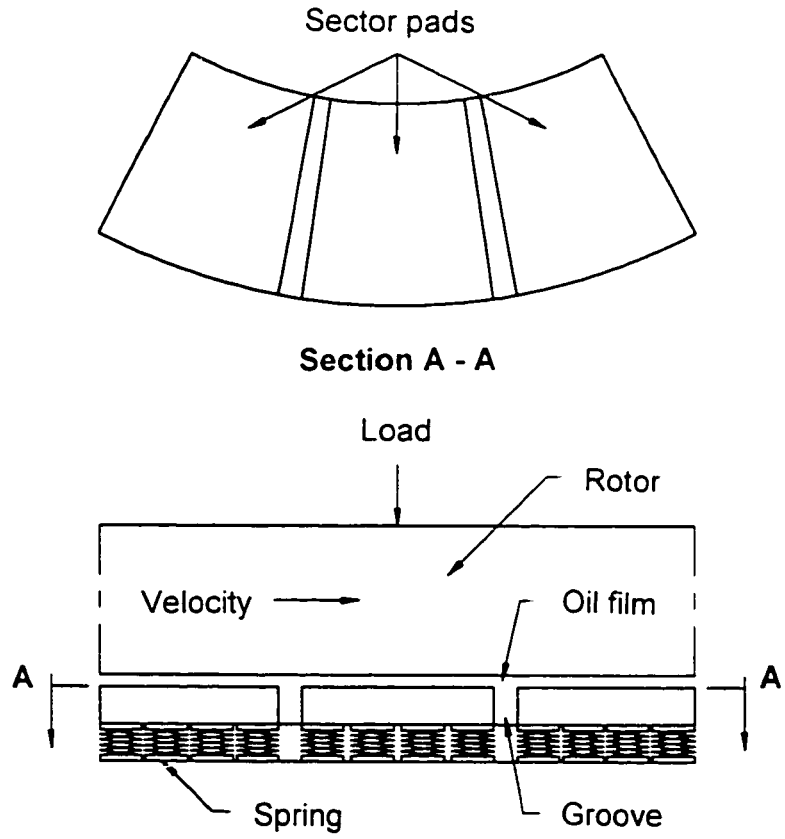

Figure 1.1. Three segments of a large spring-supported thrust bearing

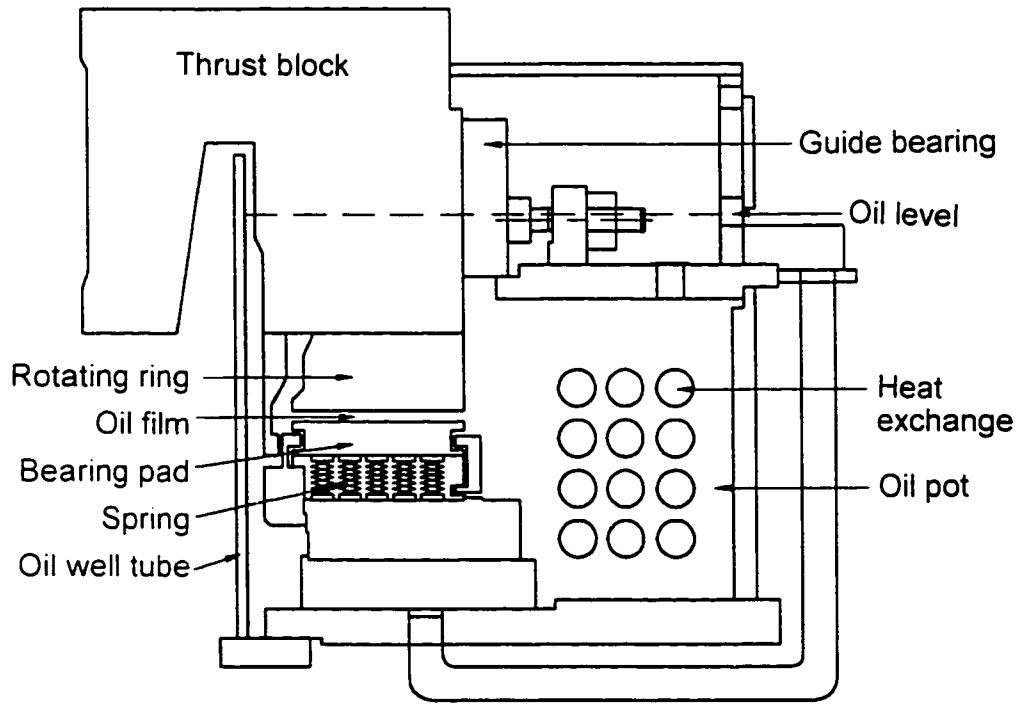

Figure 1.2. Vertical section of a typical bearing assembly

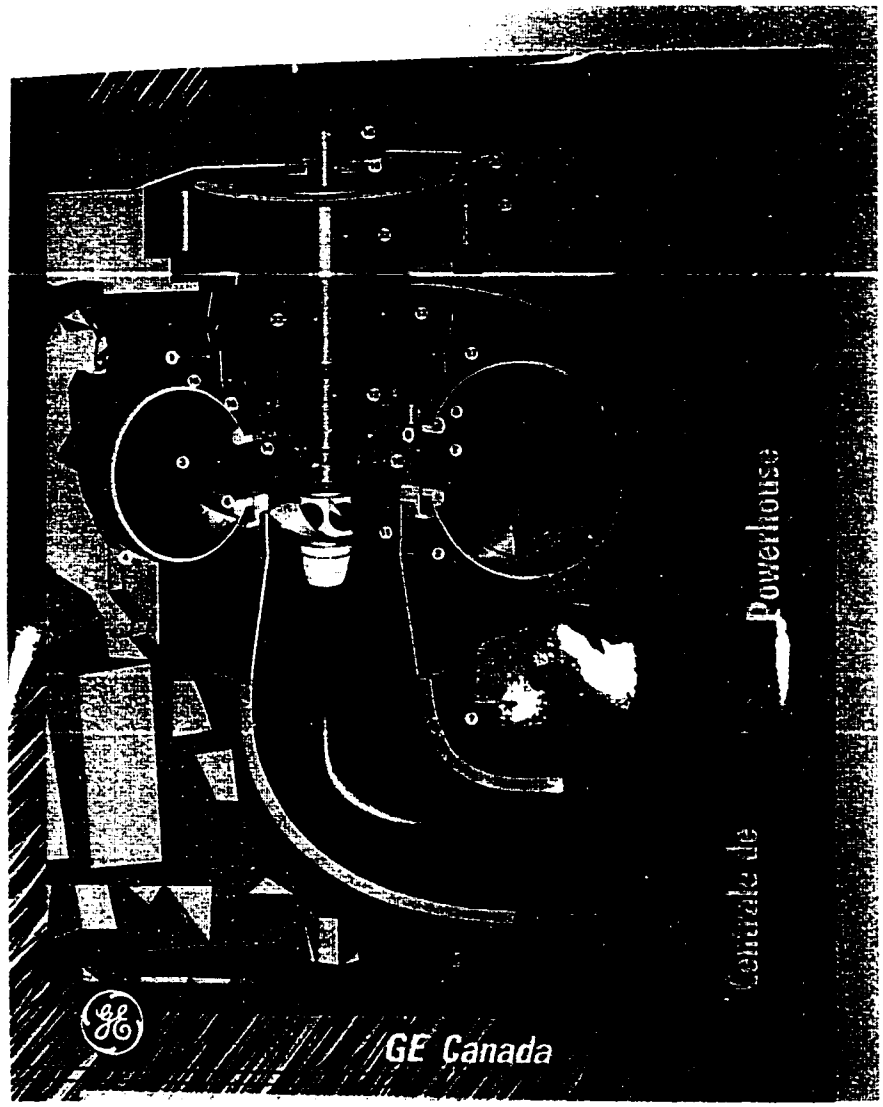

1. Draft tube liner
2. Discharge ring
3. Stay ring
4. Spiral case
5. Pit liner
6. Bottom ring
7. Wicket gate
8. Outer head cover
9. Intermediate head cover
10. Inner head cover
11. Kaplan runner
12. Turbine shaft
13. Thrust bearing support
14. Guide bearing
15. Operating ring
16. Wicket gate operating mechanism
17. Servomotors
18. Oil head
19. Exciter
20. Upper bracket
21. Stator
22. Rotor
23. Generator shaft

Figure 1.3. Hydroelectric generator

supported by a set of 47 springs located under the pad. A groove with a constant width of 52.3 mm separates the pads circumferentially. The upper surface or "rotor" consists of a flat, continuous "rotating ring" (Figure 1.2) that is attached to the thrust block and the rotating shaft. This shaft connects the rotor to the hydraulic turbine. Under normal operating conditions, the total load on this thrust bearing is 12 MN (2.7×10^6 lbs) and the speed is 20.9 rad/s (200 rpm). A lubricating oil film, with a minimum thickness of about 50 μm, exists between the surface of each pad and the surface of the rotor. This oil film prevents the direct contact between pad and rotor surfaces. The flow in the oil film is usually laminar but can be turbulent when rotor surface velocities are high. The physics of the oil film is described as thermohydrodynamic lubrication with the additional influence of thermoelastic pad deflection. This physics can be explained by describing the main features of the oil flow, the heat transfer and the pad deflection.

Oil Flow

The moving rotor surface entrains oil into the film. This flow is in the plane of the rotor and pad surfaces, in the direction of rotor rotation across the inlet (or leading) radial edge of the pad, eventually leaving the pad across the outlet (or trailing) radial edge of the pad. However, the flow encounters a converging gap between pad and rotor surface and a pressure is generated as a consequence. As a result of this pressure, the oil film can carry a load and also some of the oil is pushed out the side of the film across the inner and outer circumferential edges of the pad. It is possible to have some flow back across the leading edge of the pad if the pad it tilted to give a large inlet film thickness. Additionally, a very small pressure gradient occurs through the thickness of the film that drives a small flow. However, this flow component has little influence on overall momentum transfer in the film.

Heat Transfer

Thermohydrodynamic lubrication occurs when the energy generated by the shearing of the lubricant film increases temperatures and causes a significant reduction in viscosity. Although the friction involved in the shearing of the lubricant film is low compared to

many tribological applications, the size of these thrust bearings can result in a relatively large power loss of about 500 kW and an associated temperature rise in the oil film of about 40 °C above the oil pot temperature. This power loss is significant enough to be a factor in the overall design optimization of the unit. Furthermore, the temperature rise causes a drop in oil viscosity as well as a convex thermal distortion of the thrust bearing pad, known as crowning, and both of these phenomena can reduce the film thickness and thus risk direct surface contact between pad and rotor.

Once energy is generated in the film, it is convected by the flow in the plane of the rotor and pad surfaces towards the inner, outer, trailing and occasionally leading edges of the pad. Conduction in this plane is negligible compared with convection. Generated energy is also conducted and convected to the pad and rotor surfaces. In this case, conduction dominates but convection can contribute substantially in some regions. The convection is accomplished by the small flow through the thickness of the film as mentioned in the previous section. The large temperature gradients through the thickness of the film compensate for the small flow to give a fairly high convective heat transfer.

The thermohydrodynamic lubrication involves more than just heat transfer in the oil film because heat is transferred into both pad and rotor. Furthermore, heat is carried by the oil flows beyond the lubricant film and by the moving rotor. These peripheral heat flows influence the temperature distribution of the film mostly by removing energy from the film except in the inlet zone where energy is added. The removal of energy from the film is governed by the heat transfer across the back surface of the pads, into a rather stagnant oil flow around the spring supports, and the heat transfer across the various surfaces of the rotor into either air or oil. The addition of energy in the inlet zone occurs because the upstream bearing and the flow across the groove influence the temperature of the incoming rotor and adjacent oil that is entrained. Essentially, the flow across the trailing edge of the upstream pad injects hot oil into the groove between the pads where a turbulent boundary layer develops adjacent to the rotor surface. The warm moving rotor on one side and the cooler oil from the depths of the groove on the other side both influence the convective heat transfer in this boundary layer. The region of the boundary

layer immediately adjacent to the rotor is entrained across the leading edge of the pad into the oil film.

Pad Deflection

While the bearing is in operation (usually under steady state conditions), the bearing pad is deflected by bending moments from both the imposed temperature and the imposed pressure distributions. The deflected pad shape influences the oil flow, heat transfer and ultimately film thickness and it must be considered. The thermal bending causes a convex deflection and the pressure bending causes a concave deflection. The net effect is a relatively flat shaped pad. The springs that support the pad have pre-load applied to them through a central bolt. When the load on the bearing pad is below the pre-load value, the springs do not deflect, thus give a stiff support. There are no springs at the leading edge of the pad so that the centre of effect of the springs is towards the trailing edge of the pad to promote a tilting of the pad to produce converging film geometry necessary for fluid film lubrication. On the bearing pad, there is a thin layer of a soft metal alloy (Babbitt) as noted previously. This layer does not contribute to bending stiffness but it is designed to protect the bearing. If direct surface contact (or wiping) does occur, the soft Babbitt layer on the pad surface is designed to shear thus minimizing the possible damage to the rotating ring surface (Figure 1.2) and pad itself. However, a bearing failure is still expensive to repair and there is a serious loss of revenue while the generator is not functioning.

Non-linear Effects and Stability

The spring-supported thrust bearing is a non-linear system that may have very different performance for small changes in the input conditions and perhaps an unstable operation leading to direct surface contact and bearing failure. For example, progressive thermal bending, sudden transitions to turbulent flows and random pad vibrations have been known to occur in large thrust bearings.

The thrust bearings usually run under steady state conditions, but a "thermal ratchetting" can occur in which thermal bending causes an increasingly convex pad shape

(called crowning) that causes a thinner lubricant film leading to increased temperature which causes a simultaneous decrease in viscosity and an increase in pad crowning, both of which cause film thickness to continue to drop until eventually wiping of the bearing occurs (Ettles and Advani, 1980). This phenomenon is not well understood. However, the distributed spring-support (in contrast to the pivot support) may introduce a large enough pressure deflection to produce a concave shape that tends to counteract thermal crowning thus reducing the risk of thermal ratchetting.

As discussed above, the oil flows might be turbulent in the bearing film and are almost certain to be turbulent in the groove. Turbulence could cause the non-linear effect of a large change in performance (Pinkus and Wilcock, 1980) for a small change in input conditions, if the bearing operates close to a major transition to turbulence. However, transition to turbulence in bearing films is associated with thicker films and increased heat transfer rates. Thus, although transitions to turbulence may cause non-linear behaviour in the relationship of input parameters to behaviour, there is unlikely to be instabilities leading to bearing failure.

Vibration of bearing pads can occur in thrust bearings under low load conditions. However, in most applications of large spring supported thrust bearings in hydroelectric generators, the substantial weight of the rotor and hydraulic turbine are always acting. In addition, the present spring supported thrust bearings have springs with a preload applied as mention previously. The preloaded springs stiffen the system response during lower load conditions which tends to increase natural frequencies and thus reduce the risk of vibrations. Also, the bearing system is immersed in the oil pot (Figure 1.2) and consequently has a built in damping element.

Non-linear effects and stability issues have been discussed above and could influence bearing performance in the field and experimental studies in the laboratory. However, none of these effects have been experienced in the experimental study of the present thesis and, to the best of the present author's knowledge, they have not occurred in the field.

1.2 Scope of the Investigative Approach

The overall aim of GE Hydro is to maintain reliable and efficient electric generators by improving their design thus maintaining their leadership in this industry. The economic factors associated with hydroelectric generator design have resulted in the need for developing thrust bearings capable of supporting larger loads at higher operating speeds. A simple scaling up of existing functional designs risks bearing failure and thus a research and development program is warranted. The large loads and considerable size of the required bearings make full scale simulation in the laboratory very expensive and a trial-and-error approach with field testing potentially even more expensive. A small experimental apparatus can be built but the thermal and elastic influences on the performance cannot be well presented. In other words, there is a size effect (Ettles, 1980) which cannot be modelled exactly by a small-scale apparatus. Thus, the development of reliable thrust bearings with low power losses becomes increasingly difficult.

One approach to solve this problem is to build a test facility with a thrust bearing of comparable size to those in the field and study the influence of load, speed, oil pot temperature and some geometric variations (thrust bearing pad thickness and spring arrangement) on thermohydrodynamic lubricant flow and thermoelastic pad deflections under steady state conditions. Then the experimental data can be compared with results predicted by a numerical model. Once satisfactory agreement has been obtained by refining both the numerical model and the experiments, the numerical model can be used to predict full sized thrust bearing performance. Although such an approach is fundamental to many engineering research and development programs, it has not been applied, until now, to large spring-supported, sector pad thrust bearings. The present investigation concentrated on experiments and did not develop new theory, except for some implementation details for finite element analysis of pad deflection.

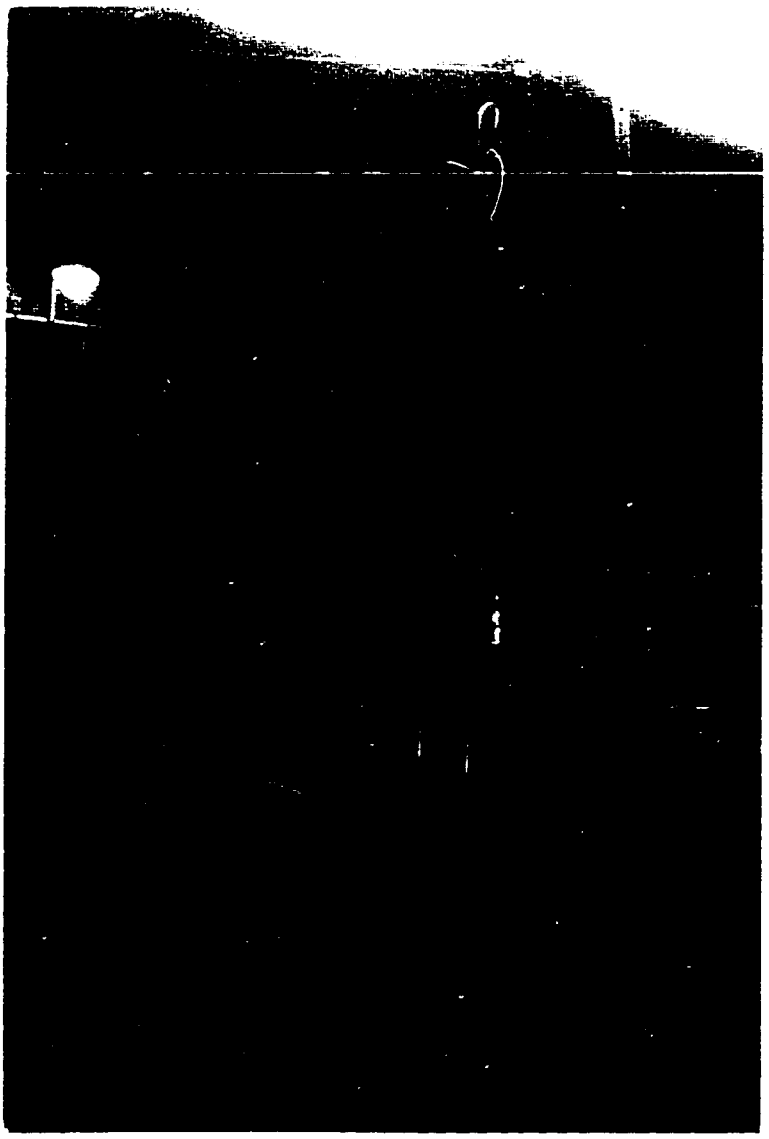

Figure 1.4. Photograph of the thrust bearing apparatus

The test facility for the present research program was built by GE Hydro starting in 1990 and completed when the loading system was mounted in 1994. The apparatus is located at GE Hydro's "Dominion Engineering Works" in Montreal (Figure 1.4). The thrust bearing in the apparatus has 1.168 m outer diameter and 0.711 m inner diameter with 12 bearing pads each supported by up to 15 springs. Although it is smaller than most (but not all) thrust bearings in service, it can be subjected to high *specific loads* (total load divided by pad surface area) of up to 7 MPa (310 kN/pad) and to high rotational speeds of up to 83.8 rad/s (800 rpm) compared with those encountered in current practice. Various combinations of load and speed have been examined in the present study. Numerous temperature and pressure sensors are located in the apparatus and four displacement probes of the eddy current type (made by DYMAC, a Scientific-Atlanta Inc. subsidiary, San Diego, California, U.S.A.) are located in the thrust block and rotation ring and sweep over the thrust bearing pads. They are intended to provide continuous circumferential measurement of oil film thickness at four radial locations. The use of displacement probes to measure film thickness in large thrust bearings, although not unique, is not well documented in the academic literature and development of this technology is an important part of the experimental program. In the present experiments, two pad thicknesses have been studied along with three spring arrangements.

The numerical model consists of a software package GENMAT (Bearing Sciences Inc., 202 Van Wies Point Road, Glenmont, NY 12077, U.S.A.) which has been developed specifically for the analysis of large spring-supported sector pad thrust bearings by Ettles (1991) with more than 20,000 lines of FORTRAN coding. In GENMAT, the thermohydrodynamic lubrication analysis involves the three dimensional variation in viscosity which follows from the simultaneous solution of a generalized Reynolds equation and a reduced form of energy equation. The heat and oil flow in the bearing are modelled in three dimensions using a control volume approach. Boundary layer equations are solved numerically to obtain a representation of the convective oil flow in the bearing groove. The thermoelastic pad deflection calculations are based on the thin plate theory using finite differences to solve the resulting partial differential equation. GENMAT

permits a transition from laminar to turbulent flow in both bearing film and the groove, and subsequently models these turbulent flows. Because it performs very complex modeling with many judicial approximations and because experimental comparisons are needed urgently, any development of the software GENMAT is beyond the scope of the present thesis.

Many iterative loops are built to the program for solving simultaneous equations and globally satisfying conservation of mass, momentum and energy for the thrust bearing. GENMAT is used to predict the experimental results, thus allowing extensive comparisons.

As mentioned previously, GENMAT provides numerical predictions of the pad deflection using the approximate representation of thin plate theory. A three-dimensional finite element model has been developed using a software package ABAQUS (Hibbitt, Karlsson & Sorensen Inc. U.S.A.) to provide a check to the pad deflection calculation in GENMAT. The model includes both thermal and mechanical effects on pad deflection.

1.3 Objectives

The objectives of the present research program are as follows:

1. To commission the test facility.

2. To build a small laboratory apparatus to characterize the behaviour of the displacement probes under various pressure and temperature conditions.

3. To perform experiments under steady state running conditions of various load, speed, oil pot temperatures and lubricants using the thrust bearing test facility with different pad thicknesses and spring arrangements.

4. To carry out numerical analysis of the thrust bearing performance using GENMAT and develop a finite element model using software ABAQUS for the pad deflection and compare with the GENMAT pad deflections.

5. To compare the results of the numerical analysis with the experimental data.

1.4 Outline of the Thesis

The present research program is intended to perform the experimental study to help reveal the complicated physics of the large spring-supported thrust bearings and to establish the fidelity with which a software package (GENMAT) represents spring-supported thrust bearing performance thus leading to improved designs using GENMAT. This first chapter has discussed both experimental and analytical approaches of the present study and provided some background regarding the development of the experimental apparatus.

In Chapter 2, the physics of large thrust bearings is explained further. The two types of support mechanism for thrust bearings, pivots and springs, are described. The intent of both supports is to allow the pad to tilt and deflect to a configuration favourable to fluid film lubrication. The hydroelectric generators made by GE Hydro have spring-supported thrust bearings and there is very limited academic literature on these bearings. However, considerable literature on large pivoted pads exists and is relevant to the present study. In the review of the experimental studies reported in Chapter 2, most of the cited papers involve pivoted pads. In review of the analytical studies, the various assumptions are identified and involve both pivoted and spring-supported pads.

The numerical analysis was performed using the software package (GENMAT) that was specially developed for the analysis of spring-supported thrust bearings and the results were compared with the experiments. This software package is introduced in Chapter 3. Also in Chapter 3, a finite element model is described for the calculation of thrust bearing pad deflection (based on the well-known software package ABAQUS) and compared with the GENMAT calculations of pad deflection for a typical case. The ABAQUS model was developed to attempt to provide a theoretical check on GENMAT. The thrust bearing experimental apparatus and instrumentation are described in Chapter 4. The experimental methods are described in Chapter 5 along with the test strategy.

In Chapter 6, experimental results are compared with the numerical analysis of GENMAT. To develop some perspective on the range of results obtained in this comparison, two typical cases have been examined, with differences in bearing pad geometry, in load, in speed, in oil viscosity and in both instrumentation and technique

used for oil film measurement. Because of the discrepancies are found in oil film measurement using the displacement probes, their behaviour is investigated using a small laboratory apparatus in Chapter 7.

Factors influencing the thrust bearing performance are discussed in Chapter 8. Large amounts of experimental data with comparison to the numerical predictions are displayed to provide better understanding of the thrust bearing performance under various bearing geometries, lubricant viscosities, loads and rotational speeds. Conclusions and recommendations for future work are presented in Chapter 9.

Chapter 2

Theoretical Background and Previous Experimental Work

Fluid film lubricated bearings are used in a variety rotating machines, particularly for the applications with heavy loads, high velocities and long service times. In hydroelectric generators, the vertical load is carried by large sector pad thrust bearings that cannot function without full fluid film lubrication. For large thrust bearings, the two basic pad support mechanisms are pivots and springs (Vohr, 1981). The intent of both pivot and spring supports is to allow the pad to tilt slightly to provide an optimal converging-diverging gap between pad and rotating ring which is required for the hydrodynamic generation of fluid film lubrication (Figure 2.1). The hydroelectric generators made by GE Hydro have spring-supported thrust bearing pads and the academic literature specifically relating to spring-supported pads is not extensive. However, the more comprehensive literature on large pivoted pads is relevant because the physics is quite similar and thus studies involving bearings with both types of supports are discussed in the following sections.

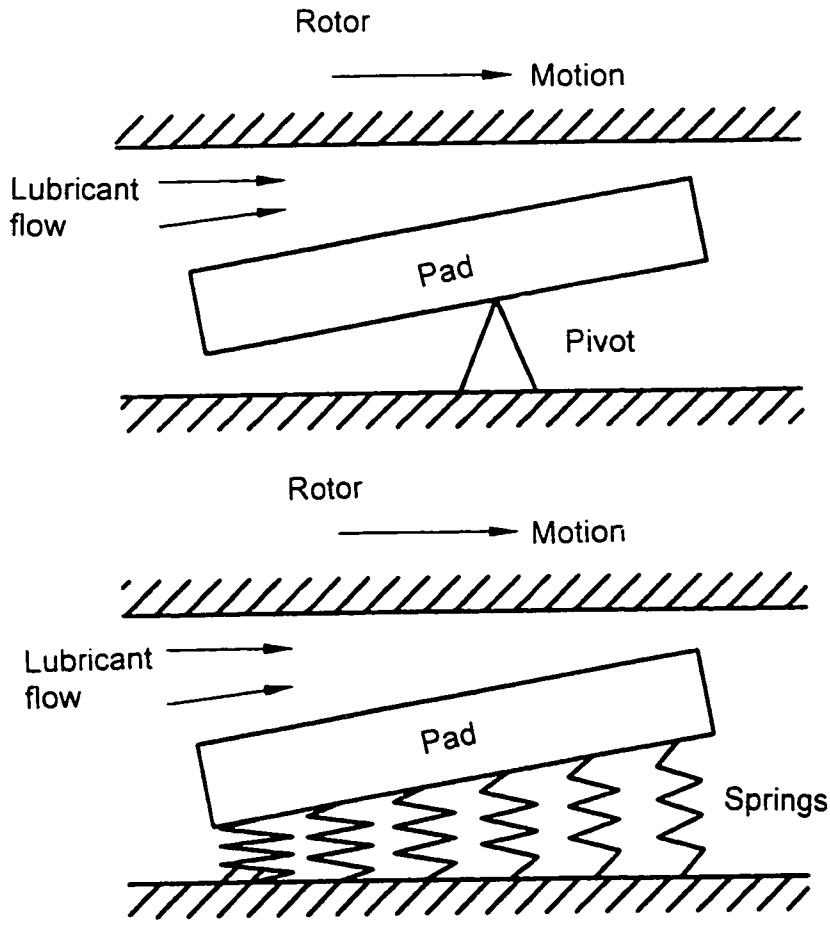

Figure 2.1. Two basic pad support mechanics: pivot and spring

2.1 Experimental Studies

As mentioned previously, for large thrust bearings used in hydroelectric generators, the size and high loads make full scale experiments extremely difficult. As a result, the typical experimental apparatus is of a small scale and represents only a few of the features of large thrust bearing performance. Furthermore, experiments have not been performed, to the author's knowledge, on spring-supported sector pad thrust bearings with the exception of a few temperature measurements provided by Vohr (1981). Thus the present review of experimental studies reports almost exclusively on pivot-supported thrust bearings which do exhibit quite similar behaviour (Table 2.1).

Thrust Bearing	ID (m)	OD (m)	Number of Pads	Max. speed (rad/s)	Max. load (MN)	Max. specific load (MPa)
Baudry *et al*	1.32 -	2.04 2.44	- -	10.47 12.57	5.71 9.07	- -
Elwell *et al*	0.42	0.79	8	31.41	1.14	3.8
Kawaike *et al*	0.915	1.765	4	41.89	3.76	9
Vohr*	-	0.65	4,8		-	4.1
Neal	0.079	0.149	3,4,6,8	418.88	0.024	-
Tanaka *et al*	0.322	0.474	-	125.66	-	0.8
Qu *et al*	2.45	3.9	18	62.83	30	4

* only study with spring-supported pads.

Table 2.1. Information of thrust bearing experiments

Baudry *et al* (1959) performed experiments on two pivot-supported large thrust bearings installed in a power plant (Table 2.1) for the purpose of seeking a better design for higher loading. Oil film pressure was measured using pressure taps in the pad and temperature was measured with thermocouples close to the pad surface. The temperature measurements were used to determine the pad distortion and the viscosity of the oil in the film. Oil film thicknesses were measured by using specially designed electromagnetic gauges (small reluctance gauges in a complex AC bridge circuit) which were mounted in the pad at a number of locations (Figure 2.2) and output voltages were recorded on an oscillograph. It was reported that the thermal distortion of the runner was negligible relative to both the thickness of the oil film and the distortion of the pad, in their experiments. The effect of the pad deflection on the performance of the thrust bearing was discussed. One oil film thickness and one temperature rise for each of the test bearings were compared with three simple analyses and some agreements were obtained. However, the analytical methods neglected thermal distortion of the pad and the viscosity variation with temperature throughout the oil film. The lack of detailed comparison of pressure, temperature and oil film thickness made it difficult to assess the impact of the simplifications in the model.

Elwell *et al* (1964) presented results for a pivoted sector pad thrust bearing (Table 2.1). Fluid film thickness, temperature on the pad surface and temperature through the pad thickness were measured. The temperature measurements were made at several locations in the pad and in the oil groove using copper-constantin thermocouples. Film thickness measurements were carried out using two different systems which were independent of each other (Figure 2.3). The first was a mutual inductance system which relied on the runner magnetic properties, in that, the transducer was unaffected by the condition of the oil film, but was influenced by the magnetic properties of the runner material. Voltage output of the system was a linear function of the separation between runner and pad (oil film thickness). The second used capacitance probes which were not influenced by the magnetic properties of the runner, but depended on the oil dielectric properties which were influenced by temperature and pressure in the oil film. In this case, voltage output of the system was a nonlinear function of the oil film thickness.

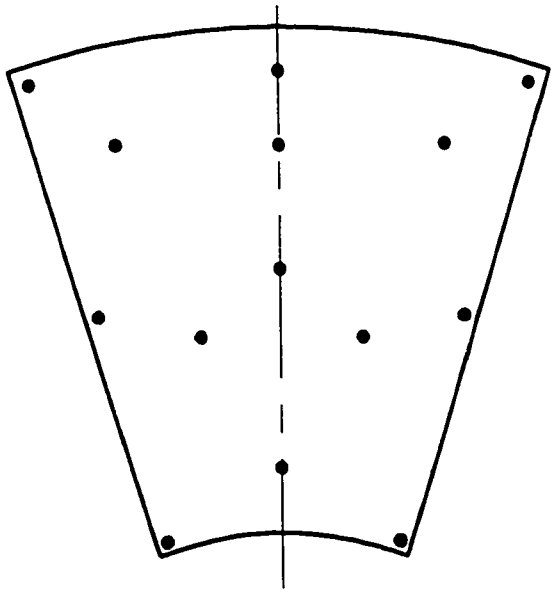

Figure 2.2. Location of electromagnetic gauges in the experiments of Baudry et al (1959)

Overall accuracy of the film measurements was estimated at ±5 μm for each of the systems. Ewell *et al* used the analysis developed by Sternlicht *et al* (1961a, 1961b) to predict temperature and oil film thickness and compare with the test data in a few locations. They found that measured temperatures were generally lower than analytical predictions and that measured oil film thicknesses were consistently lower than analytical predictions. Additional comparisons of Elwell *et al*'s results to theory were made by El Saie and Fenner (1988b) as discussed in a subsequent section in this chapter.

A test facility was built by Kawaike *et al* (1977) to study the thermal distortion in pivoted sector pad thrust bearings (Table 2.1). The loading system consisted of a hydraulic piston acting on the rotor through a hydrostatic bearing. The test bearing pads were thick enough, apparently, to make pad deflections from pressure negligible. Eight proximity probes of the eddy current type were installed at the leading and trailing edges of one pad to measure film thickness. However, there was no detailed information on the probes. Ten thermocouples were embedded at the leading edge and trailing edge to measure the pad temperature. Four thermocouples were installed through the pad thickness at a central location to measure the thermal gradient through the pad. Thermal distortion had a significant effect on bearing performance. Unfortunately, numerical analysis was not performed on these test bearings and thus the generality of the findings was impaired.

To compare with his analytical prediction of bearing temperatures, Vohr (1981) performed laboratory tests on a 0.65 m diameter bearing with 4 and 8 bearing pads (Table 2.1). The experimental study was concentrated on bearing temperature measurement by means of thermocouples installed very close to the surfaces of the pads. To check pad to pad variation on temperature, thermocouples were installed in pads located on opposite sides of the bearing and measurements from the two pads were within 0.5 °C of each other, and usually identical. By varying the bearing pad number, the effect of groove width on temperature was studied. It has found that the experimental temperatures near the trailing edge of the pad agreed very well with analytical predictions for both groove widths, but those near the leading edge were somewhat below the analytical results. However, according to the author, the analytical results were for the

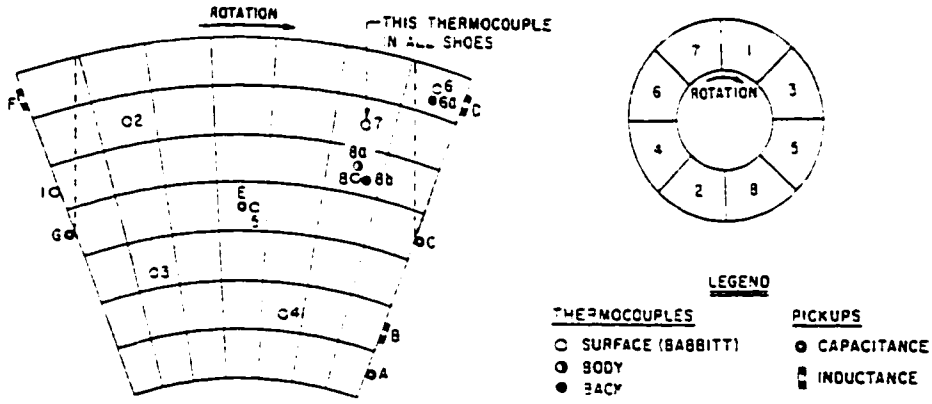

Figure 2.3. Location of bearing pads and transducers in the experiments of Elwell et al (1964)

bulk film temperatures and, because of heat conduction, the measured bearing surface temperatures were below the bulk temperatures as expected.

Tests were conducted by Neal (1979, 1982) on a small bearing (Table 2.1) in which the operating temperatures were of particular interest. The apparatus consisted of a multi-pad test bearing and a hydrostatic loading plate. In these tests, different pad arrangements were used, and it should be noted that the pads were not exactly sector shaped (Figure 2.4). Thermocouples were mounted in the pads along a circumferential arc approximately at the mean radius of the pad, and in the oil pot between the pads (Figure 2.4). Since the oil supply rate to the pot was fixed, the oil pot temperature varied with load and speed. Tests were conducted at four different speeds, from 105 to 419 rad/s, and they showed that the measured temperatures near the pad surface provided an indication of bearing performance. The effects of load, speed, oil supply rate and number of pads on these temperatures were explored. However, oil film thickness and pressure were not measured. A comparison with theory was provided by El Saie and Fenner (1988b), as discussed in a subsequent section in this chapter.

Tanaka *et al* (1985) performed experiments on a relatively small pivot-supported sector pad thrust bearing (Table 2.1). Load was applied to the bearing by a "hydrostatic actuator" which might have been a device similar to the one used by Kawaike *et al* (1977). Film thickness profiles were measured by mounting three proximity probes of eddy current type in the runner so that the pad surface was scanned along three different radii and the profiles were showed on an oscilloscope screen. However, no further details were reported. The maximum temperature was found near the trailing edge and the outer edge while the minimum temperature was found at the leading edge near the inner edge. With increased load, the oil film thickness decreased as a whole and the tilt in the circumferential direction (pitch angle) of the pad decreased. The thermal distortion of a pad surface was convex and the minimum oil film thickness was not always at the trailing edge. Although results were shown for various running conditions, there was no theoretical analysis for comparison purposes. Larger thrust bearings might behave quite different and thus results could not be applied to them with certainty.

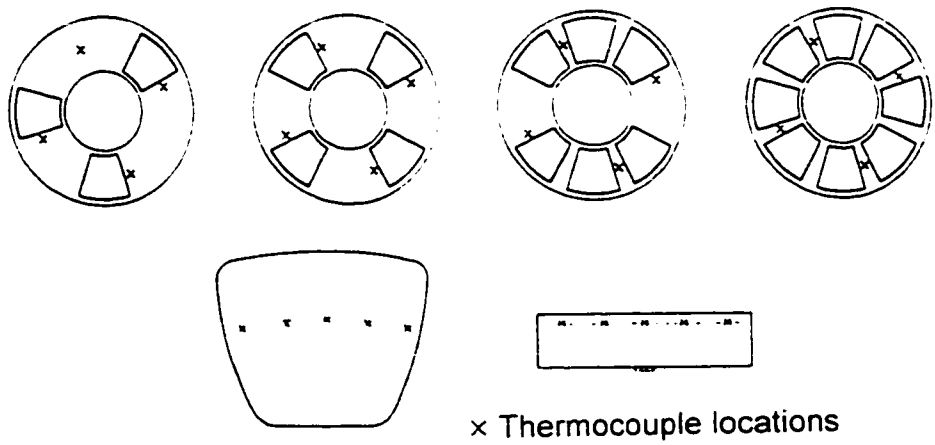

Figure 2.4. Pad arrangement and geometry for the experiments of Neal (1979, 1982)

Finally, Qu *et al* (1993) reported that a test facility was built in China for research and development of large pivoted sector pad thrust bearings (Table 2.1). Load was applied by a hydraulic system. A high pressure oil lifting system was provided for the bearing during starting and stopping procedures to prevent possible surface damage. Fluid film thickness between the runner and the pad was to be measured using proximity probes of the eddy current type embedded in the pad. In addition, film pressure and temperature were to be measured. Unfortunately, no complete experimental results have been published.

2.2 Theoretical Studies

In contrast to the relevant experimental studies there are many more relevant analytical studies to consider. It is convenient to classify papers as being *specific* or *general* where *specific* means that the main topic deals with only one or two of the physical phenomena involved in large thrust bearing behaviour while *general* means that the paper purports to provide an analysis of the entire thrust bearing behaviour. For example, specific papers deal with topics such as thermohydrodynamic lubrication, flow across the groove and lubricant flow through the thickness of the film. General papers, however, integrate all of the physics into a single overall model, although they often approximate some of the mechanisms in a manner that is believed to maintain an overall accuracy in their results. In all of the literature considered in the present thesis, it can be observed that specific papers do not include thermoelastic deflection of the pads while general papers always attempt some treatment of it. In the following sections, specific papers are discussed first under a number of headings and then, in the last section, the general papers are discussed.

2.2.1 Thermohydrodynamic Lubrication

Thermohydrodynamic lubrication involves the simultaneous solution of the generalized Reynolds equation for lubricant flow and the reduced energy equation for heat flows. In

thermohydrodynamic lubrication, temperature varies throughout the lubricant and thus both viscosity and density, which are function of temperature, vary in the plane and through the thickness of the lubricant. In addition, three dimensional lubricant flow is found in the convection terms of the energy equation. For bearings of infinite width, Colynuck and Medley (1989) presented a concise summary of the equations for thermohydrodynamic lubrication and these equations are repeated below with some additional comments that are related to the present thesis. (For bearings of finite width, such as the sector pad geometry of large thrust bearings, the same physics applies but the equations and the analytical manipulations are slightly more complicated.)

The conservation of momentum is represented by a reduced version of the Navier-Stokes equations.

$$\frac{\partial p}{\partial x} - \frac{\partial}{\partial z}(\eta \frac{\partial u}{\partial z}) = 0 \tag{2.1}$$

$$\frac{\partial p}{\partial z} = 0 \tag{2.2}$$

Conservation of mass gives the continuity equation.

$$\frac{\partial(\rho u)}{\partial x} + \frac{\partial(\rho w)}{\partial z} = 0 \tag{2.3}$$

Conservation of energy is represented by a reduced thermal energy equation.

$$\frac{\partial}{\partial x}(\rho u c_p T) + \frac{\partial}{\partial z}(\rho w c_p T - k\frac{\partial T}{\partial z}) = \eta(\frac{\partial u}{\partial z})^2 \tag{2.4}$$

where conduction in the x-direction and compressional heating are considered negligible.

Lubricant viscosity and density can be considered unique functions of temperature, such as

$$\eta = \eta_0 e^{\beta(T-T_0)}, \qquad \rho = \rho_0 e^{\gamma(T-T_0)} \tag{2.5}$$

and the influence of pressure can be neglected. More realistic expressions for the influence of temperature on viscosity and density could be substituted here without making the analysis more complicated. Because they were comparing theoretical procedures, Colynuck and Medley (1989) did not require such realism.

Since Equation (2.2) indicated that p is a function of x only, Equation (2.1) is integrated twice with respected to z with the boundary conditions

$$u = U \text{ at } z = 0 \quad \text{and} \quad u = 0 \text{ at } z = h$$

to give

$$u = M\frac{dp}{dx} + NU \tag{2.6}$$

where

$$M = F_1(z) - \frac{F_1(h)}{F_0(h)}F_0(z), \qquad N = 1 - \frac{F_0(z)}{F_0(h)}$$

and

$$F_j = \int_0^z \frac{z^j}{\eta}dz, \qquad j = 0, 1$$

Equation (2.6) implies

$$\frac{\partial u}{\partial z} = \frac{1}{\eta}(K_1 Z + K_2) \tag{2.7}$$

where

$$K_1 = \frac{dp}{dx}, \qquad K_2 = -\left(\frac{F_1(h)K_1 + U}{F_0(h)}\right)$$

For a control volume spanning the film, Equation (2.3) implies

$$\int_0^h \frac{\partial(\rho u)}{\partial x}dz + [\rho w]_0^h = 0 \tag{2.8}$$

Applying Leibnitz's rule, noting that w=0 at both z=0 and z=h and substituting from Equation (2.6) give

$$\frac{d}{dx}\left[\int_0^h (\rho M\frac{dp}{dx} + \rho NU)dz\right] = 0 \tag{2.9}$$

which is a form of the generalized Reynolds equation. For a specified film geometry, the above equations can be applied in numerical procedures (Figure 2.5) to solve for temperature and pressure distributions described by Colynuck and Medley (1989).

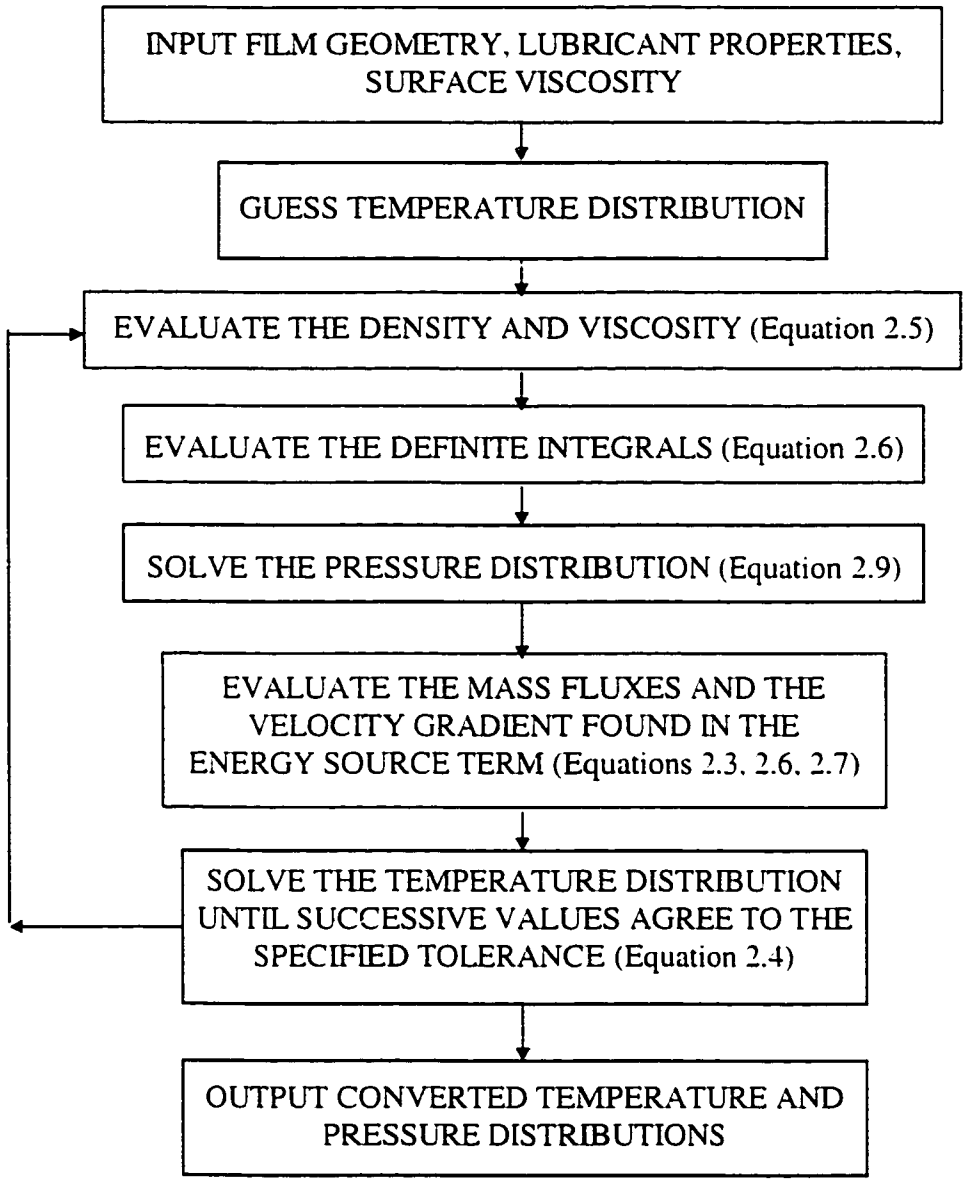

Figure 2.5. Flowchart for iterative procedure used in the numerical solutions of Colynuck and Medley (1989)

Dowson and Hudson (1963a) performed the first full thermohydrodynamic analysis and, in addition, allowed the heat to flow into the surfaces. They pointed out that viscosity changes with temperature imposed a serious reduction on the load carrying capacity. Although they only solved a two dimensional bearing, they estimated the need to perform a full thermohydrodynamic analysis to obtain an accurate representation of the thermal effects on the lubrication of large thrust bearings.

Huebner (1971a) and Kim *et al* (1983) performed full thermohydrodynamic analysis in three dimensions of thrust bearings but neglected thermal and elastic deflection of the surfaces. Kim *et al* compared their full thermohydrodynamic results to those obtained when the temperature was averaged through the film thickness and demonstrated a need for a full thermohydrodynamic solution to obtain accurate results.

2.2.2 Numerical Analysis

Choosing numerical methods has played a major role in the analysis of thrust bearings performance. Conventional finite differences were used by Dowson and Hudson (1963) and later by Hahn and Kettleborough (1967) to model the lubricant and heat flows of thermohydrodynamic lubrication. These numerical analyses had difficulty if reverse flow occurred in the inlet zone and Ettles (1980) suggested a form of finite difference that maintained local conservation of both mass and energy (control volume formulation) and then used upwinding to treat reverse flow regions if they occurred. Also, Ettles emphasized the importance of local conservation of mass and energy in improving the accuracy of the numerical model. However, Colynuck and Medley (1989) found similar accuracy of a control volume formulation when compared to a conventional finite difference formulation but noted that the control volume formulation did allow a simple treatment of reverse flow using upwinding.

In the region of the lubricant film where the surfaces diverge, cavitation often occurs. Mathematically, this means that a free boundary exists in the plane of the lubricant film along which the pressure and the pressure gradient normal to the boundary fall approximately to zero. In reality, lubricating oils can sustain a small negative gauge pressure but including this more complex fluid behaviour has a negligible effect on the

overall load capacity. Numerically, the cavitation boundary can be located accurately by setting negative pressures to zero within the iterations of a Gauss-Siedel matrix solver. Apparently this approach was used by Ettles and Anderson (1991) and Ettles (1991) in their finite difference formulation of thermohydrodynamic lubrication.

Finite element analysis of thermohydrodynamic lubrication was performed by Tieu (1973), Huebner (1974b) and Ma and Dong (1995). These finite element analyses did not conserve mass locally but such formulations were performed recently by Gero and Ettles (1988) and Kumar and Booker (1994). These analyses treated domains of arbitrary shape with reverse flow and included cavitation, but they were relatively elaborate and complex formulations. It should be pointed out that the elaborate formulations of the finite element method for lubrication analysis may not be worth the effort since there seems to be no advantage in accuracy or computational effort compared to a mass and energy conserving control volume formulations (Ettles and Anderson, 1991).

To apply numerical methods to the deflection of the bearing pad, various models have been developed. Baudry *et al* (1958) investigated the influence of the pad deflection considering the bearing pad as a beam, and addressed the need to balance the thermal deflection against that due to the hydrodynamic pressure. Sternlicht *et al* (1961) first applied the biharmonic equation with finite differences to the centrally pivoted thrust bearing pad. Vohr (1981) determined the elastic bending of the pad by pressure and temperature gradient using Ritz methods and in the thermal deflection analysis, temperature was assumed to vary linearly through the pad thickness.

Robinson and Cameron (1975) used the biharmonic bending equation and included elastic and thermal deflection. The equation was solved using a finite difference technique along with a correction for shear by Ettles and Anderson (1991) and by Ettles (1991).

El-Saie and Fenner (1988a) claimed to have improved deflection analysis by applying a polynomial difference technique to the pad deflection considering the thermal stress moment. Compared with other numerical techniques, it combines some of the features of both finite difference and finite element methods. This formulation had the property that a coefficient matrix needed only to be calculated once and stored, then, it

could be multiplied by the local pressure vector when required to determine the nodal deflections. The formulation also allowed for varying pad thickness. They stated that their method had been extensively tested and was shown to give satisfactory results. Unfortunately, comparisons of pad deflections predicted by El-Sain and Fenner with these predicted by Ettles and Anderson (1991) were not found in the literature.

Seyler (1991) developed a computer program using finite element analysis to model the pad deflection caused by both pressure and temperature. He compared his results to the finite difference deflection solutions of Ettles and did not obtain good agreement. It was not known whether the discrepancies were due to the different behaviour of the truncation error in the two solutions or the approximations involved in thin plate theory employed by Ettles (1991).

Recently, Ashour *et al* (1991) and Sinha *et al* (1993, 1994) also solved the biharmonic equation to estimate the elastic deflection of a spring supported thrust bearing pad. However, their modelling ignored thermal effects and thus their solutions were not applicable to large thrust bearings.

Brockett *et al* (1996) reported a full thermohydrodynamic analysis with thermoelastic pad and *runner* deformation for sector pad thrust bearings. The runner was the part of the rotor on the bearings surface and, apparently, it was a disc of some axial thickness attached to the rotating shaft. In their solutions, all of the analysis was performed with the finite element method. They claimed to have the only full sector pad thrust bearing analysis which included thermal and mechanical expansion-contraction of the material of the bearings surfaces. However, no comparisons were made with the thermoelastic models of other investigators. It was concluded that the deformation of the runner led to smaller minimum film thicknesses and increased temperatures with increasing load. A lower film temperature could be obtained, therefore, at the expense of minimum film thickness when the runner deforms. It was also found that as the runner thickness increased, the influence of the runner deformation on the bearing performances was smaller. However, the bearings and the runners considered in this study were very small (outer radius: 152.4 mm. runner thickness: 12.7 mm and 25.4 mm), for large bearings and runners, there might be of different behaviour.

2.2.3 Turbulence and Inertial Influences in the Film

Turbulence and inertial influences, when treated in detail, could have significant effects on thrust bearing performance (Pinkus and Wilcock, 1980). Neglecting the inertia terms was a simplification of the previously derived Reynolds equation (Equation 2.9). The inertial effects were discussed in laminar flow bearings by Launder *et al* (1978) who suggested that the effect cannot be neglected routinely in the design of fluid film bearings for optimum performance. Non-linearity of the governing simultaneous partial differential equations made solutions difficult to achieve.

Transition from laminar to turbulent flow is likely to occur in a thrust bearing under high-speed conditions. A theoretical study of thermal effects in thrust bearing operating under turbulent conditions was reported by Huebner (1974c) who presented a three-dimensional solution. Hasimoto and Wada (1984) extended this work and included pad deflection in analyzing turbulent characteristics of sector-shaped and tilting-pad thrust bearings. However, transition Re numbers were not reported.

Innes (1991) described a detailed investigation performed using a large scale model of a single tilting-pad to obtain information on the transition to turbulence. Based on their work, the transition Re number ($Re=\rho vl/\eta$, where ρ=density, η=viscosity) was determined to be about 1200 which was found to be independent of a pad-length-to-inlet-gap ratio.

According to Vohr (1981), the spring-supported thrust bearings used by GE Hydro had laminar flow in the film, although flow in the groove was turbulent. Ettles (1991) agreed with Vohr that the film was usually laminar but did introduce a turbulence model in his software package (GENMAT) that permitted regions of turbulence.

2.2.4 Flow in the Groove

The problem of the flow in the groove was complicated by the intermixing of the cool "supply" oil from the bath and hot oil from the upstream bearing film. Such effects were important because the entire thermal characteristics of the bearing were influenced. Ettles

and Cameron (1968) studied this problem under laminar flow conditions. They applied boundary layer theory in a two-dimensional model to estimate the amount of heat that was carried across the inter-pad groove and into the next pad, and reported that the viscosity of the oil entering the load carrying film was much different from that of the supply oil. The quantity of heat carried over into the next pad was found to be 70% - 95 % of the heat leaving the previous pad. Ettles and Cameron (1968) then introduced a "hot oil carryover factor" and provided experimental data for this parameter as a function of the leading to trailing edge film thickness ratio.

However, Vohr (1981) pointed out that the circulation flow in the groove of the hydro generator thrust bearings is three-dimensional and turbulent. He used solutions for the thermal boundary layer across the groove to calculate the heat transferred to the cold oil in the groove but allowed a global energy balance on a control volume, consisting of film, groove and bearing pad, to set the film inlet temperature. An iterative procedure was developed in which a constant groove inlet oil temperature was estimated at the trailing edge of the upstream bearing. Once all the heat and lubricant flows were calculated, the average film outlet temperature was compared to that of the groove inlet oil temperature. Since the heat flows were dominated by the generation from shearing the oil film, the constant groove inlet temperature did not dominate the solution and could be adjusted and the calculations repeated until groove inlet and film outlet temperatures were equal. Vohr's overall analysis provided reasonably accurate predictions of the operating temperature (a particular temperature in the pad that was monitored in the field for hydroelectric generators made by GE Hydro) of large spring-supported bearings both in the field and in the laboratory which suggested that his approach to dealing with the thermal influence of the flow across the groove was reasonably accurate and perhaps an improvement over the hot oil carryover factor of Ettles and Cameron. In a written discussion of the paper by Heshmat and Pinkus (1986), Ettles stated that he believed that the approach of Vohr's was the best estimate currently available and later Ettles (1991) incorporated this method into his GENMAT software package.

2.2.5 Complete Numerical Models of Large Thrust Bearing Performance

Baudry *et al* (1958) made an early attempt at overall modeling of thrust bearings by including the influence of the load and thermal deformation. The need to balance the thermal deformation against the deflection due to the hydrodynamic pressure was discussed. But, unfortunately, the interaction between the film pressure and the pad deflection was not included.

Sternlicht *et al* (1961a) presented an adiabatic analysis of the oil film on an elastic, centrally pivoted sector thrust bearing pad. They accounted for the viscosity variation with temperature and allowed for elastic deflection of the pad by solving the biharmonic equation with finite differences. Sternlicht *et al* (1961b) carried out a similar analysis including, in addition, the effect of thermal gradients on pad deflection. They solved the Reynolds and energy equation using finite differences and obtained both pressure and temperature distributions.

For a given load, speed, and bearing geometry, Castelli and Malanoski (1969) added the effect of heat conduction through the pad but used a constant temperature through the film thickness and showed that as the inlet temperature was increased, the difference between it and the maximum temperature remains essentially constant. Thus, to reduce maximum temperature, one must reduce the inlet temperature.

Realizing the importance of thermal deformation and elastic deflection, Ettles (1976) modeled both but set temperature and thus constant viscosity through the thickness of the film. He previously discussed hot-oil-carry over model which was used to predict film inlet temperature. Later, Ettles (1980) studied the size effects in tilting pad thrust bearings and discussed the methods of accommodating or reducing thermal distortion. For a pad with any given support system the design could be scaled up directly if only elastic distortion was considered. However this was not the case for thermal distortion which tended to increase directly with bearing size. He illustrated this concept with the deflection of a cantilever thrust bearing which did not exhibit any size effect for

only elastic deflections, but the thermal deflections were shown to increase in proportion to bearing size. Ettles stated that

> "In principle it should be possible to scale up successful thrust bearing design as machines increase in size. In practice this has led to serious and expensive bearing failures."

In numerical analysis, Ettles (1980) suggested that great care must be taken to satisfy flow conservation exactly. If this was not done the unbalanced flow can act as a source or sink term to increase or decrease the temperature continuously as the iterative solution proceeded. The radius of the pivot-supported disk that was located under sector pad was also studied in some detail and shown to have significant effect on the load capacity of the bearing. As a direct consequence of thermal distortion, the maximum obtainable load decreased exponentially with bearing size. By considering experimental studies of other investigators, Ettles suggested some methods to increase the load capacity and decrease the maximum temperature by using a two-piece pad consisting of a thin Babbitt plate supported on a thick pivoting base. Also, reducing the temperature difference through the pad was an additional method of reducing thermal distortion.

Since bearing temperatures were such an important aspect of the design of the thrust bearing, Vohr (1981) developed a method to predict the operating temperature of spring-supported thrust bearings used by GE Hydro. He had available the computer program from Castelli and Malanoski (1969) which was capable of modeling the behaviour of tilting pad thrust bearings. Their elastic model had been was taken from Sternlicht *et al* (1961a) and was extended by Vohr to include thermal deformation of the pads. As discussed previously, Vohr used a global energy balance approach to deal with peripheral heat flows including the groove. For the film, the simplifying assumption that the temperature could be considered constant across the thickness of the bearing film was made and so the solution procedure only considered temperature variation in the plane of the bearing but not through the film thickness. He assumed that the springs provided, in essence, a uniform pressure support for the bottom of the pad. The overall analysis was insensitive to some of the peripheral heat transfer processes and thus inaccuracies in the corresponding heat transfer coefficients still led to good results. Vohr's predictions of

operating temperature (defined previously in Section 2.2.4) were quite accurate when compared with his laboratory experiments and with some field measurements.

A thermohydrodynamic analysis with thermal deformation and pressure induced pad deflections was presented by El-Saie and Fenner (1988a). For pivot-supported pads, this analysis was an attempt to model all of the main aspects of thrust bearing behaviour. Their work consisted of theoretical treatment as well as comparison to experimental results. As mentioned previously, the method of pad deflection analysis adopted in their work was a polynomial difference technique. To reduce the complexity of their solution, a quadratic temperature profile through the film was assumed. Heat transfer of the pad and runner was modeled using a finite difference formulation with the pad model being fully three-dimensional whereas the runner temperature was modeled as two-dimensional (varying in the radial and axial directions only). The solution procedure effectively considered all of the main aspects of the bearing analysis.

El-Saie and Fenner (1988b) compared their theory with experimental results for a large thrust bearing with pivot-supported pads. Since this particular experimental study was not published in a refereed journal, information had to be taken from the paper by El-Saie and Fenner. The thrust bearing had an outside diameter of 2.95 m and inside diameter of 1.5 m and there were ten pads. The rotational speed was 9 rad/s (86 rpm) with an oil pot temperature of 48 °C and maximum loads up to 16 MN. Extensive temperature measurements in the pad using thermocouples were carried out. Apparently, the oil film thickness was not measured. Comparison between the theory and these experimental results showed that good agreement occurred with the maximum temperature and with the leading edge temperature. Furthermore, El-Saie and Fenner used the measured temperatures to predict temperature contours at the pad surface for comparison with theoretical temperature contours. The shapes of the temperature contours and their magnitudes were very similar (Figure 2.6). The maximum temperature occurred away from the central arc and towards the trailing edge.

El-Saie and Fenner also had experimental results from Elwell *et al* (1964) which were described previously in Section 2.1. Comparisons were made with oil film thickness and temperature at the pad centre.

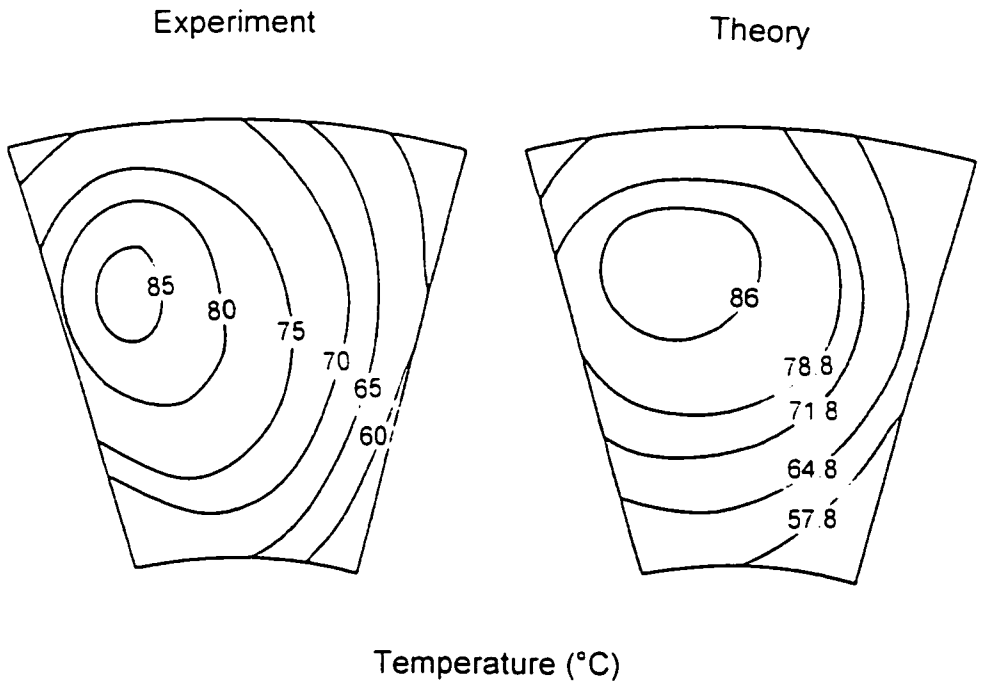

Figure 2.6. Experimental and theoretical temperature contours at a tilting pad surface from El-Saie and Fenner (1988b)

The numerical prediction of the oil film thickness were up to about 7 μm higher than the experimental results which indicated good agreement considering the experimental accuracy of ±5 μm and the simplifying assumptions of the analysis. The numerical prediction of pad surface temperature was a maximum of about 4 °C higher than the experimental measurements.

Finally, for the experimental results obtained by Neal (1979,1982) for a small thrust bearing which were described in Section 2.1, the numerical results were compared to the experimental data. It was found that the numerical prediction of pad surface temperature was a maximum of about 5 °C higher than the experimental measurements.

The comparisons between predicted and measured performance of three sizes bearings have been demonstrated the reliability of the proposed theoretical model for tilting pad thrust bearing analysis. However, their numerical model could not be applied directly to large spring-supported thrust bearings.

2.3 Program GENMAT

A numerical model for large spring-supported thrust bearings was developed by Ettles (1991). It included thermohydrodynamic lubrication, heat flowing into both pad and runner, thermal deformation of the pad and elastic deflection of the pad. The model was implement by a software package called GENMAT. GENMAT was written specifically for the spring-supported thrust bearings of GE Hydro.

The thermal and fluid flow solution methods of GENMAT were based on Ettles and Anderson (1991). They addressed the main difficulty in obtaining a solution when reverse flow in the inlet region occurred by using "upwinding" as discussed in a previous section. They discussed the benefit of using a full thermohydrodynamic lubrication analysis and pointed out that a full treatment of the thermoelastic pad deflection must be included to maintain the advantage of full thermohydrodynamic representation of the film.

The pad deflection for GENMAT was modified to consider the spring preload which was required in this design to control the vertical displacement of the pad under low loads. Through some illustrative examples, Ettles (1991) showed that a significant increase in specific load capacity could be obtained by proper control of the thermoelastic deformation. Specifically, the judicious placement of springs under the pads could lead to better control of the elastic deformation and thus improved performance. Ettles (1991) could not make any comparisons with experimental results because with the exception of the few measurements of Vohr (1981), no such data existed.

2.4 Concluding Remarks

A literature review was presented for large thrust bearing subjected to thermo-hydrodynamic lubrication with thermoelastic pad deformation. There are many numerical models which approximate various features of the bearing physics. In order to develop a comprehensive model with accurate results, experimental studies are essential. However, such studies are very few, especially for spring-supported pads, and usually do not involve one investigator performing both analysis and experiments.

Chapter 3

Numerical Analysis of Thrust Bearing Performance

The computer program GENMAT (discussed briefly in Chapter 2), was developed by Dr. C. M. Ettles (Bearing Sciences Inc., 202 Van Wies Point Road, Glenmont, NY 12077, U.S.A.) specifically for the analysis of spring-supported thrust bearings. The thermoelastic pad deflection model in GENMAT was based on a finite difference solution of the biharmonic equation based on thin plate theory with a shear correction. In the present thesis, a finite element model using the commercial software package ABAQUS was developed for the pad deflection to provide a check on the deflection model in GENMAT.

In this chapter, a summary of the features of GENMAT and ABAQUS are presented and comparisons are made between predictions of pad deflection using these two software packages. This approach serves the purpose of explaining the specific features of GENMAT that is used extensively in providing predictions for comparison with experimental data in subsequent sections of the present thesis. In addition, the comparison of pad deflections from GENMAT with those of ABAQUS provides some initial steps in assessing the accuracy of the GENMAT predictions.

3.1 The GENMAT Software

GENMAT is a software package for the analysis of spring-supported thrust bearing that considers the bearing heat and oil flow in three dimensions (Ettles; 1991, 1994a, 1994b, 1995a, 1995b). GENMAT consists of about 20,000 lines of FORTRAN coding and has a thermohydrodynamic treatment of the oil film with a thermoelastic treatment of the pad deflection. It allows the user to specify the load, surface velocity, lubricant, oil pot temperature and geometry of the thrust bearing. GENMAT outputs film thickness, temperature and pressure distributions. A complex nesting of iterative loops, each with relaxation factors, is found in GENMAT and allows the simultaneous solution of the various partial differential equations that describe the physics of the problem.

In the following sub-sections, some details of GENMAT are presented that are considered relevant to the interpretation of the numerical predictions of the experimental data in the present thesis. However, it is important to note that no part of GENMAT has been written by the present author and thus GENMAT is only part of the present thesis to the extent that it provides numerical predictions to compare with experimental data. The detail presented in this thesis is summarized from technical reports submitted to GE Hydro by Ettles (1994a, 1994b, 1995a, 1995b) and from journal publications by Ettles (1991) and Ettles and Anderson (1991). The calculations of the present thesis were performed using Version 3.4 of GENMAT (Ettles, 1995b).

3.1.1 Lubricant Flow

A three dimensional grid defines the boundaries of control volumes (Figure 3.1). At the centre of each control volume, temperatures and pressures are specified, linked by algebraic expressions and solved in a finite difference type of method in which conservation of mass is applied locally to each control volume following the general procedures described by Patankar (1980).

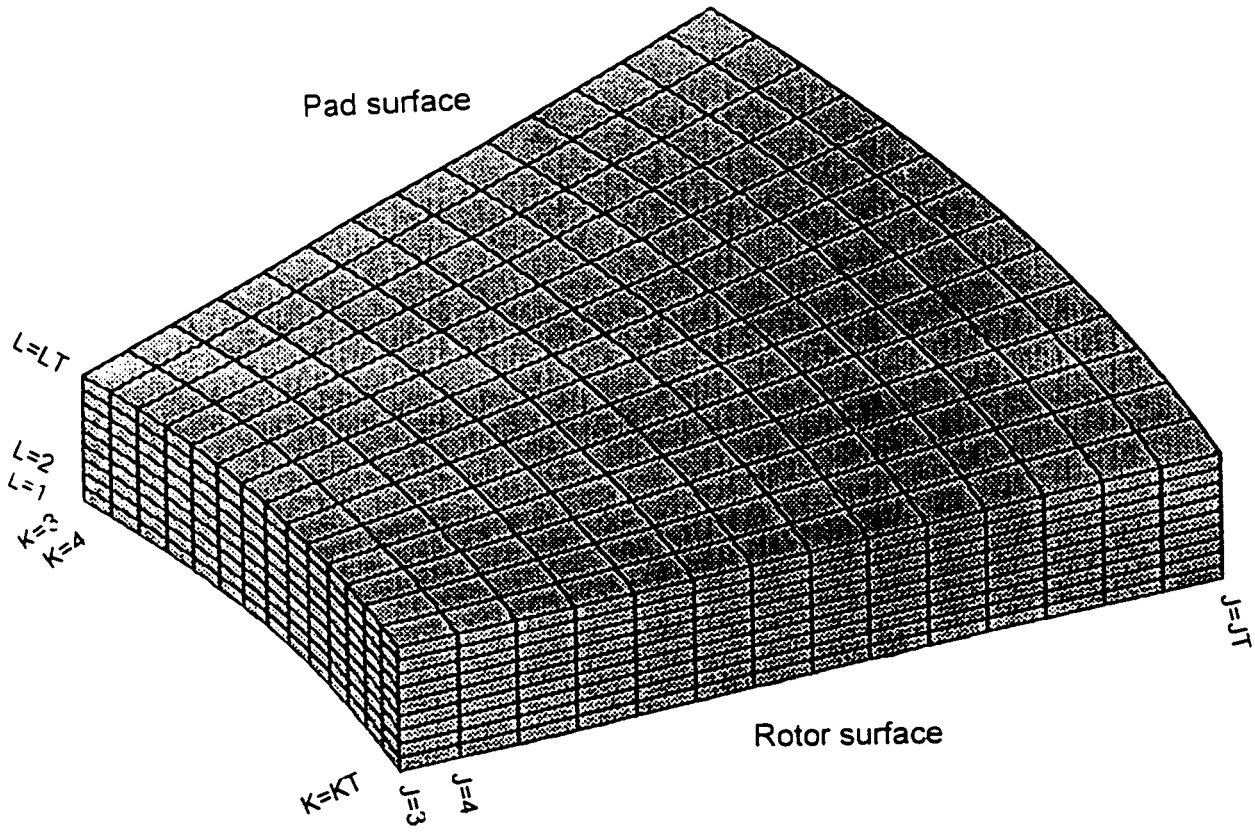

Figure 3.1. The computational grid within the film for the lubricant flow and temperature distribution (J, K and L are indices relating grid positions to arrays within GENMAT, and JT, KT and LT are the maximum values)

For lubrication mechanics, the conservation of momentum can be represented by:

$$\frac{\partial p}{\partial r}=\frac{\partial}{\partial z}\left(\eta\frac{\partial u}{\partial z}\right) \tag{3.1}$$

$$\frac{1}{r}\frac{\partial p}{\partial \theta}=\frac{\partial}{\partial z}\left(\eta\frac{\partial v}{\partial z}\right) \tag{3.2}$$

$$\frac{\partial p}{\partial z}=0 \tag{3.3}$$

and the conservation of mass can be represented by

$$\frac{1}{r}\frac{\partial}{\partial r}(ru)+\frac{1}{r}\frac{\partial v}{\partial \theta}+\frac{\partial w}{\partial z}=0 \tag{3.4}$$

These expressions represent the viscosity as Newtonian and the density as constant. The viscosity varies with temperature throughout the three-dimensional grid and when required linear interpolation is used to determine viscosities at the control volume faces. However, the lubricant flow in the z-direction is assumed negligible (as indicated by Equation 3.3) and this permits the viscosity variation through the thickness of the film to be represented by definite integrals that can be solved numerically. Thus, a single pressure acts throughout each column of control volumes that span the film thickness. The resulting simultaneous equations for pressure are solved using a Gauss-Siedel routine with successive over-relaxation.

Once flows in the r-direction and the θ-directions are determined by numerical analysis (hopefully with good accuracy), the full expression for conservation of mass (Equation 3.4) is applied to the columns of control volumes that span the thickness of the film to numerically "back out" the z-direction velocity (w) and thus provide an estimate

of the flow in the z-direction. This flow in the z-direction is subsequently included as a convective heat flow in the solution of the energy equation.

These procedures and simplifications have been described in the academic literature (Ettles, 1991; Ettles and Anderson, 1991; Colynuck and Medley, 1989). However, in finding the flow in the z-direction, Colynuck and Medley used an approach that, although based on the same theory, had more algebraic complexity in representing the velocities over the control volume faces than Ettles (and consequently GENMAT which was developed by Ettles). It was considered unlikely that these differences had much effect on the overall accuracy of GENMAT.

So far the description of GENMAT modeling has been for laminar flow in the film with negligible inertial effects. In most cases that are analyzed in the present thesis, the preceding description of the flow modelling is likely to be adequate. However, GENMAT had built-in provisions for modeling turbulent flow using Reichardt's eddy viscosity distribution that was implemented depending on a local film Reynolds number (Ettles, 1994). Thus, it was possible to have some regions of turbulent flow in the fluid film. Some considerations of circumferential and centrifugal (radial) inertial effects were also included. However, only the centrifugal inertial was included in Version 3.4 of GENMAT. Since density is not sensitive to the temperature change, density remains constant for case study in GENMAT. Also, viscosity variation due to pressure is ignored since the pressure is not high enough to cause a significant change.

Finally, to deal with cavitation in diverging regions of the fluid film, the Sommerfeld boundary conditions are applied in which negative pressures are allowed to exist during the iterative pressure calculations but are set to zero for the calculation of load. Using the Sommerfeld rather than the usual Reynolds boundary conditions avoided convergence problems without introducing significant modeling error. For most of the bearings analyzed in the present thesis, cavitation did not occur until the trailing edge where the Sommerfeld boundary conditions would be entirely adequate.

3.1.2 Heat Flow

The same three-dimensional grid that is used for the lubricant flow is also used for the heat flow (Figure 3.2) and the following form of the reduced energy equation is applied to the fluid film:

$$\rho c\left(u\frac{\partial T}{\partial r}+\frac{v}{r}\frac{\partial T}{\partial \theta}+w\frac{\partial T}{\partial z}\right)=\frac{1}{r}\frac{\partial}{\partial r}\left(kr\frac{\partial T}{\partial r}\right)+\frac{1}{r}\frac{\partial}{\partial \theta}\left(\frac{k}{r}\frac{\partial T}{\partial \theta}\right)+\frac{\partial}{\partial z}\left(k\frac{\partial T}{\partial z}\right)+\eta\left[\left(\frac{\partial u}{\partial z}\right)^2+\left(\frac{\partial v}{\partial z}\right)^2\right] \tag{3.5}$$

Once again, a control volume formulation is used which conserves mass and energy locally and the lubricant flow through the film thickness is determined as described in the previous section. The convected fluxes are "upwinded" to avoid convergence problems (Ettles, 1991). If some portion of the flow is turbulent, an adjustment is made to the viscosity and to the thermal conductivity in the reduced energy equation. As before, the matrix solver is a Gauss-Siedel routine with successive over-relaxation.

The heat flows in the pad and rotor are solved in a similar manner to those in the film except that only heat conduction is involved. A three-dimensional grid is used in the pad (Figure 3.2) and with various surface heat transfer coefficients to provide the boundary conditions at the pad sides and bottom, the temperature distribution is determined. A similar approach is taken for the rotor. The temperature distribution in the pad is used in subsequent thermoelastic deflection analysis. Heat flows in both pad and rotor are sensitive to the values of heat transfer coefficients at the boundaries.

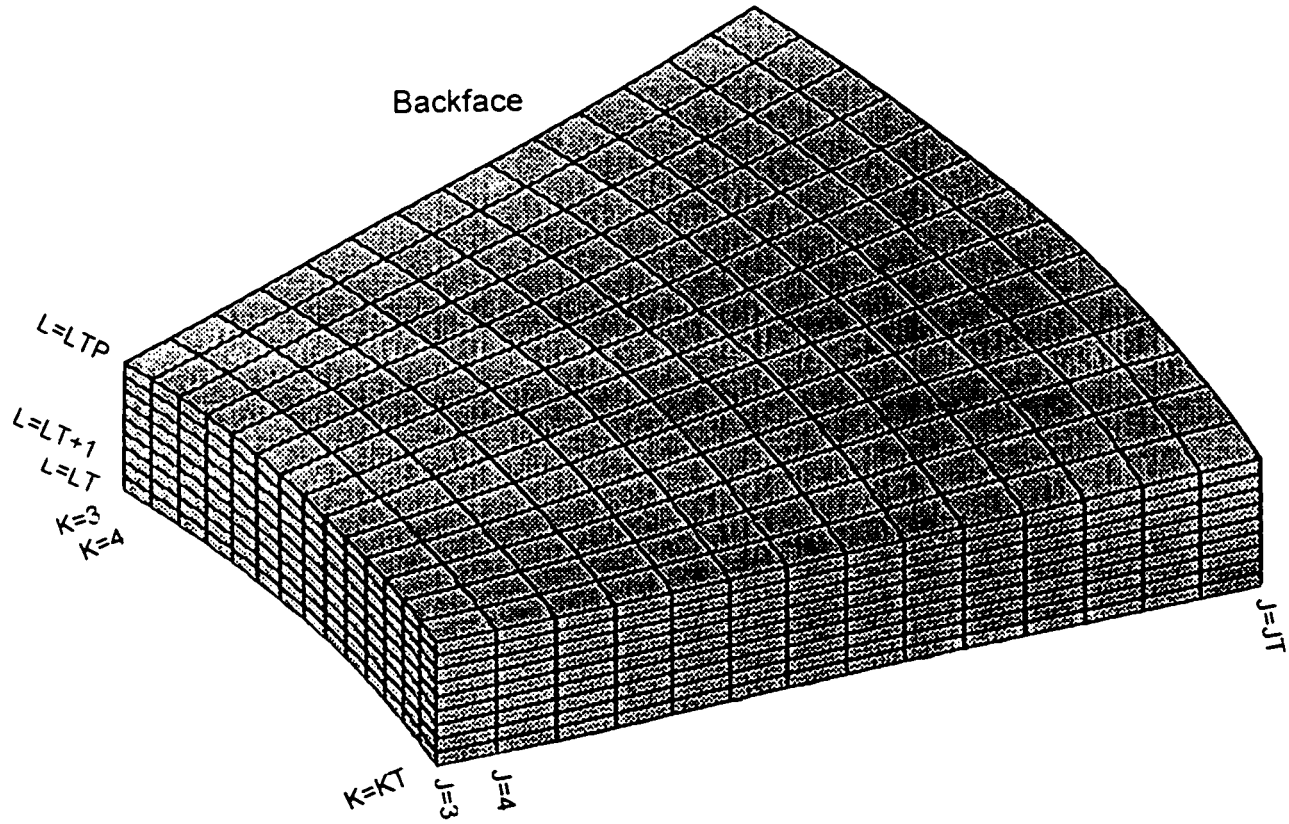

Figure 3.2 The computational grid within the pad for the temperature distribution (J,K and L are indices relating grid positions to arrays within GENMAT and JT, KT and LTP are the maximum values)

3.1.3 Flow Across the Bearing Groove

GENMAT uses boundary layer theory to represent the flow starting at the outlet of one pad across the groove to the inlet of the next pad. For the thermohydrodynamic numerical modeling of a particular pad this "hot oil carry-over" from the upstream pad determines the "initial" inlet boundary condition (which may be modified by backflow as the iterative solution proceeds). Radial flow in the groove is neglected, the circumferential curvature is neglected and thus a two-dimensional Cartesian formulation is employed. The boundary layer equations are solved numerically (Ettles, 1991) and a turbulence model is used when required (Ettles, 1994a). In this case, the effective viscosity is found using Mellor's law of the wall.

3.1.4 Thermoelastic Deflection of the Pad

The local deflection of the pad is found by the finite difference solution of the fourth-order biharmonic equation for bending. This equation is an approximate representation based on a "thin-plate" approximation of the pad. The pad bending is caused by the mechanical stress from a combination of imposed film pressure on the top of the pad and reaction forces of the springs on the back face of the pad. Also, pad bending is caused by thermal stresses arising from the imposed temperature distribution. A correction factor for shear stress is applied to reduce the error caused by the thin plate approximation. The biharmonic equation for bending and thermal deflection is

$$\nabla^4 w = \frac{p'}{D} - \frac{1}{D(1-\upsilon)}\nabla^2 M_T \tag{3.6}$$

where

∇^4 = *biharmonic differential operator*

∇^2 = *harmonic* (*Laplacean*) *differential operator*

$$D = \frac{E\, t_h^{\,3}}{12(1-\upsilon^2)}$$

p' = effective local pressure on the pad
(fluid film pressure minus spring "pressure")

M_T = thermal moment

E = elastic modulus

v = Poissons' ratio

t_h = pad thickness

The springs on the back face of the pad have their influence distributed proportionally to the surrounding points in the finite difference grid. As mentioned previously, the springs require that a certain load (called the "preload") be exceeded before deflection proportional to load occurs. This non-linear aspect of the overall spring force-deflection relationship is not represented in the applications of GENMAT in the present thesis and thus it is assumed that all spring loads exceed the preload. This assumption is examined in subsequent discussions. A grid with non-uniform spacing is used for the pad deflection calculation (Figure 3.3) and the equation set is solved directly using a banded matrix algorithm. GENMAT interpolates to apply the temperature to the deflection grid and to apply the calculated deflections to the computational grid of the film (Figure 3.1).

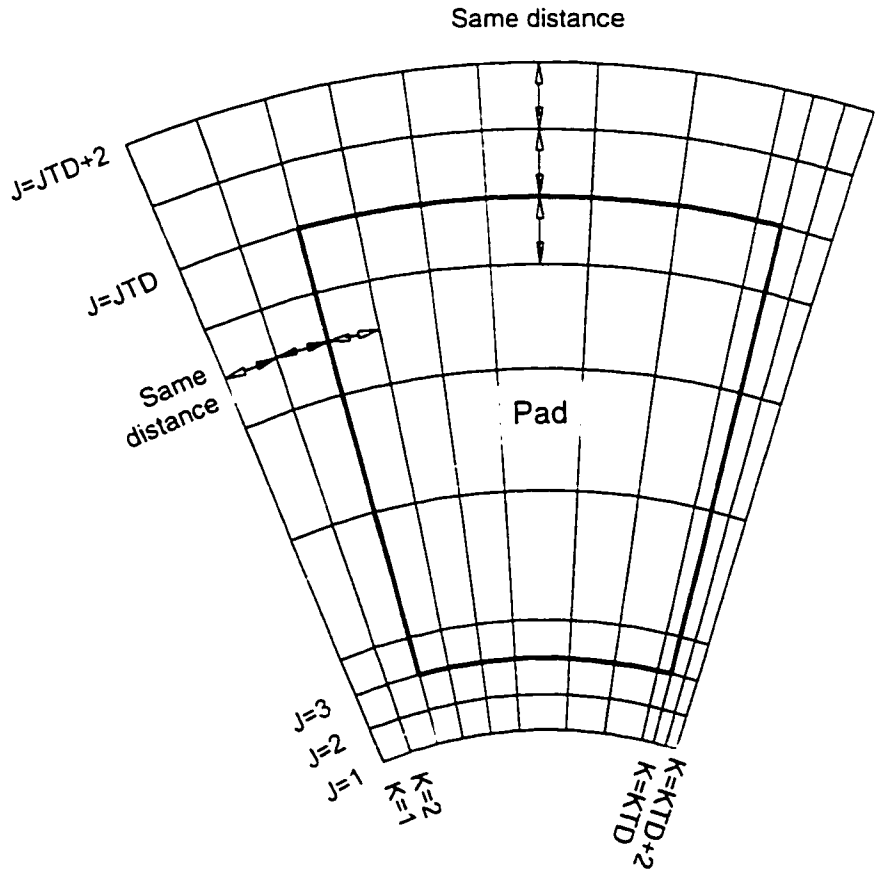

Figure 3.3. The computational grid for pad deflection

3.1.5 Some Numerical and Physical Considerations

In GENMAT, linking the numerical model to physical reality and obtaining accurate numerical solutions requires some specific features. An understanding of some of these features is important for the comparison of GENMAT numerical predictions with experimental data in the present thesis.

Pad Crowning

The undeflected pad can be given a convex parabolic surface geometry or crown in both the radial and circumferential directions. For pure circumferential crowning, the deviation from a flat plane is equal along radial lines and symmetric about the central radial line. Similarly, for pure radial crowning, the deviation from a flat plane is equal along circumferential lines and symmetric about the central circumferential line. Also, it is possible to impose a concave surface geometry.

Pad Balancing

Static equilibrium in the direction of the film thickness dictates that the pad is loaded equally on the top face by the oil film pressure and on the bottom face by the springs reaction forces. Furthermore, the pad must be tilted both in both radial and circumferential directions until the moments about any point sum to zero. It is convenient to consider the unique point (centre-of-effort) about which the moments caused by the oil film pressure and the moments from the spring reaction forces each sum to zero. An iterative procedure is used which involves the successive curve fitting of centre-of-effort coordinates and tilt angles to hasten convergence by providing an extrapolated value for the next specified tilt angles (Ettles, 1994).

Pad Grounding Condition

A balancing procedure is applied, as discussed in the previous section, to impose static equilibrium on the out-of-plane moments. According to Ettles (1995a), to solve Eqn. (3.6), boundary conditions are required to prevent translation and rotation. Apparently, Ettles found it both convenient and accurate in GENMAT to apply the boundary condition of $w = 0$ at three nodes that were widely spaced, in an approximate equilateral triangle, with the nodes about half way between the pad centre and the edges. These boundary conditions were chosen in preference to earlier attempts at trying to impose $\partial w/\partial r = \partial w/\partial \theta = w = 0$ at the centre-of-effort but the relatively coarse grids of the deflection calculation led to unrealistic pad shapes.

Treatment at Interface Between Pad and Film

Control volumes in the pad interact directly with control volumes in the oil film (Figure 3.4). Assuming the temperature varies linearly within the control volume with a common value at interface, the conducted local heat flux into the film is:

$$q = \frac{A k_p k_o}{t_p k_o + t_o k_p} (T_p - T_o) \tag{3.7}$$

where q = heat flux k = thermal conductivity

T = temperature t = distance from grid node to interface

A = area of the control volume interface

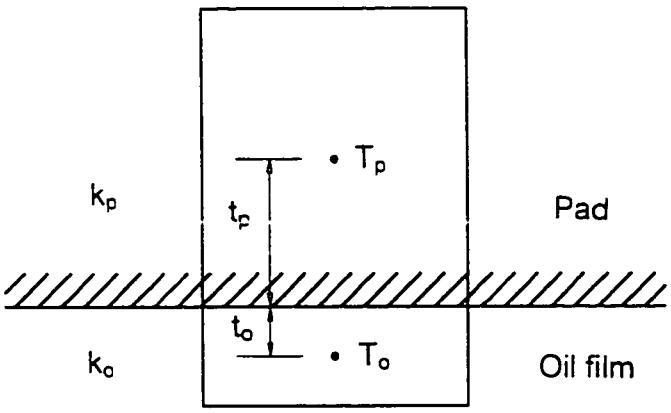

Figure 3.4. Control volumes at the pad-film interface

This direct connection gave a common thermal solution domain for pad and film thus avoiding the need for an approximate approach involving a surface heat transfer coefficient

Surface Heat Transfer Coefficients

The other five surfaces of the pad are exposed to slowly moving oil from the oil pot that is maintained at a constant temperature by heat exchangers. The heat transfer from these surfaces is approximated by surface heat transfer coefficients. These heat transfer rates are important, particularly at the back face of the pad, because they influence the film and pad temperatures which in turn affects the thermal distortion and hence the rate of heat generation in the film and so on.

To estimate the surface heat transfer coefficients, empirical expressions have been developed from temperature measurements from several pivot-supported bearings (Ettles, 1987) and modified according to temperature data from the thrust bearing test facility described subsequently in the present thesis.

Ram Effect at the Leading Edge

Ettles (1995b) argues that viscous effects in the inlet zone at the leading edge of the pad serve to reduce the inlet boundary pressure to a value much lower than might be expected when only the boundary layer flow in the groove is considered. In GENMAT, a "semi-empirical" value for inlet pressure is adopted.

3.1.6 Running the Program

The code of GENMAT is self-contained and no library routines are required. Combining a spring and pad data file with a general data file forms the GENMAT input file. These two data files are obtained by running the data generation programs provided with GENMAT. Some of the input data remains the same from run to run and thus the data generation programs may not be used for every run.

Spring and Pad Data File

This data file contains the coordinates, stiffness and preload of the springs along with the pad geometry and rotor thickness. The groove between the pads has a uniform width but in the calculations of the present thesis, this geometry is approximated within GENMAT as sector shaped. As a result, the groove increases in circumferential width in the radial direction. This approximation allows a cylindrical coordinate system to be employed in the numerical analysis.

General Data File

The general data file contains running conditions, physical properties and "numerical" parameters. The running conditions include quantities such as the oil pot temperature, rotational speed, lubricant grade following the classification of the ISO (International Standards Organization) and the load applied to an individual pad. The physical properties include surface heat transfer coefficients for pad and rotor; shaft and rotor dimensions; both thermal and elastic material properties and pad crowning. The numerical parameters include specification of the grids for temperatures, pressures and pad deflections; convergence criteria and relaxation factors.

3.2 Finite Element Analysis of Pad Deflection

A finite element analysis of the spring-supported pad was achieved using the commercial package called ABAQUS (Hibbitt, Karlsson & Sorenson, Inc. 1994). The main input was a file that specified the required options and gave the data associated with these options.

A three- dimensional finite element model was developed for a pad that included both thermal and mechanical effects. The model used the converged temperature and pressure distributions from a GENMAT analysis of a typical bearing from the experiments reported subsequently in the present thesis and the deflection of the pad was calculated. The specific intention in this section of the present thesis was to compare the pad deflections calculated by ABAQUS with those predicted by the deflection model in GENMAT. It was suspected that the deflection model in GENMAT introduced some inaccuracy because it was based on a finite difference solution of the biharmonic plate bending equation. Even if the deflection model in GENMAT was accurate enough, it also has limitations on its ability to model complex pad geometries (a steel pad with a thick copper backing plate, for example). The finite element modeling in the present thesis was preliminary in nature since only one case was examined in the present thesis.

However, it was hoped that some indication would be gained regarding the strategic value of trying to develop a finite element deflection model as an option for GENMAT. Furthermore, it was expected that some insight would be gained into the inner workings and accuracy of GENMAT that would be useful in subsequent comparisons of experimental data with the numerical predictions of GENMAT.

3.2.1 Preprocessing Program

The preprocessing program was developed in the FORTRAN language and included the generation of a uniform three dimensional grid (or mesh), the nodal distribution of spring stiffness and the converged values of both pressure and temperature distributions from GENMAT. The output of the preprocessing program was the ABAQUS input file.

3.2.2 Modeling Details

The finite element model consisted of elements, a mesh (or grid), element attributes and boundary conditions.

Element Selection

In the present thesis brick elements with 8 nodes were used with spring elements representing the supporting springs. Brick elements with 20 nodes could have been used but run times would have increased and thus they were not employed.

Mesh Generation

The uniform mesh for the pad was generated by a short FORTRAN code, written by the present author and placed in the preprocessing program. The mesh size could be varied easily. However, in the case examined, it was convenient to set the mesh size the same as in GENMAT because the ABAQUS model was using pressure and temperature output from GENMAT. The resulting aspect ratio of the elements was about 4.3 and this value violated the usual practice of keeping the aspect ratio below 2. This element shape may have caused some inaccuracy in the results. The supporting spring elements were added to complete the three-dimensional mesh (Figure 3.5).

Element Attributes

The spring elements presented a special problem. Since the centre of a spring was unlikely to coincide with a grid node, the spring stiffness had to be distributed to the corner nodes of the element over which it acted (Figure 3.6). This was accomplished by a geometric proportioning. If the distances of the spring centre to the nodes 1, 2, 3, 4 were l_1, l_2, l_3, l_4, then the proportion P_n of the spring stiffness allocated to node n was:

$$P_n = \frac{1/l_n}{\sum_{1}^{4} 1/l_n}, \qquad \text{where } n=1, 2, 3, 4 \tag{3.8}$$

Several springs can contribute to the stiffness assigned to a node.

When the values of spring stiffness were assigned to the appropriate grid nodes, a new pattern of springs was generated in the finite element model to simulate the spring arrangement. For a bearing with a 15 spring arrangement (Figure 3.7), the pattern in the ABAQUS model was as shown in Figure 3.8.

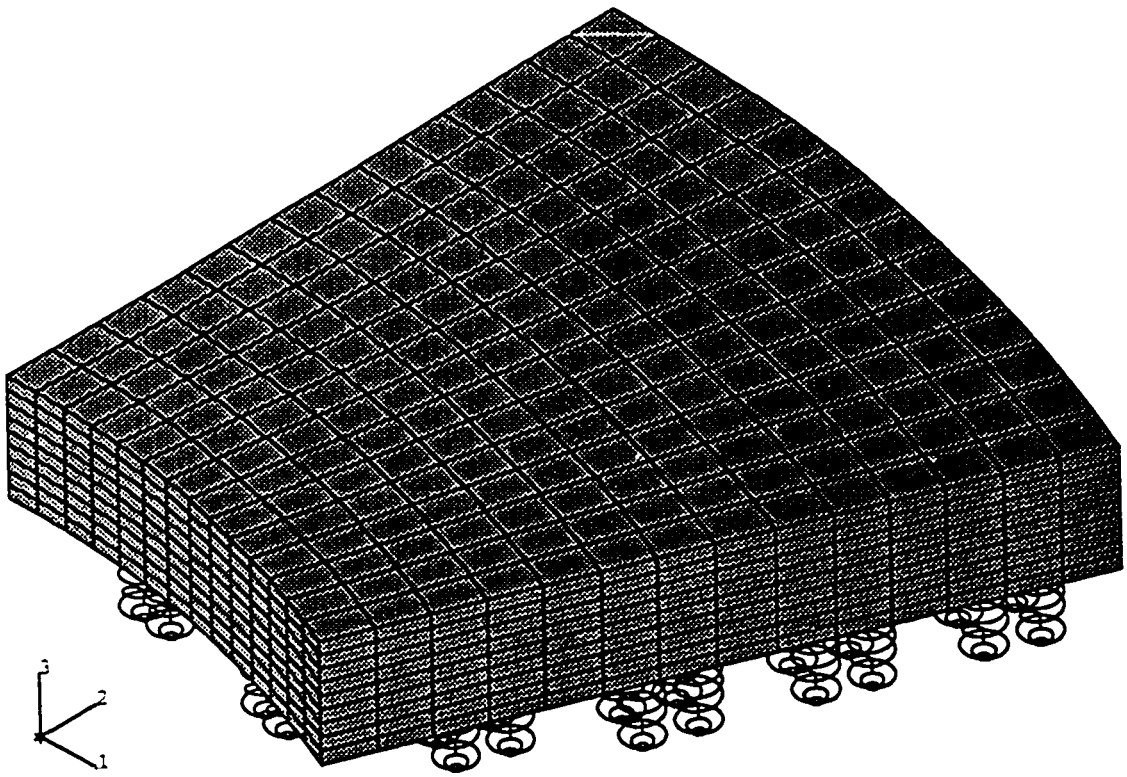

Figure 3.5. Mesh and spring elements

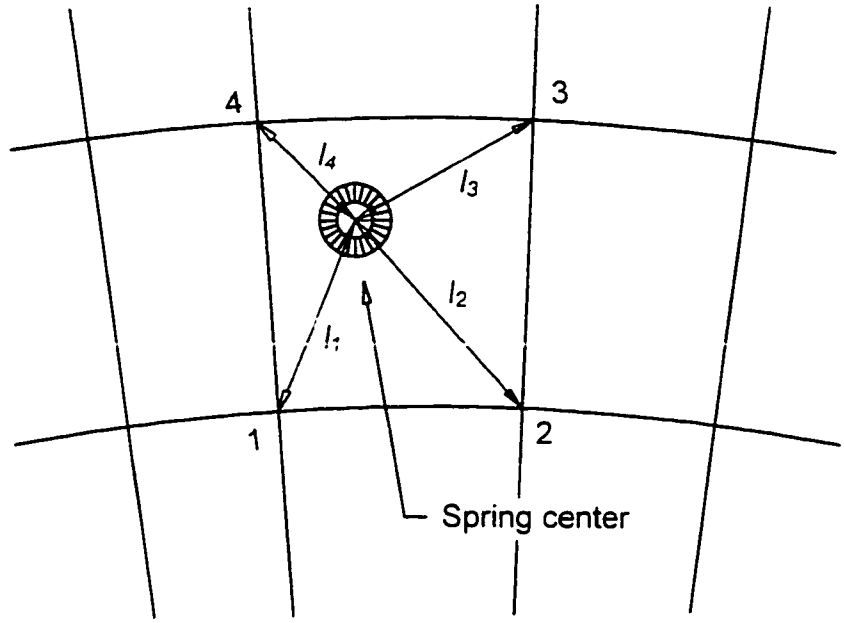

Figure 3.6. Spring stiffness allocation

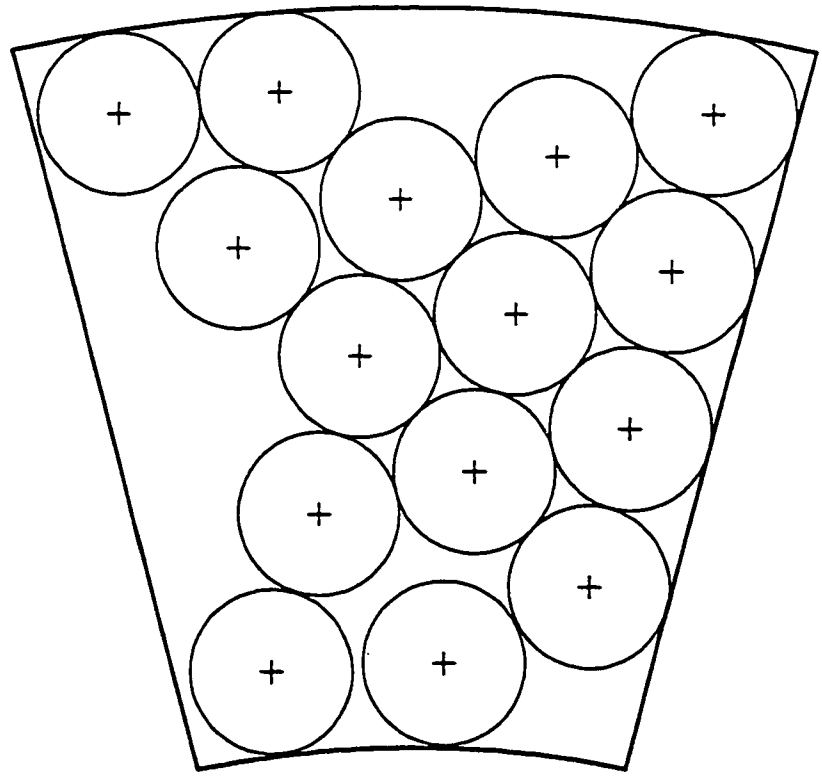

Figure 3.7. Spring set (15 Springs)

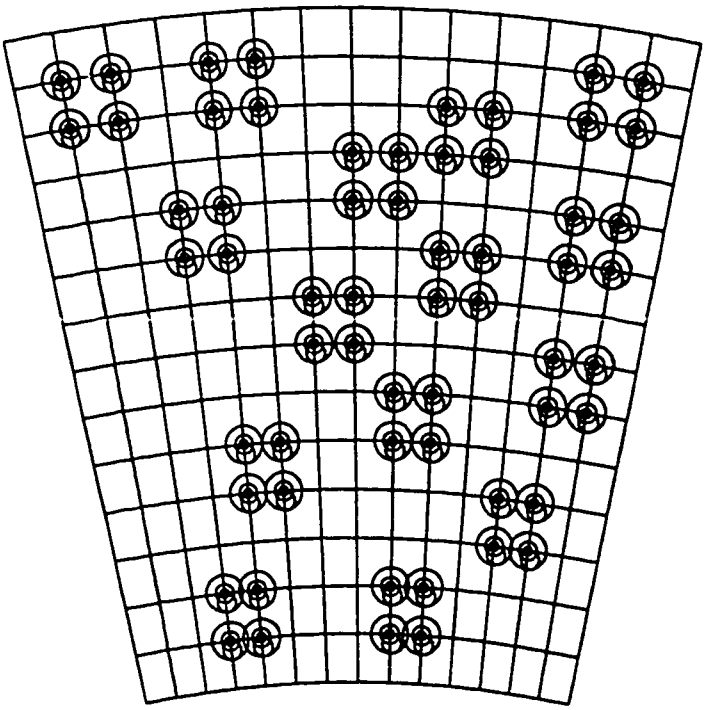

Figure 3.8. Spring simulation pattern (15 Springs)

Another element attribute was the pressure and temperature values from the GENMAT output that were read into ABAQUS and assigned to the corresponding grid nodes. Pressure was on the top surface of the pad, applied as the nodal loads, while temperature was distributed throughout the whole pad.

Material properties were also defined for the pad material and applied to the elements. In this case, they included elastic modulus, Poisson's ratio, thermal conductivity and coefficient of thermal expansion.

Boundary Conditions

Boundary conditions were applied to constrain the spring-supported pad in the radial and circumferential directions. In the spring-supported thrust bearings, the fluid film applied shear stress to the pad surface pushing it circumferentially in the direction of rotor motion and radially outwards until the outer and trailing edge met stationary metal surfaces. This constraint was represented by the following boundary conditions:

$$\begin{aligned} u_\theta = 0, \quad u_r = 0 \qquad & \textit{at outer -trailing edge corner} \\ u_\theta = 0 \qquad & \textit{at inner - trailing edge corner} \end{aligned} \tag{3.9}$$

as shown in Figure 3.9. These boundary conditions were applied at the midpoint of the pad thickness.

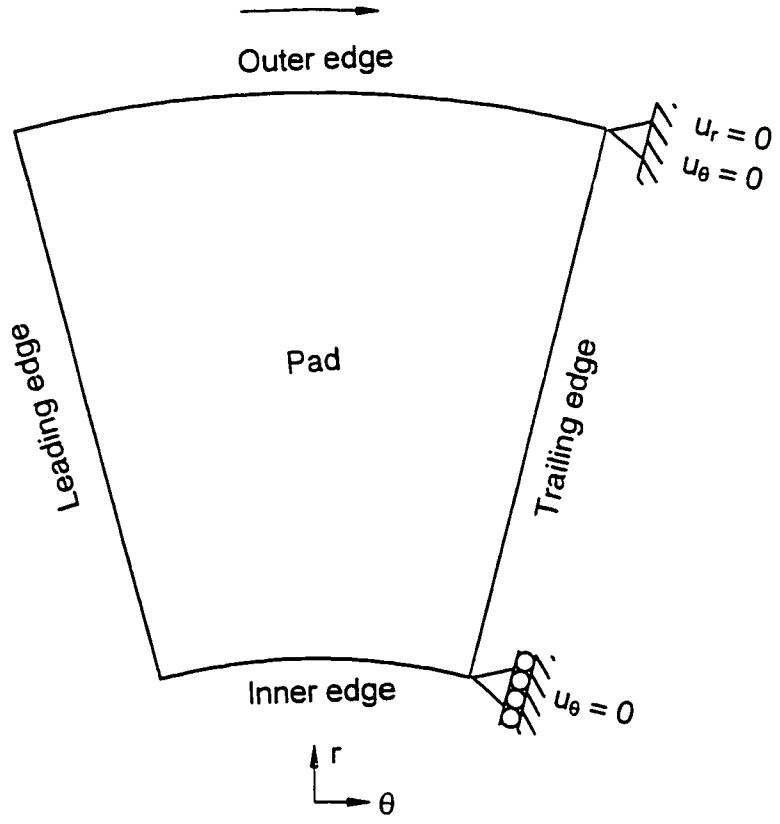

3.3 Comparison of GENMAT and ABAQUS Pad Deflections

A single case (Table 3.1) was analysed by GENMAT to produce converged pressure and temperature distributions for input into the ABAQUS model and the deflections predicted by ABAQUS was compared with the film shape calculated by GENMAT.

Specific load	Rotation speed	Lubricant	Oil pot temperature	Spring set
4 MPa	500 rpm	Terreso 46	70 °C	15 springs

Table 3.1 Input conditions for the case examined

The pad position at the minimum film thickness predicted by GENMAT was aligned with the minimum deflection predicted by ABAQUS. Then, the output values from each software packages were converted to relative deflection values with the same origin.

An effective way to make the comparison was to create contour maps of the two film thickness distributions (Figure 3.10). When this was done, it was clear that the ABAQUS model predicted more circumferential tilting of the pad. Furthermore, the ABAQUS model located the zero relative deflection at the outer corner of the trailing edge whereas the GENMAT model predicted it at about 1/3 of the way inwards from this outer corner along the trailing edge.

The difference between the two models was difficult to interpret with only one case to consider. The calculation grids were quite coarse and thus both models might be somewhat inaccurate. The ABAQUS model had a high aspect ratio that may have introduced error as mentioned previously. With the influence of an individual spring was distributed to the four nodes nearest to its centre rather than representing its true shape and thus the local pad bending was not modelled precisely. Furthermore, a small discrepancy in the pad balancing of GENMAT might cause the ABAQUS model to predict a different pad tilt. However, the tilt might have returned to a value close to the GENMAT prediction, if the ABAQUS model was then capable of participating in the iterations of the full GENMAT solution. On the other hand, there might be somewhat more inaccuracy in the GENMAT deflection model than that of ABAQUS.

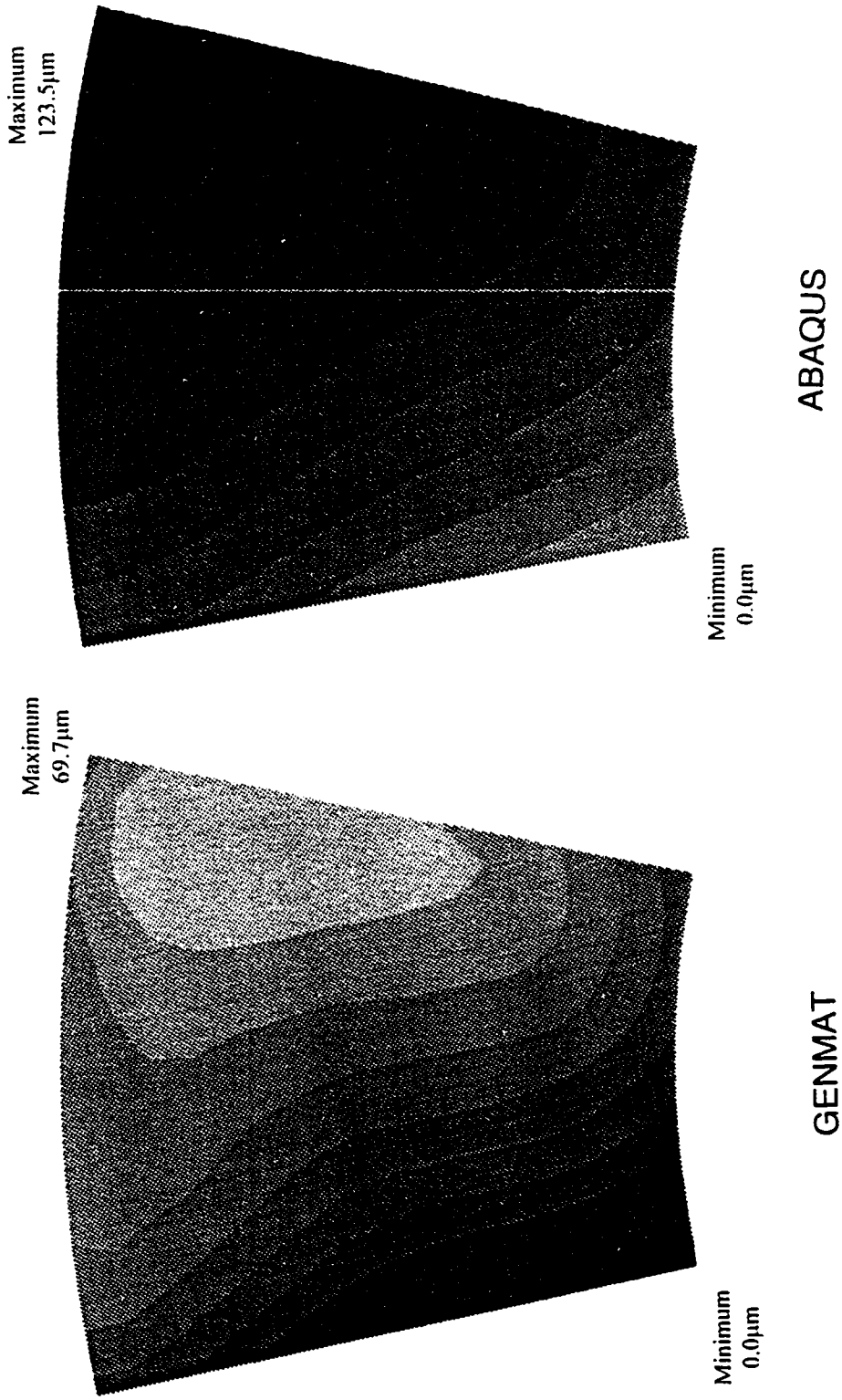

Figure 3.10. Comparison of pad deflections predicted by GENMAT with those predicted by ABAQUS

3.4 Concluding Remarks

The GENMAT software package is very complex and provides a rigorous treatment of the physics of spring-supported thrust bearing lubrication. Based on the single case compared with a finite element analysis using the ABAQUS commercial package, there is a suggestion that perhaps an option should exist in GENMAT to conduct a finite element analysis to determine pad deflection. However, a more extensive appraisal of this complex issue was beyond the scope of the present thesis. Another way to investigate the accuracy of the GENMAT deflection model is to compare its predictions to experimental data. This comparison is performed in subsequent chapters of the present thesis.

Chapter 4

Laboratory Test Facility

In 1990, construction began on a laboratory test facility (Figure 4.1) for large thrust bearings at the Dominion Engineering Works in Montreal sponsored by the Generator Engineering Group of GE Hydro. The major development of the test facility occurred over a four year period as described in detail by the internal reports of GE Hydro written by Grant (1991), Monk (1991), Mizgala (1994) and Yuan (1994a). The construction was completed in June 1994 with the installation of the loading system. The spring-supported thrust bearing in this apparatus had an outside diameter of 1.168 m thus making it large enough to simulate some of the features of large thrust bearings in the field. In the experiments, load, speed, oil pot temperature, oil viscosity grade, pad thickness and spring arrangement were varied and pressure, temperature, oil film thickness were measured at a number of locations in the thrust bearing pad. Also, temperatures of other part of the apparatus such as thrust block, rotating ring, oil pot, springs, driving motor and cooling system were measured using thermocouples and resistance temperature detectors (RTD's). In this manner, thrust bearing performance was explored.

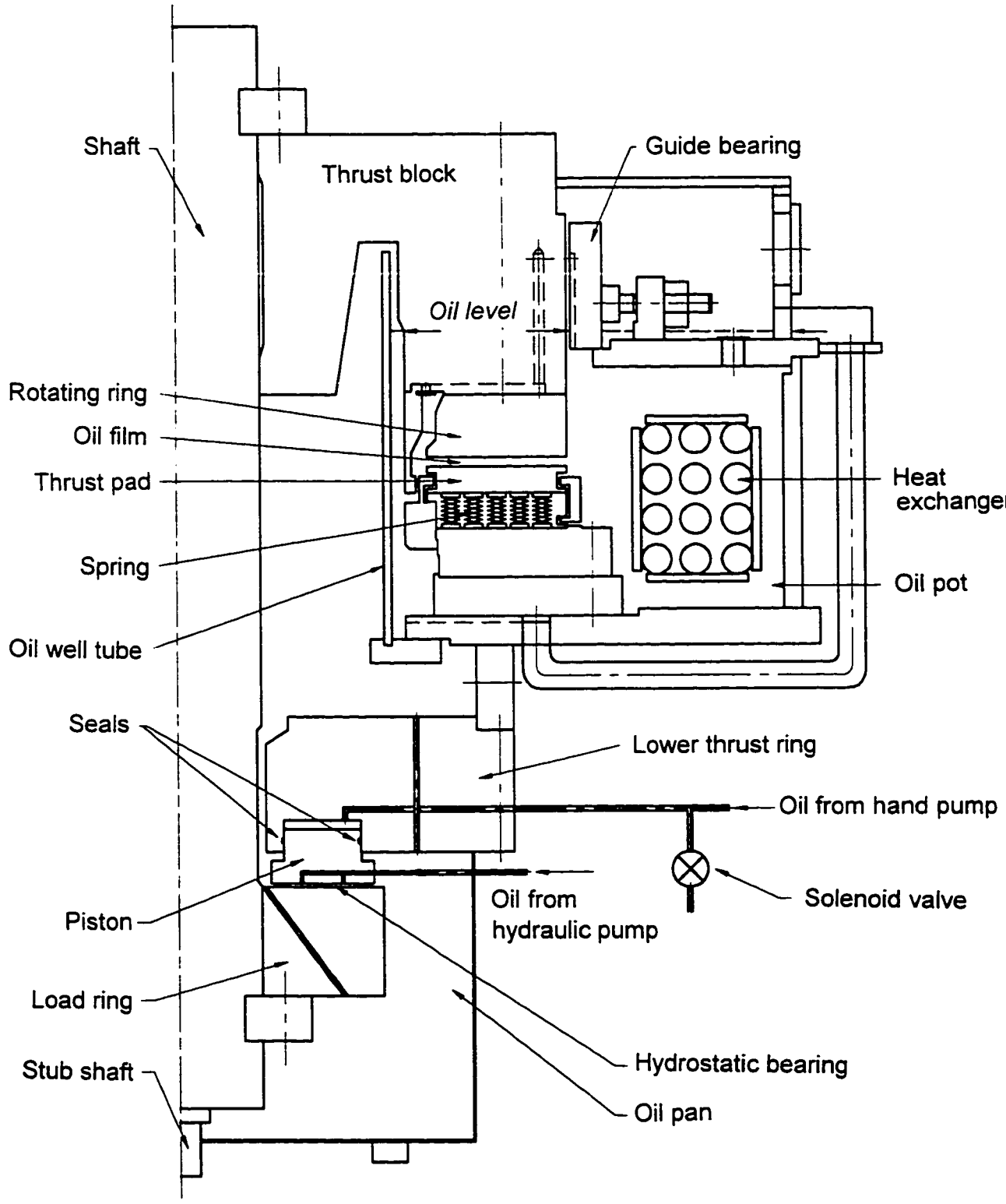

Figure 4.1. A cross section of the test facility

4.1 Component Systems

4.1.1 Thrust Bearing

The rotor (thrust block and rotation ring) of the bearing was loaded against stationary spring-supported sector pads which were constrained radially by segmental guide bearing pads (Figure 4.1). The rotor was driven by a 224 kW DC motor with an adjustable speed controller. The test facility was designed to permit speeds up to 800 rpm (corresponding to a maximum surface velocity of 49 m/s) and specific loads (average pressure) in the thrust bearing up to 7 MPa. An air blower provided cooling for the drive motor. Lubricant was supplied by emersing the entire thrust bearing and the lower half of the guide bearings in an oil pot.

The sector pad of the thrust bearing had a ring groove in the center (Figure 4.2) into which high pressure oil could be pumped at start-up to provide hydrostatic oil films between pad and rotating ring to provide surface protection during the start-up. On the top of the pads, there was a thin layer of soft Babbitt (Figure 4.2) which was present to minimize the damage to the rotating ring surface and the pad itself should an unforeseen film break down occur or if contaminant particles were present in the oil. The pad thickness dimension included the Babbitt layer.

The pads were part of a set of 12, distributed symmetrically in the circumferential direction (Figure 4.3) to form a thrust bearing with an outer diameter of 1.168 m (46 inches) and an inner diameter of 0.711 m (28 inches). The grooves between pads all had a constant width of 52.3 mm which meant that the leading and trailing edges of the pads did not follow radial lines exactly and thus the pads were not perfect sector shapes (Figure 4.3). Based on the above dimensions, the total surface area of the pads was 0.531 m^2. The pads were mounted in a oil pot consisting of an annular tank with a steel outer wall but a plexiglass inner wall called the "oil well tube" (Figure 4.4).

Pads of two different thicknesses were tested, one was 41.2 mm (1.62 inches) and the other was 30.2 mm (1.19 inches). The groove and pad thickness dimensions were typical of full-scale bearings in service and, therefore, heat conduction through the pad

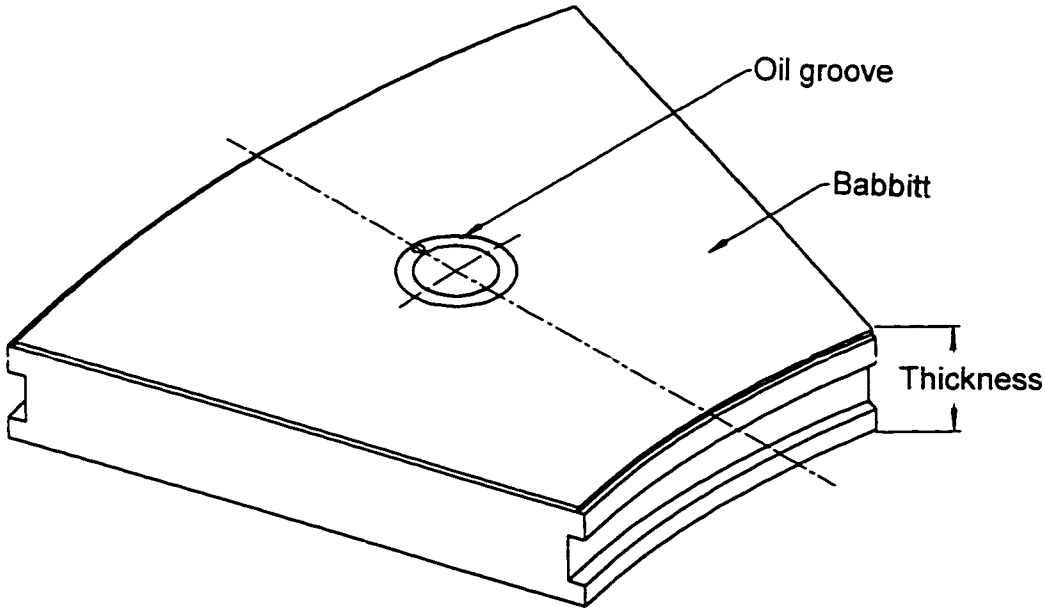

Figure 4.2. The thrust bearing pad

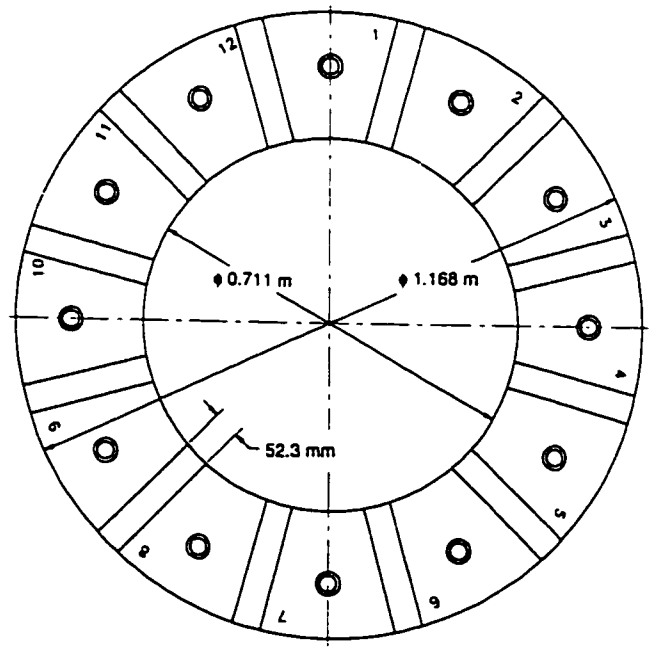

Figure 4.3. The pad arrangement
(specific pad numbers referred to in subsequent description of instrumentation)

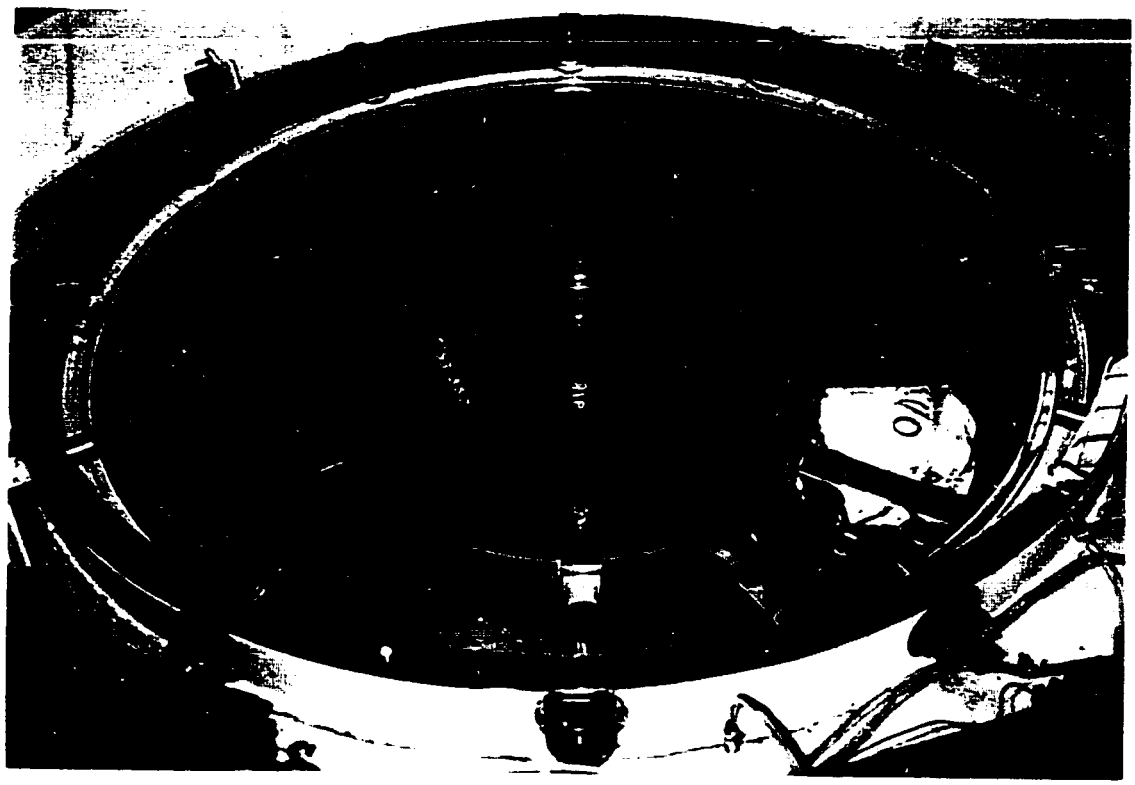

Figure 4.4. The thrust bearing pads in the oil pot

thickness and convective heat transfer in the groove should be representative of full-scale bearings. However, many bearing pads in service are larger, both radially and circumferentially, and as a result, the test bearing pads had lower deflections than pads in service for the same average film pressure.

The thrust bearing pads were supported by springs (Figure 4.5). Each spring had a 50 mm diameter, a 3.65 MN/m stiffness and a 7.56 kN compression preload (Figure 4.6). As mentioned previously, a central bolt with end plates applied the preload and the load on the spring had to exceed the preload before any deflection occurred. Thus, the springs provided a stiff mounting to avoid pad vibration and exhibited non-linear rather than the usual linear load-deflection behaviour found in most mechanical devices. Three different spring arrangements were tested. Arrangement no. 1 had 15 springs located over most of the back face pad (Figure 4.7a), arrangement no. 2 had springs removed from the leading edge to give only 11 springs per pad (Figure 4.7b) and arrangement no. 3 had 12 springs per pad (Figure 4.7c).

4.1.2 Loading System

The load was imposed by a hydraulic piston of annular shape which had inner and outer piston rings to seal the pressure chamber as shown previously in Figure 4.1. The piston pushed down on the lower end of the rotor shaft through a load ring when oil was pumped into the pressure chamber with a hand pump. The load was calculated from the product of chamber pressure and piston area plus the weight of the rotor. Conceptually, this loading system was similar to that employed by Kawaike *et al* (1977).

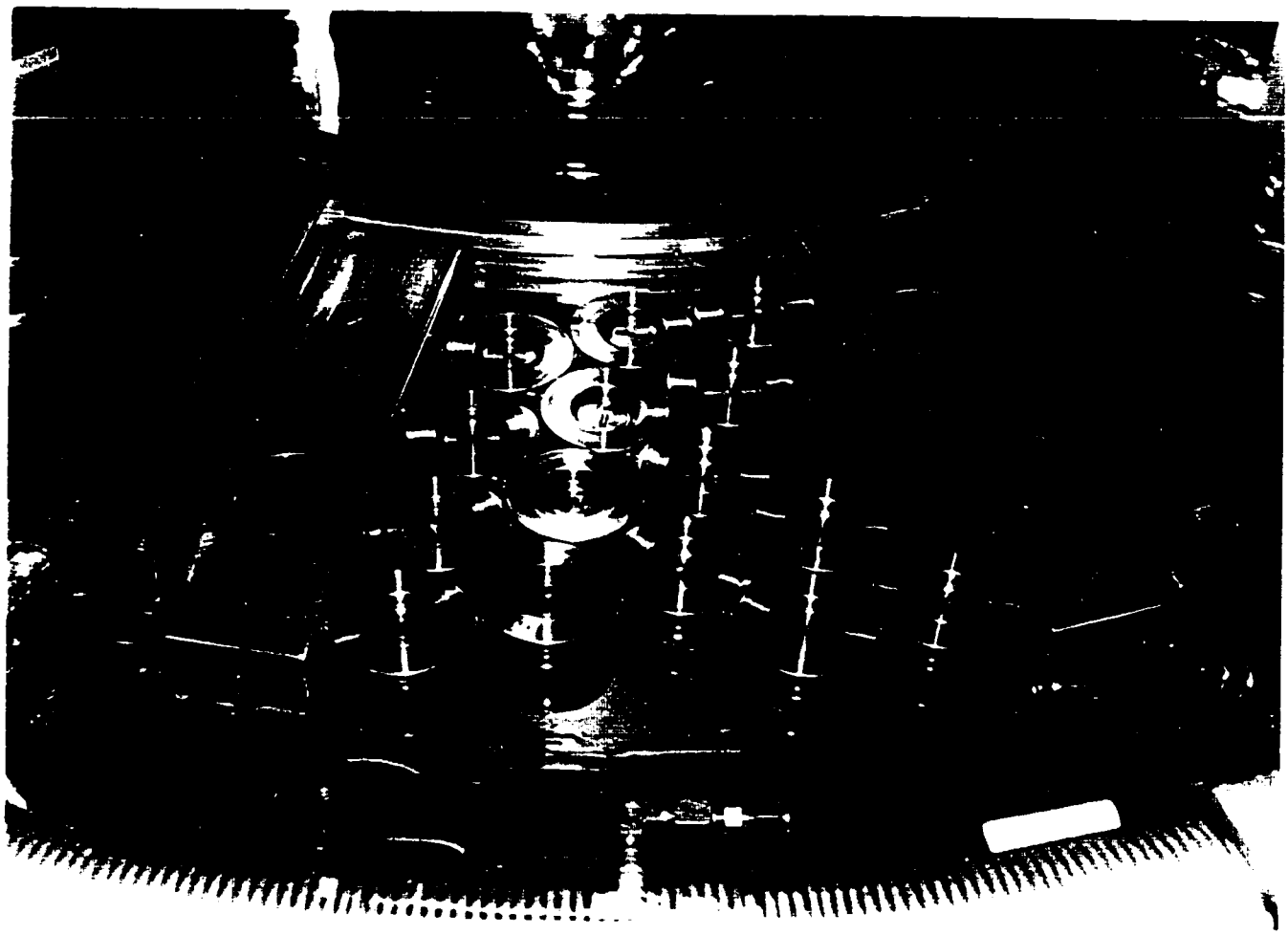

Figure 4.5. The springs supporting the pads

Figure 4.6. A spring used to support the thrust bearing pad

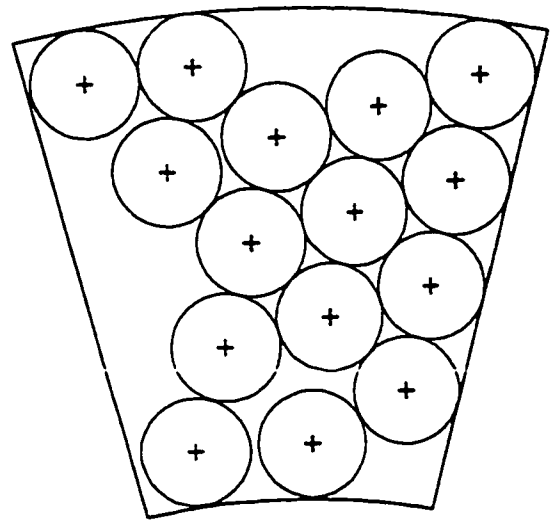

(a) No. 1

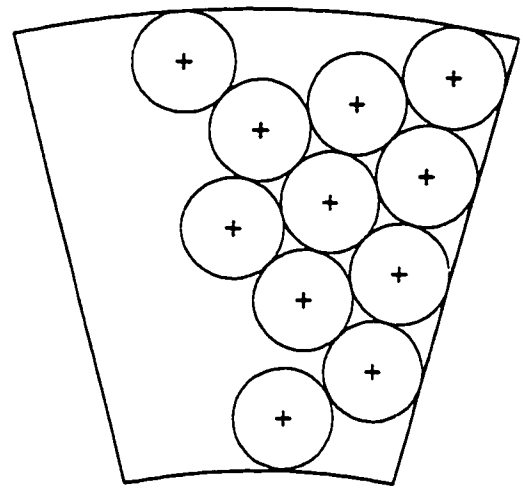

(b) No. 2

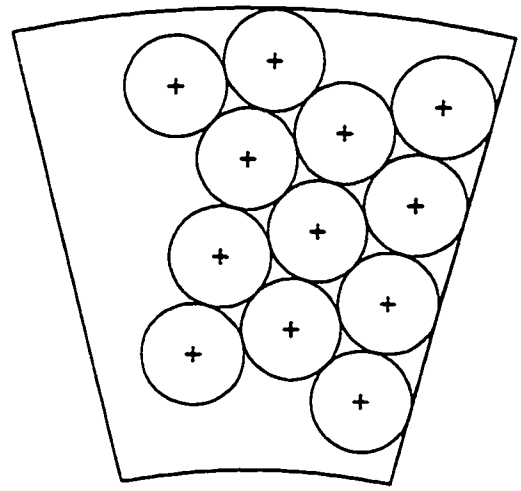

(c) No. 3

Figure 4.7. The spring arrangements

The load was applied to the moving rotor through a hydrostatic bearing onto a load ring on the lower part of the shaft (Figure 4.1) thus avoiding direct surface contact. The hydrostatic bearing had six inner and six outer pockets (Figure 4.9).

4.1.3 Oil Supply Systems

Oil supply systems were essential for running the apparatus in that thin oil films prevented direct surface contact with the associated high friction and surface damage. Under steady state operation, the guide and thrust bearings had low pressure oil available for entrainment. However, the ring groove of the thrust bearing and hydrostatic bearing of the loading system needed a high pressure oil supply.

Oil supply to thrust bearing

Oil supply systems were required to provide relatively cool oil for entrainment into the film of the thrust bearing and the guide bearing. Thus, the thrust bearing and the lower half of the guide bearing were immersed in an oil pot which was kept at constant temperature by adjusting the water flow rate through two internal heat exchangers (Figure 4.8). A passive pumping system was driven by the motion of the rotor to circulate the oil thus reducing local temperature gradients. Oil was pumped radially outward, through channels in the rotor between the thrust block and the rotating ring, by centrifugal force, to flow into the oil pot (or directly into the guide bearing). From the oil pot, flow occurred radially inward through the grooves between the pads to be available for entrainment at the leading edge of the thrust pads and to mix with some of the hot oil from the trailing edge of the "upstream" pad. The oil flow rates could be adjusted by using various orifices and baffle plates.

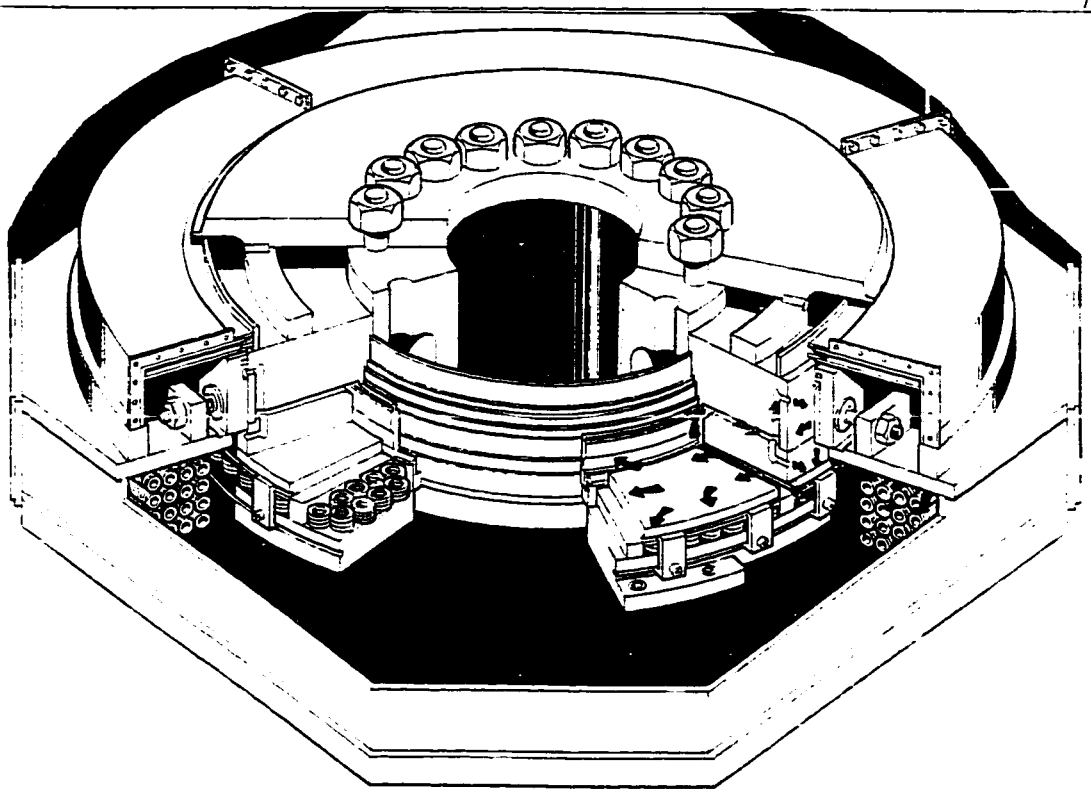

Figure 4.8. Oil supply to thrust bearing

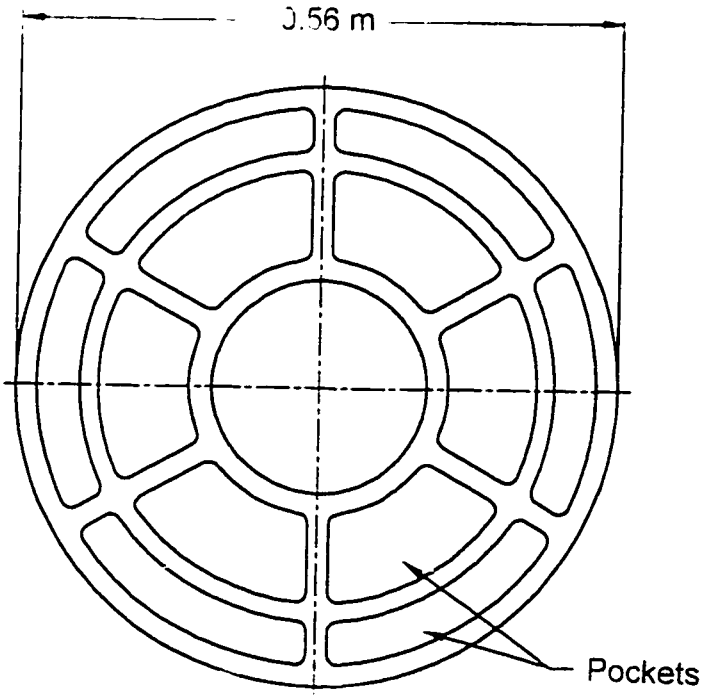

Figure 4.9. The hydrostatic bearing of the loading system

Hydrostatic system for the test bearing

To provide protection of the bearing surfaces during start-up and shut-down, the pad had a ring groove in the center into which oil was injected with a 1.1 kW pump. This hydrostatic oil film could be maintained when the rotor was stationary, thus allowing a small amount of lateral motion and very gradual rotation by hand, both of which were useful during the set-up of the guide bearing and finding the voltage output from the displacement probes corresponding to zero film thickness (as discussed in next chapter).

Oil supply to the hydrostatic bearing of the loading system

The pockets of the hydrostatic bearing (Figure 4.9) had oil supplied by a 37.3 kW pump through a manifold. Compensation was provided by capillary tubes and orifices in series between the manifold and the pockets. The oil was cooled by heat exchangers in the pump reservoir. A solenoid valve was attached to the hand pump line to relieve the pressure in the event that the pump for the hydrostatic bearing failed.

4.2 Instrumentation

The test facility had various types of instrumentation to measure the temperature of the thrust bearing pad, film pressure and film thickness. This instrumentation provided the experimental data as explained subsequently. Also, temperatures were measured at numerous other locations, including the thrust block and rotating ring (Figure 4.10), guide bearings, the groove between the pads and the oil pot. In addition, temperatures and flow rates of the cooling water were measured along with power input to the drive motor which allowed a calculation of overall power loss of the thrust and guide bearing system. The test facility had more instrumentation which measured quantities such as pressure in the hand and hydrostatic bearing pumps of the loading system, runout of the rotor shaft and the level of the oil in the pot.

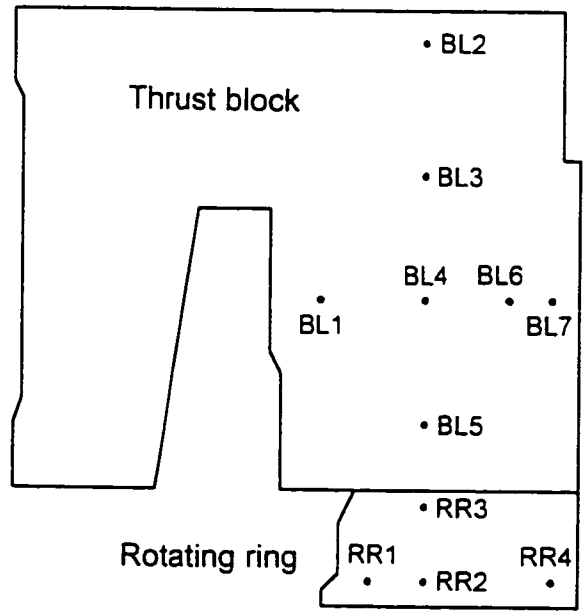

Figure 4.10. Temperature measurement in the rotor

(BL = Block, RR = Rotating Ring)

4.2.1 Temperature Measurement

Most of the temperature measurements were made with Copper-constantan thermocouples but some measurements were made with resistance temperature detectors (RDT's). The RDT's were physically larger than the thermocouples and thus did not provide a temperature at as precise a location. However, RTD's were used in generator thrust bearings in service and, thus, they were used in a similar manner in the test facility to monitor temperature in two of the thrust pads at the same location, in one of the guide bearing pads and in the hydrostatic bearing of the loading system. One of the RTD's in the thrust bearing pad and the one in the hydrostatic bearing were connected to an alarm box which provided an audible warning if temperatures exceeded expected maximums. A further four RTD's were used to measure the inlet and outlet water temperatures of the two internal heat exchangers in the oil pot.

Pad no. 7, with a pad thickness of 41.2 mm had 10 thermocouples (TC1, TC2, ...TC10) in it. Thermocouples TC1, TC2 and TC3 were located through the pad thickness at the trailing edge where TC1 was closest to the pad surface, while the others were spread over the pad area in the mid plane of the pad thickness (Figure 4.11). Pad no. 7 with pad thickness of 30.2 mm had 14 thermocouples in it. Some were located through the pad thickness at the outer edge of the pad, others were spread over the pad area in the mid plane of the pad thickness (Figure 4.12).

4.2.2 Pressure Measurement

Pressure taps were located in the thrust pad, with the connecting tubes from the outer edge of the pad (Figure 4.13) to analogue gauges which were located outside the bearing and gave the pressure values. Most of the available space was used by these connecting tubes and thus it was not possible to measure pressure on the same pad as temperature. At many of the other locations in the test facility pressures were low enough to allow pressure taps to be connected to manometers.

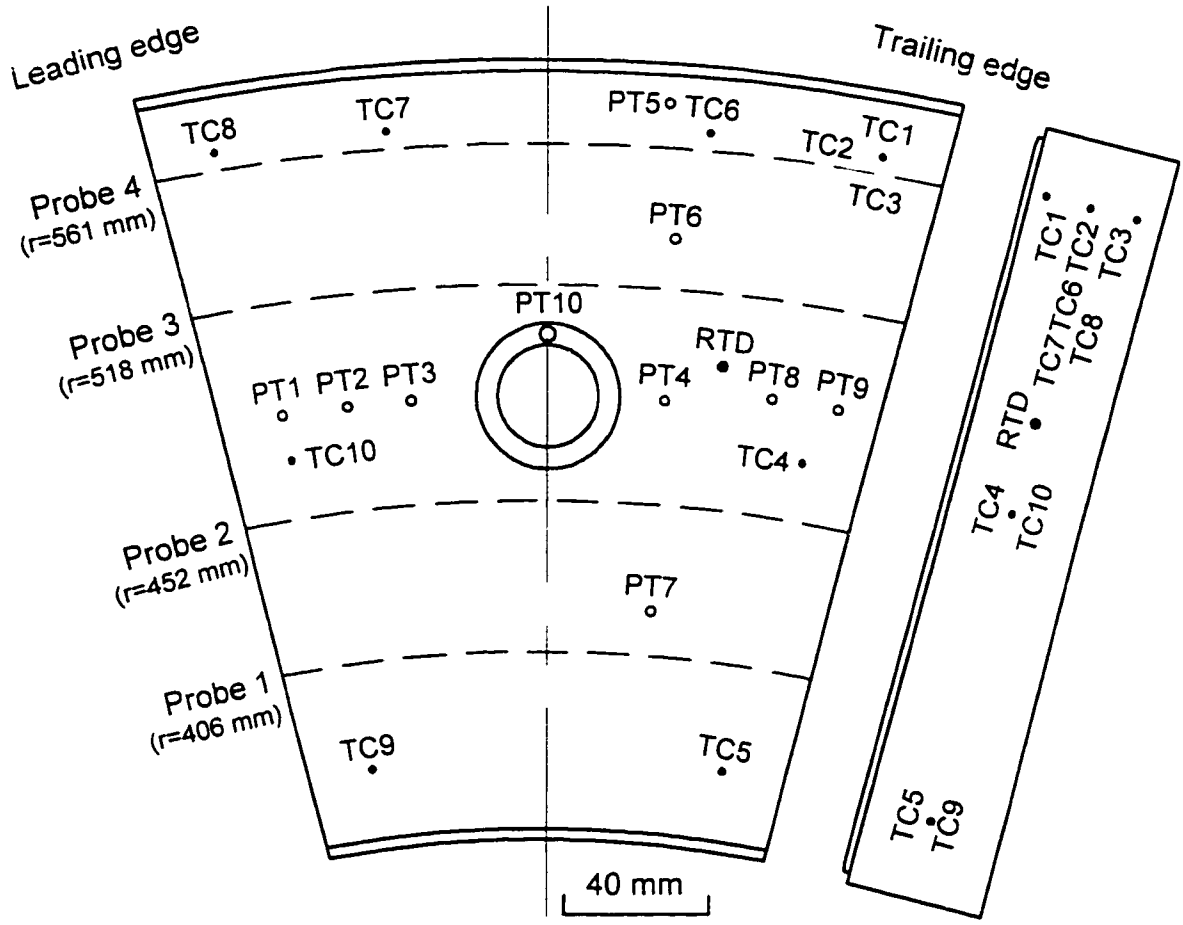

Figure 4.11. Location of all instrumentation

(pad thickness of 41.2 mm)

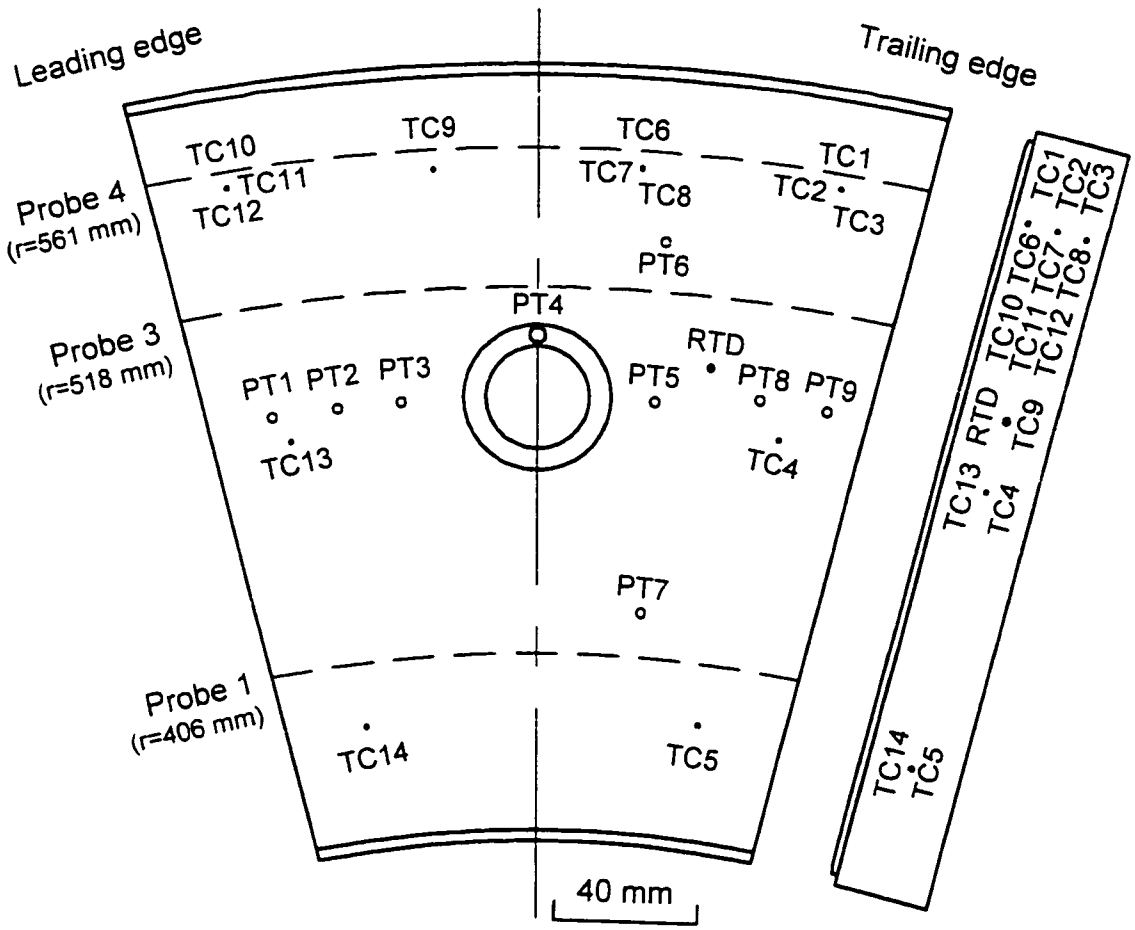

Figure 4.12. Location of all instrumentation

(pad thickness of 30.2 mm)

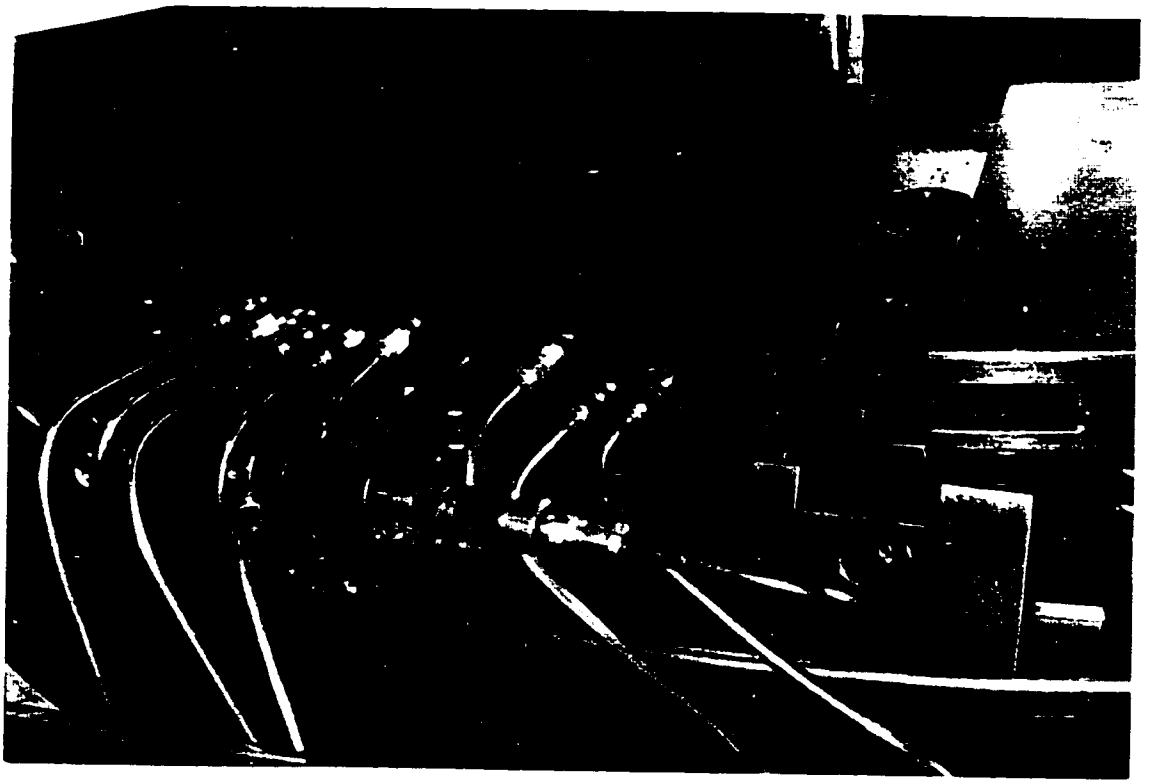

Figure 4.13. Photograph of the pressure taps

Pad no. 10 with pad thickness of 41.2 mm had 10 pressure taps (PT1, PT2, ... PT10) in its surface (Figure 4.11). Pad no. 10 with pad thickness of 30.2 mm had 9 pressure taps in its surface (Figure 4.12). Basically, pressure profiles from the inner edge to the outer edge and from the leading edge to the trailing edge could be obtained from these pressure taps.

4.2.3 Oil Film Thickness Measurement

To measure film thickness, capacitance or inductive methods have been suggested for hydrodynamic bearings with metallic surfaces. Both methods have advantages and disadvantages as discussed by Ettles (1968). For the inductive methods, Ettles recommends calibration *in situ* because the large variations of permeability found with ferrous materials and the difficulty in predicting the response using theory. In the present study, an inductive method was chosen. Five displacement probes of the eddy current type (made by DYMAC, a Scientific Atlanta Inc. subsidiary, San Diego, California, USA) were used to measure the oil film thickness between the rotating ring and the thrust bearing pads. This type of probe was developed originally for more general use in rotating and reciprocation machinery to sense distance between the probe tip and an electrically conductive surface. Similar probes were apparently used by Kawaike *et al* (1977) and Tanaka *et al* (1985).

Four displacement probes were placed in the rotor (Figure 4.14) to measure the oil film thickness between the rotating ring and the thrust bearing pads. The probes were mounted vertically in holes of 19 mm diameter just beneath the rotating ring surface (0.2 - 0.5 mm), and epoxy was used as a grouting agent. Tanaka *et al* (1985) also had displacement probes in the rotor. As the rotor turned, the probes passed over each of the thrust bearing pads in turn (path shown in Figure 4.11 and Figure 4.12). To obtain output from the probes, four signal wires and two input wires ran down the inside of the shaft to a slip ring located on the stub shaft as shown previously in Figure 4.1. The slip ring allowed a transfer of electrical signals between rotating and stationary components. An additional Probe no. 5 was located in the pad towards the leading edge (Figure 4.15) and

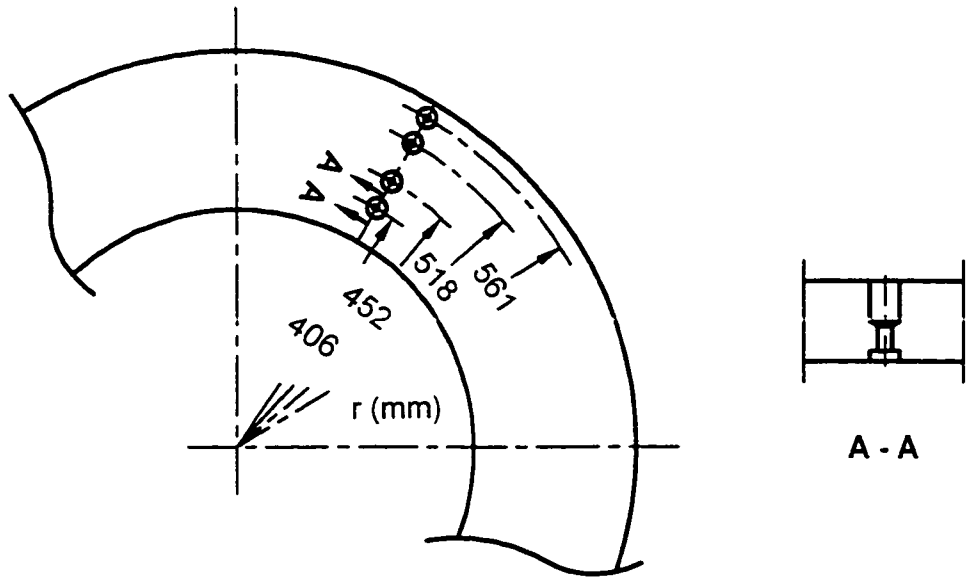

Figure 4.14. Locations of displacement probes in the rotor for measuring film thickness

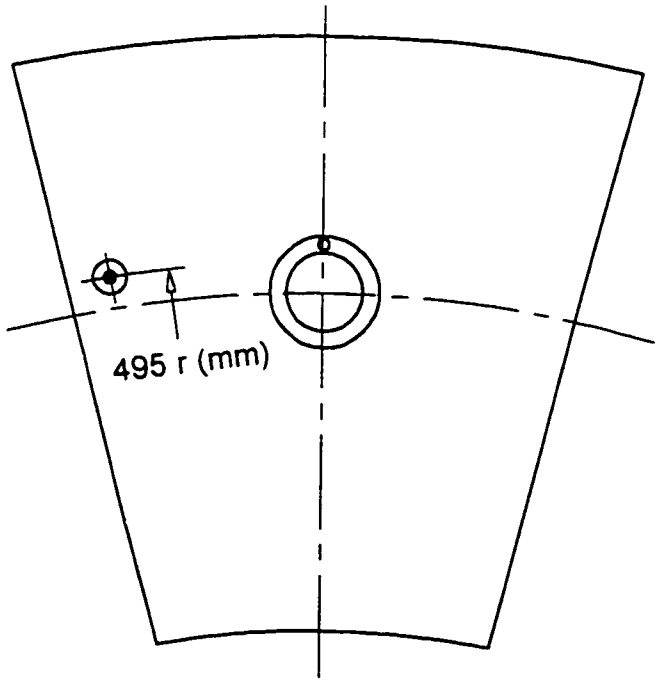

Figure 4.15. Location of probe no. 5 (in thrust bearing pad)

provided a reference datum on that spot. Before running experiments, the displacement probes were calibrated at room temperature with the rotor stationary, as discussed in a subsequent chapter.

The dynamic output signals were measured by a rapid response oscillographic chart recorder (Figure 4.16), made by Honeywell (Fort Washington, Pennsylvania, USA) or a SD390 dynamic signal analyzer (Figure 4.17), made by Scientific Atlanta Inc. (San Diego, California, USA). The "*analogue recorder*" was a multi-channel instrument which obtained and displayed the dynamic signals from the displacement probes process on light sensitive paper in a sequential manner thus introducing a small delay into the acquisition. The "*digital analyzer*", a sophisticated multichannel dynamic analysis system (Microsoft windows based), allowed virtually instantaneous acquisition, analysis and display of wave-form signals, along with post-processing of acquired data. The probe output voltages were recorded by the digital analyzer, converted to displacement values using the slope from the calibration procedures. A more detailed discussion of the probe calibration and data treatment is given in next chapter. Both voltages and displacements were displayed on the screen and stored in data file. The hard copy was available through the printer connected to the analyzer.

4.3 Concluding Remarks

The laboratory test facility provided the capability of measuring pad temperatures, film pressures and film thicknesses in a relatively large thrust bearing. This experimental data characterized thrust bearing performance and was used in subsequent comparisons with numerical analysis.

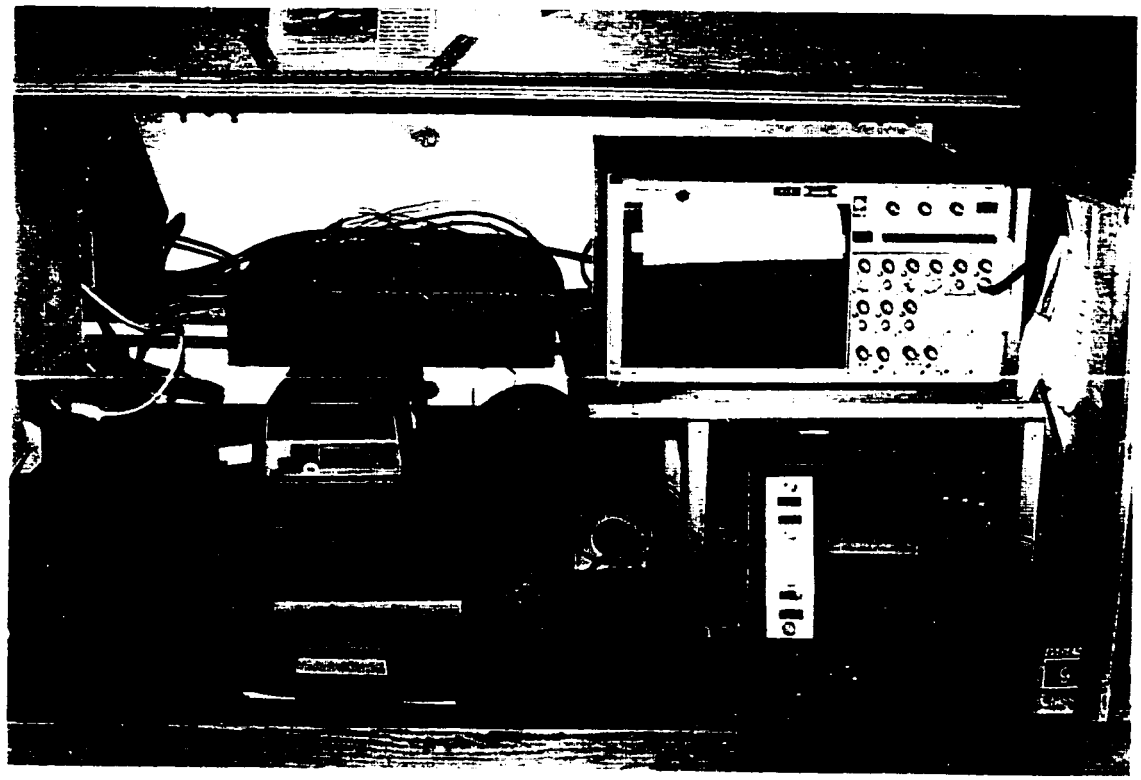

Figure 4.16. Rapid response oscillographic chart recorder

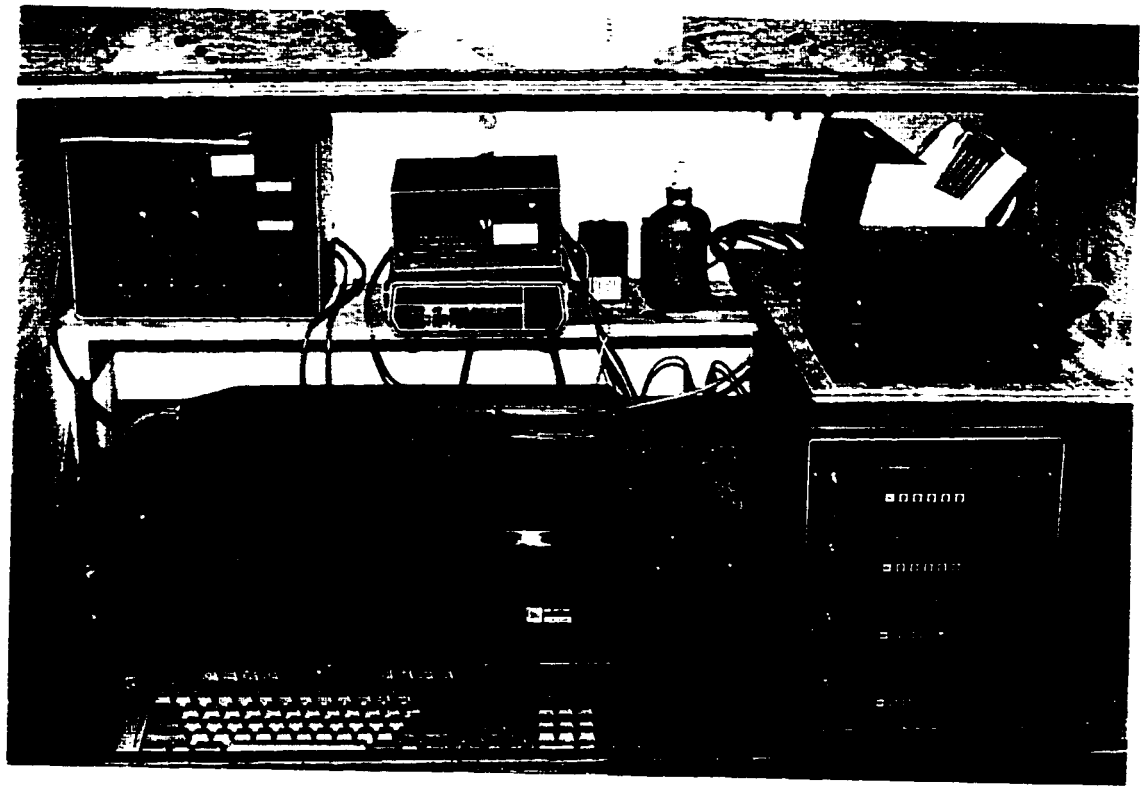

Figure 4.17. SD390 dynamic signal analyzer

Chapter 5

Experimental Methods

Before running the experiments, the displacement probes that were mounted in the test bearing were calibrated. Then, preliminary tests were carried out to check the performance of the test facility as a whole, including the instrumentation and the loading system. Finally, the experimental procedure was established and data collection could begin.

5.1 Displacement Probe Calibration

As described previously in Chapter 4, the oil film thickness between the thrust bearing pads and the rotor was measured by eddy current displacement probes, four of which were mounted in the rotor and one mounted in pad number 2. According to the technical specifications, an individual probe at a particular temperature had a linear relationship between output voltage and distance from the tip to the opposing bearing surface. However, the output voltage level increased with increasing temperature and each probe was likely to have a somewhat different voltage-distance-temperature relationship. Thus, a calibration procedure was conducted on each of the probes after they were mounted in

the apparatus. This calibration established a slope for the linear voltage-distance relationship for each probe over the distance range it would encounter in subsequent experiments. The calibration was performed at room temperature because the rotor had to be raised and lowered repeatedly to place shims of various thickness between the surfaces and thus maintaining any other temperature would have been very difficult.

The effective use of the *in situ*, room temperature calibration slopes depended on four important factors:

1. The voltage-distance data had to indicate a linear relationship over the relevant distance range. This factor had to be judged upon examining the calibration data collected and considering the uncertainty levels of the data.

2. During the actual test runs, an accurate procedure had to be developed to obtain the voltage corresponding to zero film thickness at the operating temperature of the probe. Efforts were made to achieve this objective, as discussed subsequently. The extent to which temperature influenced the output voltage of the probe was examined in a laboratory investigation described in a later chapter.

3. The slope of the voltage-distance calibration curve had to be independent of temperature. Initially, this independence was assumed but the slope behaviour with temperature was examined in a laboratory investigation described in a later chapter.

4. The output voltage of the probe had to be independent of the film pressure. Initially, this was assumed but the influence of pressure on voltage levels was examined in a laboratory investigation described in a later chapter.

5.1.1 Detailed Procedures

Shims of various thicknesses (25.4, 50.8, 127.0 μm) were used by themselves or in combination for the calibration. Before the calibration was performed, the oil pot was drained and the drive motor on the top of the apparatus was removed by an overhead crane. Then, the rotor was lifted vertically by the overhead crane to permit access to the pad surfaces. Two shims (or groups of shims) were placed in a radial orientation on pad no. 11 so that the rotor could be lowered down with the probes located between the shims, and additional shims of the same thickness were placed on pad no.'s 2, 3, and 7 (Figure 5.1). Having a shim (or group of shims) on pad no. 2, allowed its probe to be calibrated along with the probes in the rotor. The additional shims were intended to keep the rotor surface parallel to the pad surfaces although this was unlikely to be totally effective since the resting heights and inclinations varied somewhat from pad to pad. Thus, to ensure that all shims were in contact with the rotor, loads were applied through the hydraulic piston of the load system by applying various pressures with a hand pump. The pressure of the hand pump was increased until the probe output voltages remained constant for a given set of shims. The influence of load on probe output voltage was significant, especially when distances were low and there was a hysteresis involved with loading and unloading (Figure 5.2). The calibration procedure evolved to the following steps.

1. The rotor was lowered onto the pads with zero separation (without any shims in place) so that the probes in the rotor were located over pad no. 11 at the position shown in Figure. 5.1 and the probe output voltages were recorded. Hand pump pressure was increased through 0.689, 1.379, 2.068, 2.758, and 3.447 MPa which corresponded to loads of 0.366, 0.732, 1.098, 1.464 and 1.830 MN on the bearing (or specific loads of 100, 200, 300, 400, 500 psi) until probe output voltage was the same for successive loads* (see footnote on Page 84).

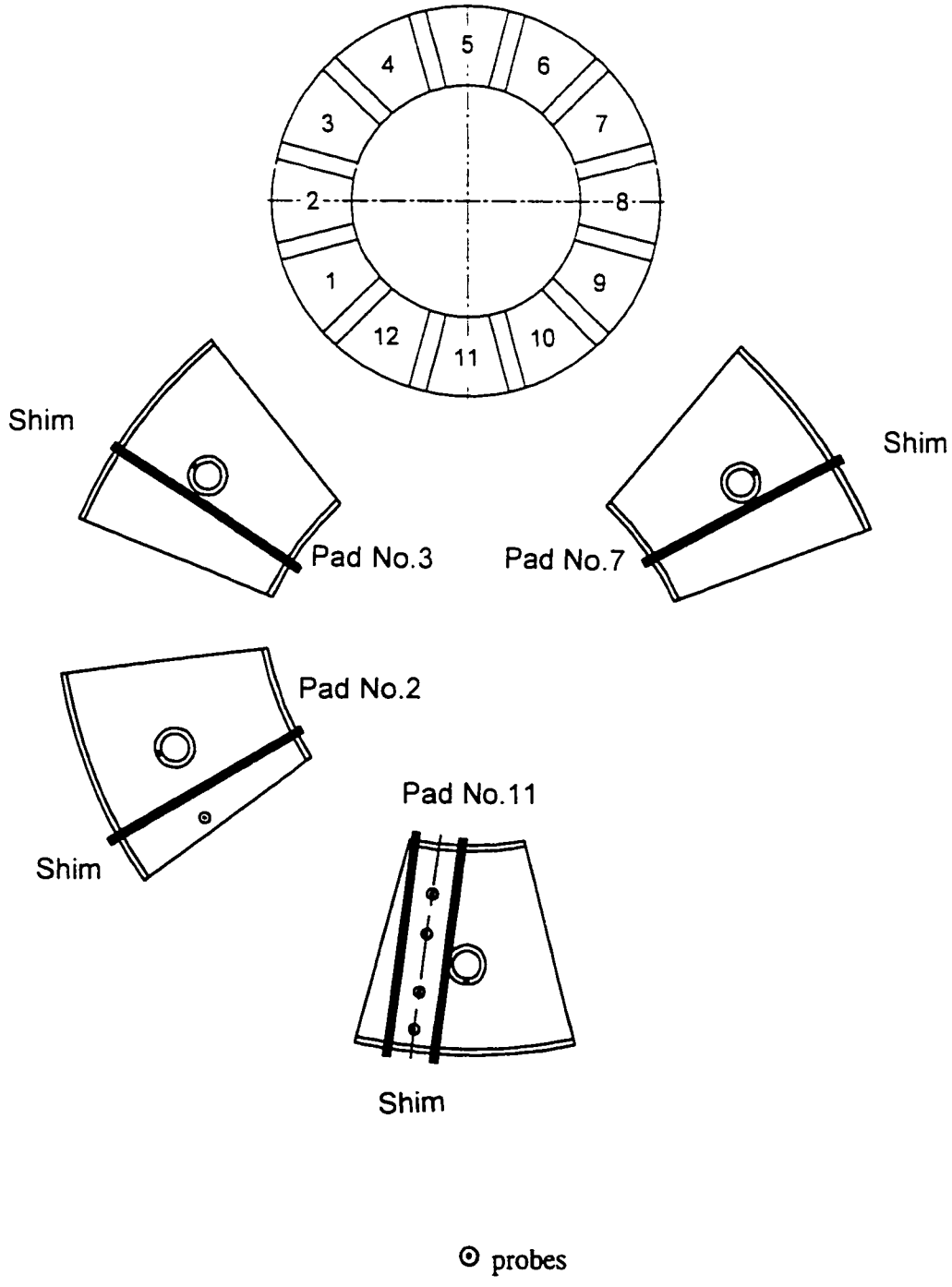

Figure 5.1. The placement of the shims during room temperature calibration

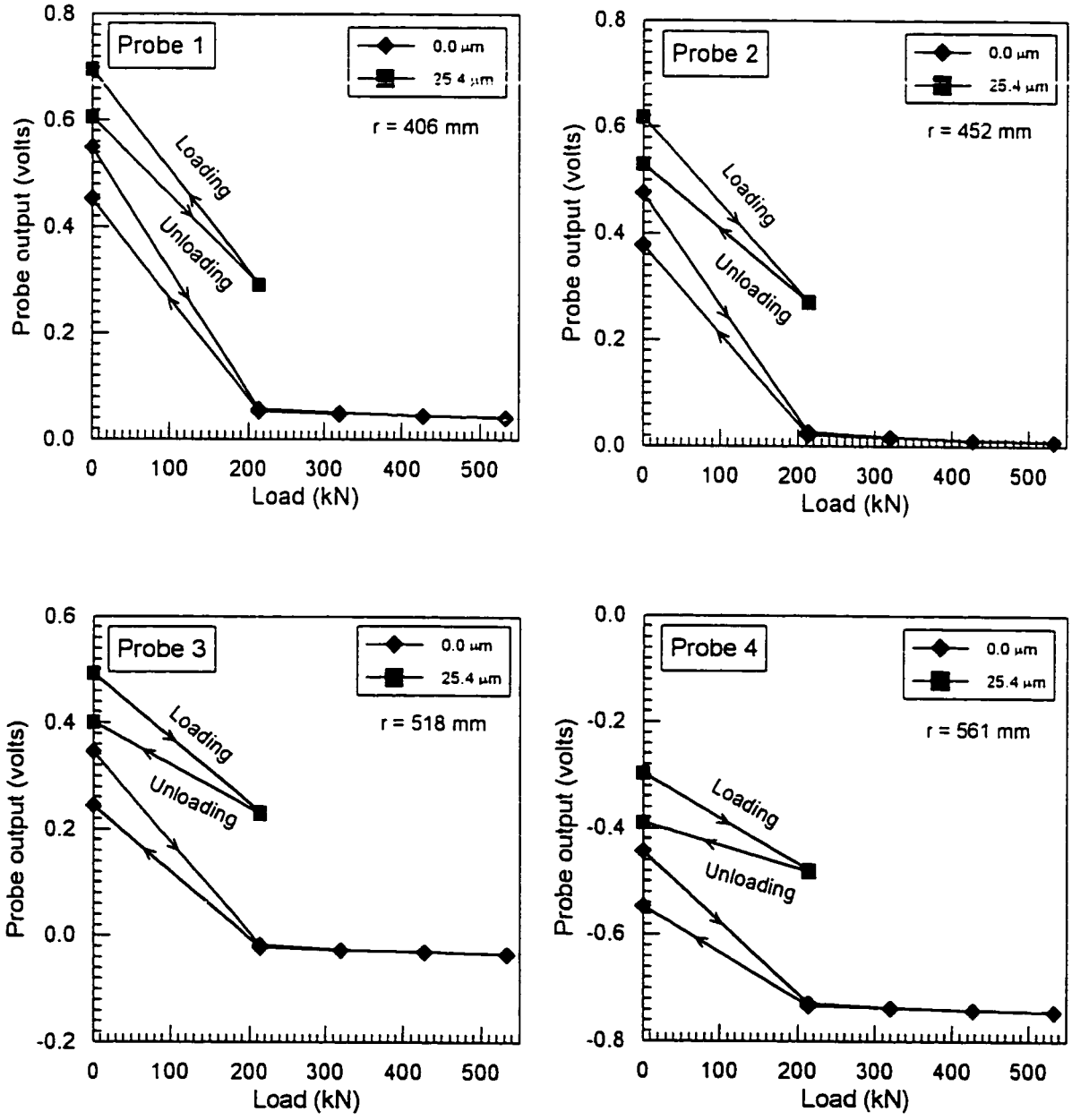

Figure 5.2. Influence of load on probe output voltage

2. The rotor was lifted and shims of 25.4 μm (1 mil) thickness were placed as shown in Figure 5.1 and the probe output voltages were recorded. Loads were increased through the same sequence as in Step 1 until probe output voltages were the same for successive loads*. Usually, this occurred at a lower load that in step 1.

3. Step 2 was repeated for various combinations of shims so that the separations between rotor and pad were 50.8, 76.2, 101.6, 127.0, 254.0, 381.0, 508.0, 635.0 and 762.0 μm (which corresponded to 2, 3, 4,5 10, 15, 20, 25 and 30 mils).

4. Step 1 was repeated to check the voltage at zero separation.

5.1.2 The Calibration Curves

The calibration curves for probes 1 to 4 were obtained by a linear least square fit of the data obtained from calibration procedure (Figure 5.3). These probes were in the rotor at an estimated depth of approximate 130 μm and faced the Babbitt surface of the pad.

A similar calibration curve was obtained for probe 5 (Figure 5.4) which was buried in the pad (pad no. 2) at a depth of about 635 μm and faced the steel surface of the rotor. The slope of calibration curve was much less than those for probes 1 to 4 because it was further away from the opposing surface. Also, having steel rather than Babbitt as a target surface might have had some influence on the slope along with the fact that each probe seemed to have a slightly different behaviour.

---

* The actual experiments were performed over several days and started before the load influence was realized. Consequently, Steps 1 - 4 were performed at each of the load imposed by the hand pump rather than the more time efficient procedure of increasing the load for a given set of shims. If the calibration were to be repeated, the method provided would be employed.

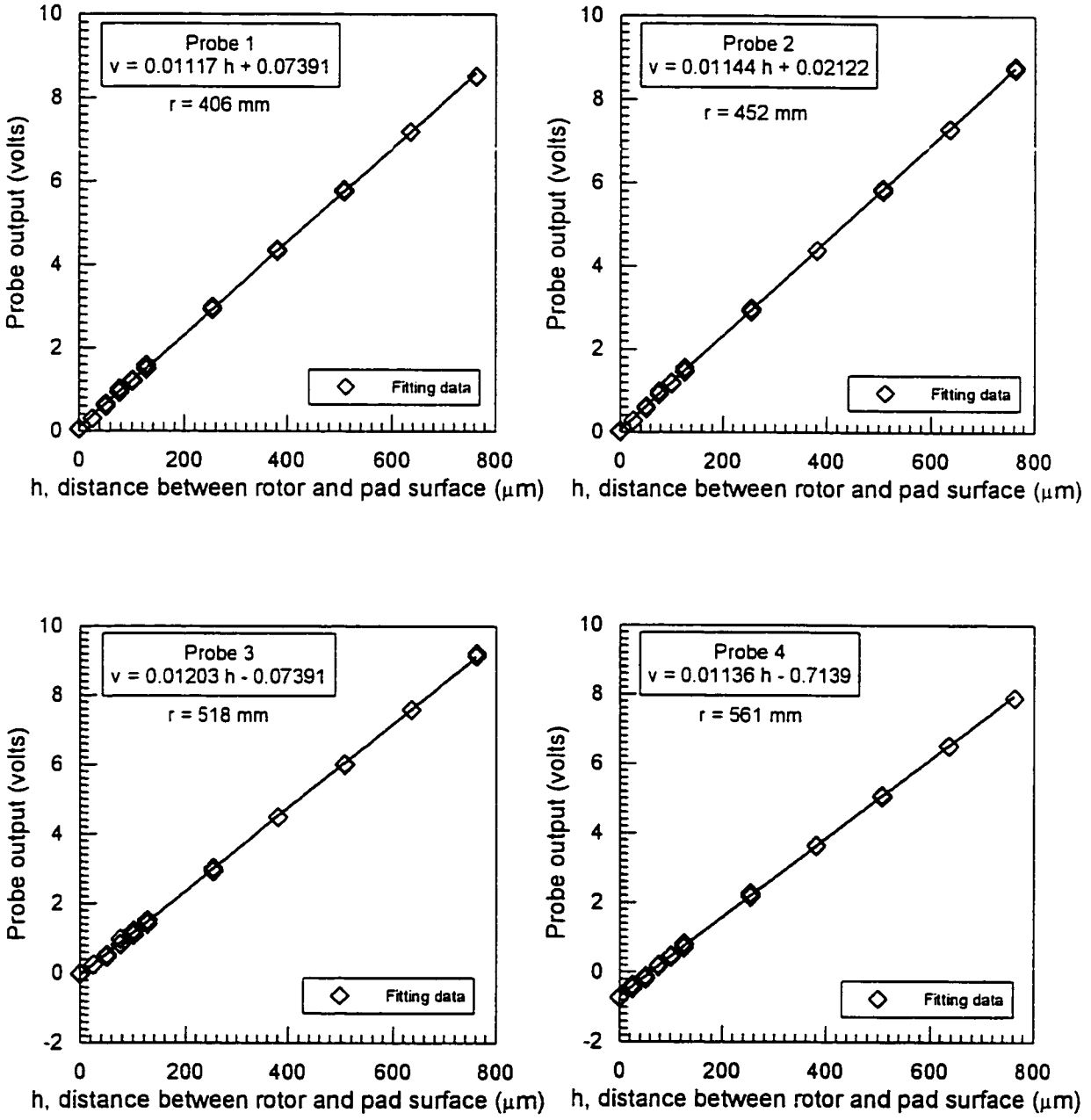

Figure 5.3. The room temperature calibration of probes 1 - 4

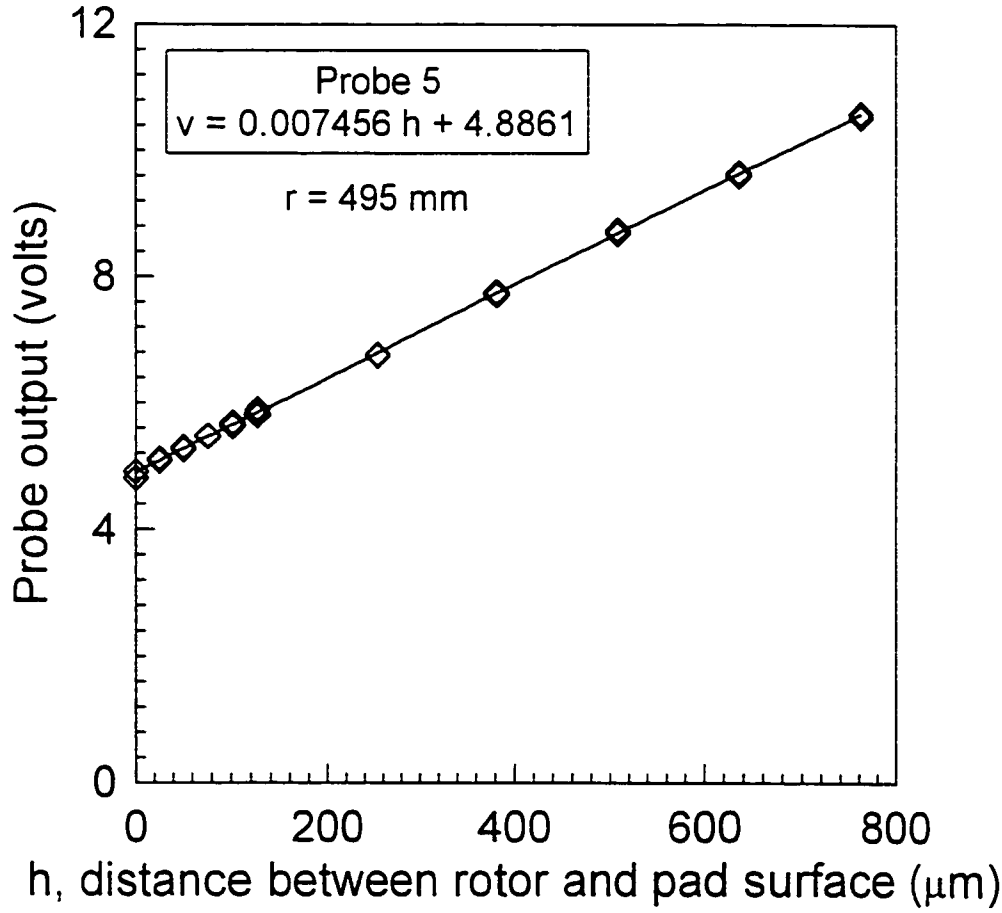

Figure 5.4. The room temperature calibration of probe 5

The room temperature calibration curves were as follows:

$$\textit{Probe 1:} \quad v = 0.01130\,h + 0.07391 \tag{5.1}$$

$$\textit{Probe 2:} \quad v = 0.01144\,h + 0.02881 \tag{5.2}$$

$$\textit{Probe 3:} \quad v = 0.01203\,h - 0.07599 \tag{5.3}$$

$$\textit{Probe 4:} \quad v = 0.01142\,h - 0.7139 \tag{5.4}$$

$$\textit{Probe 5:} \quad v = 0.007456\,h + 4.8861 \tag{5.5}$$

where

v = probe output voltage (v), h = distance between rotor and pad surface (μm)

During operation of the apparatus, h was equivalent to the oil film thickness.

The data acquisition system used the slopes of these curves to convert voltages to film thicknesses. The intercepts were eliminated by rapidly stopping the test and recording a voltage corresponding to zero voltage. However, because the test facility ran at high temperatures (about 84 °C), the room temperature slope over-estimated the actual slope thus giving a smaller film thickness (when measured voltage drop was divided by the slope) than really occurred. The extent of this error is discussed in subsequent sections of the present thesis. During the experiments, the experimental apparatus needed to be dismantled a number of times for modifications. During subsequent re-assembly, the calibration curves were checked before starting to make sure they had not changed.

5.2 Performance Checks

Some tests were conducted to check the performance of the experimental apparatus. The "static" tests were conducted when the rotor was stationary while a "dynamic" test was conducted when it was in motion. The dynamic test was performed under steady state conditions in which the temperature variation over time was minimal. In these tests, a variation of 0.5 °C in 45 minutes at 50 °C was considered acceptable. The tests were performed on all thrust bearings (Figure 4.7) which were to be tested.

5.2.1 Static Tests

The static tests were conducted periodically throughout the test program. Many of the static tests involved the loading system which could function when the rotor was stationary.

Hydraulic Piston and Hand Pump for the Load System

The spacing between the lower end of the load ring and the hydraulic piston (Figure 5.1) was measured to be sure that it did not exceed 12.7 mm at 4.5 MPa. If it did, the bearing would be forced against the clips which were used to support it during installation.

The hand pump was used to apply a pressure to the hydraulic piston which in turn applied load to the test bearing (Figure 5.1). To check the seals in the hydraulic piston-cylinder arrangements the pressure was applied and left for 30 minutes. If the pressure did not drop, the test was passed.

Hydrostatic System for the Test Bearing

Another hydraulic pump, rated 1.1 kW, injected an oil film between the rotating ring of the rotor and the thrust bearing pads during start-up and shut-down. To check this system, a mechanical (dial) gauge was used to measure how high the rotor was lifted. The test was passed if the rotor was lifted 120 μm. Blocked orifices or other faults in the system were expected to reduce this characteristic value and thus a problem with the system would be indicated.

Next, the hydraulic pump was shut off suddenly and if the solenoid valve closed to maintain pressure in the oil groove, this test was passed. In yet another test, an attempt was made to start the motor that drove the rotor without turning on the hydraulic pump for the hydrostatic system of the test bearing. An automatic switch was supposed to act to prevent the motor from starting. Thus, the inability to start the motor was considered a successful result for this test.

5.2.2 Dynamic Test

The dynamic test was performed when the motor was in motion as a check on faults that may not show up in static testing. The vertical and radial variations in rotor position (or runout) were measured using a mechanical (dial) gauge when running at 21 rad/s (200 rpm) under various loads. To pass this test, both positional variations or "runout" of the rotor had to be small (less than 2.54 mm) and independent of speed. Also, significant vertical runout should only be present when the load system was turned off. Furthermore, radial runout had to be constant after 21 rad/s (200 rpm) and independent of load. Compliance with all of these requirements was needed to pass the dynamic test.

One further requirement was needed to pass the dynamic test. The hydraulic pump was rated at 37.3 kW and produced a flow rate of 1.137×10^{-3} m^3/s (15 gal/min) to maintain an oil film between the hydrostatic bearing surface and the load ring. The safe working condition was determined by continuous temperature measurements from an RTD located just below the stationary hydrostatic bearing surface. Compliance consisted of the temperature never exceeding a specified alarm value throughout the dynamic test.

5.3 Protocols for the Main Experiments

Performance checks and some preliminary tests were used to ensure that the apparatus was ready for service. Protocols were developed to guide the actual experiments. The present section describes these protocols, including those related to oil film thickness measurement.

Experimental data values were collected when the apparatus was running under steady state conditions, which meant that the temperature variation over time was minimal. These data values included:

- motor speed, current and voltage
- load piston pressure
- water flow rate through the heat exchangers in the oil pot

- pressure in the film and groove
- temperature in pad and groove along with rotor temperatures at shut-down
- oil film thickness, including the zero value at shut-down
- qualitative observations of the drain hole flow rate in the guide bearing segment and the depth of oil behind the guide bearing

The protocols involved in obtaining the data were organized under three headings: start up, running and shut-down.

5.3.1 Start up

1. Before turning the power on, the whole apparatus was inspected visually for abnormalities. This included checking the oil level in the pot and in the tank of the pump for hydrostatic bearing in the load system.

2. When the analogue recorder was used, the slopes of the calibration curves (see Section 5.1.3) were input. For 0.2 volts per division, 25.4 mm (1 inch) on the analogue recorder display corresponded to 25.4 μm (1 mil). When the digital analyzer was used, the calibration equation slopes were input and a frequency of data point collection of 1000 times the rotor speed was set.

3. A sequence of switches was closed to supply power to the various electrical components.

4. The pump for the hydrostatic system of the test bearing was turned on along with the pump for the hydrostatic bearing of the load system. The speed controller for the drive motor was set to 10.5 rad/s (100 rpm) and the motor slowly came up to that speed. Once 10.5 rad/s was reached the pump for the hydrostatic system of the test bearing was turned off. The motor speed was then increased, usually to 21 rad/s (200 rpm).

5. The required load was gradually applied using the hand pump. As the hand pump pressure was increased, the motor current was kept below 575 A to avoid overheating damage. This was achieved by simply letting the apparatus run at a particular load until oil temperature increased, viscosity dropped and the motor current dropped in response to lower power losses in the bearing.

6. Once the required load was reached, the speed was increased to the desired value. As before, the motor current was monitored and kept below 575 A and thus there was a limit to the motor speed for a specific values of load and oil viscosity.

7. The cooling water for the pump of the hydrostatic bearing in the load system was turned on along with the cooling water for the heat exchangers in the oil pot. The flow rate of the water supplied to the heat exchangers in the oil pot was adjusted until the desired oil pot temperature was achieved. Once again, the motor current had to stay below 575 A and thus there was a limit to how low an oil pot temperature could be obtained. Steady state was achieved when oil pot temperatures measurements, taken 45 minutes apart, had a variation less than 0.5°C.

5.3.2 Running

8. Temperatures from thermocouples and RTD's were recorded along with all pressure gauge values. If the analogue recorder was used, the oil film thickness curves on the light-sensitive paper were obtained at a suitable paper speed to give clarity and with a length of paper sufficient to record at least one sweep of the oil film thickness for each pad. If the digital analyzer was used, digital data files were recorded automatically at the specified frequency and stored on disc.

9. Occasionally, the above data collection step was repeated to check for consistency.

5.3.3 Shut-down

10. The pump for the hydrostatic system of the test bearing was turned on. The cooling water to the heat exchangers of the oil pot and to the pump for the hydrostatic bearing of the load system was turned off and the load was removed by releasing the hand pump pressure. Then, the motor was turned off and the rotor positioned so that the probes were over pad number 11 (shown in Figure 5.1).

11. The pump for the hydrostatic system of the test bearing was turned off. A specific load of 1.13 MPa was applied by setting an output pressure of 3.45 MPa (500 psi) on the hand pump and the voltage outputs of the displacement probes (for measuring the film thickness) were evaluated by an *analogue recorder* or a *digital analyzer*. This voltage output was meant to correspond to a film thickness of zero at the operating temperature of the probes and thus the entire shut-down protocol had to be performed as fast as possible to avoid significant temperature changes which were known to influence output voltages (as described in a later chapter). While it needed less than 2 minutes to stop the rotor and place it in the data collecting position, it took another 2 minutes or so to collect the displacement data using the *analogue recorder* compared with the *digital analyzer*. This additional time was required because of the sequential procedure of data collection as mentioned previously in Chapter 4.

12. The rotor temperatures were then recorded by reading a Voltmeter that was connected to the various thermocouples in the thrust block and rotating ring.

13. Finally, the hand pump pressure was released and all power input was turned off.

5.4 Concluding Remarks

The calibration of the displacement probes, the performance checks before running experiments and the detailed experimental protocols were described in this chapter. The application of the displacement probes to measure oil film thickness in large thrust bearings was complex and a separate laboratory apparatus has been developed to explore the characteristics of the displacement probes as described in a subsequent chapter. It has been shown that both voltage level and slope were influenced by the temperature of the probe.

Thus, using a slope obtained at room temperature rather than the actual temperature at which they were subjected to in the testing, introduces some error into the measurements. In addition, the voltage determined at zero film thickness might not have been measured at the same temperatures as during testing. Further discussion of the uncertainty in the measurement of absolute values of film thickness is discussed in subsequent chapters.

Chapter 6

Comparison of Numerical Predictions With Experimental Data for Two Bearing Configurations

Over the last three years, many bearing configurations were studied with various operating conditions, spring set arrangements and pad thicknesses. In addition, both an analogue recorder (Figure 4.16) and a digital analyzer (Figure 4.17) were employed to obtain the output voltages from the displacement probes. The choice of these data acquisition devices influenced the accuracy of the film thickness measurements. For the present research, the capacity to examine bearing behaviour theoretically with numerical analysis has been discussed in Chapter 3 while the capacity to examine bearing behaviour experimentally has been discussed in Chapter 4 and Chapter 5. A comparison of theoretical predictions with experimental data would permit some assessment of the fidelity with which each approach represented reality. Good agreement between theory and experiment would improve the confidence with which the software package GENMAT could be applied to analysis of existing bearings in hydroelectric generators and design of future bearings.

In the present thesis, comparisons of theory and experiment were made for a large number of bearing configurations. However, in this chapter, a comparison is made for only two typical bearing configurations (or "cases") with the intent of addressing in detail the many specific and common issues arising from the comparison of theory with experiment.

The two cases were chosen carefully to have as many different features as possible in the experiments. They had differences in pad thickness, number of springs (and thus spring arrangement), oil grade and rotational speed. The analogue recorder was used in one case, the *digital analyzer* was used in the other.

6.1 Geometry and Operating Conditions

As mentioned above, two cases were examined. The bearing geometry (Table 1), operating conditions (Table 2) and oil properties (Table 3) were different for the two cases. Case 1 had higher rotational speed, thicker pads, an oil of higher ISO viscosity grade and a larger number of springs than Case 2. Also, the spring arrangements were different for Case 1 (Figure 4.7a) and for Case 2 (Figure 4.7c).

Thrust Bearing Feature	Case 1	Case 2
Outer diameter (m)	1.168	1.168
Inner diameter (m)	0.711	0.711
Overall thickness (mm)	41.1	30.2
Groove width (mm)	52.3	52.3
Number of Pads	12	12
Number of Springs	15	12

Table 6.1. Thrust Bearing Geometry

Conditions	Case 1	Case 2
Lubricant ISO grade	46	32
Load per pad (kN)	177	177
Rotational speed (rad/s)	52.4	31.4
Oil pot temperature (°C)	70	70

Table 6.2. Operating conditions

Parameter	Case 1	Case 2
ISO* viscosity grade	46	32
ν (cSt) at 40°C	48.0	33.5
ν (cSt) at 100°C	6.70	5.45
ρ (g/ml) at 15°C	0.873	0.868

*International Standards Organization

Table 6.3. Oil properties

A cylindrical coordinate system (Figure 6.1) was defined to permit the plotting of both numerical predictions and experimental data. As discussed in Chapter 4, pressure taps (PT's) were located in one pad whereas thermocouples (TC's) and resistance temperature detectors (RTD's) were located on another. Scaled drawings were composed which gave the exact location of the instrumentation on a single pad for Case 1 (Figure 4.11) and for Case 2 (Figure 4.12). Four displacement probes for measuring film thickness were employed in Case 1 but some malfunction occurred with Probe 2 and thus only the remaining three displacement probes were employed in Case 2. In case 1, TC's were distributed through the thickness of the pad at one r-θ location whereas in Case 2, TC's were distributed through the thickness of the pad at three r-θ locations. Also, Case 1 had an extra pressure tap at the outer edge compared with Case 2 (Figure 4.11 and Figure 4.12).

6.2 Influence of Load on Pad-to-Pad variation in Film Thickness

The pads were mounted at nominally the same height on assembly of the bearing. However, small variations in the mounted heights occurred and thus a slightly higher pad would carry somewhat more load. The pre-loaded springs exacerbated this problem by preventing a higher pad from being pushed down (to allow lower pads to carry load) until the pre-load values were exceeded. Thus, it might be expected that at lower values of the total load applied to the bearing, there would be some variation in the load per pad. This situation had significant implications on comparisons between numerical predictions and experimental data.

The numerical analysis in the GENMAT software package assumed that all pads were the same and carried the same load. The experimental strategy made the same assumption by not having any instrumentation specifically for the measurement of the load on each pad. Furthermore, in placing temperature and pressure instrumentation on different pads and conducting the displacement probe calibration on another pad, the tacit assumption was made that all pads carried the same load. If they did not, the measured values of film thickness, temperature and pressure distributions would not be for the same load conditions and could not be related directly to each other or to the numerical predictions of the GENMAT software package.

Fortunately, the displacement probes swept over all of the pads in the thrust bearing and recorded a voltage that was related to the film thickness. This allowed a check on pad-to-pad variation in film thickness. If this variation were small, the load on each pad would be the same. Checking this behaviour was an essential first step in comparing numerical predictions with experimental data.

The load per pad value of 177 kN quoted in Table 6.2 corresponded to a total load of 2.124 MN. Some preliminary tests were performed with the lower total loads of 1.334 MN and 1.728 MN . Following the procedures outlined in Chapter 5, the film thickness was measured for each pad by Probe 1 using the analogue recorder at an r-θ location of (0.406m, 3.94°) which was the inside trailing edge portion of the pad. In contrast to the

lower total loads, the pad-to-pad variations in the measured film thickness values were quite small at the highest total load of 2.124 MN (Table 6.3) which was used in cases 1 and 2.

	Total Applied Load (MN)		
	1.334	1.728	2.124
Pad No.	Film Thickness (μm)		
1	18.5	17.6	15.5
2	26.0	21.9	16.0
3	23.5	20.5	17.0
4	21.0	18.5	17.0
5	25.5	23.0	15.0
6	28.0	23.5	16.2
7	23.2	21.5	15.5
8	26.5	22.0	15.7
9	25.4	21.7	17.0
10	23.0	23.0	18.0
11	25.5	26.0	16.2
12	24.5	22.8	17.5
Avg.	24.2	21.8	16.4
Std. Dev.	2.48	2.14	0.87

Table 6.4. Oil film thickness measured by Probe 1 at the r-θ location of (0.406m, +3.94°)

The low pad-to-pad variation was also illustrated with the data collected by the digital analyzer (Figure 6.2). When the GENMAT software package was applied with the same loads as in Table 6.3 (assuming that the load per pad was uniform), the majority of the springs were loaded beyond their pre-load values only for the highest load of 2.124 MN. Thus, it seemed plausible to suggest that once total loads were high enough to ensure that most of the springs were loaded beyond their pre-load, the original height differences between the pads had a minimal effect on the load per pad variation. At any

rate, for the loads used in cases 1 and 2, the pad-to-pad variation was very small and the numerical predictions of the GENMAT software package could be compared with the measured film thickness, temperature and pressure values with the assurance that essentially the same load per pad acted in the numerical analysis and for all of the measured values. However, a comparison of numerical predictions with experimental data was still performed for the lower total loads, as presented in a subsequent chapter along with further discussion.

6.3 Results and Discussion

The two cases are presented separately to reinforce the inter-dependence of the film thickness, temperature and pressure data for each case. The nature of the agreement between film thickness predicted by the software package of Ettles (1991) and that measured in the experiments, should be related to the agreements for temperatures and pressures. The oil properties of ISO 46 and 32 that were used in the software package were taken from a stored data base. Unfortunately, these properties did not correspond exactly to those of the actual oils used, as discussed by Ferguson *et al* (1998) but the influence of this inconsistency on the theoretical predictions was judged to be small.

6.3.1 Case 1

A comparison of the experimental and theoretical film thickness for Case 1 did not show good agreement (Figure 6.3). The film thickness values were determined by a measurement system, which included the analogue recorder. The system had some inherent filtering and further manual filtering from taking average discrete values by hand from the plots on the recorder. The overall precision of the film thickness values was estimated as about ± 4 μm and bars indicating this range have been placed on Figure 6.3. However, the accuracy of the film thickness measurement was probably influenced by a

"fixed" error of unknown magnitude arising from the determination of probe output voltage corresponding to zero film thickness. Attributing this inaccuracy to the experimental measurements rather than the numerical predictions was suggested by the measurement of zero or near zero film thickness values by three of the four displacement probes. Such low values were unlikely without severe surface damage to the test pads which was not observed. While the inaccuracy was linked to the experiments, an actual value for uncertainty in the absolute values of the measured film thickness could not be quantified.

However, it was felt that the pad shape had been measured with quite good fidelity. The comparison of the experimental and theoretical results supported this suggestion except for a tendency of probe 4, which passed over the outer edge of the pads, to give about the same values as the theoretical prediction over the inlet half of the pad whereas the other probes consistently underestimated the film thickness. Perhaps in this instance, the probe measurement should have underestimated film thickness but instead gave an agreement that was fortuitous. The software package might have given a reduced film thickness in this region because of a somewhat inaccurate value of heat transfer coefficients or imprecision in the thermoelastic deflection modelling which just happened to correspond to the experimental results. Although a considerable effort had been made to try to accurately measure and correlate the heat transfer coefficient to various bearing features, it was very difficult to specify accurately since it varied over the pad surfaces and changed with features such as the pad geometry, rotational speed, spring packing and oil viscosity. An empirical formula was used to calculate a heat transfer coefficient in GENMAT and it remained constant over all the pad surfaces where it was needed. Another plausible explanation, that would also produce fortuitous agreement, was the possibility that the runner was crowning slightly (a possibility discussed subsequently in this chapter), thus increasing the actual film thickness just enough to agree with theoretical predictions (which had not included runner crowning).

Although the inaccuracy of the film thickness measurements permitted only qualitative comments regarding the fidelity of the theoretical modelling, the temperature measurements were much more accurate and thus comparisons with theory were

quantitative and meaningful. First, the accuracy of the temperature measurements must be considered. Following Kline and McClintock (1953) a measurement uncertainty value should be given along with a further estimate of the "odds" of finding the true temperatures within this range of the measured values. Thus, it was estimated that the odds were 20 to 1 that the true temperatures were within ± 2°C of the measured values. Although some clarity was introduced by the use of the word "odds", such terminology was considered to suggest a rather cavalier attitude towards the fidelity of the measurements. Thus, in the rest of the present thesis, the quoted ranges (such as ± 2°C) *were referred to as the estimated uncertainty range at the 95% confidence level.* This range included the random errors in the thermocouple devices and the slight random variations in the thermal equilibrium imposed by the test facility. This estimated uncertainty range at the 95% confidence level was based on our experience with the experiments. Occasional repeat tests had been performed and contributed directly to this experience. However, in general, the financial resources were not available to perform the multiple repeat testing necessary for a statistical analysis. Furthermore, such a statistical analysis would be complicated by the difficulty in creating exactly the same experimental conditions in the rather complex experimental facility and was considered unlikely to provide a substantial improvement in the evaluation of the true temperatures. Finally, the introduction section of Kline and McClintock (1953) noted four factors (related to fixed bias of both observers and instrumentation) "which tend to lessen the effect of repetition" on improving the accuracy, thus suggesting that even if such repetition were performed the benefits might not be forthcoming.

Comparison of theoretical with experimental temperatures indicated quite good overall agreement (Figure 6.4). Small differences which did occur between theory and experiment, were considered to be caused by the measurement uncertainty of ± 2°C (slightly larger than the size of a data point in Figure 6.4 and thus too small to be represented graphically) and, to a larger extent, by the likelihood of some inaccuracy in the pad shapes predicted by the software package. The temperature results suggested that the software package might provide a good overall prediction of temperatures in large spring-mounted thrust bearings. The agreement between theoretical and experimental

temperatures in the present study was as good as that found by Ali El-Saie and Fenner (1988b) for a large pivot-supported thrust bearing. Furthermore, the same sort of agreement was found to extend over a wider range of operating conditions in a special study on the influence of oil viscosity on power loss by Ferguson *et al* (1998).

Unfortunately, theory predicted much smaller pressures in the central region of the pad than were measured in the experiments (Figure 6.5). The uncertainty range of the pressure measurements was estimated as ± 0.2 MPa (slightly smaller than the size of a data point in Figure 6.5 and thus not shown graphically) at the 95% confidence level. The small uncertainty range suggested that the fairly large differences between the measured data and the predictions of the software package were attributable to inaccuracies in the theoretical modeling.

One explanation for the seemingly contradictory result of quite good temperature agreement but rather poor pressure agreement was the possibility that temperatures were not influenced so much by film thickness distribution whereas the opposite was true for pressures. If film thickness at the inlet half of the outer edge were larger than predicted by the software package, as suggested previously, then pressures would drop in that region and increase in the centre of the pad in order to carry the imposed load.

6.3.2 Case 2

Somewhat better agreement between theory and experiment was achieved for the film thickness values of Case 2 (Figure 6.6). The scatter in the results was shown clearly because discrete data values were directly plotted from the files generated by the data acquisition system (whereas with the system used for the Case 1 measurements had both internal and manual filtering as mentioned in the previous section). Much of this scatter was caused by electronic noise involved in passing the probe voltages in the moving rotor through slip rings. If a curve was fit through the discrete data from the data acquisition system, the overall precision of this curve was slightly better than that obtained with the system used for case 1. However, without more extensive studies, the overall precision was estimated at ± 4 μm about a fitted cubic polynomial through the discrete data which

was the same as estimated for the system in case 1. For the sake of clarity, the fitted curve of the discrete data are not shown in Figure 6.6, but bars indicating the estimated precision are presented.

Probe 1, in particular, showed good agreement between theory and experiment in both film thickness magnitudes and surface shape. This good agreement was attributed to a better determination of the probe output voltage corresponding to zero film thickness, which was part of the measurement procedure as mentioned earlier in Chapter 5. However, as in case 1, the "fixed" error associated with establishing the voltage at zero film thickness could not be quantified and thus the uncertainty range of the absolute values of measured film thickness could not be specified and the following comments had to be considered qualitative in nature. In any event, a rather strange deviation in the apparent agreement occurred for probe 3 over the trailing half of the pad. The discrepancies in this region might indicate imprecision in the thermoelastic deflection modeling of the software package. The measured film thickness of probe 4 values gave a surface shape similar to that predicted by the software package, but the magnitudes were lower. The lack of agreement might have occurred because of inaccurate output voltages for zero film thickness. It could be further speculated that the lower rotational speed of the rotor and lower overall temperatures might have prevented significant crowning of the rotor, which had been suggested in Case 1 (and which would have tended to increase measured film thickness, thus masking the differences between theory and experiment).

In addition, the experimental results from the data acquisition system tended to drop right at the trailing edge of the pad. In a subsequent laboratory simulation, this drop was found to disappear when the data sampling rate was increased while the rest of the film thickness data remained the same. Thus the low film thickness values at the trailing edge were not considered to represent physical reality.

The same estimated uncertainty ranges at the 95% confidence level as in case 1 were applied to temperatures and pressures in Case 2. As in case 1, the theoretical and experimental temperatures agreed quite well (Figure 6.7) and this agreement was as good as that found by Ali El-Saie and Fenner (1988) and similar to that found by Ferguson *et al* (1998). The experimental pressures were always slightly higher than those predicted by

theory (Figure 6.8), but the differences were not as great as in Case 1, perhaps significant crowning of the rotor did not occur because speeds, oil viscosities and thus film temperatures and temperature gradients were lower than in Case 1. It did seem likely, however, that since measured pressures (which were quite precise as mentioned in the Case 1 discussion) were always slightly higher that theoretical, that the software package was over-estimating pressure (perhaps as a consequence of underestimating film thickness) in some regions in which pressure measurements were not taken.

6.3.3 Some Comments on Agreement Between Theoretical and Experimental Data

For large thrust bearings, no other studies had such extensive comparisons of theoretical and experimental film thickness, temperature and pressure distributions. The agreement between theoretical and experimental results, although not perfect, did provide solid support for the utility of the GENMAT software package in predicting large spring-supported thrust bearing behaviour. In particular, theoretical and experimental temperatures were in quite good agreement. The agreement for pressures was not as good but the theoretical pressure distribution was likely to be very sensitive to slight inaccuracies of the film thickness (and more specifically the pad shape) in theoretical modelling. The fixed error of unknown extent from the determination of the voltage equivalent to zero film thickness made the comparison of theoretical and experimental film thicknesses qualitative in nature. However, theoretical and experimental pad shapes did seem to agree reasonably well.

If the software package was considered to be providing a reasonable representation of physical reality, then detailed contour maps of the film thickness, temperature and pressure distributions for Case 1 and Case 2 were considered instructive (Figure 6.9).

6.4 GENMAT Simulation: Thermal Crowning of the Rotor

The comparison of the pressure on the thrust bearing pad showed that there were large differences between the experiment and the theory, particularly for Case 1. As discussed in the previous section, thermal crowning of the runner might have caused this and the GENMAT software package did not include a feature to simulate the runner thermal deflection. However, it was possible to assume an equivalent pad crowning geometry and input this into the software where it remained as the starting pad shape throughout the various iterations involved in the numerical analysis. In this way, the possible influence of rotor crowning could be investigated in a qualitative manner.

After a number of trials it was found that a symmetric thermal crown in the radial direction of 60 μm could be applied to Case 1 to give numerical predictions of pressures that were very close to those measured experimentally (Figure 6.10). The predicted temperatures remained in close agreement with measurements and the film thickness did not change much (and were apparently still subject to a large fixed error). However, the fact that a plausible rotor crown could be represented in the GENMAT software package and gave good agreement with measured pressures strongly suggested that rotor crowning should be included in future numerical analysis.

6.5 Concluding Remarks

Some quite close agreement occurred between experimental and theoretical film thickness, particularly for Case 2. However, there was a problem with establishing an accurate value for the displacement probe output voltages at zero film thickness which compromised the accuracy of most of the measured film thickness values. Furthermore, some differences between the experimental and theoretical pad shapes occurred that could not be attributed to the problem of establishing the voltage at zero film thickness.

Also, measured pressures were usually higher than those predicted by theory in both of the examined cases. The differences between measured and predicted pressures might have been caused by thermal crowning of the rotor giving thicker films than predicted by theory at the outer edge of the bearing with possible contributions from imprecise thermal boundary conditions or by inaccuracies in the thermoelastic deflection model within the software package.

In contrast, temperature agreement between theory and experiment was quite good for both cases. This agreement made a strong argument in favour of the ability of the GENMAT software package to represent physical reality in general in spite of specific disagreements in the film thickness and pressure values.

Much of this chapter will be published in a journal paper (Yuan et al, 2000).

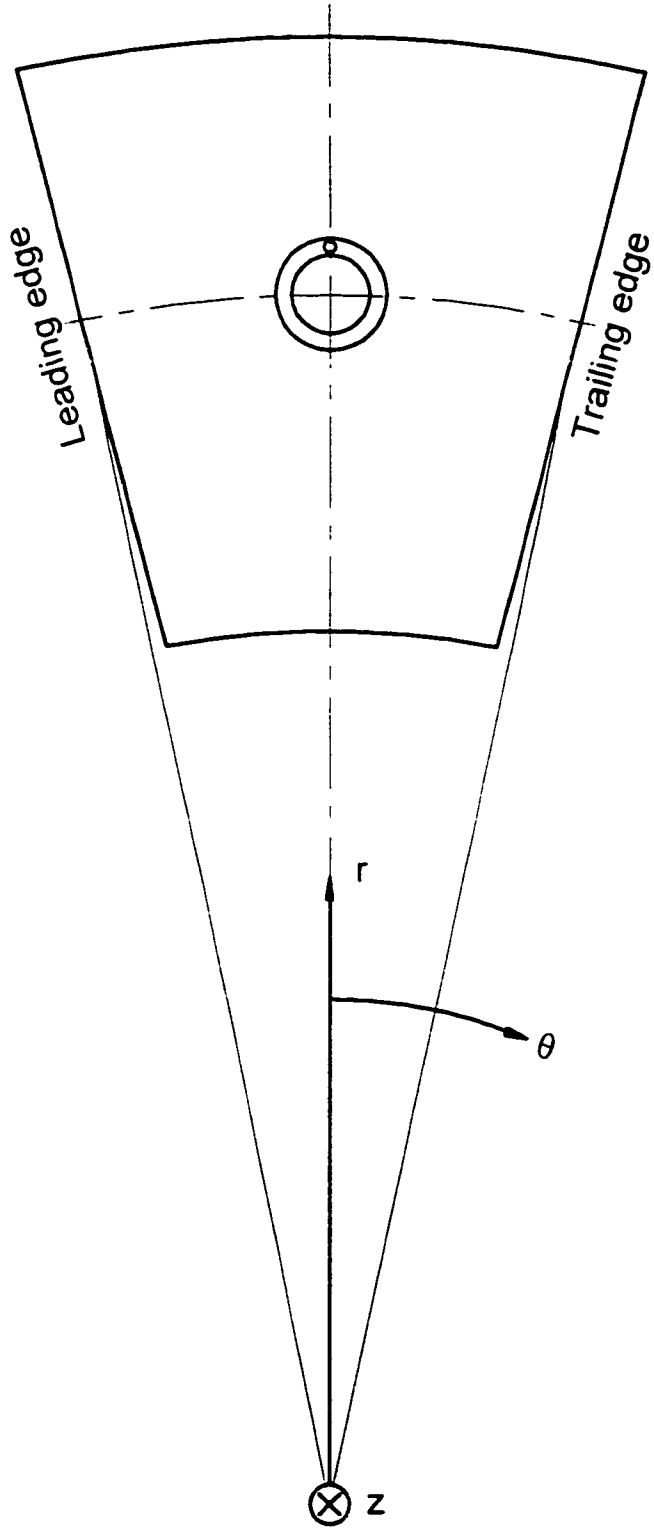

Figure 6.1. Coordinate system with the positive z-axis extending into the page (Note that the pad was not a perfect sector shape)

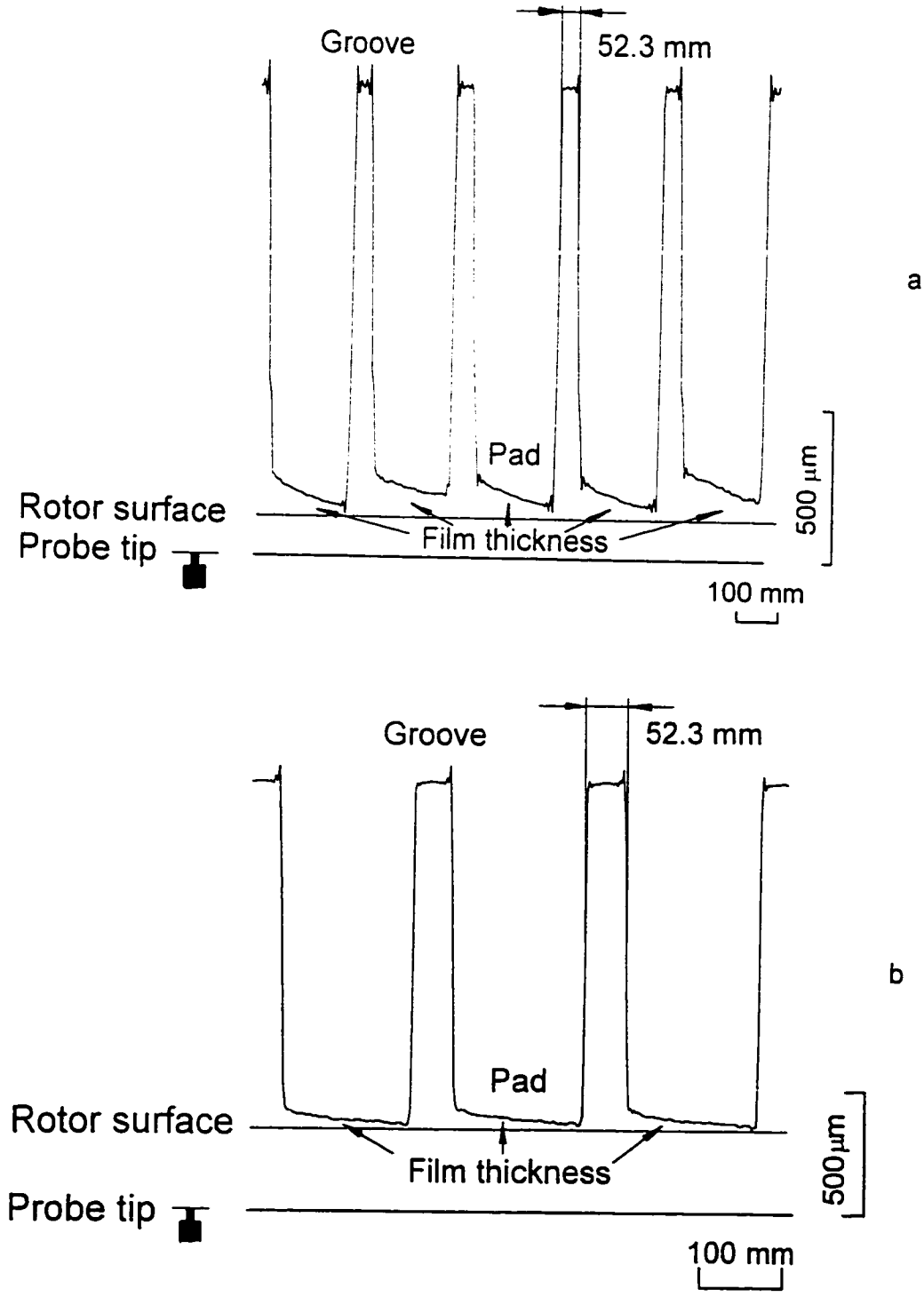

Figure 6.2. Oil film thickness patterns from digital analyzer

a. Load: 1.334 MN (44 kN/pad), b. Load: 2.124 MN (177 kN/pad)

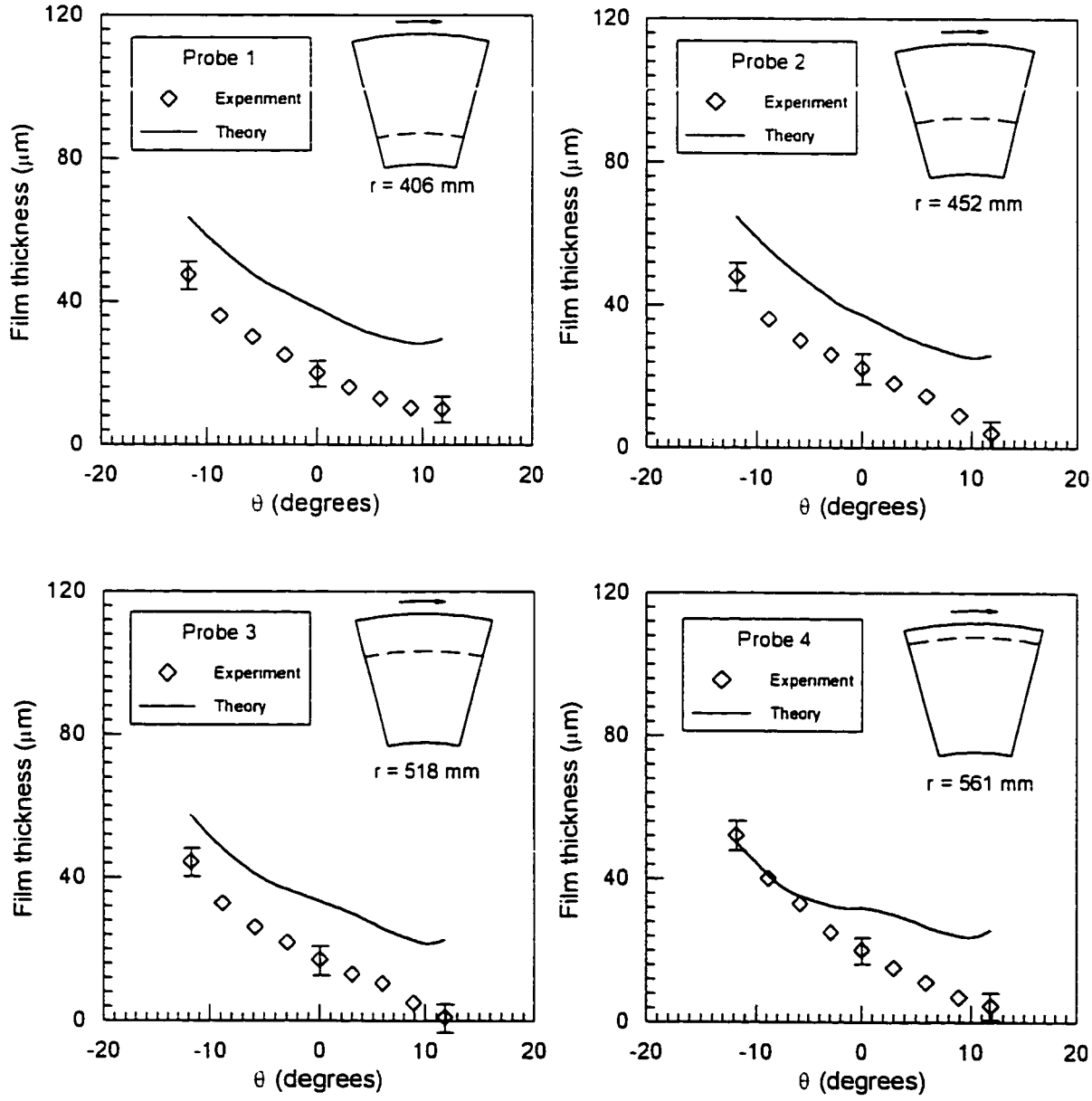

Figure 6.3. Experimental and theoretical film thicknesses for Case 1 at various radial locations

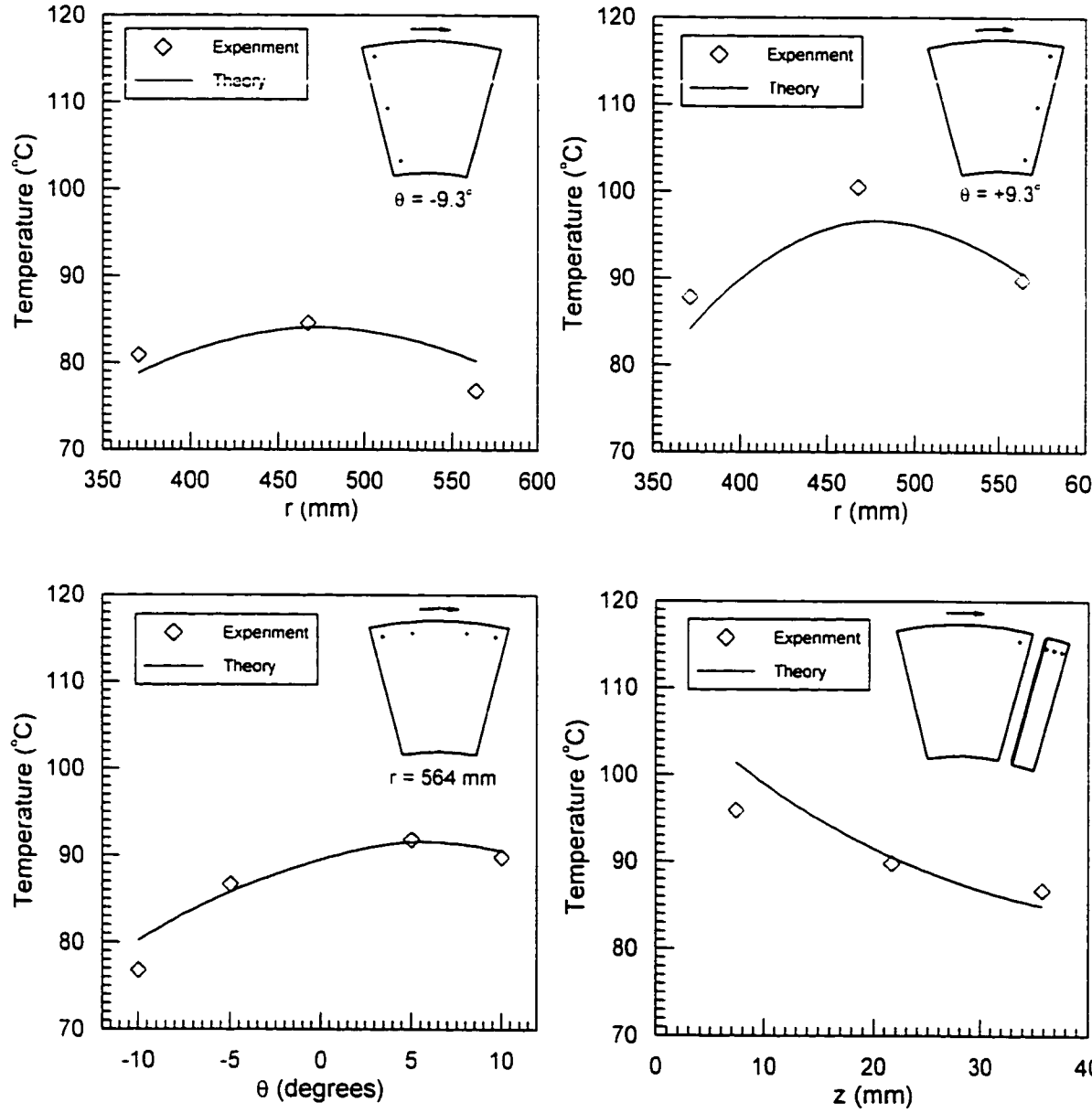

Figure 6.4. Experimental and theoretical temperatures for Case 1 at various locations

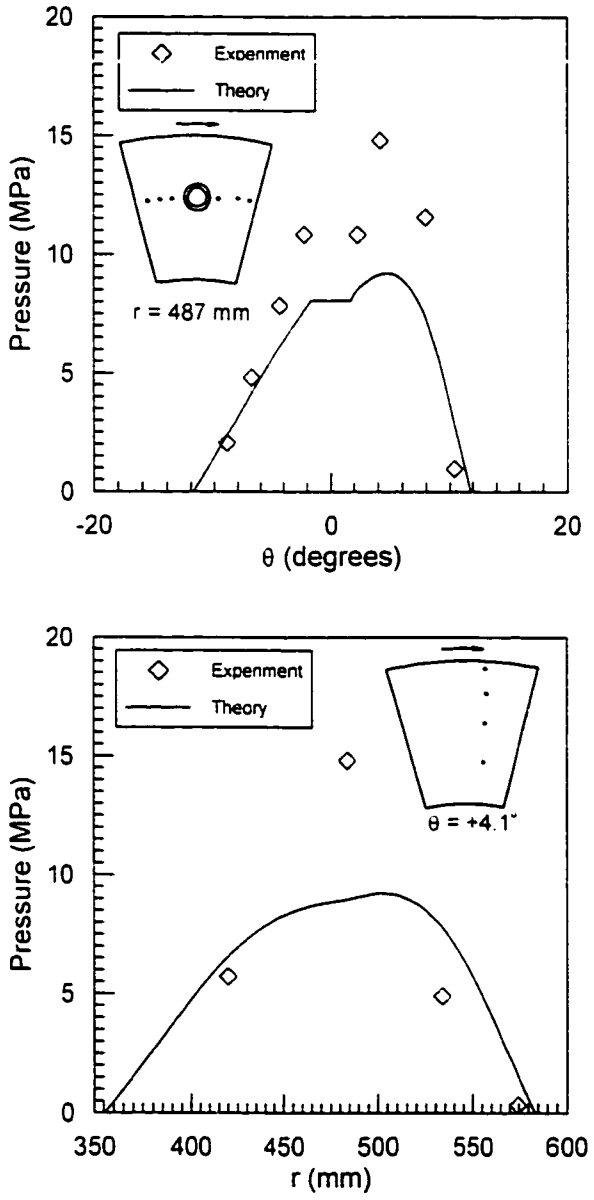

Figure 6.5. Experimental and theoretical pressures for Case 1 at various locations

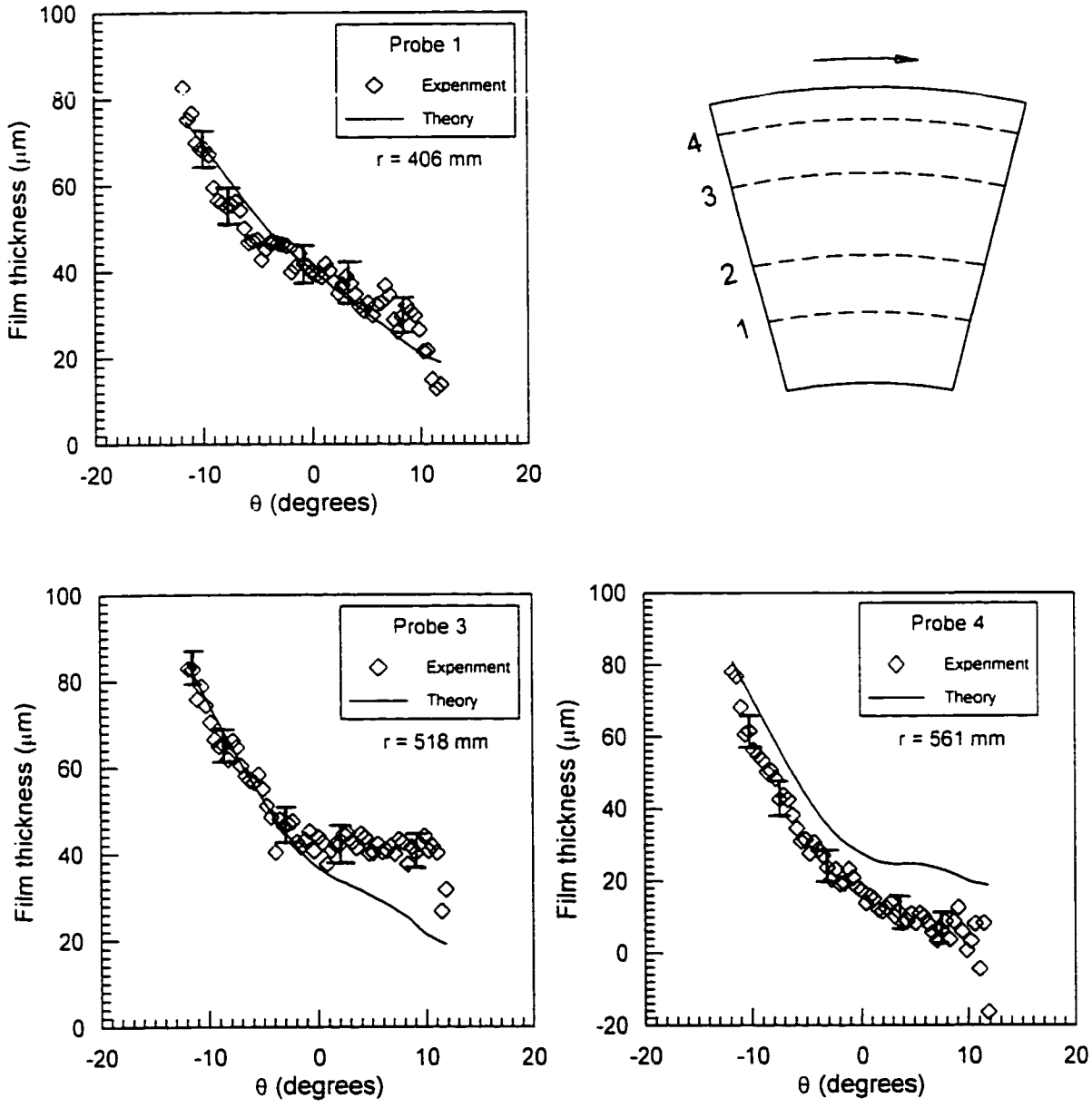

Figure 6.6. Experimental and theoretical film thicknesses for Case 2 at various radial locations

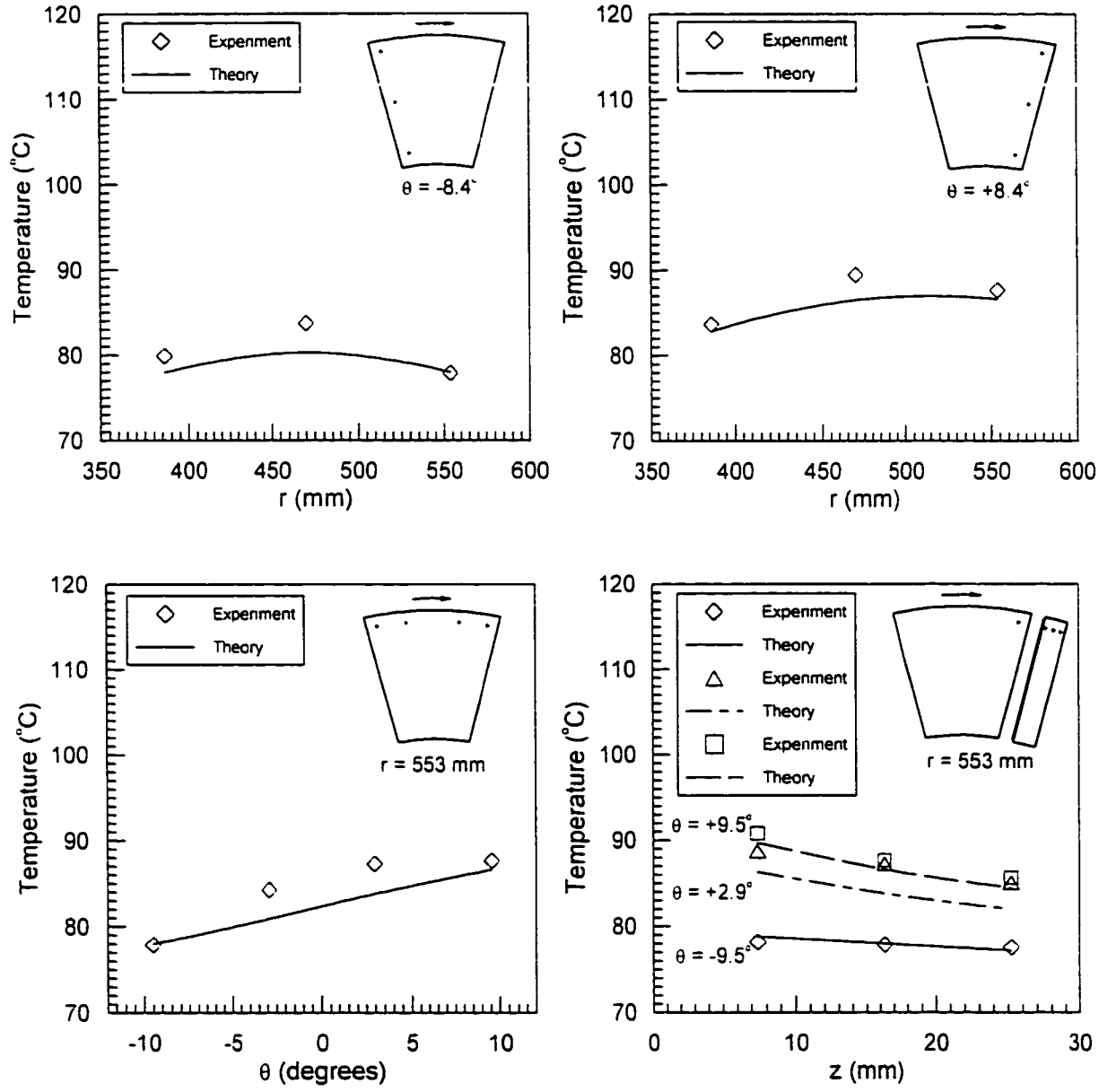

Figure 6.7. Experimental and theoretical temperatures for Case 2 at various locations

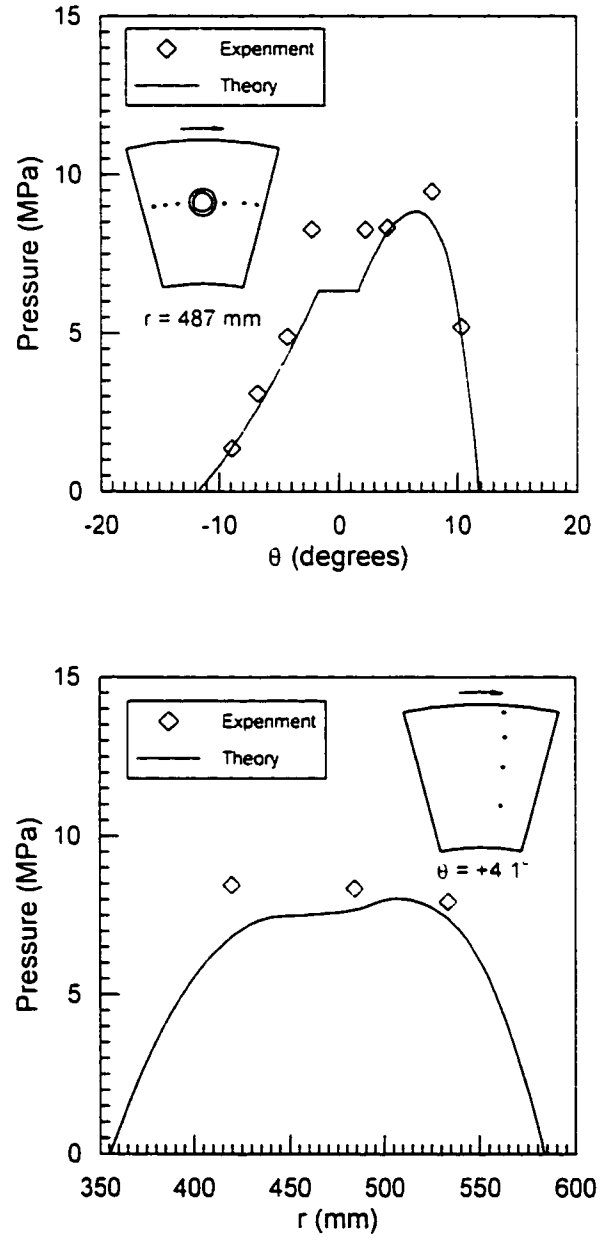

Figure 6.8. Experimental and theoretical pressures for Case 2 at various locations

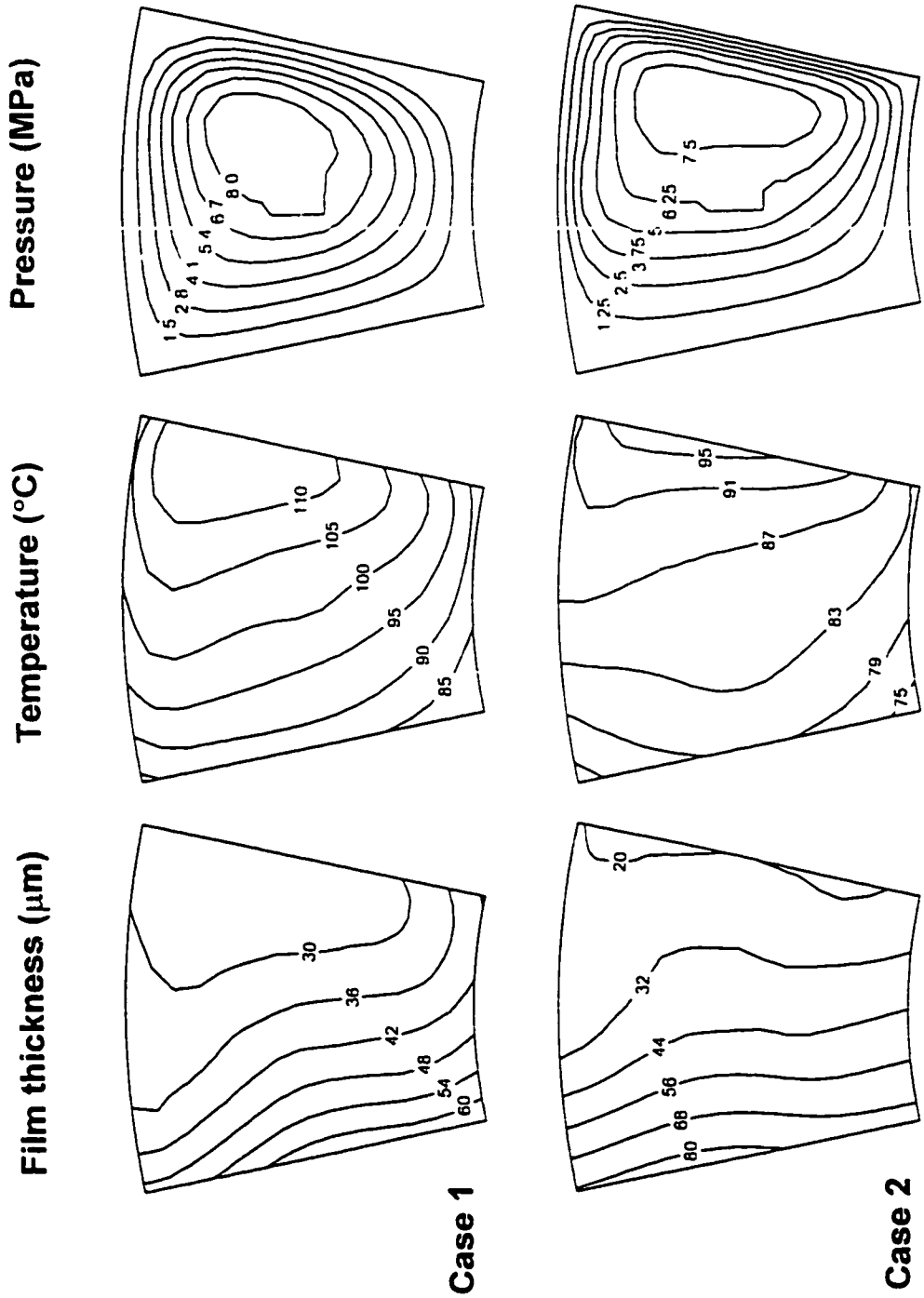

Figure 6.9. Contour maps of film thickness, temperature and pressure for both cases

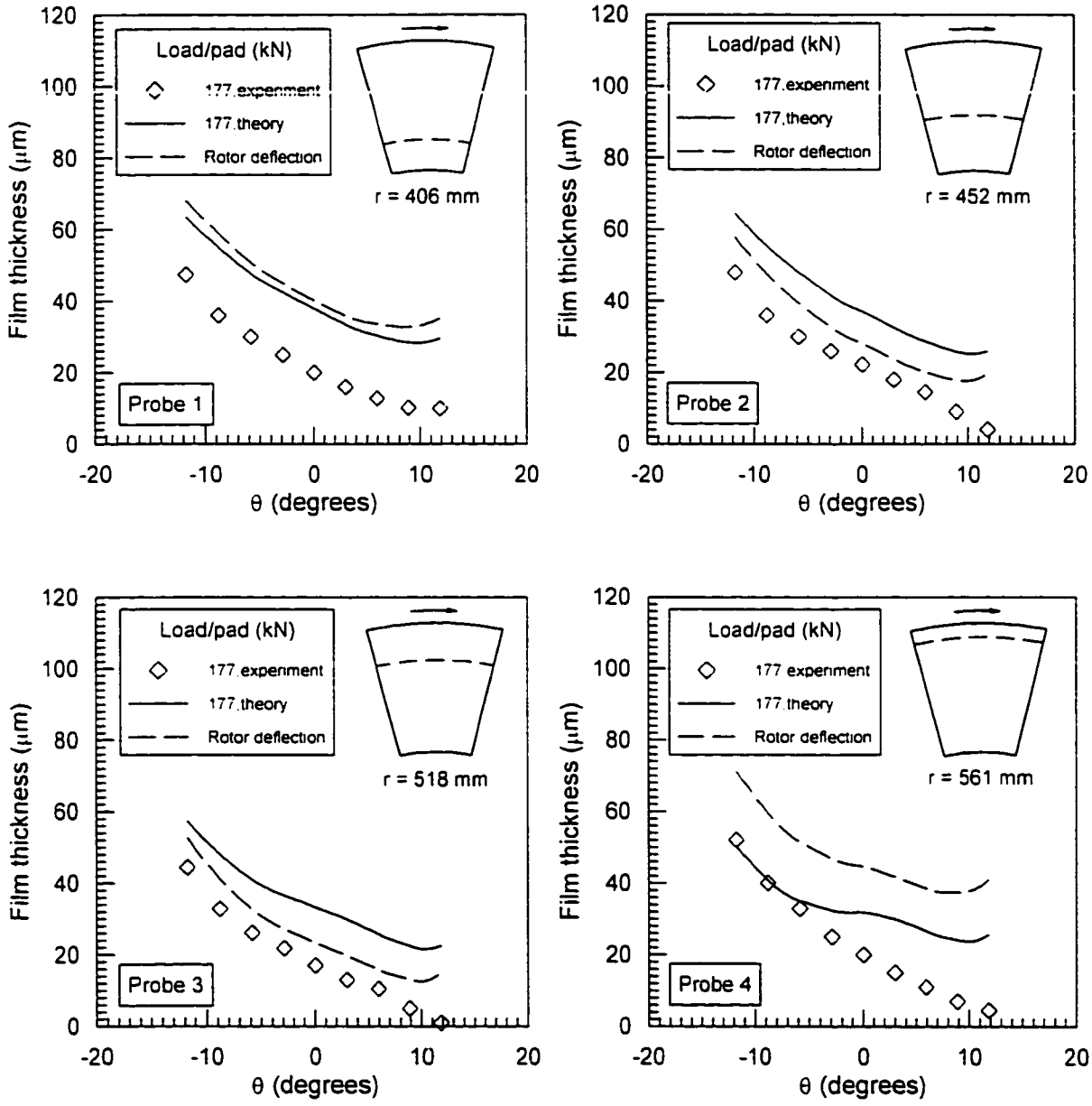

Figure 6.10a. Experimental and theoretical film thicknesses for Case 1 assuming a symmetric rotor crown of 60 μm

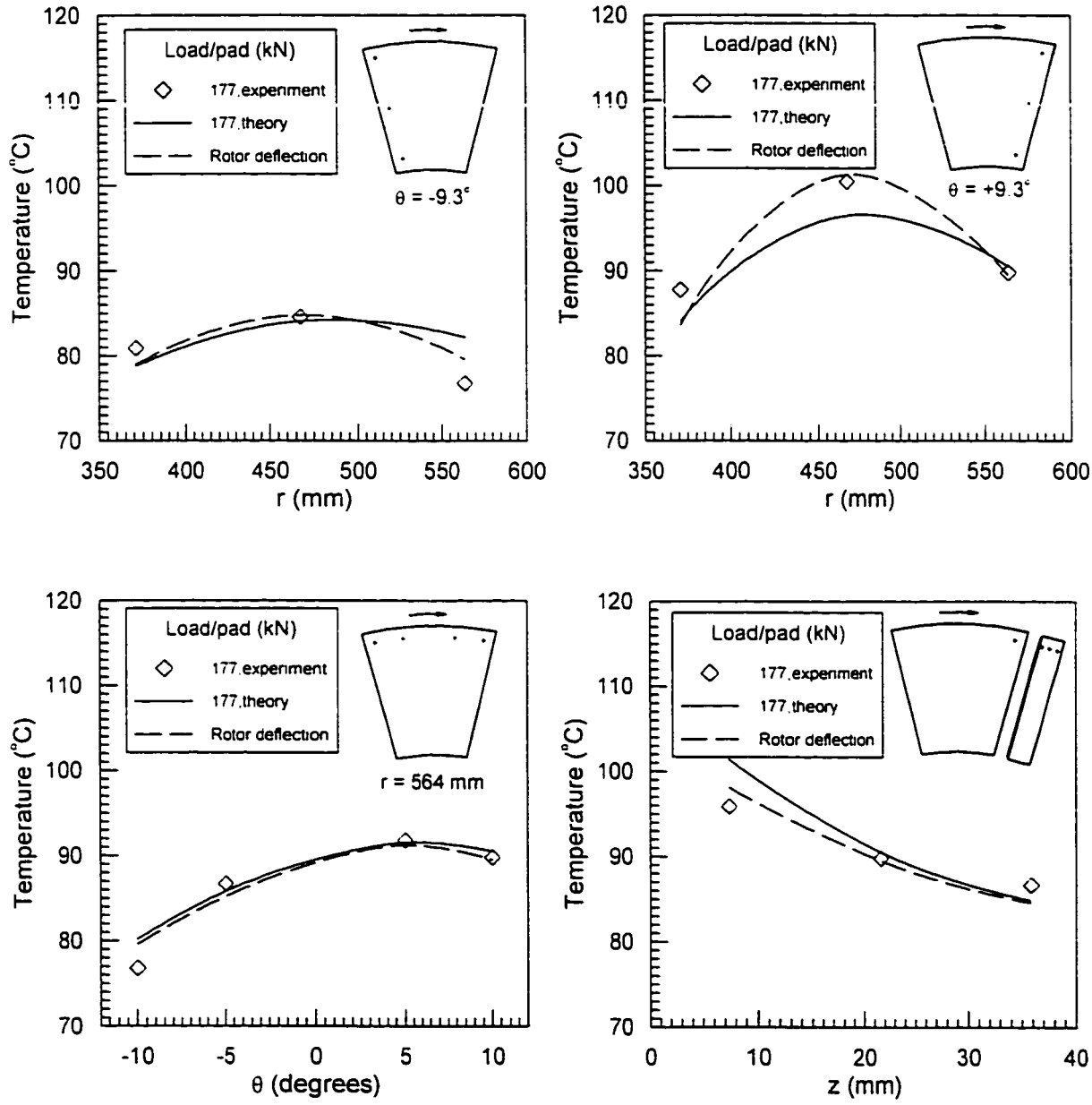

Figure 6.10b. Experimental and theoretical temperatures for Case 1 assuming a symmetric rotor crown of 60 μm

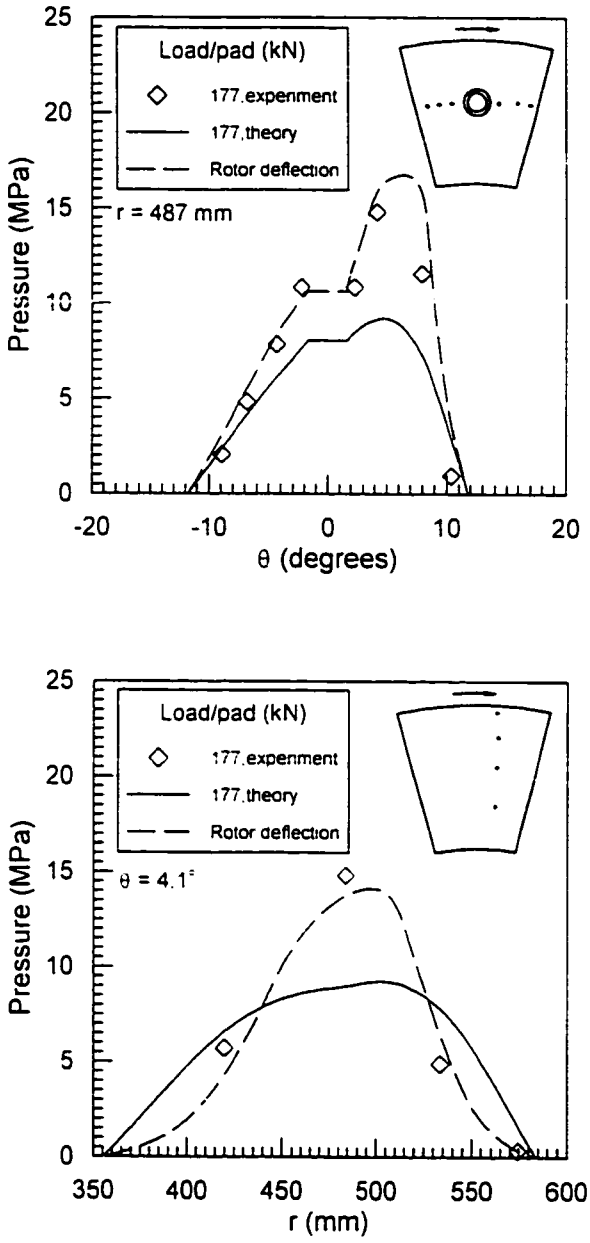

Figure 6.10c. Experimental and theoretical pressures for Case 1 assuming a symmetric rotor crown of 60 μm

Chapter 7

Investigation of Displacement Probe Behaviour

One of the most important features of thrust bearing performance is to maintain a continuous oil film between the lower part of the rotor or the rotating ring and the bearing pad surfaces. Knowledge of the film thickness allows a direct assessment of the risk of surface contact and subsequent bearing failure.

Clearly, there were problems with the film thickness measurements presented in Chapter 6. Some of the probes always gave measured values that were a relatively constant amount below those predicted by the GENMAT software package (Figure 6.2). In some cases, the measured film thicknesses were so low that they became negative. The similar shape of the measured films and the presence of measured film thicknesses that were negative while the test bearings continued to function without the high friction associated with surface contact (which would have caused the drive motor to stall) suggested that problems existed with the measurement system. One possible explanation was that the slope of the voltage-distance relationship changed at the higher operating temperatures. Also, the low film thickness values could be caused by an increase in probe temperature (above that of its value during operation) when the voltage corresponding to zero film thickness was obtained. This increase on probe temperature might have occurred because the pad had a

higher surface temperature than the rotor. Finally, there could have been some influence of the film pressure on the probe output voltage. The behaviour of the output voltage from the displacement probes as a function of temperature and pressure thus became an important issue in considering the results obtained. This behaviour was examined by calibrating a probe under controlled conditions of temperature and pressure in a "laboratory" apparatus. This laboratory calibration involved recording output voltages from the probe placed at various distances from small samples of bearing surfaces while immersed in oil. The probe, bearing surface samples and oil were all contained within a small pressure vessel with heating coils wrapped around it. Efforts were made to use this laboratory calibration to help interpret the film thickness results obtained from the test facility and to directly link the laboratory and test facility calibrations.

7.1 Laboratory Apparatus

A model M60 eddy current probe was connected to a model M600 probe "driver" by an M900 extension cable to form the DYMAC displacement probe system (DYMAC, a Scientific Atlanta Inc. subsidiary, San Diego, California, U.S.A.) as shown in Figure 7.1. This probe system was placed in an apparatus (Figure 7.2) which consisted of a small pressure vessel, heating coils, a hand pump and an electric circuit for reading the output voltage. This apparatus was intended to subject the probe to the same conditions that it sustained in the test facility.

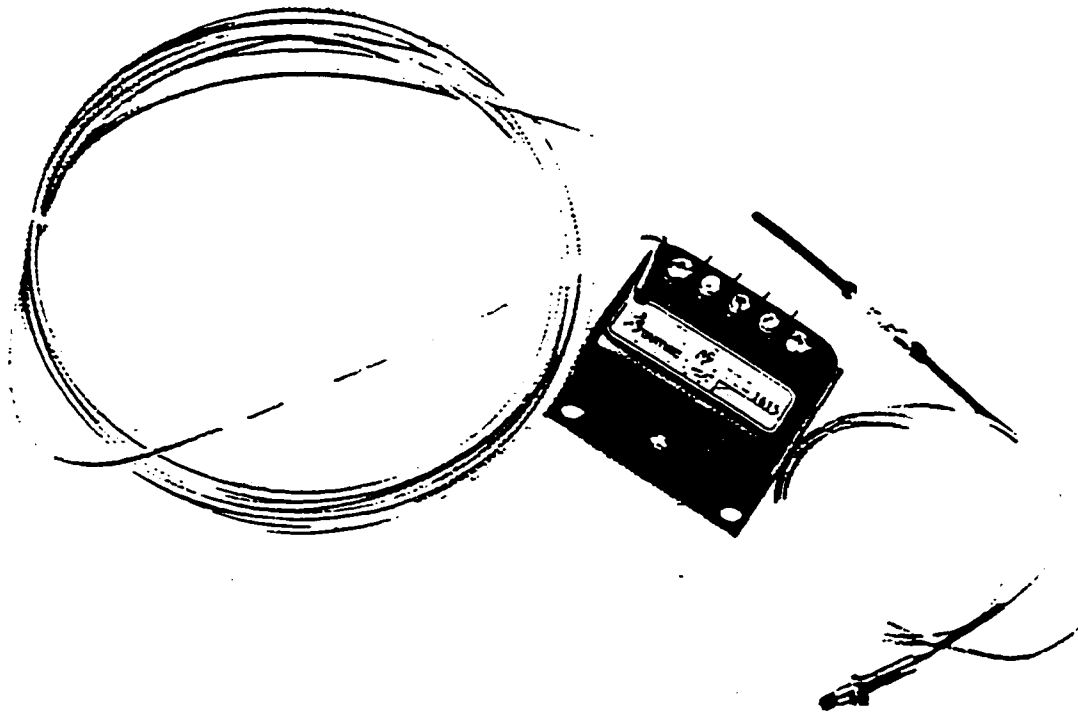

Figure 7.1. An Eddy current displacement probe

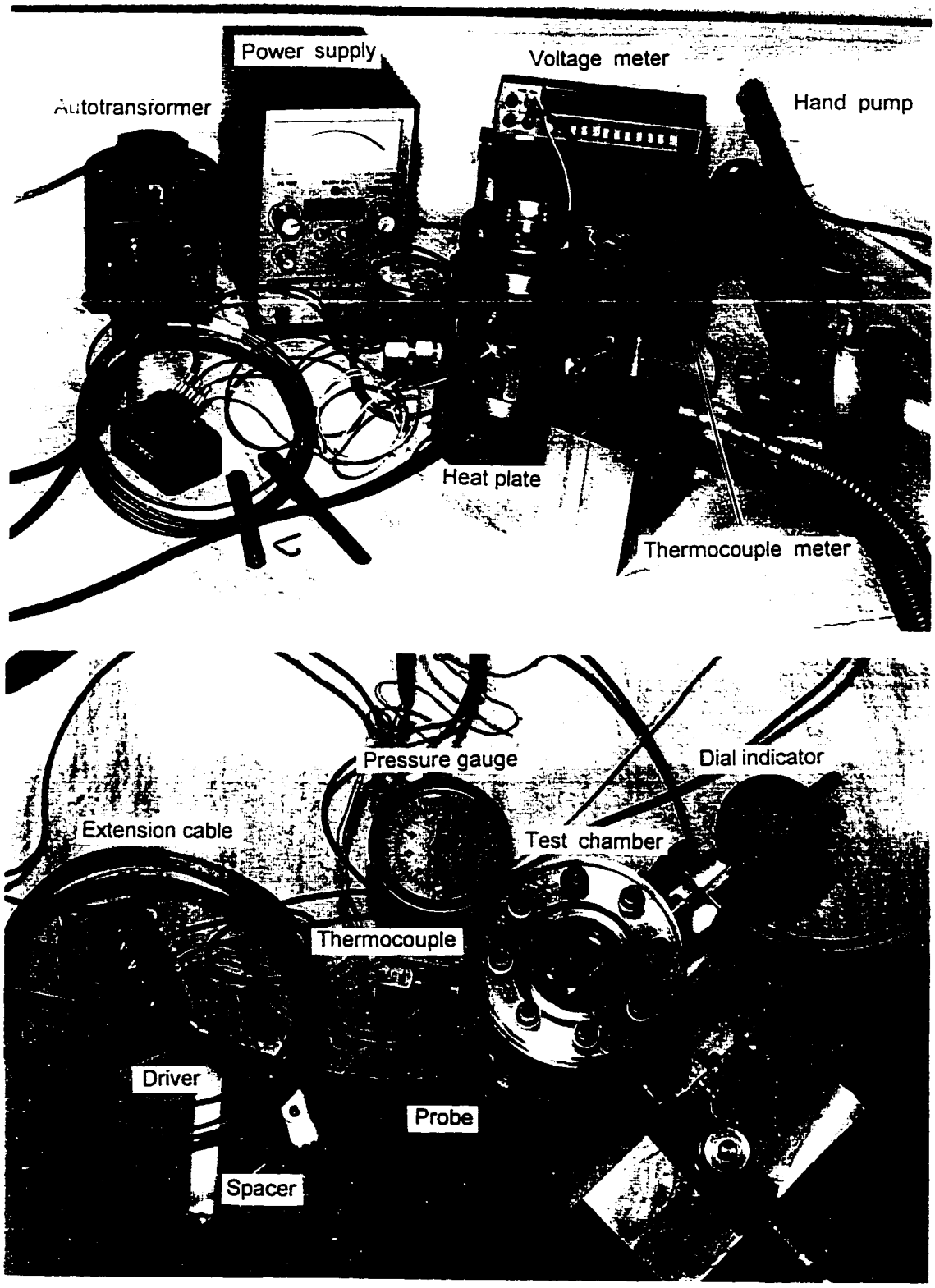

Figure 7.2. Two views of the test apparatus showing the various components

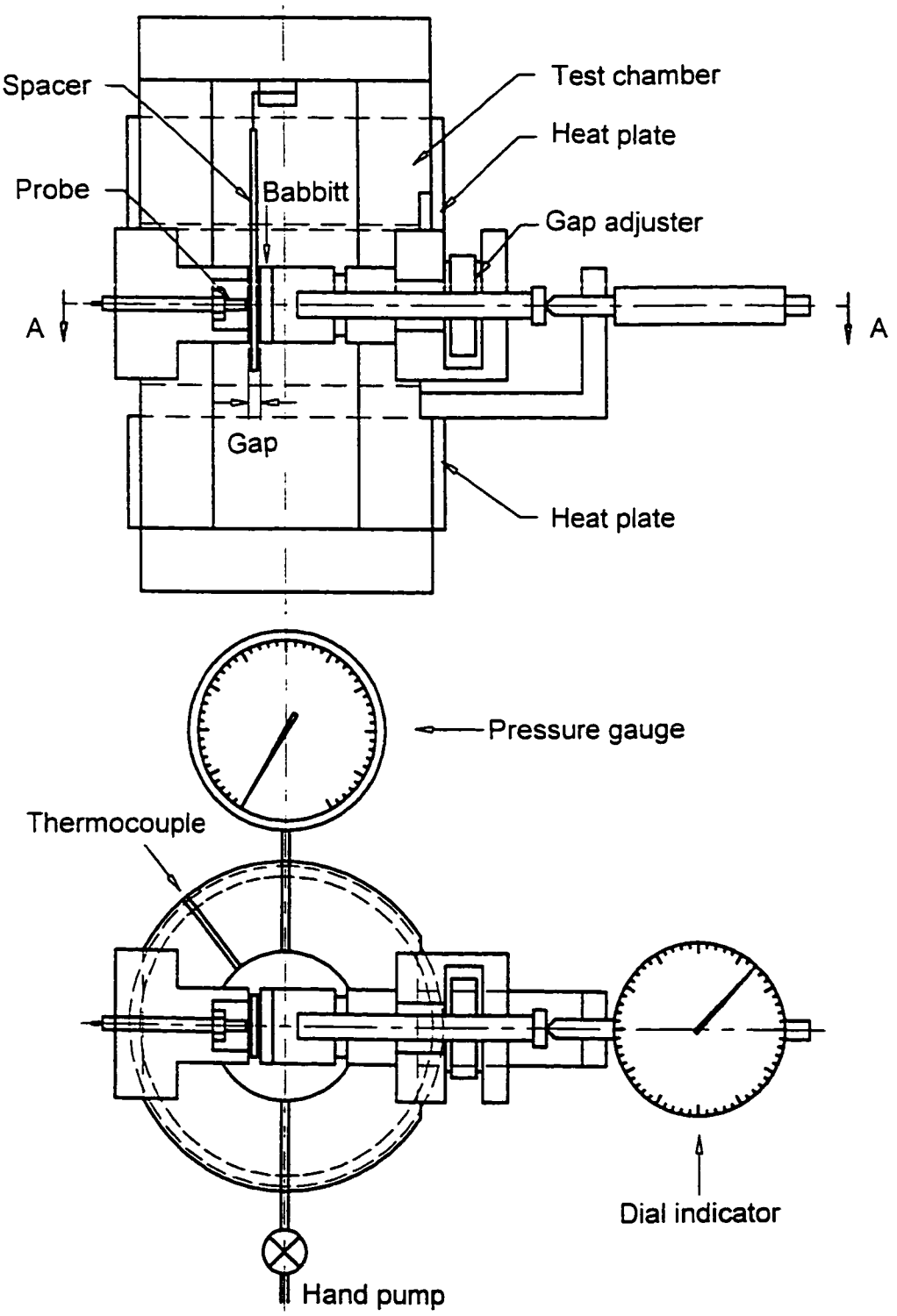

Figure 7.3. The configuration of the apparatus within the pressure vessel

7.1.1 Pressure Vessel

The pressure vessel was an aluminium tube (Figure 7.3) which was sealed at both ends using circular plexiglass plates bolted in place with O-ring seals. The transparent plexiglass end-plates were chosen so that the pressure vessel interior could be visually observed during testing procedures. The pressure vessel was filled with a light, clear oil (Mentor 29 made by Imperial Oil Ltd., Sarnia, ON). Within the pressure vessel, the displacement probe was mounted on one side with a dial indicator (for mechanically measuring displacement) on the other side. Both sides were sealed to prevent oil leakage. The end of the dial indicator was attached to a small "target" block of steel covered with a Babbitt layer to simulate the surface of the thrust bearing pad. The surface of the target block was set to the same position each time by turning a fine-threaded screw that pushed the block towards the probe tip. Thin spacers of known thickness were hung with a small wire from the top end-plate and used in the calibration procedures described subsequently.

As mentioned in Chapter 4, some of the later experiments in the test facility were conducted with a displacement probe mounted in the pad surface. This probe had the steel rotor surface as the target. Since material influenced the output voltage of the probe, special tests were completed in which the Babbitt-steel block was replaced by one of steel alone.

Three additional holes were drilled into the pressure vessel walls. A thermocouple went into one hole to measure temperature near the probe tip, the outlet pipe of the hand pump used another hole and a pressure gauge was mounted in the third hole. The pressure vessel was designed to withstand pressures up to 6 MPa and temperatures up to 120 °C.

7.1.2 Heating and Pressurising Systems

Two semi-circular heating plates were placed around the outside wall of the pressure vessel to provide the energy needed to raise the internal chamber temperature (Figure 7.2). Wires were connected between the plates and a "variable autotransformer" which permitted the input voltage to be set and controlled the energy input and thus ultimately controlled the chamber temperature. A simple hand pump was used to pressurise the oil in the internal

chamber. The thermocouple and pressure gauge mentioned above monitored chamber conditions and provided feedback for setting the input voltage to the heating plates and hand pump pressure, respectively.

7.1.3 Electrical System

The electrical system consisted of a custom probe "driver" connected by special extension cables to the probe and also to a 24 volt power supply which was capable of delivering a current of 25 mA (Figure 7.4). The required output voltage (V) was measured with a conventional voltmeter.

7.1.4 Displacement Probe Mounting

The displacement probe was mounted in the chamber wall through a steel retaining block which was itself bolted into the wall of the pressure vessel (Figure 7.3). Following the recommendations of the operating manual, a spherical region of *radius* equal to the probe tip *diameter* (Figure 7.5a) was kept free from any metal other than the "target" surface, to ensure that only the target surface influenced the output voltage. Thus, a cavity had to be shaped to contain the probe and avoid any interference. In the laboratory apparatus the cavity was the same size as that found in the test facility mounting of the probes and both were sufficiently large to avoid interference. The probe was threaded into a hole at the bottom of the cavity and locked firmly in place with a nut. Epoxy was used to fill in the cavity around the probe tip. The distance between probe tip and the retaining block surface was carefully set to 50 μm.

Also, the magnetic field from the probe tip had a conical shape (Figure 7.5b) and would bend around a target surface within the cone. Thus, the target surface in the laboratory apparatus was made large enough to extend well beyond the cone of the magnetic field. In the test facility this was always the case except when the probes in the rotor passed over the edges of the pads.

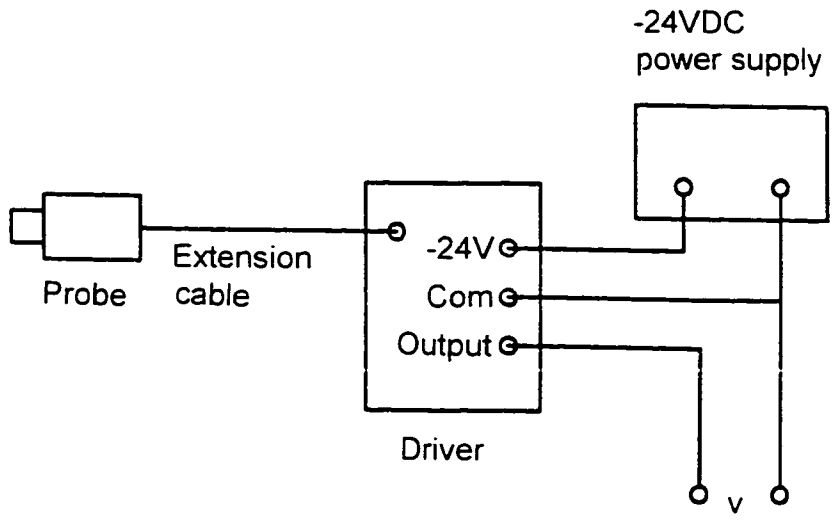

Figure 7.4. The electrical system

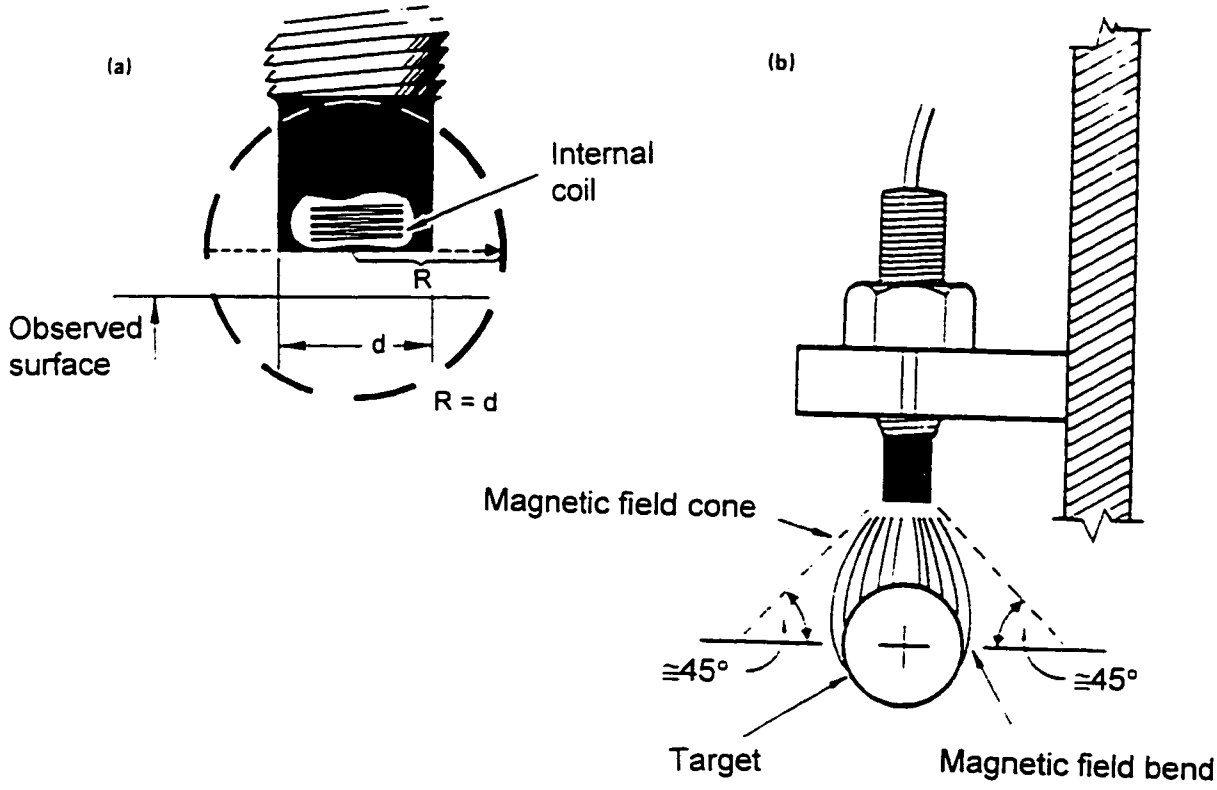

Figure 7.5. The magnetic field at the probe tip
a. Zone to be kept free of all metal except the target surface.
b. The cone shape of the magnetic field.

7.2 Calibration Procedure for the Gap Measurement

A fine-threaded screw (about 1 mm axial travel per revolution) with a large disc for a head allowed a manual adjustment of the gap (Figure 7.3). The dial indicator gave accurate feedback on the actual displacement of the block (target surface). However, setting the gap to the zero gap position was difficult because the epoxy deformed somewhat when pushed from one side by the probe tip and the other side by the contacting target surface. This "compliance" problem was solved by inserting spacers of varying thickness into the gap. These spacers were hung with a small wire from the upper end-plate to facilitate their insertion when the chamber was filled with oil. When inserted into the gap they rested on the outer edges of the retaining block rather than on the epoxy surface of the cavity containing the probe.

The calibration procedure involved decreasing the gap using the fine-threaded screw until the spacer was pressed with just enough force to allow it to move when pulled in the lateral direction by applying a small force through the supporting wire. After gaining some experience with this procedure, an ability to set the gap to hold the spacer lightly but firmly was developed without pulling laterally to check. This ability was useful when access to the pressure vessel interior was difficult because the oil was pressurised. The spacer was then removed and the gap was decreased by the thickness of the spacer so that it became "zero". The dial indicator then gave a reading corresponding to zero gap. However, when the gap was at zero, the probe tip itself was exactly 50 μm from the target surface as it was placed during mounting. Slight imprecision in the screw motions and the dial indicator positioning made it necessary to check the gap zero setting with spacers of various thicknesses (25.4 μm, 50.8 μm and 127 μm) periodically during the testing. Furthermore, testing at higher temperatures required re-setting the zero because of thermal distortions of the target and retaining blocks.

When testing at elevated pressures, the probe position relative to the retaining block surface was not expected to change because it was locked in place at the bottom of the cavity by a nut. However, the gap itself could increase as the pressure shifted either the retaining

or the target block. Thus, it is particularly important to perform the calibration procedure that was described above.

7.3 Experimental Conditions

An individual experiment was considered a single voltage measurement corresponding to a unique combination of target surface material, chamber gauge pressure, chamber temperature and gap separation (Table 7.1). The individual experiments were divided into groups (Table 7.2). Group 1 was given the descriptive label of the *temperature test with the Babbitt target surface*. Group 2 was the *pressure test with the Babbitt target surface*. Group 3 was the *temperature test with the steel target surface*. Some 1215 individual experiments were performed (Table 7.2), but only 318 of these were unique because all individual experiments were repeated three or four times.

Temperature was always set first because it took some time for steady state to be reached and to achieve a particular temperature required a series of adjustments to the variable autotransformer (control was manual rather than automatic). Next, the pressure was set and then the calibration procedure for the gap was performed as described in the previous section.

Group No.	Target Surface Material	Gauge Pressure (MPa)	Chamber Temperature (°C)	Probe tip to Target Block (μm)
1	Babbitt	0	24, 34, 44, 54, 64, 74, 84, 94,104	50, 100, 150, 200, 250, 300, 350, 400, 450, 500, 550, 600, 650, 700, 750, 800, 850, 900, 950
2	Babbitt	0, 0.69, 1.38, 2.76, 4.14, 5.12	24, 54, 84	50, 100, 150, 200, 250
3	steel	0	23, 50, 87	50, 100, 150, 200, 250, 300, 350, 400, 450, 500, 550, 600, 650, 700, 750, 800, 850, 900, 950

Table 7.1. An overview of the experimental conditions

Group No.	No. of Unique Experiment.	No. of Repetitions of Each Unique Experiment.	Total no. of Experiment.
1	171	4	684
2	90	4	360
3	57	3	171
Grand Totals	318	--	1215

Table 7.2. The number of experiments performed

7.4. Results and Discussion

An ideal displacement probe for measuring fluid film thickness in a large spring supported thrust bearing would not be influenced by temperature or pressure and would have a linear increase in output voltage with the distance from probe tip to target surface. The probe technical information did admit that temperature influences the output voltage value. However, the influence of pressure, temperature and distance on the slope of the probe output voltage versus distance was not known. These relationships were examined in the following sections.

7.4.1 Effect of Pressure

When a Babbitt surface was the target and distance was varied in increments from 50 to 250 μm, the pressure was varied in increments from 0 to 5.12 MPa for each of these temperatures (25, 54 and 84 °C) as indicated in Table 7.1. The various pressures gave essentially identical probe output voltage for each distance and for each temperature. This result supported the assumptions made in Section 5.1 when considering the use of displacement probes in the test facility. However, it was considered possible that the rapid change in pressure, which would be experienced by the probes in the test facility but not in the laboratory apparatus, might have an influence on probe output voltage. This possibility was not examined in the present chapter.

7.4.2 Effect of Temperature and Distance on Slope

Babbitt Target Surface

When the Babbitt surface was the target, the probe output voltage in the laboratory apparatus was quite linear at room temperature of 24 °C for distances from probe tip to target surface of 50 – 200 μm (Figure 7.6). Beyond 200 μm, the probe output – distance curve became gradually non-linear. This non-linearity was not a very strong characteristic of the data. The laboratory data could be fitted from 50 – 850 μm and appear quite linear as well

(Figure 7.7). However, as temperature increased the non-linearity with distance became more apparent (Figure 7.6) which suggested that it was physically realistic even at room temperature.

In the test facility where calibrations were performed at room temperature, the probe output voltage versus distance curve had been fit as linear. However, the exact distance below the rotor surface that the probes were placed was not known. If it was less than 200 μm, the fit in the laboratory apparatus from 50 – 200 μm would be relevant to the test facility probes. The slopes of the fitted curves for the room temperature calibration of the test facility probes (Figure 5.3) were quite close to those found for the probe in the laboratory apparatus for distance of 50 – 200 μm (Figure 7.6) which suggested that the laboratory tests and test facility calibrations were examining the same physical phenomenon.

When temperature was increased, there was no test facility data to compare with the results from the laboratory apparatus. Increasing temperature caused an increase in the voltage level and a drop in the slope of the voltage-distance curve at low distance values of about 10% (Figure 7.6). The voltage-distance curve became increasingly non-linear with distance probably did not influence the accuracy of the test facility results much for probes 1 – 4, perhaps at most a 5% uncertainty, and thus only a slight violation of the probe calibration assumption 1 made in section 5.1. However, there would still be some violation of the probe calibration assumption 3 of Section 5.1. Clearly, the slope of the voltage-distance curve was not independent of temperature and this would introduce an additional uncertainty of about 10% as mentioned previously.

Thus, the total uncertainty associated with these violations was estimated at about 15% and this uncertainty was not enough to explain the zero and negative film thickness indicated in the testing reported in Chapter 6. This finding was important and suggested that the calibration of the displacement probes and the incorrect assumption upon which it was based was not enough by itself to explain the inaccuracy in the measured film thicknesses found in Chapter 6. Consequently, by default, the procedure for finding the voltage corresponding to zero film thickness was implicated in the inaccuracy of the film thickness measurements.

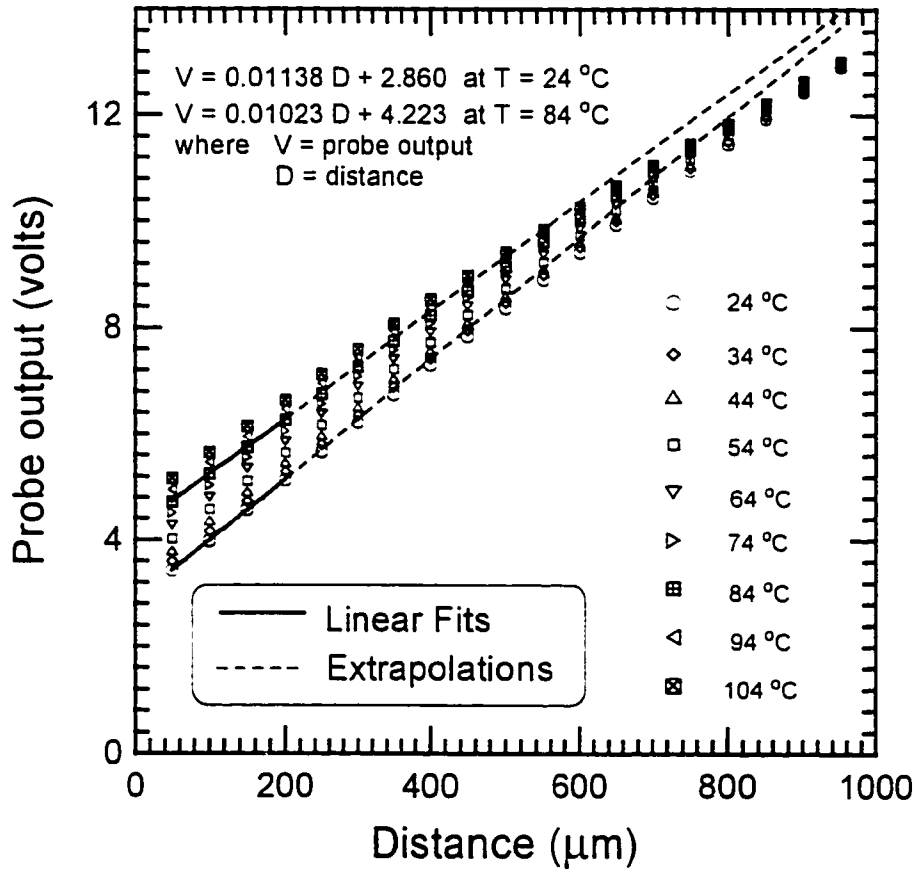

Figure 7.6. Probe output versus distance from probe tip to a Babbitt surface (simulating Probes 1 – 4 in the rotor of the bearing in the test facility)

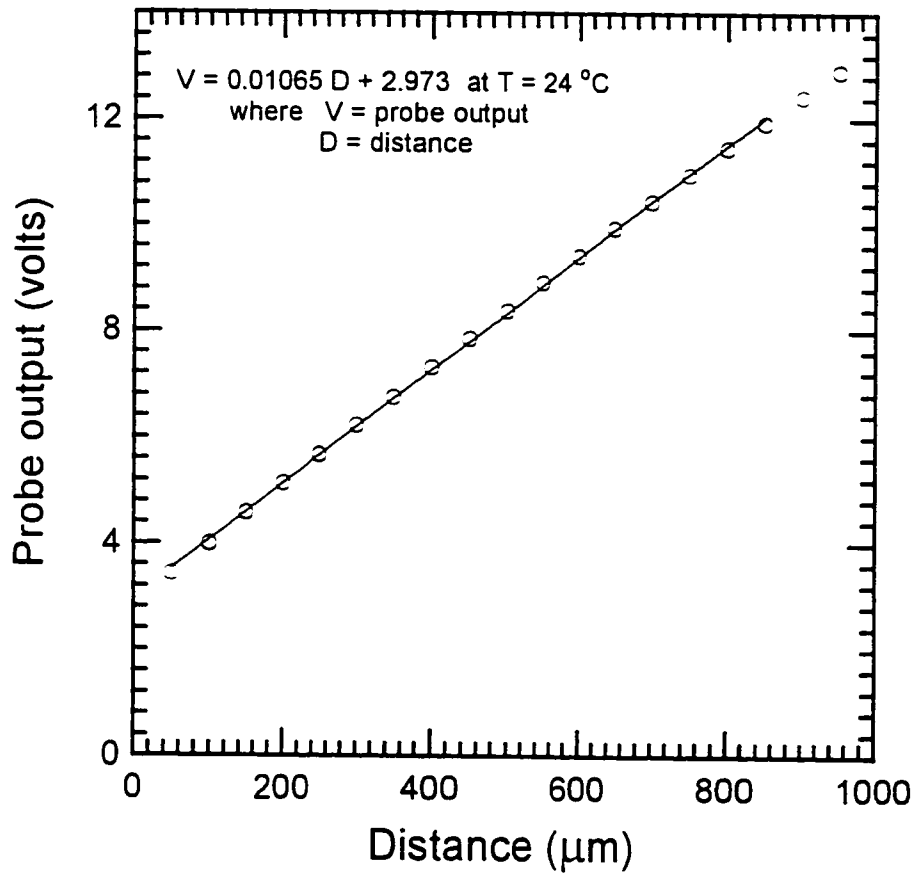

Figure 7.7. The curve fit for the T = 24 °C data in Figure 7.6 over the larger distance range of 50 - 850 µm

Steel Target Surface

When the target surface was steel, the room temperature probe output-distance curve had no hint of non-linearity (Figure 7.8) and thus differed from the results when the target surface was Babbitt. The probe output-distance equations at room temperature were

$$V = 0.007682D + 0.1338 \qquad for\ D = 50 - 200\mu m \tag{7.1}$$

and

$$V = 0.007683D + 0.1461 \qquad for\ D = 50 - 950\mu m \tag{7.2}$$

where D = distance from probe tip to steel target surface.

Also, the slope was very close to that found in the test facility calibrations (Figure 5.4). However, as temperature increased, the slope at small distance decreased and the non-linearity of the voltage-distance curve increased (Figure 7.8). While this effect was not as severe as that found with the Babbitt surface as a target, it did still exist. Also, for the steel target surface, the laboratory apparatus results could be used to design a "correction" to the results obtained with probe number 5 in the test facility. However, this correction remained rather tentative because very little data was collected with probe number 5 which had been installed only for the last test. Also, the probe used in the laboratory apparatus was not probe number 5 and each probe had a slightly different probe output versus distance behaviour.

7.4.3 Developing a Correction to the Test Facility Data for Probe Number 5

The original intent of the experiments with the laboratory apparatus had been to link the findings to the results obtained in the test facility and perhaps provide a correction to the test facility data. Unfortunately, the laboratory experiments were performed after the experiments with the test facility. The temperature of the probe numbers 1-4 in the test facility were not known exactly because the nearby temperatures were not measured while the test facility was running. The lack of temperature measurement occurred because the slip-ring connection with the rotor was already being used to capacity with the probe output

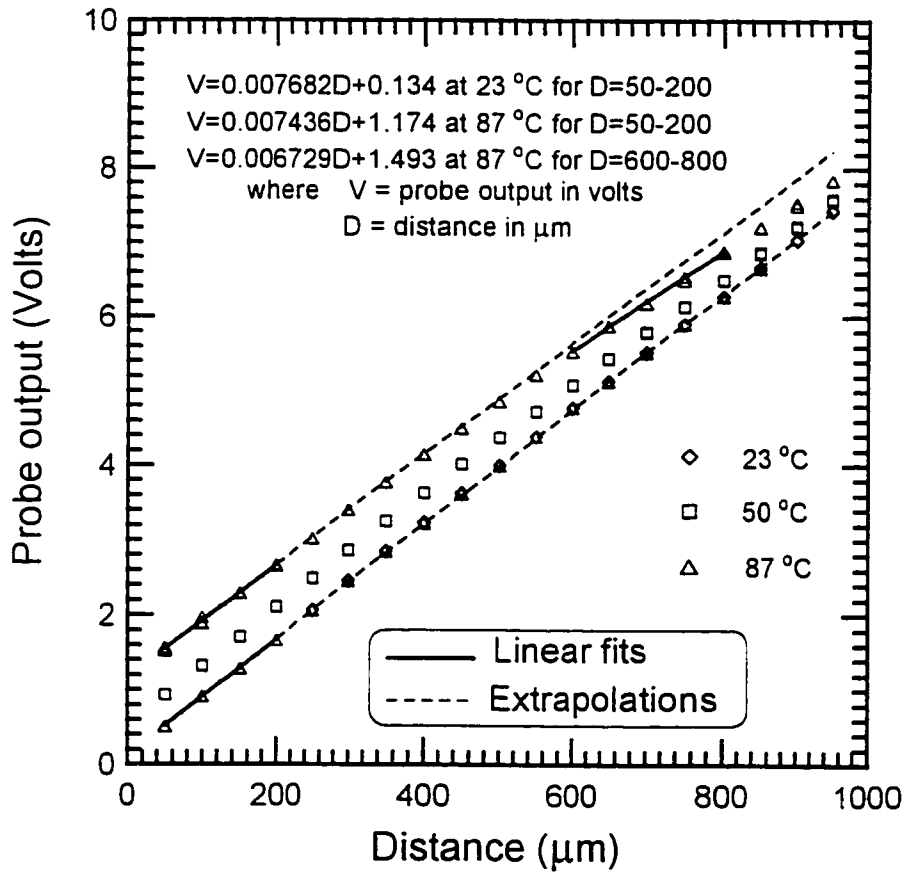

Figure 7.8. Probe output versus distance from probe tip to a steel surface (simulating probe number 5 in the pad of the bearing in the test facility)

voltage recordings. In addition, the distances from probe tip to target surface for probes number 1-4 were not known in the test facility because, at the time of installation, it was not considered necessary to place the probes at a known distance below the surface. Also, each probe was slightly different in its slope and the intercept of the voltage-distance curve with the probe output voltage axis. The intercept voltage was controlled by a variable resistor in the electric circuit and the value of the resistor in the facility circuit was arbitrarily adjusted to obtain a well-placed set of curves of the *analogue recorder*. The value of this resistor was not recorded during experiments with the test facility because it was thought that only the slope was important.

If the probe numbers 1-4 could have been calibrated in the laboratory first, then mounted with an identical electric circuit at a known distance below the surface in the test facility and had their temperature recorded while the test facility was running, then an accurate film thickness could have been measured without having to stop the rotor to determine the probe output voltage "corresponding to" zero film thickness. However, this possible approach evolved after experience was gained with the test facility and in the laboratory. It was not obvious initially.

Fortunately, probe number 5 was placed about 635 μm (25 mil) below the surface of the pad and the temperature was approximately known while the test facility was running because nearby thermocouple output was recorded. Thus, it was possible to develop a tentative link between the laboratory data and that from probe number 5 in the test facility. This link should provide a correction for the test facility data. However, it had to be assumed that there was negligible difference between the response of the laboratory probe and probe number 5. This assumption was supported by the similar slopes of the voltage–distance curves of the probe numbers 1-4 when calibrated in the test facility (Figure 5.3). In other words, provided the probes were a similar distance from the same target surface, the slopes of the voltage-distance responses were very similar. However, the actual magnitude of the voltage output also depended on the variable resistor used in the measurement circuit and this was not known for probe number 5. This introduced some uncertainty into the calibrations linking the laboratory probe performance to that of probe number 5 in the test facility.

First, it was possible to check whether the probe in the test facility was actually 635 μm below the pad surface. The calibration equation for number 5 in the test facility was given previously in Chapter 5 as follows:

$$V = 0.007456h + 4.866 \qquad for\ h = 0 - 762\mu m \tag{5.5}$$

where, h = distance between rotor and pad surface

This equation was re-written in the same form as Equations (7.1) and (7.2) to obtain

$$V = 0.007456(h + d_s) + C_1 \tag{7.3}$$

where d_s = distance from probe tip to surface

C_1 = intercept of the voltage-distance curve

For h = 0. Equation (5.5) implied that V = 4.886 or Equation (7.3) implied that

$$4.886 = 0.007456d_s + C_1$$

Assuming that Equation (7.2) was a better representative of the physics than Equation (7.1) because it was based on more data and that C_1 was the same as in Equation (7.2), then

$$4.886 = 0.7456d_s + 0.1461$$

gave d_s = 635.7 μm which was quite close to the 635 μm that the probe tip was estimated to be placed below the surface. This good agreement suggested that probe number 5 was indeed quite accurately placed about 635 μm below the surface of the pad.

For the probe in the laboratory apparatus at a temperature of 87 °C to be relevant to probe number 5 that was 635 μm below the pad surface, the following probe output versus

distance relationship was developed as shown in Figure 7.8.

$$V = 0.006792(h + d_s) + 1.493 \qquad for\ (h + d_s) = 600 - 800\mu m \tag{7.4}$$

In contrast to the data taken at room temperature, the data taken at a temperature of 87 °C did not fit a straight line over the distance range. Thus, it was important to know how far below the surface probe number 5 was placed and to choose a suitable distance range to obtain Equation (7.4).

For Case 2 in Chapter 6, the probe number 5 output was V = 5.155 when running under test conditions and V = 4.751 when the rotor was stopped and load was applied to produce zero film thickness as described in section 5.3.3. To find an expression for the film thickness when running under the Case 2 conditions, the following general form of the equations relating probe output to film thickness was considered.

$$V = m(h + d_s) + C_1 \tag{7.5}$$

where m = slope in volts/μm.

h = distance from rotor to pad surface.

d_s = distance from probe tip to pad surface.

C_1 = intercept of the voltage-distance curve.

Assuming the temperature was about 82 °C when running under test condition and when the rotor was stopped. Equation (7.5) implied

$$5.155 - 4.751 = [m(h + d_s) + C_1] - (md_s + C_1)$$

which gave

$$h = \frac{0.404}{m} \tag{7.6}$$

To find an appropriate value for the slope (m), the slope of the test facility calibration curve at room temperature given by Equation (5.5) was reduced by the same proportion as the slope of the laboratory apparatus calibration curve at room temperature given by Equation (7.2) was reduced when the calibration was performed at 87 °C over a distance of 600 to 800 μm given by Equation (7.4). This meant that the slope was estimated as

$$m = 0.007456 \times \left(\frac{0.006729}{0.007683} \right)$$

$$\text{or } m = 0.006531$$

The temperature for probe number 5 in the test facility under the Case 2 conditions was estimated to be 82 °C and the temperature for the laboratory apparatus data of Equation (7.4) was taken for 87 °C but this difference in temperature was judged to have a negligible effect on the above corrected slope. Therefore, the best estimate for the film thickness was determined by substituting the corrected slope into Equation (7.6) to obtain

$$h = 61.9 \ \mu m$$

The film thickness value obtained by the test facility data acquisition system, which used the slope of room temperature calibration of Equation (5.5), was 54.2 μm, whereas GENMAT predicted a film thickness of about 70 μm. These values were compared graphically (Figure 7.9) and suggested that the film thickness predicted by the test facility calibration at room temperature would increase by about 15% when the modified calibration was used to account for the non-linear behaviour and temperature dependent behaviour of probe number 5. However, the measured film thickness value with the modified calibration was still below the theoretical value predicted by GENMAT and the values measured using probes 1, 3 and 4 (which had been mounted in the rotor and calibrated in the test facility). Without knowing the true value for the film thickness at the location of probe 5 (r = 495 mm), it was impossible to know for certain that the modified calibration had improved the accuracy of the measured film thickness. Nevertheless, the modified calibration did seem to move the measured film thickness in a direction that was consistent with theory and the other measured values (Figure 7.9).

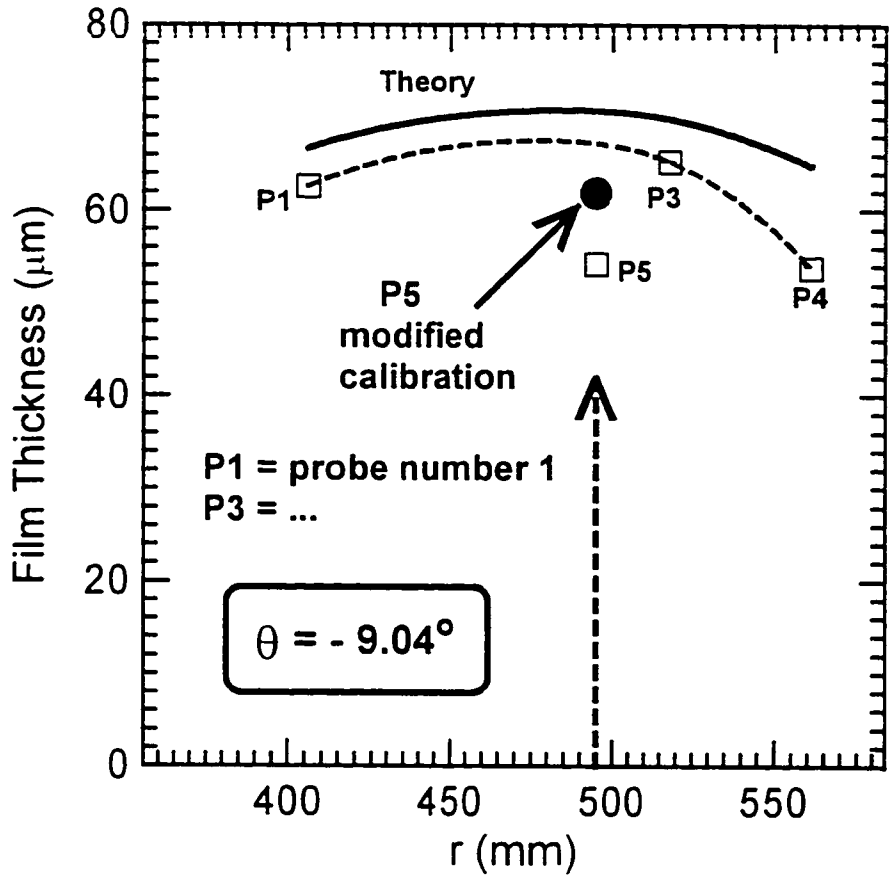

Figure 7.9. Using the laboratory apparatus to modify the calibration for probe 5 shifted the measured value closer to the theoretical prediction of GENMAT (and the values measured with probes number 1, 3 and 4)

There were other possible causes of error in the probe readings. The "zero film thickness" reading involved applying load with the hand pump to squeeze out the oil from between the surfaces. However, trapped oil films might still prevent the surfaces from making direct contact and thus the zero reading might be inaccurate. Also, since the test apparatus was running at high temperature, both rotor and pad surfaces might experience thermal distortion and not be flat. If a probe was located in a "valley" of the pad or the rotor, then a false zero would be recorded.

7.5. Concluding Remarks

When the probes were placed in the rotor, the difference between the results with the "test facility" calibration and the "laboratory calibration" was estimated at about 15%. This uncertainty was not enough to explain the inaccuracy of the measured film thickness values and the procedure for determining the probe output at zero film thickness was implicated as contributing significantly to the inaccuracy.

However, a somewhat more promising result occurred for probe number 5 (in the pad). In this case, the position of the probe below the surface was known whereas for the probes in the rotor the positions were not known. As a result, the probe output versus distance data from the laboratory apparatus could be fit by a straight line over the appropriate distance range (at a similar temperature as occurred in the test facility while running). Unfortunately, the absolute voltage level in the laboratory apparatus could not be directly linked to that in the test facility because the value of the variable resistor in the test facility circuit was not known. Still, a modification factor for the slope as a result of the elevated temperature of the running test facility at the corresponding distance range could be estimated. Using the probe number 5 output when the test facility was operating and at zero film thickness, a voltage difference was calculated and divided by the modified slope to produce a film thickness value that was closer to the theoretical predictions and to the measured value based on the output of probe numbers 1, 3 and 4. This finding provided compelling support for the suggestion that much more accurate results could have been

obtained using probes calibrated in the laboratory then placed in the test facility in a circuit with known variable resistor values at a known distance below the bearing surfaces with nearby thermocouples to measure temperatures while operating. In this manner, the temperature and distance non-linearity of the probes could have been taken into account for the film thickness measurement in the test facility.

Chapter 8

Parameters Influencing the Thrust Bearing Performance

As discussed in the previous chapters, the physics of the thrust bearing operation is very complicated and influenced by many factors. A detailed examination of two typical configurations in Chapter 6 allowed some conclusions. Comparison of the data measured in experiments with predictions obtained from the theoretical analysis of the GENMAT software package indicated that although the magnitudes of the oil film thickness did not always show good agreement, the pad shapes did correspond more closely. When the *digital analyzer* was used, both the shape and occasionally the magnitudes of the film thickness showed good agreement. These comparisons of pad shape combined with the good agreement between theoretical predictions and experimental data for temperatures suggested that GENMAT did provide a reasonable representation of the physics of the thrust bearings. However, the poor agreement for pressures suggested otherwise until varying amounts of thermal crowning of the rotor were added in the GENMAT modelling until good predictions of the experimental pressures were obtained. This amount of crowning resulted in a small reduction in film thicknesses in the central region of the pad but the pad shape stayed about the same as found in the experiments over the entire pad surface. The pad temperatures predicted for this crowned rotor were slightly closer to the

experimental data than the numerical predictions without a crowned rotor. These findings encouraged the opinion that the poor predictions of pressures were caused by not modelling rotor crowning but an actual procedure for predicting rotor crowning had not been established.

Clearly, a more reliable investigation of detailed thrust bearing performance could have been obtained if good agreements between experiment and theory were always found for film thickness magnitudes, pad shape, temperatures and pressures. If truly excellent agreement had been obtained over a wide range of cases, it would have been possible to rely on GENMAT predictions alone to investigate thrust bearing performance in detail. Unfortunately, such agreement did not occur but it was still possible to investigate a number of aspects of thrust bearing performance. The approach adopted in the present thesis was to do both experiments and theoretical analysis and to accept both measured temperatures and measured pressures as accurate subject to the uncertainty estimates given in Chapter 6. If both pad shape and temperatures agreed with the theoretical predictions, then the magnitudes of the film thicknesses predicted by GENMAT were considered to be quite accurate. This rather pragmatic approach provided some useful insights into the physics of thrust bearing performance and, more importantly, permitted design changes to be proposed which had a much better chance of success than if they had been based on theory or experiment alone.

For the sake of clarity in the present chapter, the key details of all cases are listed in Table 8.1 on the following page and all figures are placed at the end. Furthermore, the various cases are organized into groups to permit comparisons of specific bearing features. Cases 1 and 2 in Table 8.1 have been examined in Chapter 6 but they are included in the present chapter for some of these comparisons. The references to **figures** are placed in **bold type**. This organizational structure is required to allow 24 cases to be presented in various groupings and interpreted.

Case / Conditions	1	2	3	4	5	6
Load (kN/pad)	177	177	177	177	177	177
Rotational speed (rad/s)	52.4	31.4	31.4	31.4	31.4	31.4
Lubricant ISO* grade	46	32	32	32	32	46
Oil pot temperature (°C)	70	70	70	70	70	70
Overall pad thickness (mm)	41.1	30.2	30.2	41.1	30.2	41.1
Number of springs	15	12	15	15	11	15

Case / Conditions	7	8	9	10	11	12
Load (kN/pad)	177	177	177	177	177	177
Rotational speed (rad/s)	31.4	31.4	31.4	31.4	31.4	31.4
Lubricant ISO* grade	68	46	68	32	32	46
Oil pot temperature (°C)	70	70	70	40	50	60
Overall pad thickness (mm)	41.1	30.2	30.2	41.1	41.1	41.1
Number of springs	15	12	12	15	15	15

Case / Conditions	13	14	15	16	17	18
Load (kN/pad)	177	177	44	77	111	144
Rotational speed (rad/s)	31.4	31.4	52.4	52.4	52.4	52.4
Lubricant ISO* grade	32	32	46	46	46	46
Oil pot temperature (°C)	50	90	70	70	70	70
Overall pad thickness (mm)	30.2	30.2	41.1	41.1	41.1	41.1
Number of springs	12	12	15	15	15	15

Case / Conditions	19	20	21	22	23	24
Load (kN/pad)	44	111	177	177	177	177
Rotational speed (rad/s)	52.4	52.4	52.4	20.9	41.9	20.9
Lubricant ISO* grade	32	32	32	46	46	32
Oil pot temperature (°C)	70	70	70	70	70	70
Overall pad thickness (mm)	30.2	30.2	30.2	41.1	41.1	30.2
Number of springs	12	12	12	15	15	12

*International Standards Organization

Table 8.1. Cases examined in the present chapter

8.1 Geometry

Two major modifications of thrust bearing geometry were investigated. One was the thickness of the pads; the other was the arrangement and number of springs that supported each pad. These geometric features were considered to have the most influence on thrust bearing performance.

8.1.1 Pad Thickness

The thickness of the thrust bearing pads used in many of the experiments was about the same as the thickness of the thrust bearing pads used by GE Hydro in commercial service. However, because these test bearing pads were smaller both radially and circumferentially, they were much stiffer in bending than the bearing pads in service.

The bending of the spring-supported bearing pads under the influence of both the imposed film pressure distribution and internal temperature distribution was a complex phenomenon. The dimensionless groups that characterized the bending behaviour were not known and were not sought in the present investigation. However, a ratio of pad arc length at the geometric mean radius (radius that divides the sector pad into equal inner and outer areas) to the thickness of the steel in the pad (L/t) was used to provide an indication of the thrust bearing stiffness in bending. Most of the thrust bearings used by GE Hydro have this ratio in the range of 7 - 11 (Table 8.2). However, many of the bearings used in the experiments had a ratio of 5.17 (200.7 mm/38.8 mm). In order to have test bearing pads that were somewhat more representative of the stiffness of the bearings in the field, the thickness of the steel in the pad was decreased from 38.8 to 27.9 mm (the 2.3 mm surface layer of Babbitt was not considered to be important to bending). This reduced pad thickness was the minimum possible to accommodate the pressure taps and thermocouples needed to collect the data. With a ratio of 7.19, this pad fell within the range found in the bearings in the field and this suggested that an examination of the

influence of pad thickness on film thickness, temperature and pressure would have some relevance to bearings in the field (Table 8.2).

Site*	L (mm)	t (mm)	Ratio (L/t)
Churchill Falls	350.5	39.6	8.85
Furnas	330.2	39.6	8.34
Kootenay Canal	386.1	39.6	9.75
Guri I	434.3	39.6	10.97
Mica Creek	406.4	39.6	10.26
Grand Coulee	444.5	48.8	9.11
Long Spruce	401.3	39.6	10.13
Wreck Cove	259.1	36.6	7.08
Itumbiara	480.1	62.0	7.74
Mactaquac	439.4	39.6	11.10
La Grande II	391.2	39.6	9.88
Guri II**	416.6 416.6	30.2 64.5	13.79 6.46
Balsam Meadow**	320.0 320.0	36.3 50.8	8.82 6.30
Limestone	406.4	39.6	10.26
Bad Creek**	411.5 411.5	36.3 50.8	11.34 8.10
Guavio	388.6	40.9	9.50
Brisay	436.9	48.8	8.95
Gehe Yan**	431.8 431.8	36.1 50.0	11.96 8.64
THP	426.7	40.4	10.56
Test Bearing Case 3	**200.7**	**38.9**	**5.17**
Test Bearing Case 4	**200.7**	**27.9**	**7.19**

Note: t = Pad steel thickness
L = Pad arc length at the geometric mean radius

*site names used internally by GE Hydro
**these sites had two different bearing geometries

Table 8.2 Comparison of the geometry of bearings in the field with those used in Cases 3 and 4

Cases 3 and 4 had all conditions the same except the pad thickness (Table 8.3) and thus comparing them allowed an examination of the influence of pad thickness. The film thickness, temperature and pressure values were measured and predicted for each case and plotted together (**Figure 8.1**). The more flexible thinner pad could be modelled as well as the thicker pad by GENMAT since the predicted pad shape and temperatures both showed quite good agreement with experimental measurements. Therefore, the GENMAT predictions of film thicknesses were considered to be quite accurate.

The thicker pad had a larger film thickness over the outer inlet region, thus allowing more oil to flow between the runner and the thrust bearing pads (**Figure 8.1a**). The GENMAT predictions of film thickness showed somewhat more variation for the thinner pad, presumably because it was more flexible. Interestingly, the experiments with Probe 4 suggested that the thinner pad had a larger film thickness while the GENMAT predictions gave the opposite result. As discussed earlier, the GENMAT predictions were more accurate than the measured film thicknesses and thus the thinner pad had lower film thickness at the Probe 4 location (outer circumference of the bearing).

Case / Conditions	3	4
Load (kN/pad)	177	177
Rotational speed (rad/s)	31.4	31.4
Lubricant ISO grade	32	32
Oil pot temperature (°C)	70	70
Overall pad thickness (mm)	**30.2**	**41.1**
Number of springs	15	15

Table 8.3. Cases to examine the influence of pad thickness

Based on the measurements, the temperatures for the thinner pad were higher than those of the thicker pad (**Figure 8.1b**). In the radial direction, the temperatures of the thinner pad increased to reach a maximum at the outer edge, whereas those of the thicker pad reached a maximum in the middle of the pad. This higher temperature at the outer

edge suggested an increase in local energy generation because of higher shear rates and a lower local viscosity, both of which suggested lower film thickness at the outer edge for the thinner pad. These lower film thickness values were predicted by **GENMAT (Figure 8.1a)**.

According to the measurements, the thicker pad had higher pressures in the central region and thus a less uniform distribution than the thinner pad (**Figure 8.1c**). Since the film thickness distributions were fairly similar, rotor crowning might have been more extensive for the thicker pad. Such crowning could be caused by an increase and then a decrease in rotor temperature when moving out in the radial direction. This suggestion was consistent with the temperatures of the thicker pad being higher in the central region than at the outer edge.

Findings

- The numerical predictions were accurate for the 26.5% thinner pad despite its increased flexibility.
- The thinner pad had slightly lower film thicknesses along the outer edge, higher temperatures throughout the pad and a more uniform pressure distribution.

8.1.2 Spring Arrangement

Two spring arrangements were examined for each of two values of pad thickness (Table 8.4). In Group 1 with overall pad thickness values of 41.1 mm, 15 and 11 springs were used while in Group 2 with overall pad thickness values of 30.2 mm, 12 and 15 springs were used. The geometric arrangement of these various numbers of springs was described in Chapter 4. The general strategy for reducing the number of springs from 15 was to remove them from the leading edge of the pad, especially the outer leading edge. This strategy encouraged the pad to tilt, allowing more oil to flow in and thus reduce the pad temperature.

Group	1		2	
Case Conditions	4	5	2	3
Load (kN/pad)	177	177	177	177
Rotational speed (rad/s)	31.4	31.4	31.4	31.4
Lubricant ISO grade	32	32	32	32
Oil pot temperature (°C)	70	70	70	70
Overall pad thickness (mm)	41.1	41.1	30.2	30.2
Springs (numbers)	**15**	**11**	**12**	**15**

Table 8.4. Cases and groups to examine the influence of spring arrangement.

In both groups, the agreement between experiment and theory for pad shape was good but there were minor discrepancies in Probe 4 of Group 1 (**Figure 8.2a**) and Probes 3 and 4 of Group 2 (**Figure 8.3a**). For the magnitudes of the film thicknesses in Group 2, the *digital analyzer* gave film thickness magnitudes that were closer to GENMAT predictions than those obtained for Case 3, when the *analogue recorder* was used to collect the data. The agreement for temperature was very good for Group 1 (**Figure 8.2b**) but not quite so good for Group 2 (**Figure 8.3bi and 8.3bii**). Consequently, comparisons of the GENMAT predictions of film thickness were considered to be accurate for Group 1 but somewhat less accurate for Group 2.

The removal of springs from the leading edge (11 and 12 spring arrangements) caused an increase in the circumferential tilt of the pad that increased inlet edge film thicknesses (**Figure 8.2a** and **8.3a**). The increased inlet edge film thickness was significant. For Group 1 and 2, the GENMAT predictions suggested an increase of about 55 μm. For the inside trailing edge of Group 2, the film thickness was about 10 μm larger for the 12 compared with the 15 spring arrangement. However, since the accuracy was not so good for Group 2, it was not certain that this difference actually occurred. In all other comparisons in both Groups 1 and 2, trailing edge film thicknesses were about the same.

The temperatures for the arrangements with the reduced number of springs were always lower (**Figure 8.2b** and **8.3b**). These lower temperatures were a consequence of the much higher film thicknesses at the leading edge for all of the cases with less than 15 springs.

Significant differences in the measured pressure distributions were observed. Both groups indicated that for the reduced number of springs, the higher pressures moved towards the trailing edge (**Figure 8.2c** and **8.3c**). Also, the pressure distributions were more uniform for the 15 spring arrangements.

Findings

- Reducing the number of springs caused larger film thicknesses at the leading edge of the pad and lower temperatures throughout the pad but about the same film thicknesses at the trailing edge of the pad.
- Reducing the number of springs shifted the peak pressures towards the trailing edge of the pad and made the pressure distributions less uniform.

8.2 Lubricant

The thermohydrodynamic lubrication of large spring-supported thrust bearings depended on the oil properties of viscosity and density along with the constants defining the variation of each with temperature, plus specific heat and thermal conductivity. GE Hydro used the Teresso turbine oils (Imperial Oil Ltd., Sarnia, ON) and had two ways of varying lubricant properties. By selecting different ISO grades (32, 46 or 68) they could obtain progressively higher viscosities at a particular temperature and somewhat different values for the other properties of the lubricating oil. By controlling oil pot temperatures to different values, they could set and maintain different viscosities of oil in the oil pot which had an influence on oil viscosity throughout the fluid film. It was expected that oil viscosity would be the most important oil property but the manifestation of its influence was difficult to anticipate because it varied with local temperature which was itself linked to the entire thermohydrodynamic phenomenon (including thermoelastic pad deflections).

8.2.1 ISO Oil Grades

For the experiments, the lubrication oils were conveniently classified by their ISO grades (32, 46 and 68) that indicated their temperature-viscosity behaviour. However, the precise temperature-viscosity behaviours of these oils were specified by the manufacturer in accordance with the ASTM (American Society for Testing Materials) procedures (Table 8.5a). The numerical analysis employed Vogel's equation

$$\eta = Ke^{\frac{C}{T+\theta}}$$

where K, C and θ were constants determined from the specification data. The actual procedure for finding the constants was tedious as described in Ferguson *et al* (1998).

Because of this tedious calculation procedure, the GENMAT software package converted specification data for a particular set of lubricating oils that were graded as ISO 32, 46 and 68 to yield Vogel's constants (Table 8.5b) and permitted the user to characterize the oil by ISO grade alone. As mentioned in Chapter 6, this introduced an error because the actual lubricating oils had different Vogel's constants (Table 8.5c) and somewhat different viscosities at various temperatures (Table 8.5d). The effect of this error on the accuracy of the present numerical analysis of thrust bearing performance is considered in subsequent discussion.

	Temperature (°C)	ISO Grade		
		32	46	68
ν (cSt)	40	33.5	48.0	68.0
ν (cSt)	100	5.45	6.70	8.20
ρ (g/mL)	15	0.868	0.868	0.876

Note: ν = kinematic viscosity, cSt ≡ mm^2/s, ρ = density, g/mL ≡ 0.001 kg/m^3

Table 8.5a. Specification of oils used in the experiments

ISO Oil grade	Vogel's Constants		
	K (mPa s)	C (°C)	θ (°C)
32	0.06340	878.4	104.3
46	0.1354	670.9	77.85
68	0.09219	830.3	88.30

Table 8.5b. Vogel's constants of the oils used in the numerical analysis

ISO Oil grade	Vogel's Constants		
	K (mPa s)	C (°C)	θ (°C)
32	0.05799	867.2	99.88
46	0.05456	910.2	97.38
68	0.05080	957.0	95.77

Table 8.5c. Vogel's constants of the oils used in the experiments

Temperature (°C)	Viscosity (mPa s)					
	32		46		68	
	Expt	Analysis	Expt	Analysis	Expt	Analysis
80	7.20	7.45	9.23	9.49	11.8	12.8
90	5.58	5.83	7.02	7.37	8.77	9.71
100	4.44	4.67	5.49	5.89	6.74	7.58

Table 8.5d. A comparison of viscosities of oil used in the experiments with those used in the numerical analysis for some typical oil film temperatures

Experiments were performed with three ISO grades of oil for each of two values of pad thickness (Table 8.6). The cases in Group 3 had overall pad thickness values of 41.1 mm while those in group 4 had overall pad thickness of 30.2 mm.

Group	3			4		
Case / Conditions	4	6	7	2	8	9
Load (kN/pad)	177	177	177	177	177	177
Rotational speed (rad/s)	31.4	31.4	31.4	31.4	31.4	31.4
Lubricant ISO grade	**32**	**46**	**68**	**32**	**46**	**68**
Oil pot temperature (°C)	70	70	70	70	70	70
Overall pad thickness (mm)	41.1	41.1	41.1	30.2	30.2	30.2
Number of springs	15	15	15	12	12	12

Table 8.6. Conditions for various ISO grades of oil

In both groups, there was excellent agreement between experiment and theory for pad shapes with the exception of the outermost probe 4 (**Figure 8.4a** and **8.5a**). Also, the magnitudes of the film thickness were closer to GENMAT predictions for probes 1 and 3 of Group 4 (**Figure 8.5a**) in which the *digital analyzer* was used. The agreement for temperature was quite good for Group 3 (**Figure 8.4b**) but not so good for Group 4 (**Figure 8.5bi** and **8.5bii**). It was interesting to note that Group 4 showed almost identical temperatures for ISO grade 32 and 46. Consequently, comparisons for GENMAT predictions of film thickness were considered somewhat more accurate for Group 3 than Group 4.

For higher ISO grade and thus higher viscosity at a given temperature, the film thicknesses increased but only with about 2 μm between each grade for the more accurate Group 3 (**Figure 8.4a**) and about 5 μm between each grade for Group 4 (**Figure 8.5a**). Also, the pad surface temperatures increased by 2 – 5 °C between each grade (**Figures 8.4b, 8.5bi** and **8.5bii**). However, the measured pressures remained the virtually identical and thus independent of ISO grade (**Figures 8.4c** and **8.5c**)

One explanation for the lack of significant effect of lubricant ISO grade was the tendency of the higher ISO grade lubricants to increase heat generation in the film thus increasing temperature and decreasing the lubricant viscosity in the film. Therefore, the benefits of a higher lubricant viscosity associated with the higher ISO grade were mostly counteracted by the increased heat generation.

Also, the error of using lubricant viscosities in the numerical analysis that did not correspond exactly to those in the experiments (Table 8.5d) was considered unlikely to influence the accuracy much. Clearly, the large change in viscosity in moving from ISO grades 32 to 46 or 46 to 68 did not have much effect on film thickness, temperature or pressure. This confirmed the opinion in Chapter 6 and in Ferguson et al (1998) that an accurate specification of lubricant viscosity was not essential to the accuracy of numerical predictions.

Findings

- Increasing ISO grade and the associated differences in lubricant viscosity at a given temperature did not cause much change in film thicknesses, pad surface temperatures or film pressures.
- Defining a lubricant by its ISO grade alone rather than its Vogel's constants or ASTM specifications did not introduce a significant error into the calculations of the present thesis.

8.2.2 Oil Pot Temperature

Experiments were performed (Table 8.7) with four oil pot temperatures for Group 5 (Cases 10, 11, 12 and 4) with an overall pad thickness of 41.1 mm and three oil pot temperatures for Group 6 (Cases 13, 2 and 14) with an overall pad thickness of 30.2 mm.

Group	5				6		
Case / Condition	10	11	12	4	13	2	14
Load (kN/pad)	177	177	177	177	177	177	177
Rotational speed (rad/s)	31.4	31.4	31.4	31.4	31.4	31.4	31.4
Lubrication ISO grade	32	32	32	32	32	32	32
Oil pot temperature (°C)	**40**	**50**	**60**	**70**	**50**	**70**	**90**
Overall pad thickness (mm)	41.1	41.1	41.1	41.1	30.2	30.2	30.2
Springs (numbers)	15	15	15	15	12	12	12

Table 8.7. Conditions for various oil pot temperatures

The predicted pad shapes agreed quite closely with the measured ones (**Figure 8.6a** and **8.6b**) with two exceptions. Probes 4 of Group 5 in which the average slope of the measured surface profiles were larger than the predicted values and Probe 3 of Group 6 in which the average slope of the measured surface profiles were smaller than the predicted values. As usual the magnitudes of the measured film thickness values were lower than GENMAT predictions for Group 5 in which the *analogue recorder* was employed but showed similar values in Group 6 in which the *digital analyser* was employed. The temperatures showed remarkably good agreement for both groups (**Figure 8.6b**, **8.7bi** and **8.7bii**). Consequently, the predictions of film thickness made by GENMAT were considered to be very accurate for both groups. As with the different ISO grades, oil pot temperature had no effect on the pressure distribution (**Figure 8.6c** and **8.7c**)

Increasing the oil pot temperature caused a small drop in film thicknesses (**Figures 8.6a** and **8.6b**) but quite large increases in pad temperatures (**Figures 8.6b**, **8.7bi** and **8.7bii**). However, temperatures rises along the pad in the circumferential direction decreased a little as oil pot temperature increased. This tendency was more pronounced when a larger range of oil pot temperatures was examined as in Ferguson *at al* (1998).

Also, power losses decreased as discussed by Ferguson et al (1998). This behaviour was quite similar to the influence of the ISO grade in that higher oil pot temperatures caused lower film viscosities and thus lower film thicknesses. The lower ISO grades had a similar effect but lower pad temperatures.

Findings

- Higher oil pot temperatures caused a small drop in film thickness.

8.3 Load and Rotational Speed

Since loads and rotational speeds varied for bearings in the field, the influence of these conditions on bearing performance was considered important.

8.3.1 Load

Loads from 44 kN/pad to 177 kN/pad were imposed on the pad (Table 8.8) while holding rotational speed constant at 52.4 rad/s for Group 7 and 30.2 rad/s for Group 8. Also, Group 7 had an overall pad thickness of 41.1 mm, an ISO 46 lubricant and 15 springs whereas Group 8 had an overall pad thickness of 30.2 mm, an ISO 32 lubricant and 12 springs.

Group	7					8		
Case / Condition	15	16	17	18	1	19	20	21
Load (kN/pad)	**44**	**77**	**111**	**144**	**177**	**44**	**111**	**177**
Rotational speed (rad/s)	52.4	52.4	52.4	52.4	52.4	52.4	52.4	52.4
Lubricant ISO grade	46	46	46	46	46	32	32	32
Oil pot temperature (°C)	70	70	70	70	70	70	70	70
Pad thickness (mm)	41.1	41.1	41.1	41.1	41.1	30.2	30.2	30.2
Number of springs	15	15	15	15	15	12	12	12

Table 8.8. Conditions for various loads

In Chapter 6, it was noted that at loads less than 177 kN/pad, there was considerable pad-to-pad variation in the measured film thickness. This behaviour was attributed to a number of spring loads not exceeding the pre-load. In the present section, however, lower loads (< 177 kN/pad) were studied. A pad was selected arbitrarily (number 11) and film thickness was always measured over it.

The measured pad shapes were quite close to the numerical predictions for Group 7 (**Figure 8.8a**) and with the exception of Probe 3 for 44 kN/pad (the lowest load) the same good agreement occurred for Group 8 (**Figure 8.9a**). As usual, the magnitudes of the film thicknesses were closer to GENMAT predictions for some of the Group 8 cases where the *digital analyser* was used. Except for the cases with the lowest load and in Group 8 with the highest load, the temperatures agreed quite well (**Figures 8.8b**, **8.9bi** and **8.9bii**). Taken as a whole, these observations suggested that the film thicknesses predicted by GENMAT might not be as accurate as in other sections. The measured pressures seemed quite consistent with lower loads giving lower pressures (**Figure 8.8c** and **8.9c**).

It did seem apparent that lower loads caused thicker fluid films, lower pad temperatures and lower film pressures. A sharp transition in the bearing performance was not found as the load dropped except perhaps for the lowest load. Thus, spring-supported thrust bearing performance could be predicted using GENMAT even though it did not represent the non-linear springs.

Findings

- Lower loads caused thicker films and both lower temperatures and lower pressures.
- GENMAT numerical predictions were quite close to numerical predictions even though the non-linear springs were not modelled.

8.3.2 Rotational Speed

Speed of 20.9 rad/s (200 rpm) to 52.4 rad/s (500 rpm) were imposed (Table 8.9). The overall pad thickness was 41.1 mm and the number of springs was 15 for Group 9 whereas overall pad thickness was 30.2 mm and the number of springs was 12 for Group 10.

Group	9				10		
Case / Condition	22	6	23	1	24	2	21
Load (kN/pad)	177	177	177	177	177	177	177
Rotational speed (rad/s)	**20.9**	**31.4**	**41.9**	**52.4**	**20.9**	**31.4**	**52.4**
Lubricant ISO grade	32	32	32	32	32	32	32
Oil pot temperature (°C)	70	70	70	70	70	70	70
Overall pad thickness (mm)	41.1	41.1	41.1	41.1	30.2	30.2	30.2
Springs (numbers)	15	15	15	15	12	12	12

Table 8.9. Conditions for various rotational speeds

The measured film shapes did not agree very well with numerical predictions for Group 9 (**Figure 8.10a**) but the agreement of both shape was quite good for Group 10, especially at the lower rotational speeds (**Figure 8.11a**). For both groups, increasing rotational speed caused the measured temperatures to exceed the numerical predictions (**Figure 8.10b**, **8.11bi** and **8.11bii**). As rotational speed increased, the measured pressures increased at the centre of the pad for both groups (**Figure 8.10c and 8.11c**)

Increased speed caused thicker films in the inlet side of the pad but the minimum film thicknesses did not change much. Also, the pad temperatures increased and at the lower speeds, the temperatures became almost constant at as little as 10 °C above the oil pot temperature. The predictions for film thickness for Group 9 were not considered very accurate, perhaps because the higher speeds caused thermal bending effects that were not well represented in the deflection model of GENMAT. The increased pressures at the centre of the pad with increased speed suggested that perhaps the enhanced thermal

effects caused rotor crowning as discussed in Chapter 6. Alternatively, the higher speeds might have caused regions of cavitation which did not carry load thus causing an increased central pressure to compensate.

Findings

- Higher rotational speeds cause increased pad temperatures that made it more difficult to obtain accurate numerical predictions from GENMAT.
- The higher rotational speeds caused thicker films in the inlet zone but did not affect the minimum film thickness much.
- As speed increased, the central film pressures became higher.

8.4 Concluding Remarks

The preceding experimental and theoretical investigations provided a great deal of information. However, certain findings would be particularly interesting to the designer of spring-supported thrust bearings.

A lower ISO grade of oil (46 or even 32) can be used in place of the usual ISO 68 oil without much change in film thickness, pad temperature or film pressure. Numerical predictions of GENMAT remain accurate for a pad with a shape similar to those found in the field. The minimum film thickness does not always increase when springs are removed from the leading edge, even though more lubricant is entrained into the inlet zone. The accuracy of the numerical predictions of GENMAT are reduced somewhat by higher rotational speeds. Finally, there is evidence throughout the present chapter that relatively thick minimum film thicknesses of about 15 - 20 μm are remarkably unaffected by changing pad thickness, spring packing, lubricant grade, oil pot temperature, load and rotational speed. This insensitivity may discourage the designer, to some extent, but it suggests that spring-supported thrust bearings are a robust, safe machine elements. Once the risk of fluid film breakdown is reduced, designers may be able to focus on reducing energy losses along with bearing size and manufacturing costs.

Figure 8.1a, b, c, Figure 8.2a, b, c, Figure 8.3a, b, c

(Geometry – Pad thickness and spring arrangement)

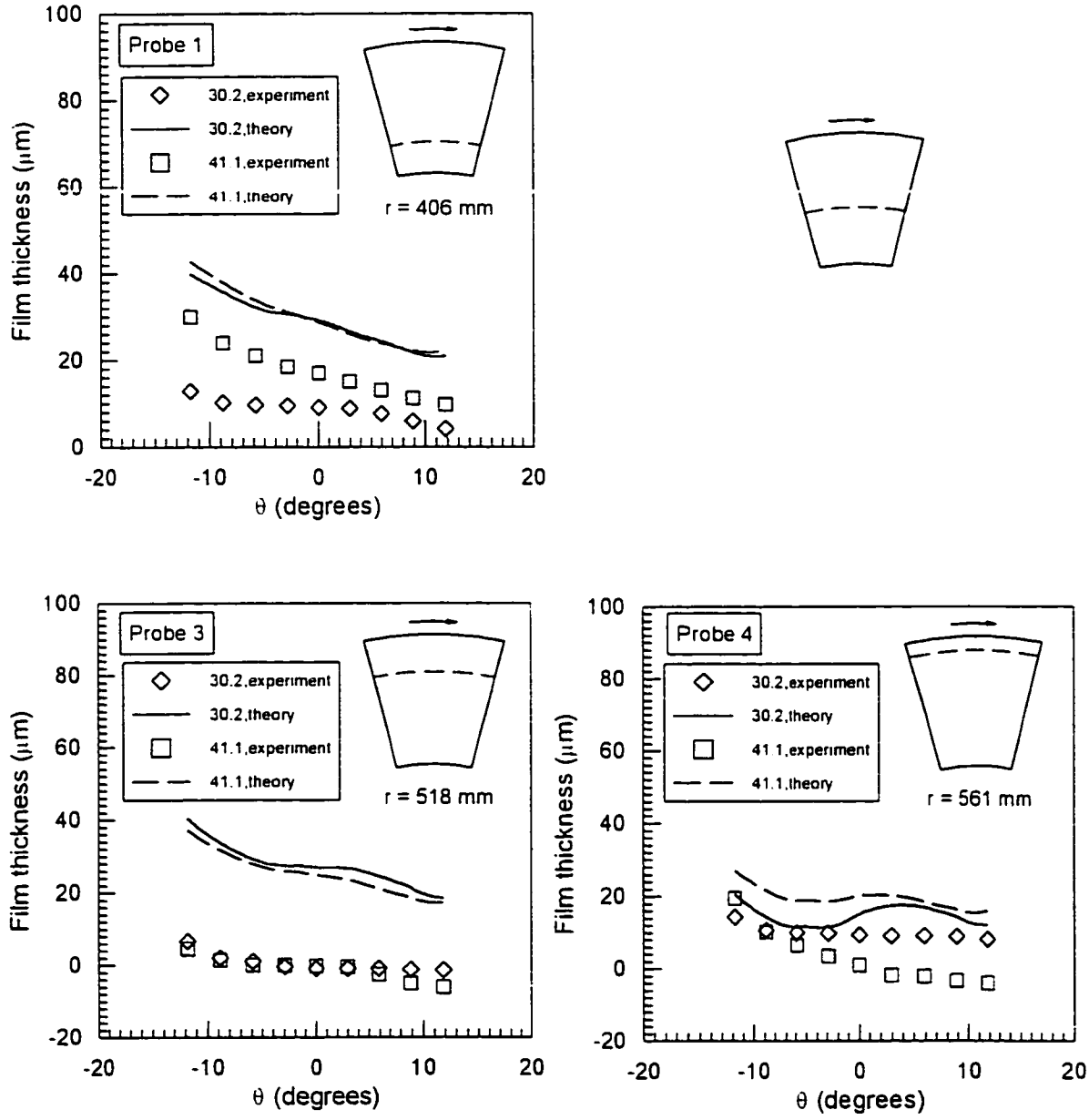

Figure 8.1a. Film thickness distribution for Cases 3 and 4 which had two different thicknesses of pads

(Numbers in the caption box are total pad thickness in mm)

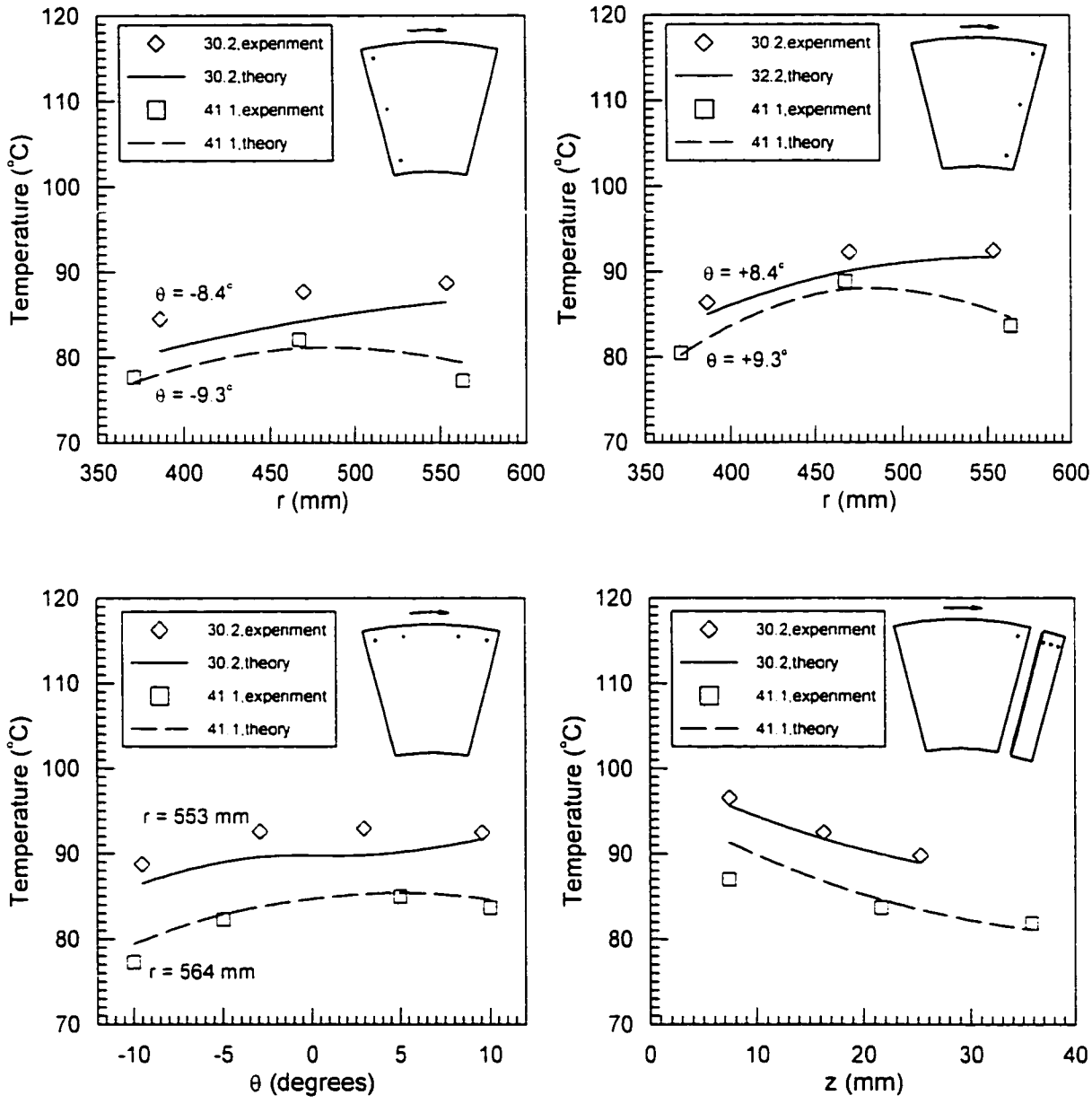

Figure 8.1b. Temperature distribution for Cases 3 and 4 which had two different thicknesses of pads

(Numbers in the caption box are total pad thickness in mm)

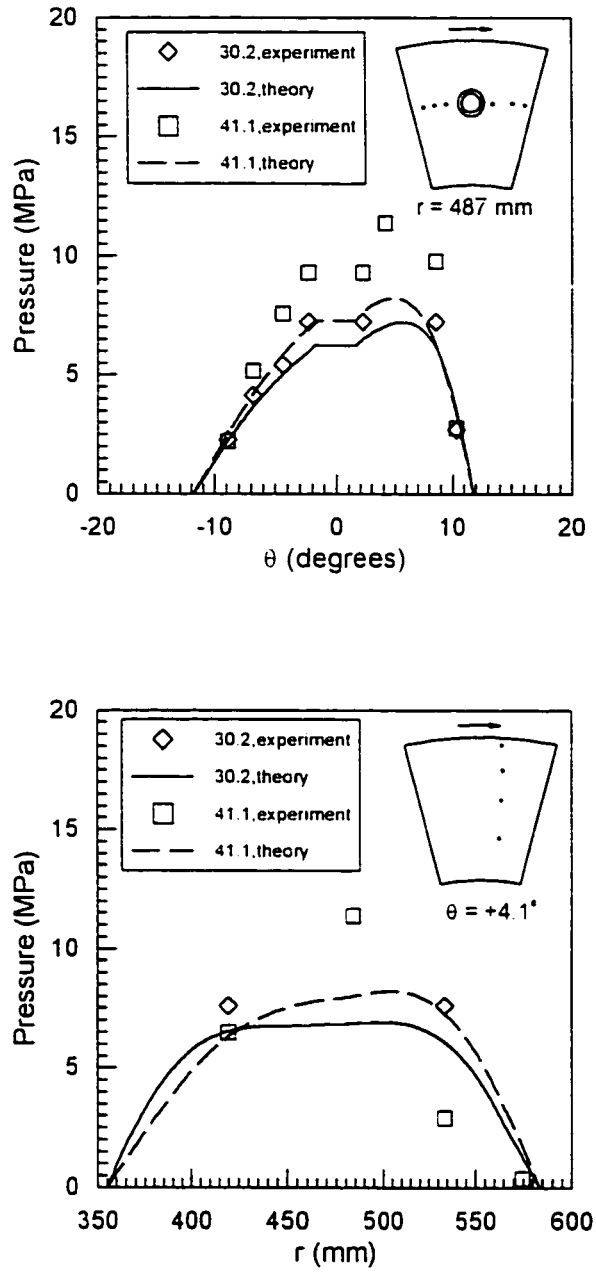

Figure 8.1c. Pressure distribution for Cases 3 and 4 which had two different thicknesses of pads

(Numbers in the caption box are total pad thickness in mm)

(For the thin pad, the central pressure probe was not functional)

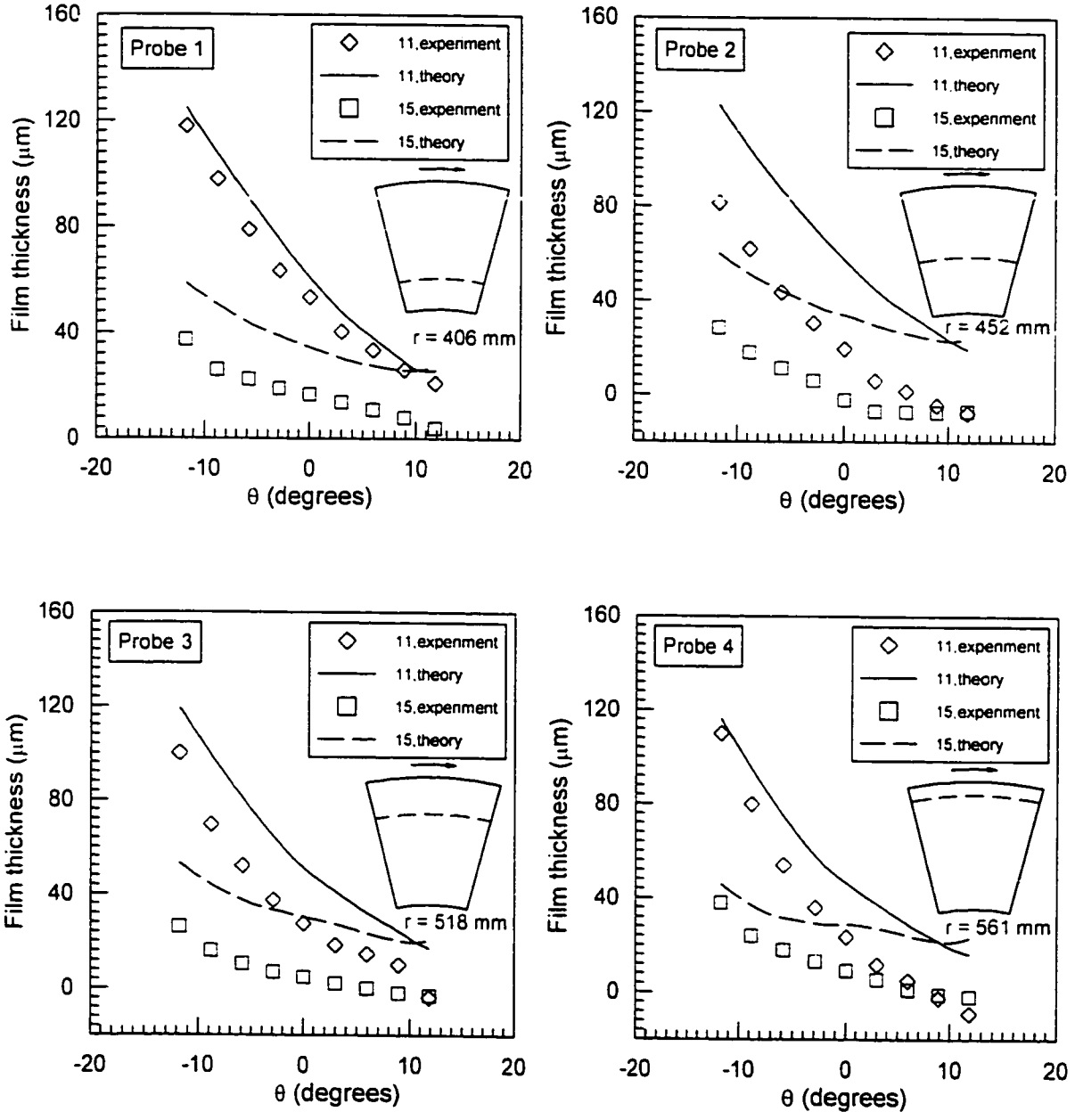

Figure 8.2a. Film thickness distribution for Group 1 (Cases 4 and 5) which had two different spring sets (11 and 15 springs) (Numbers in the caption box are spring numbers)

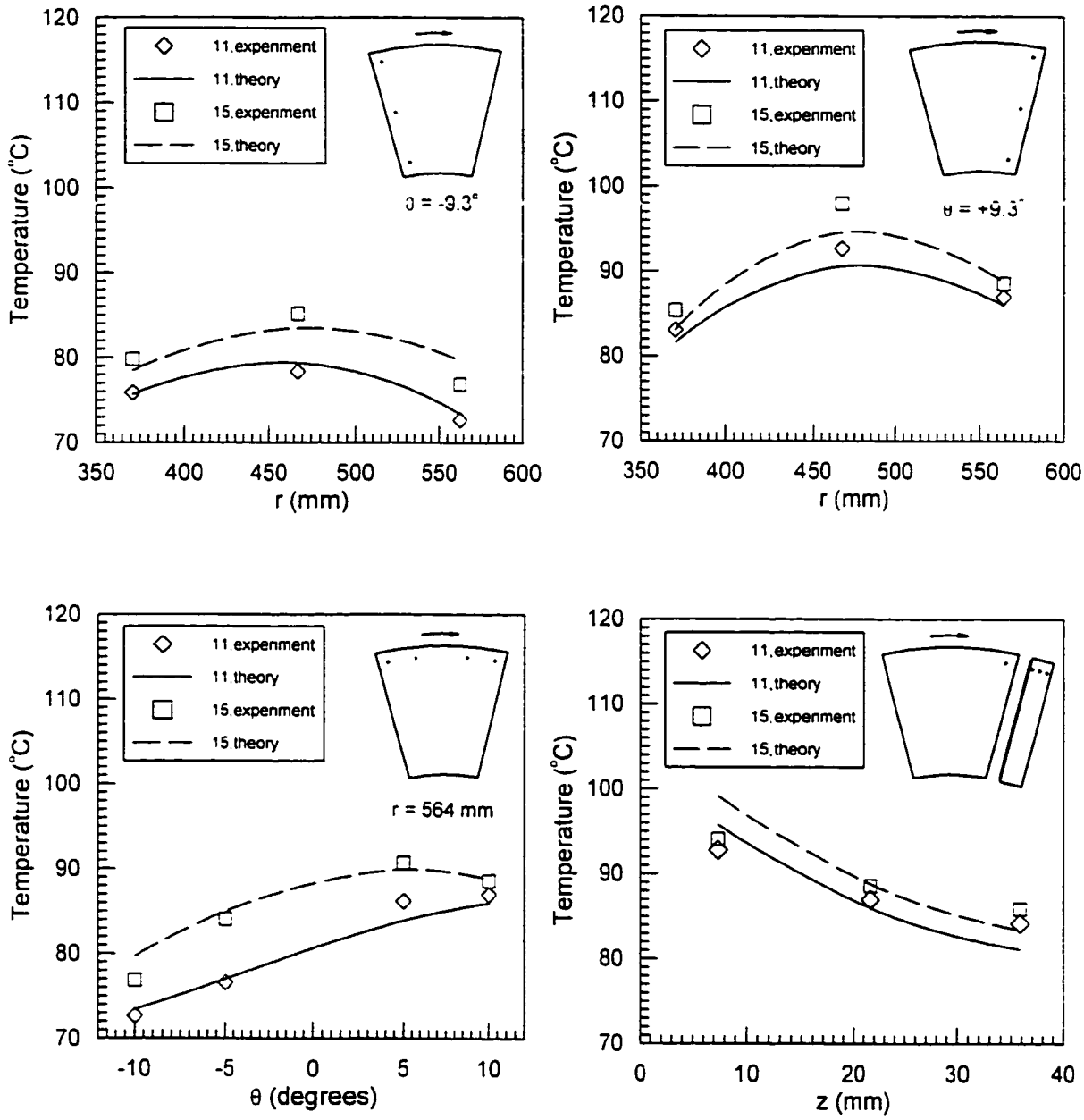

Figure 8.2b. Temperature distribution for Group 1 (Cases 4 and 5) which Had two different spring sets (11 and 15 springs) (Numbers in the caption box are spring numbers)

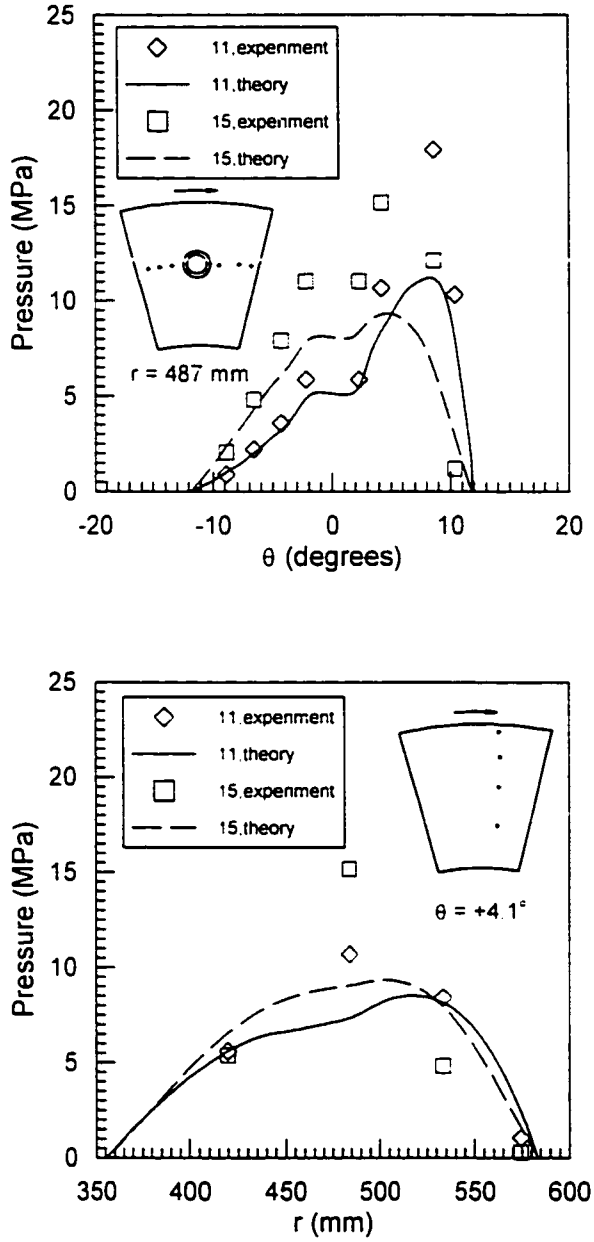

Figure 8.2c. Pressure distribution for Group 1 (Cases 4 and 5) which had two different spring sets (11 and 15 springs) (Numbers in the caption box are spring numbers)

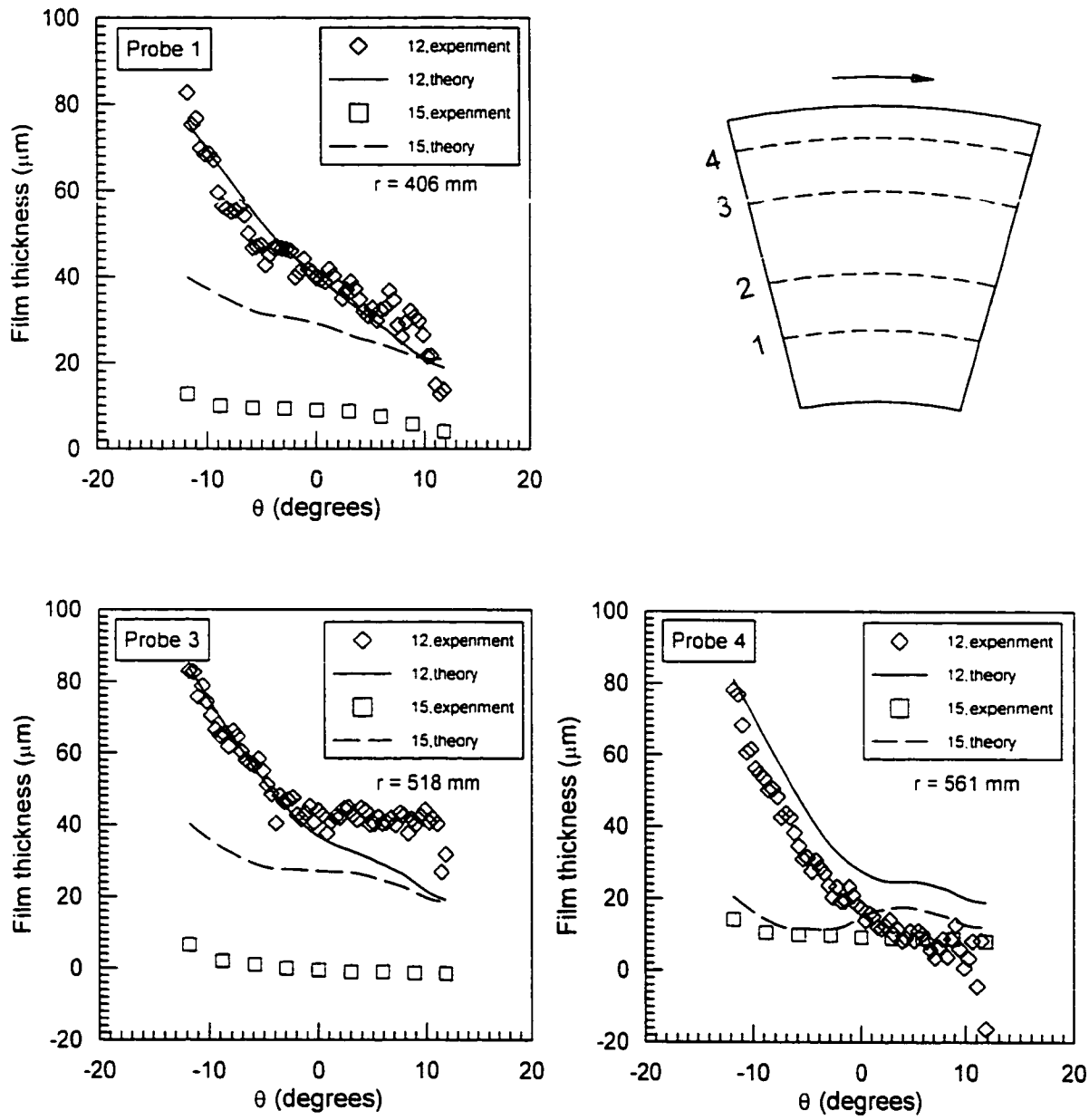

Figure 8.3a. Film thickness distribution for Group 2(Cases 2 and 3) which Had two different spring sets (12 and 15 springs) (Numbers in the caption box are spring numbers)

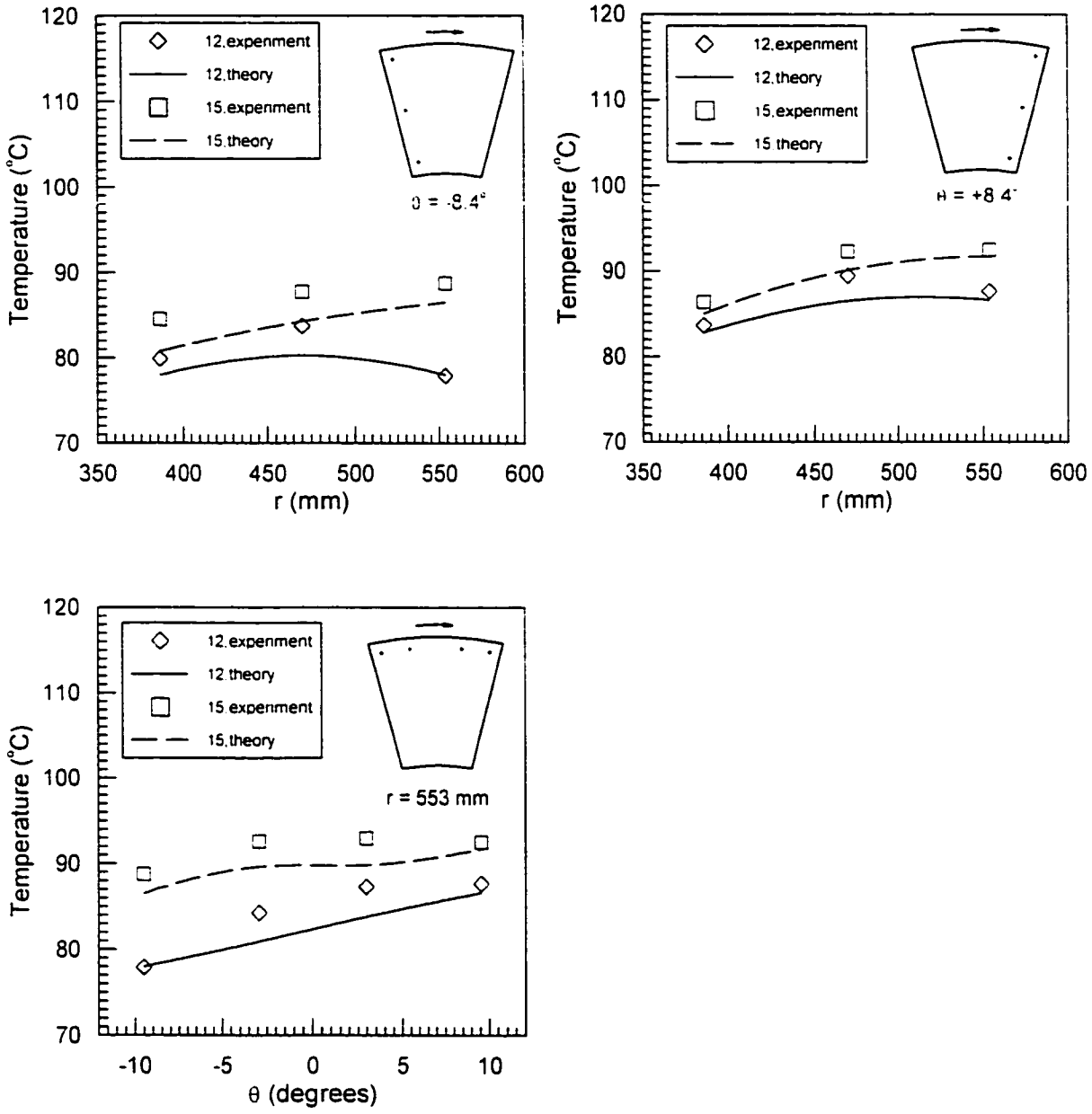

Figure 8.3bi. Temperature distribution for Group 2(Cases 2 and 3) which had two different spring sets (12 and 15 springs) (Numbers in the caption box are spring numbers)

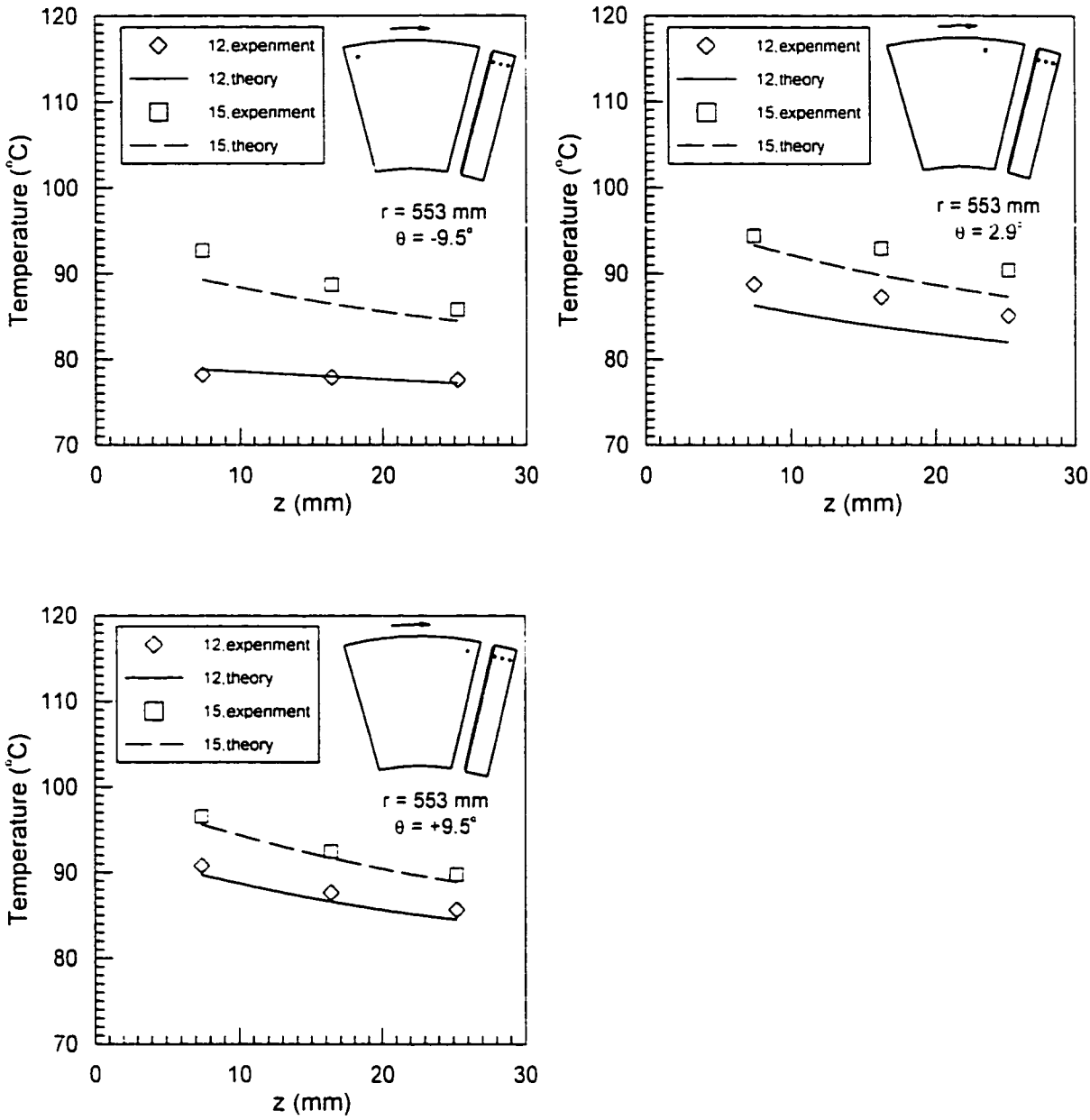

Figure 8.3bii. Temperature distribution for Group 2 (Cases 2 and 3) which had two different spring sets (12 and 15 springs)

(Numbers in the caption box are spring numbers)

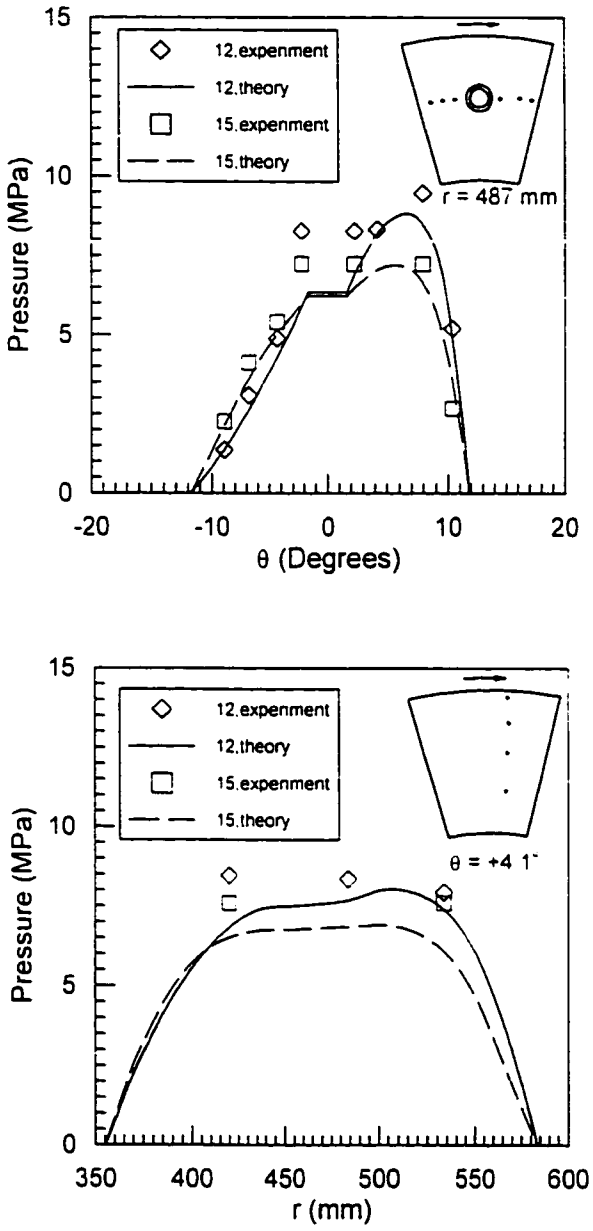

Figure 8.3c. Pressure distribution for Group 2 (Cases 2 and 3) which had two different spring sets (12 and 15 springs) (Numbers in the caption box are spring numbers)

Figure 8.4a, b, c, Figure 8.5a, b, c, Figure 8.6a, b, c, Figure 8.7a, b, c

(Lubricant – ISO grade and oil pot temperature)

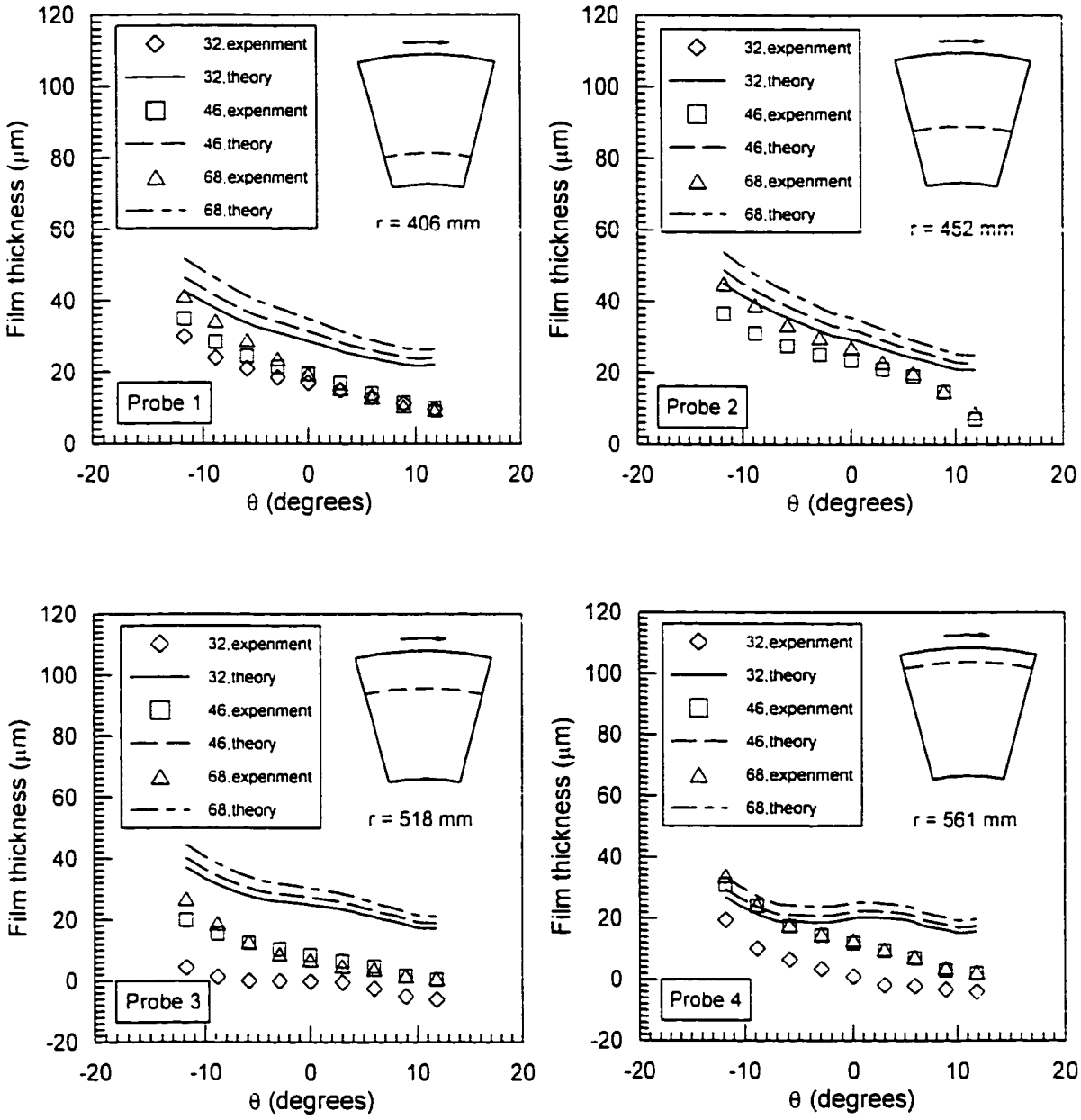

Figure 8.4a. Film thickness distribution for Group 3 (Cases 4, 6 and 7) which Had different ISO grades (32, 46 and 68)

(Numbers in the caption box are ISO grades)

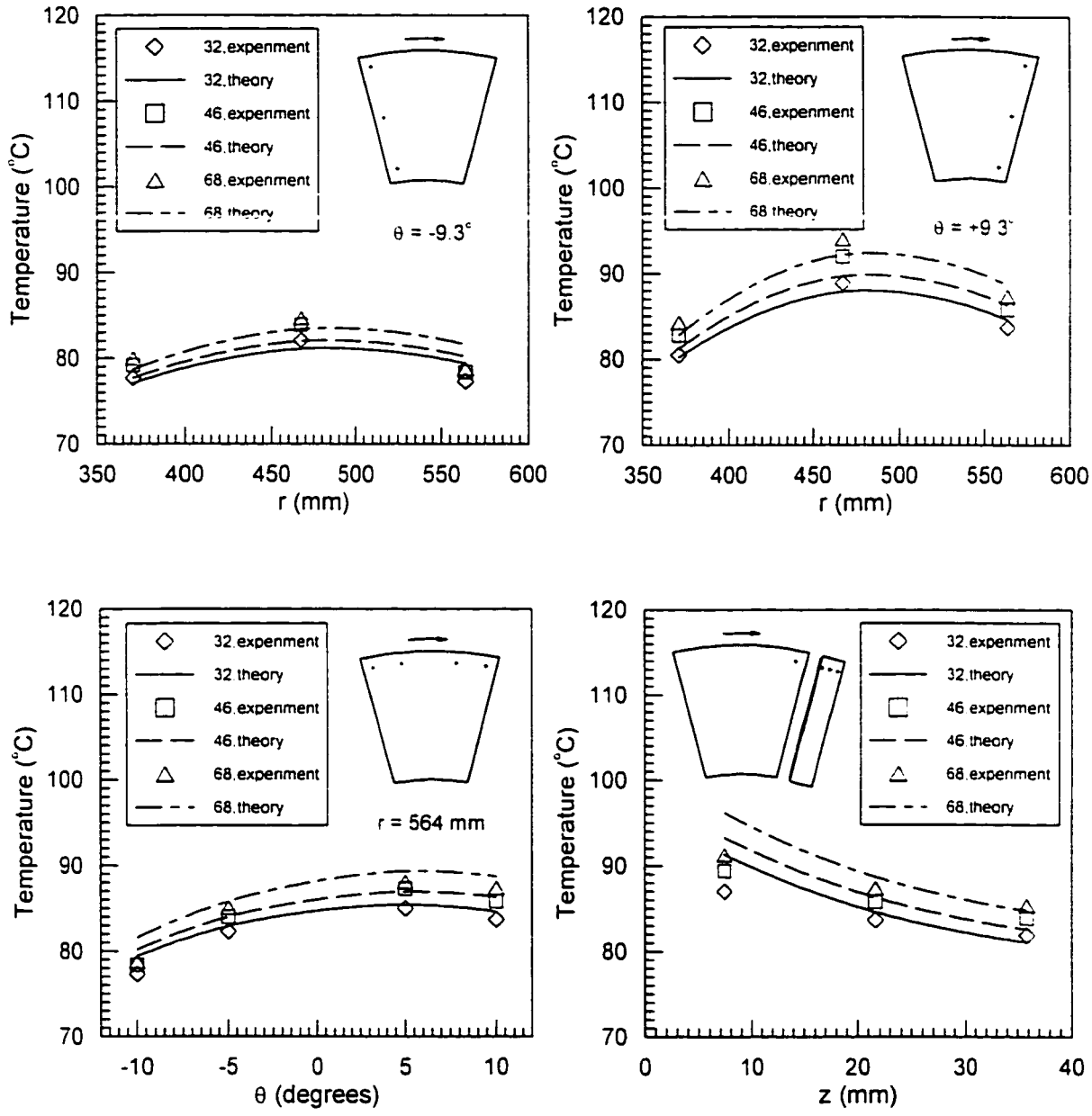

Figure 8.4b. Temperature distribution for Group 3 (Cases 4, 6 and 7) which had different ISO grades (32, 46 and 68)

(Numbers in the caption box are ISO grades)

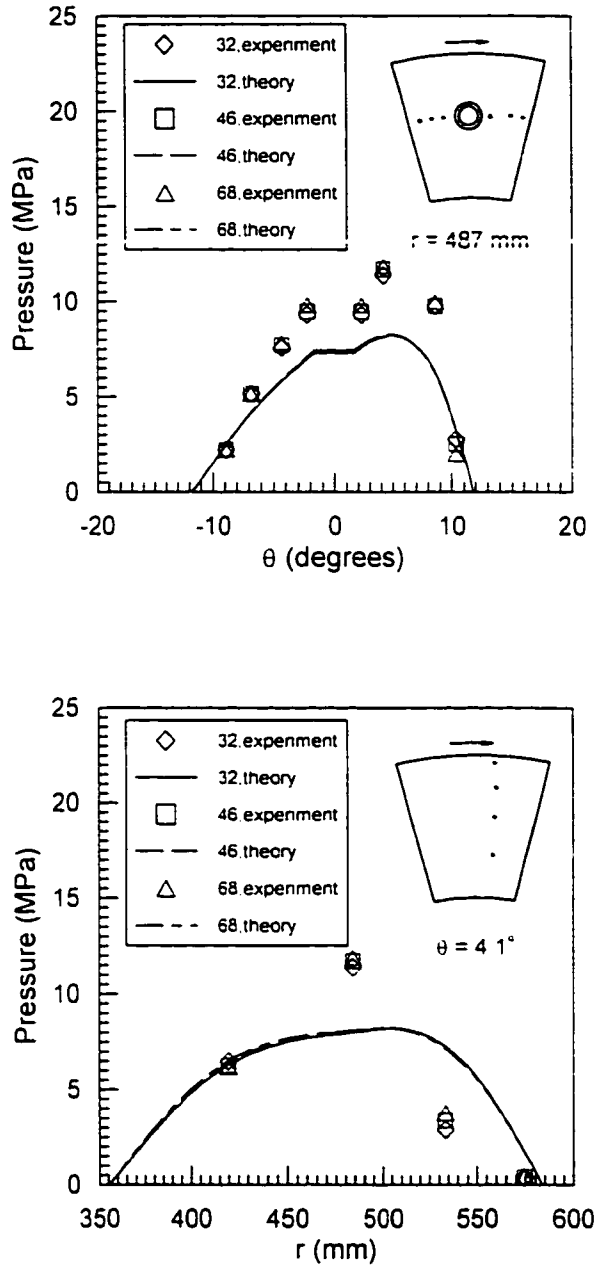

Figure 8.4c. Pressure distribution for Group 3 (Cases 4, 6 and 7) which had different ISO grades (32, 46 and 68)

(Numbers in the caption box are ISO grades)

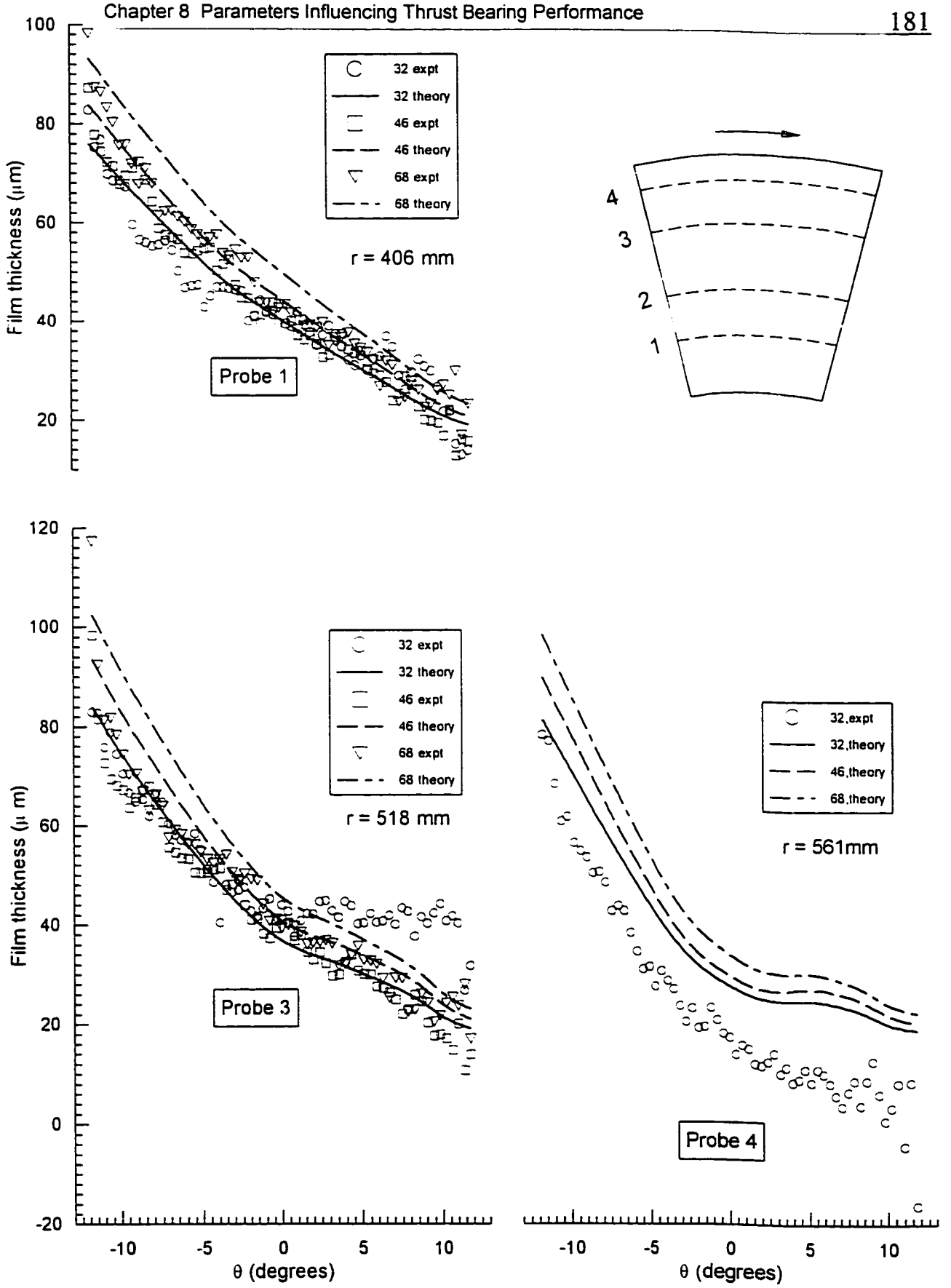

Figure 8.5a. Film thickness distribution for Group 4 (Cases 2, 8 and 9) which had different ISO grade (32, 46 and 68)

(Numbers in the caption box are ISO grades)

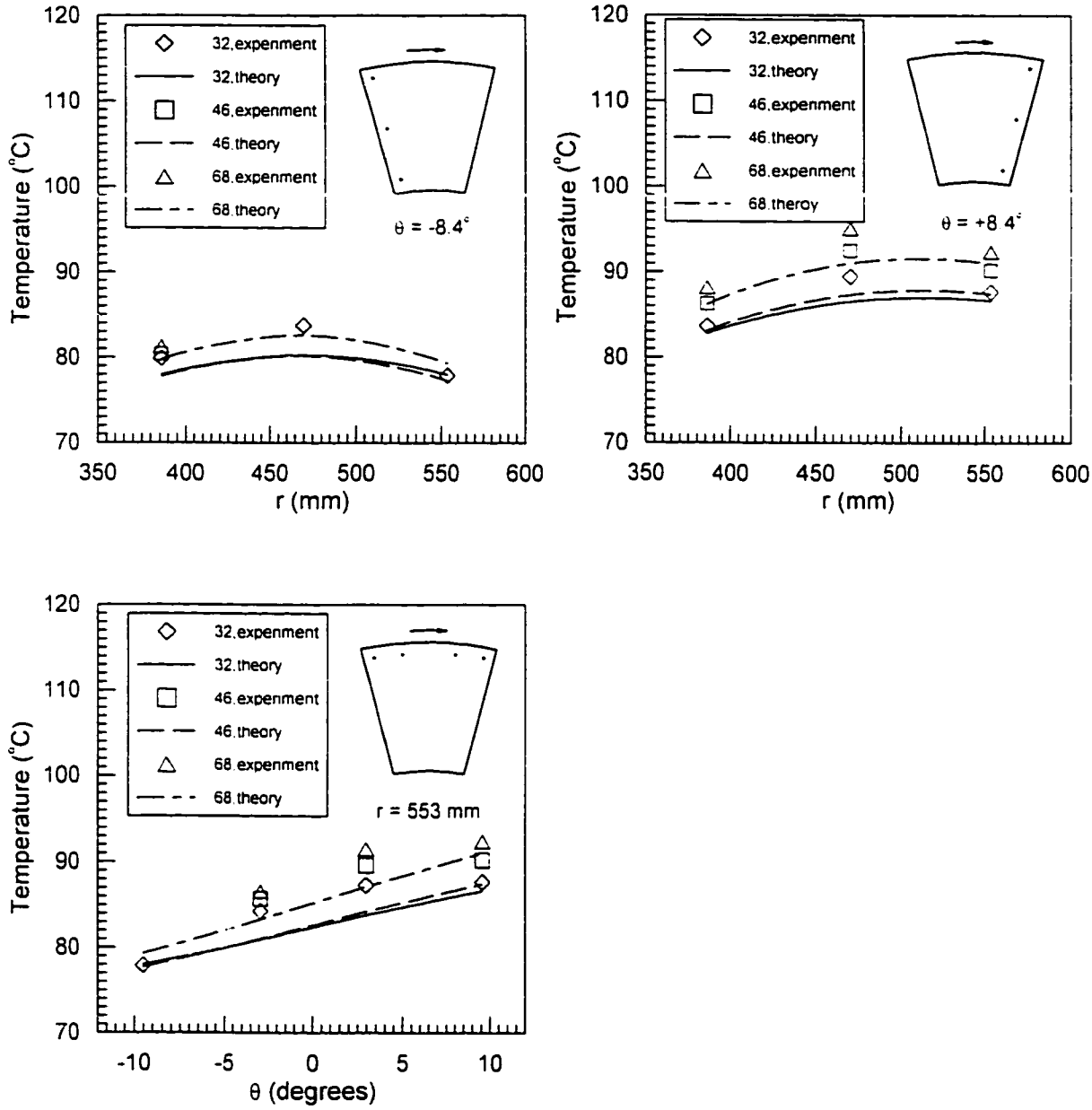

Figure 8.5bi. Temperature distribution for Group 4 (Cases 2, 8 and 9) which had different ISO grade (32, 46 and 68)

(Numbers in the caption box are ISO grades)

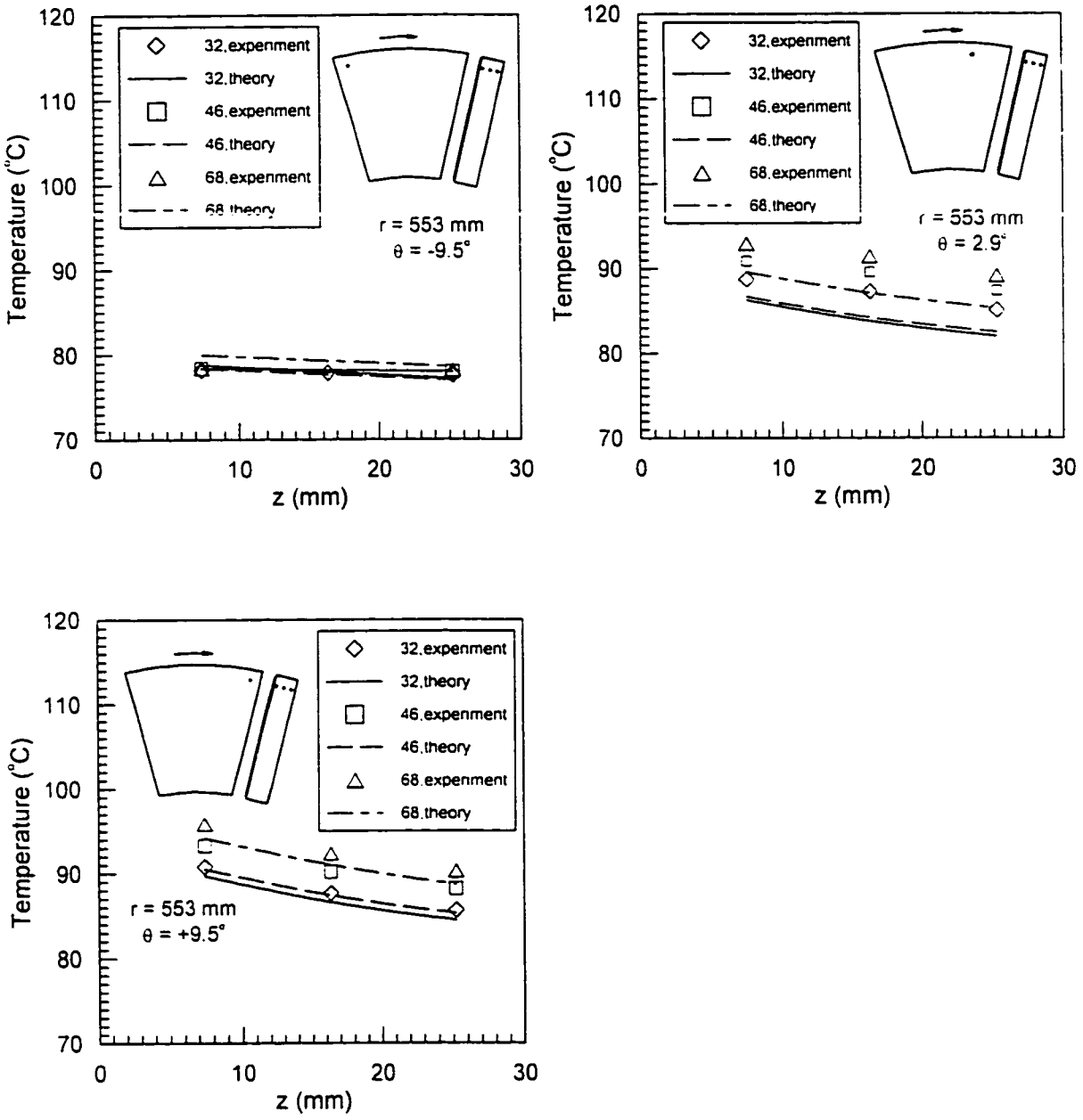

Figure 8.5bii. Temperature distribution through pad thickness for Group 4 (Cases 2, 8 and 9) which had different ISO grade (32, 46 and 68) (Numbers in the caption box are ISO grades)

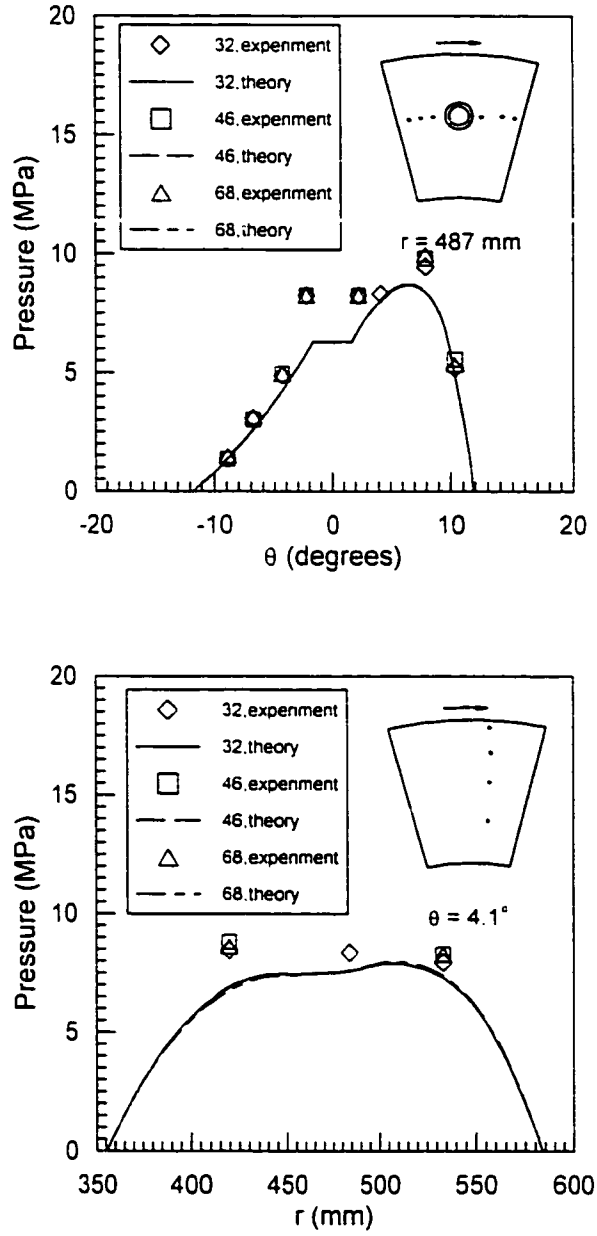

Figure 8.5c. Pressure distribution for Group 4 (Cases 2, 8 and 9) which had different ISO grade (32, 46 and 68)

(Numbers in the caption box are ISO grades)

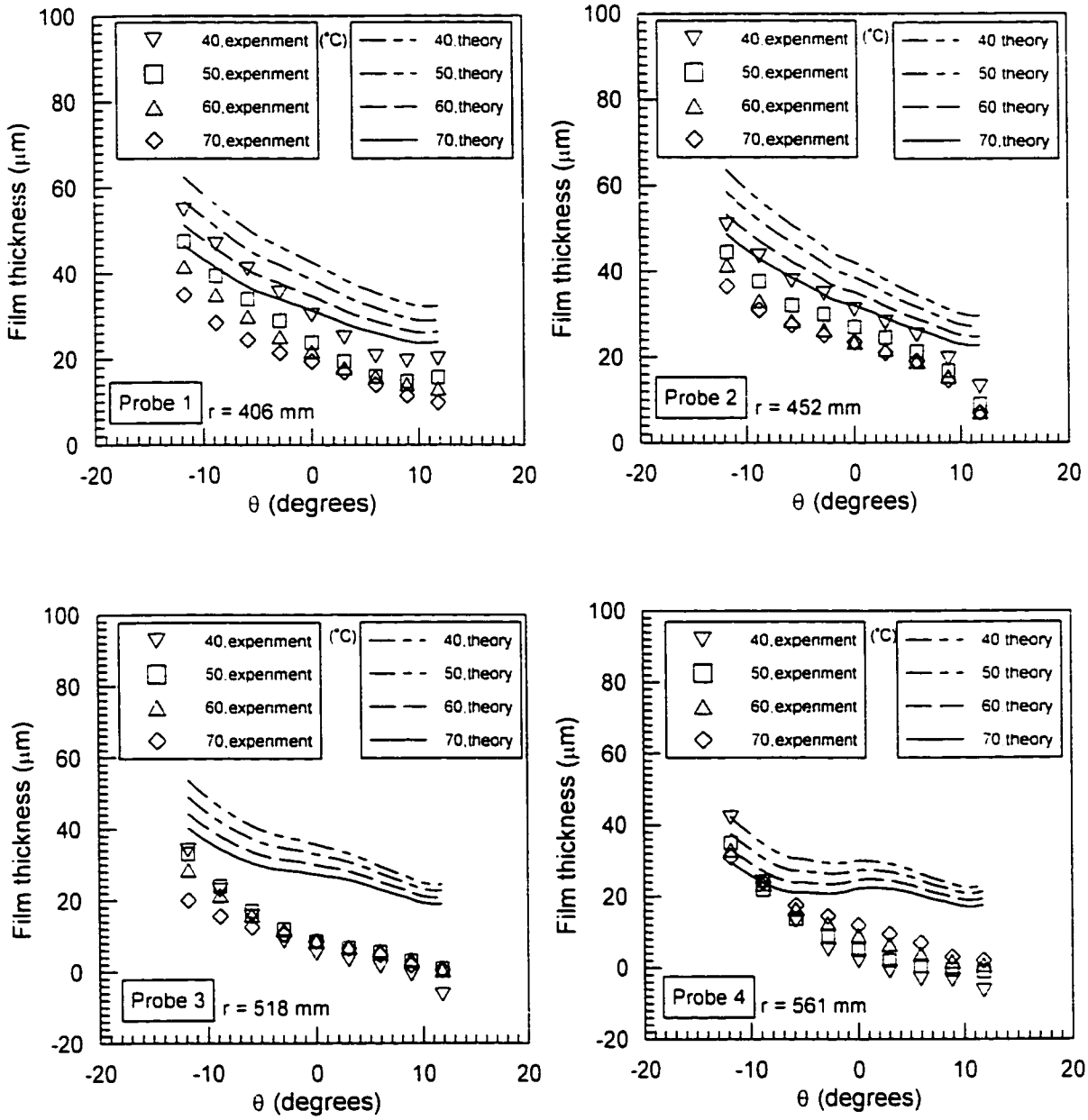

Figure 8.6a. Film thickness distribution for Group 5 (Cases 10, 11, 12, 4) which had different oil pot temperatures (40, 50, 60, 70 °C)

(Numbers in the caption box are temperatures in °C)

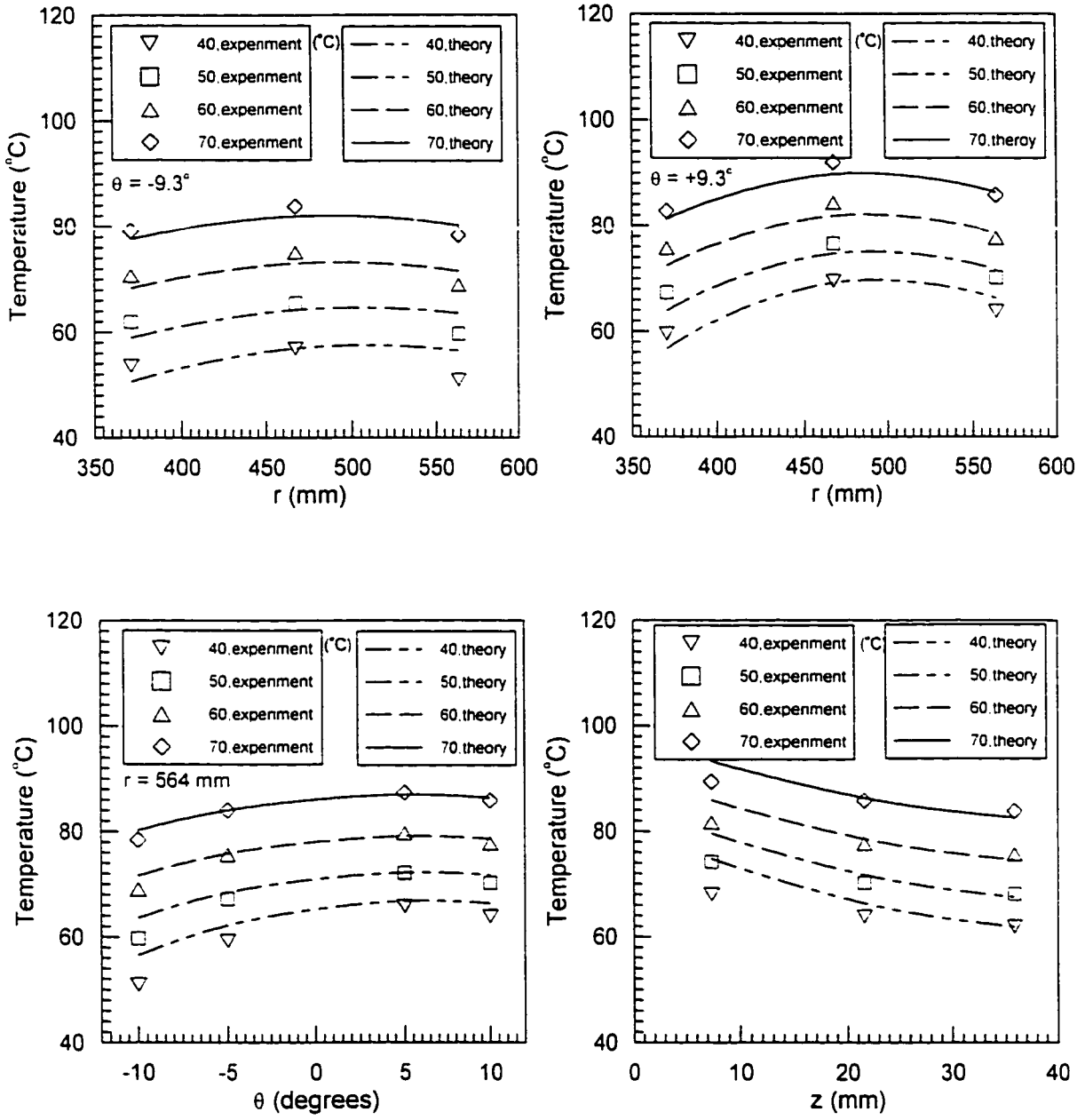

Figure 8.6b. Temperature distribution Group 5 (Cases 10, 11, 12, 4) which had different oil pot temperatures (40, 50, 60, 70 ℃)

(Numbers in the caption box are temperatures in ℃)

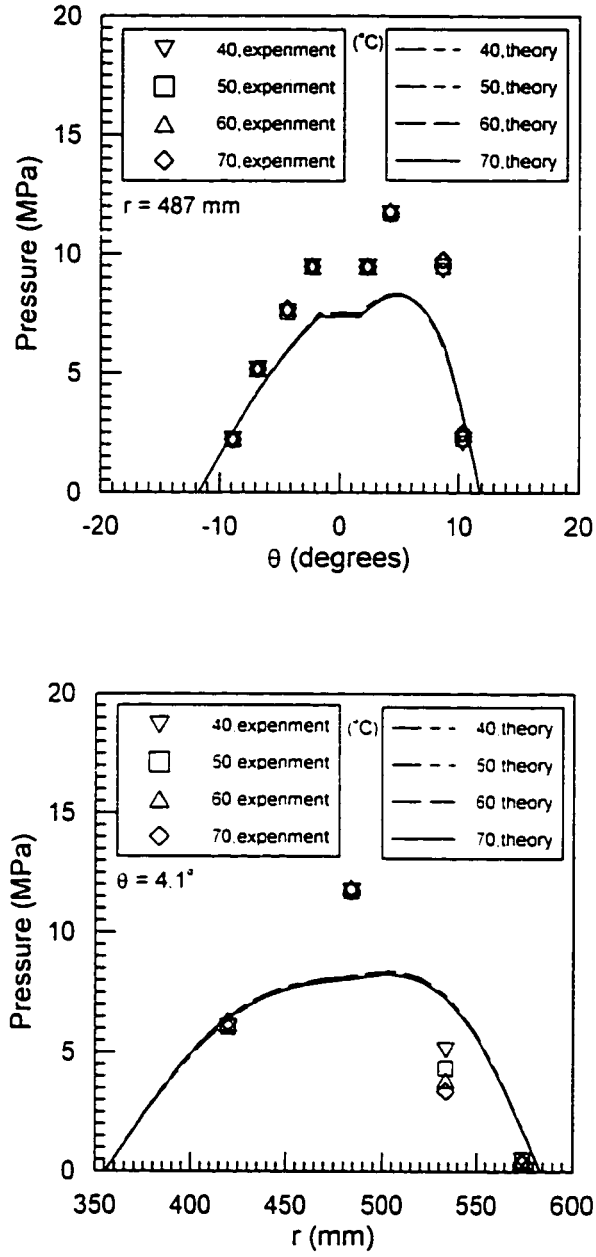

Figure 8.6c. Pressure distribution Group 5 (Cases 10, 11, 12, 4) which had different oil pot temperatures (40, 50, 60, 70 °C)

(Numbers in the caption box are temperatures in °C)

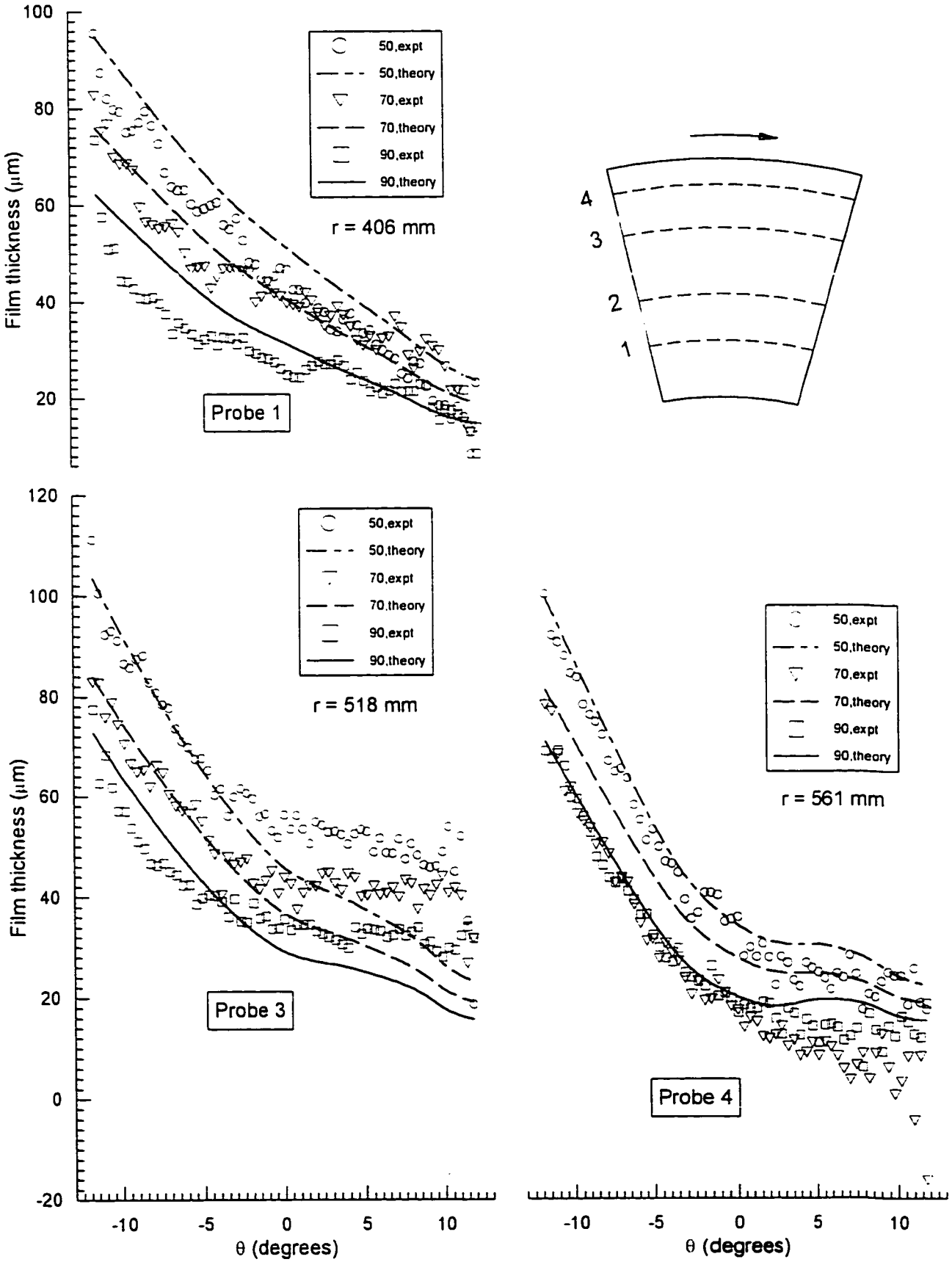

Figure 8.7a. Film distribution for Group 6 (Cases 13, 2, 14) which had different oil pot temperatures (50, 70, 90 °C)

(Numbers in the caption box are temperatures in °C)

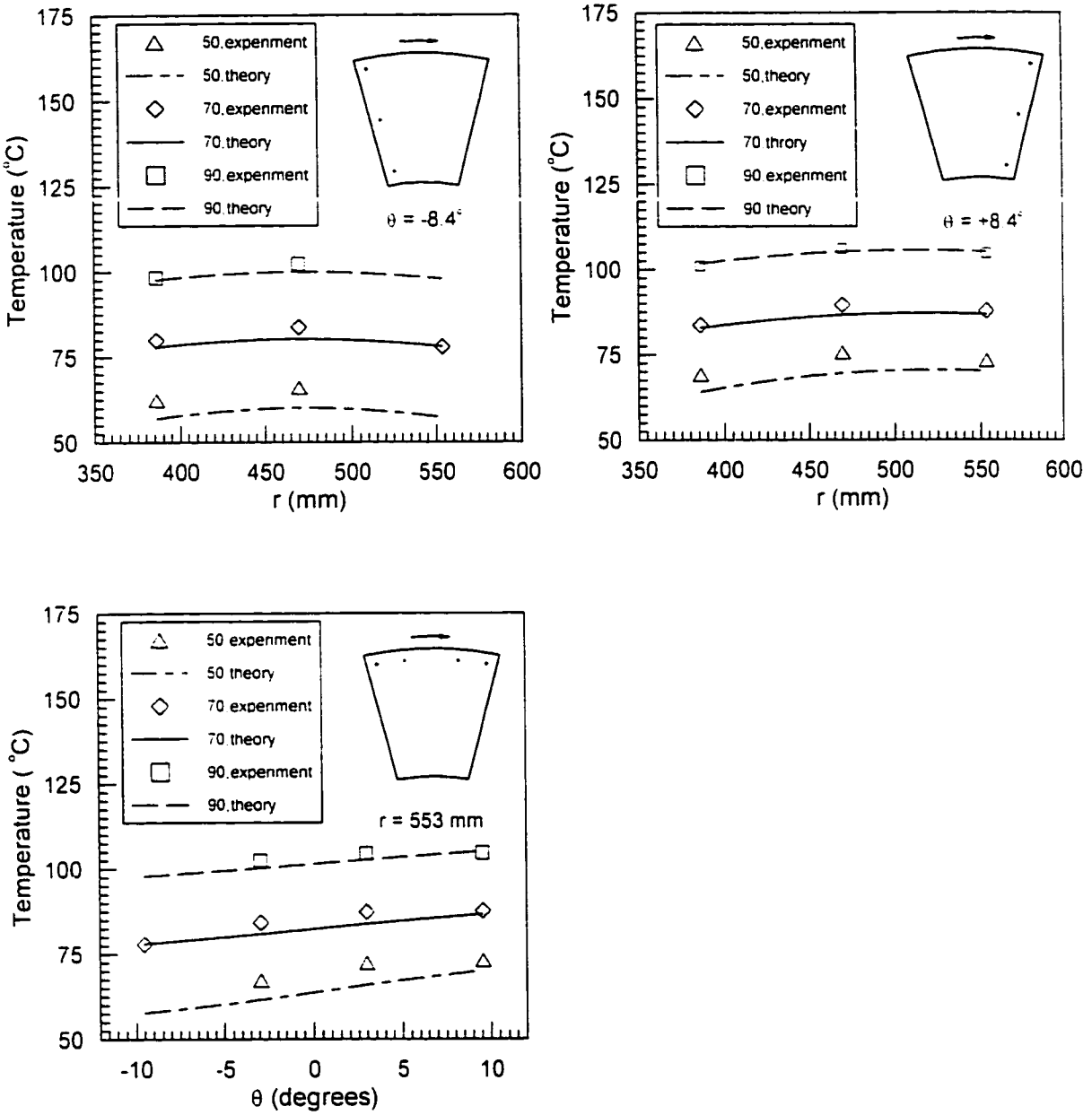

Figure 8.7bi. Temperature distribution for Group 6 (Cases 13, 2, 14) which had different oil pot temperatures (50, 70, 90 °C)

(Numbers in the caption box are temperatures in °C)

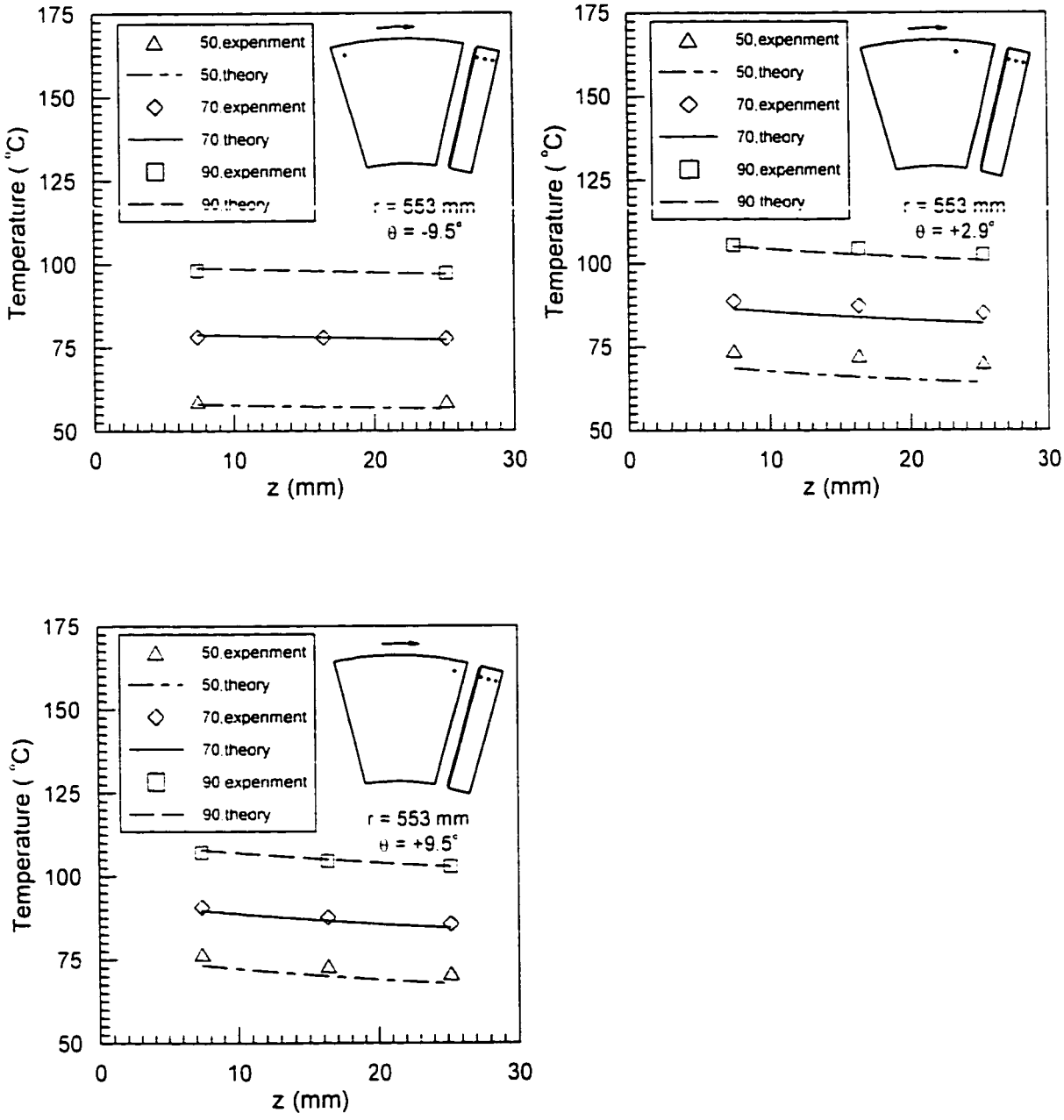

Figure 8.7bii. Temperature distribution for Group 6 (Cases 13, 2, 14) which had different oil pot temperatures (50, 70, 90 ℃)

(Numbers in the caption box are temperatures in ℃)

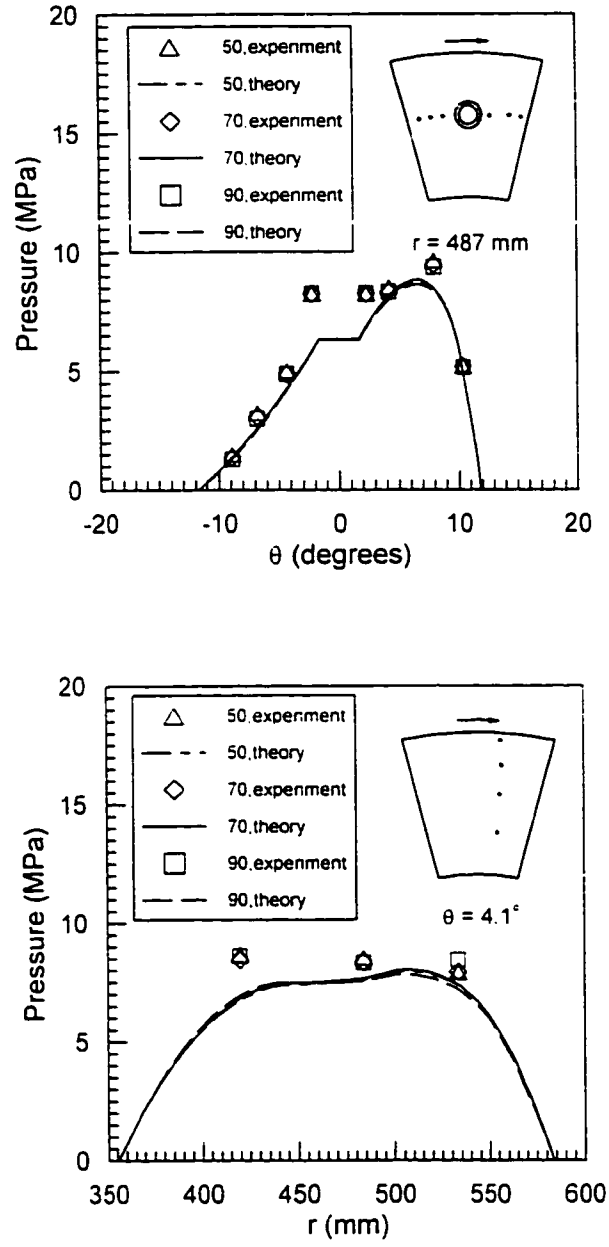

Figure 8.7c. Pressure distribution for Group 6 (Cases 13, 2, 14) which had different oil pot temperatures (50, 70, 90 °C)

(Numbers in the caption box are temperatures in °C)

Figure 8.8a, b, c, Figure 8.9a, b, c, Figure 8.10a, b, c, Figure 8.11a, b, c

(Load and Rotational Speed)

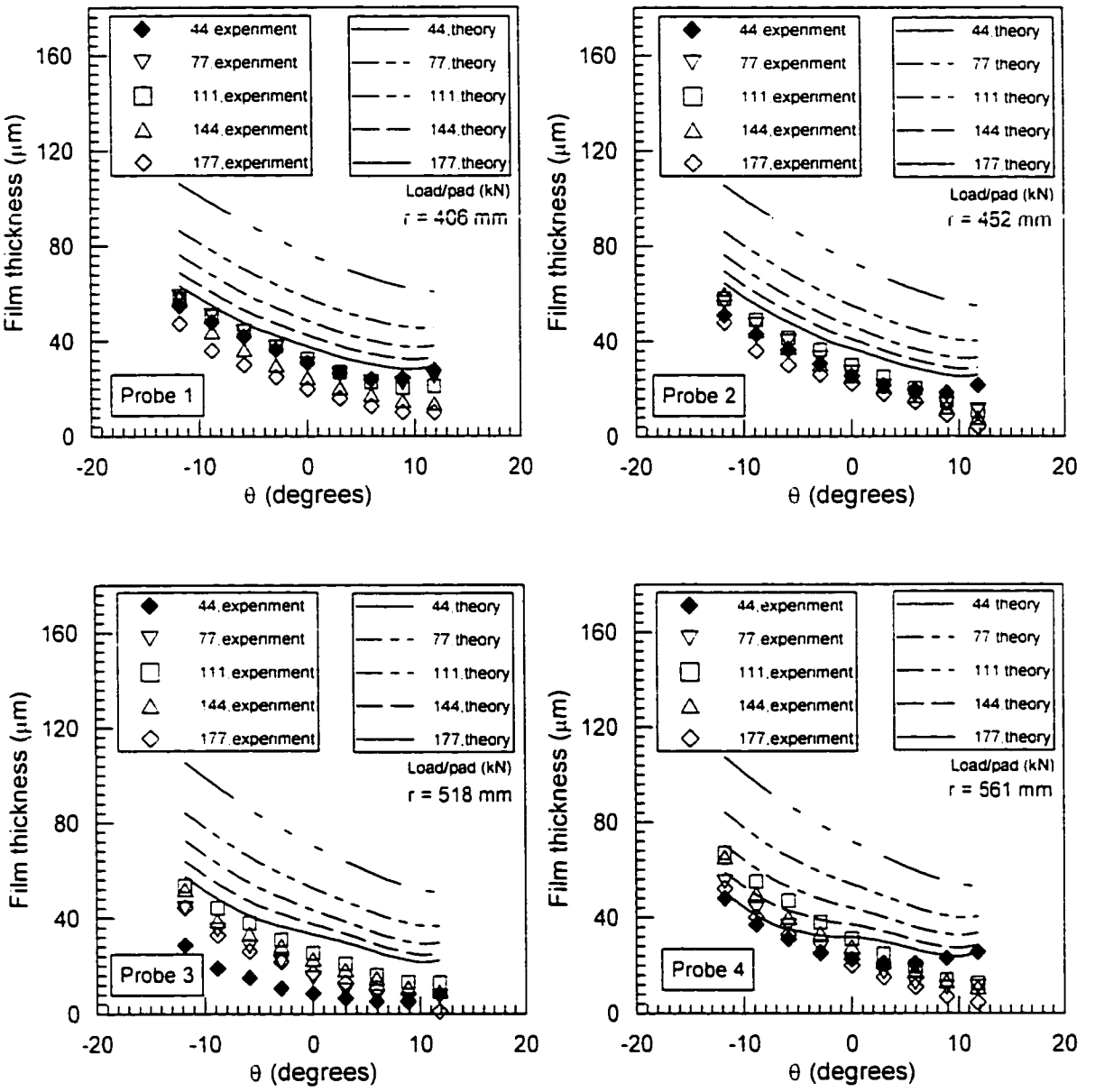

Figure 8.8a. Film thickness distribution for Group 7 (cases 15, 16, 17, 18) which had different load per pad

(Numbers in the caption box are load/pad in kN)

(Probe positions as shown in Figure 8.1a)

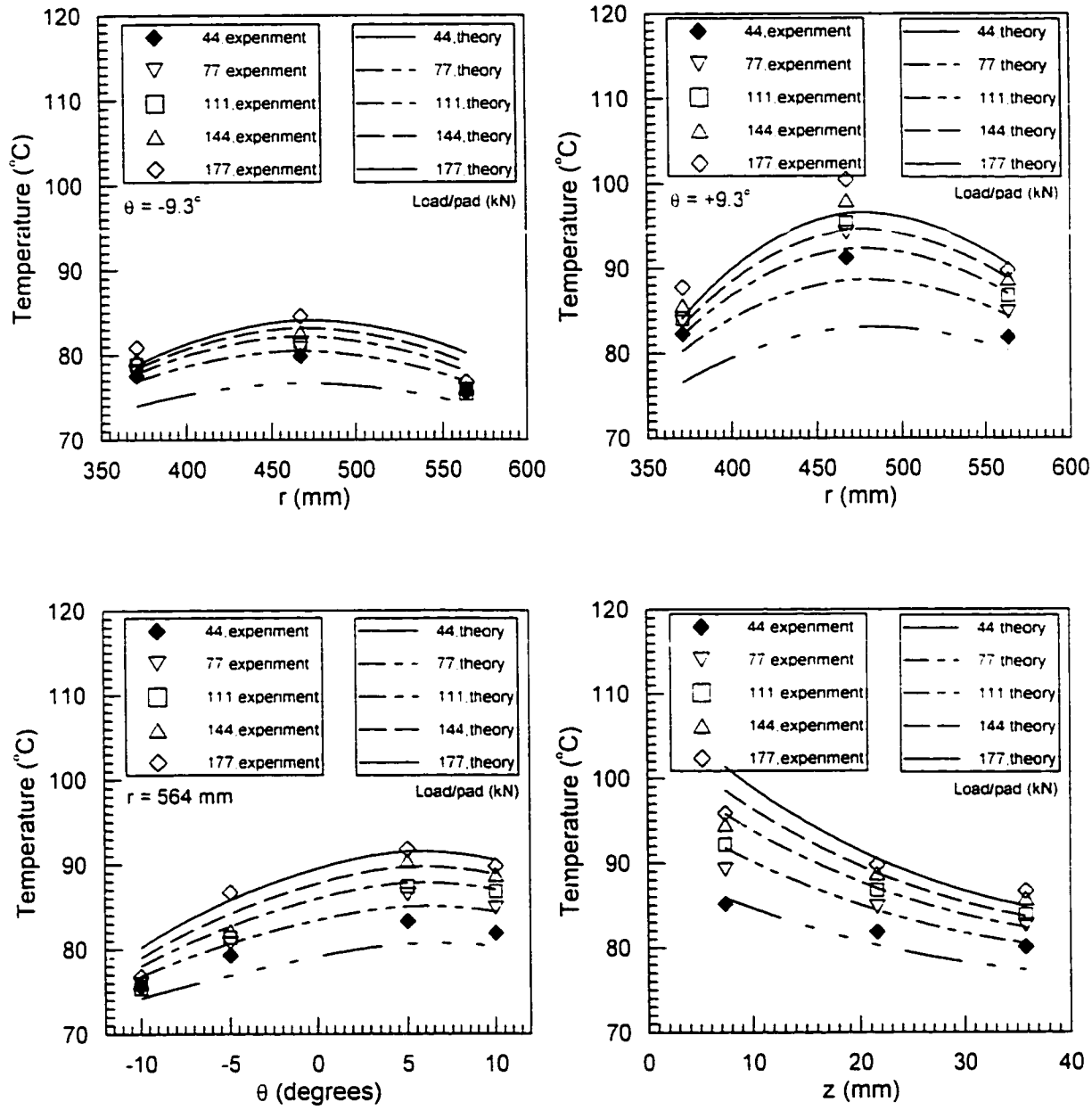

Figure 8.8b. Temperature distribution for Group 7 (cases 15, 16, 17, 18) which had different load per pad

(Numbers in the caption box are load/pad in kN)

(Thermocouple positions as shown in Figure 8.1b)

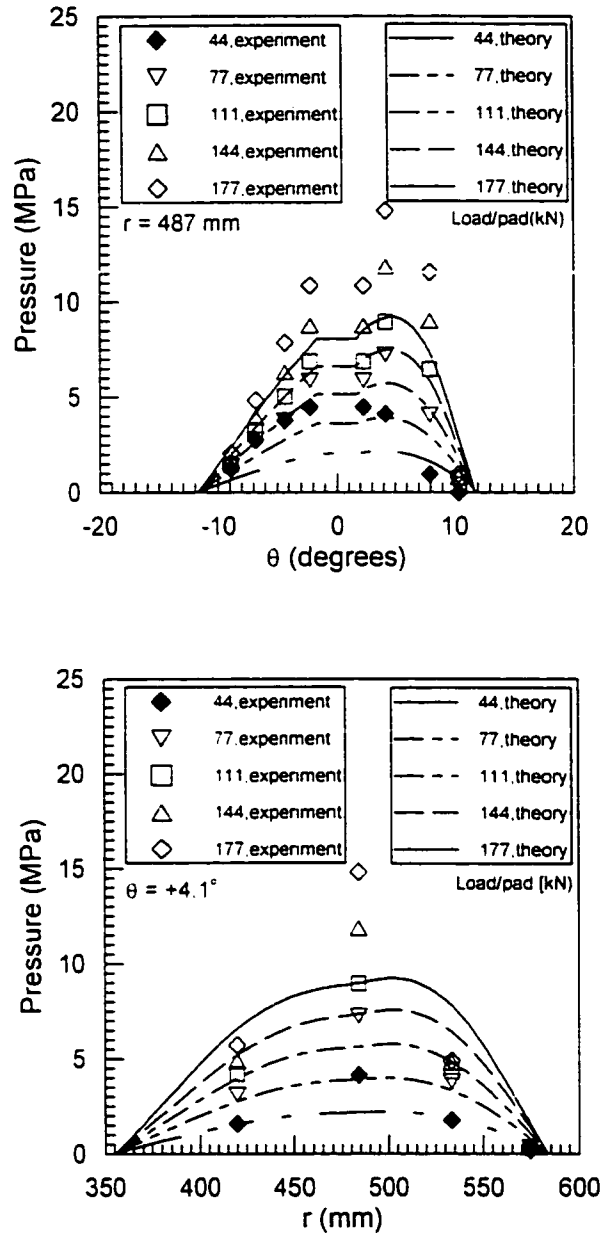

Figure 8.8c. Pressure for Group 7 (cases 15, 16, 17, 18) which had different load per pad

(Numbers in the caption box are load/pad in kN)

(Pressure probe positions as shown in Figure 8.1c)

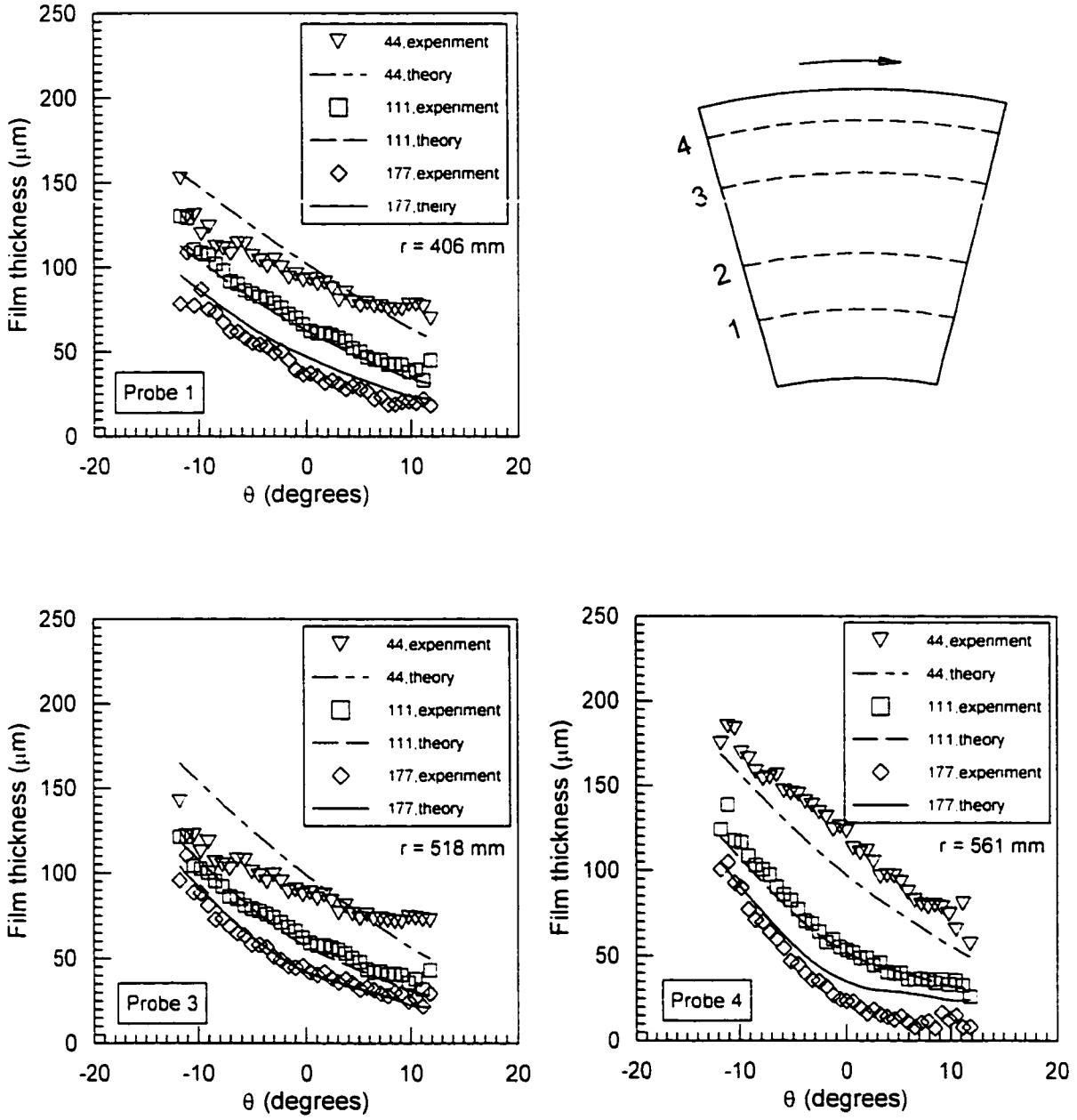

Figure 8.9a. Film thickness distribution for Group 8 (Cases 11, 20, 21) which had different load per pad

(Numbers in the caption box are load/pad in kN)

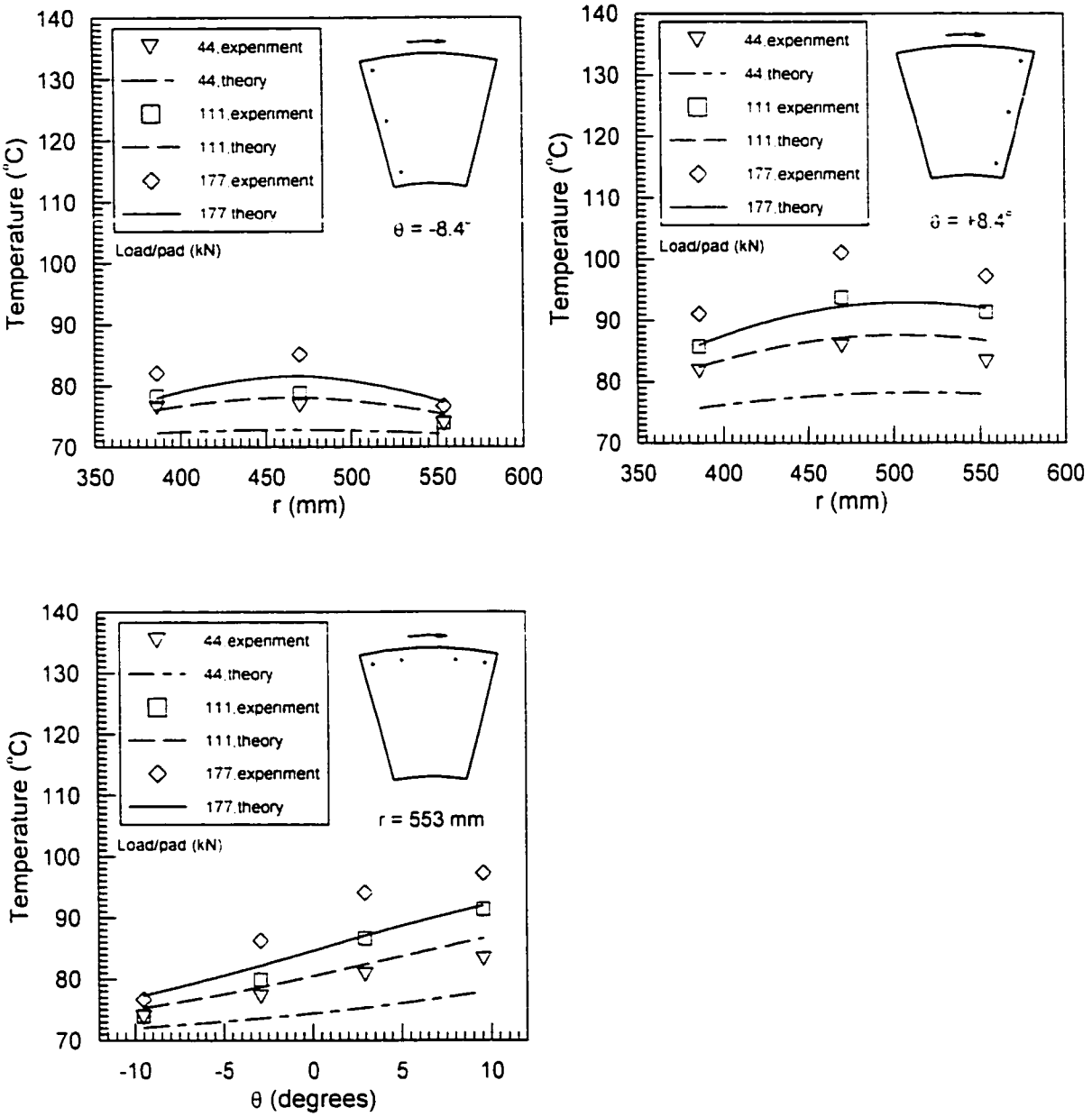

Figure 8.9bi. Temperature distribution for Group 8 (Cases 11, 20, 21) which had different load per pad

(Numbers in the caption box are load/pad in kN)

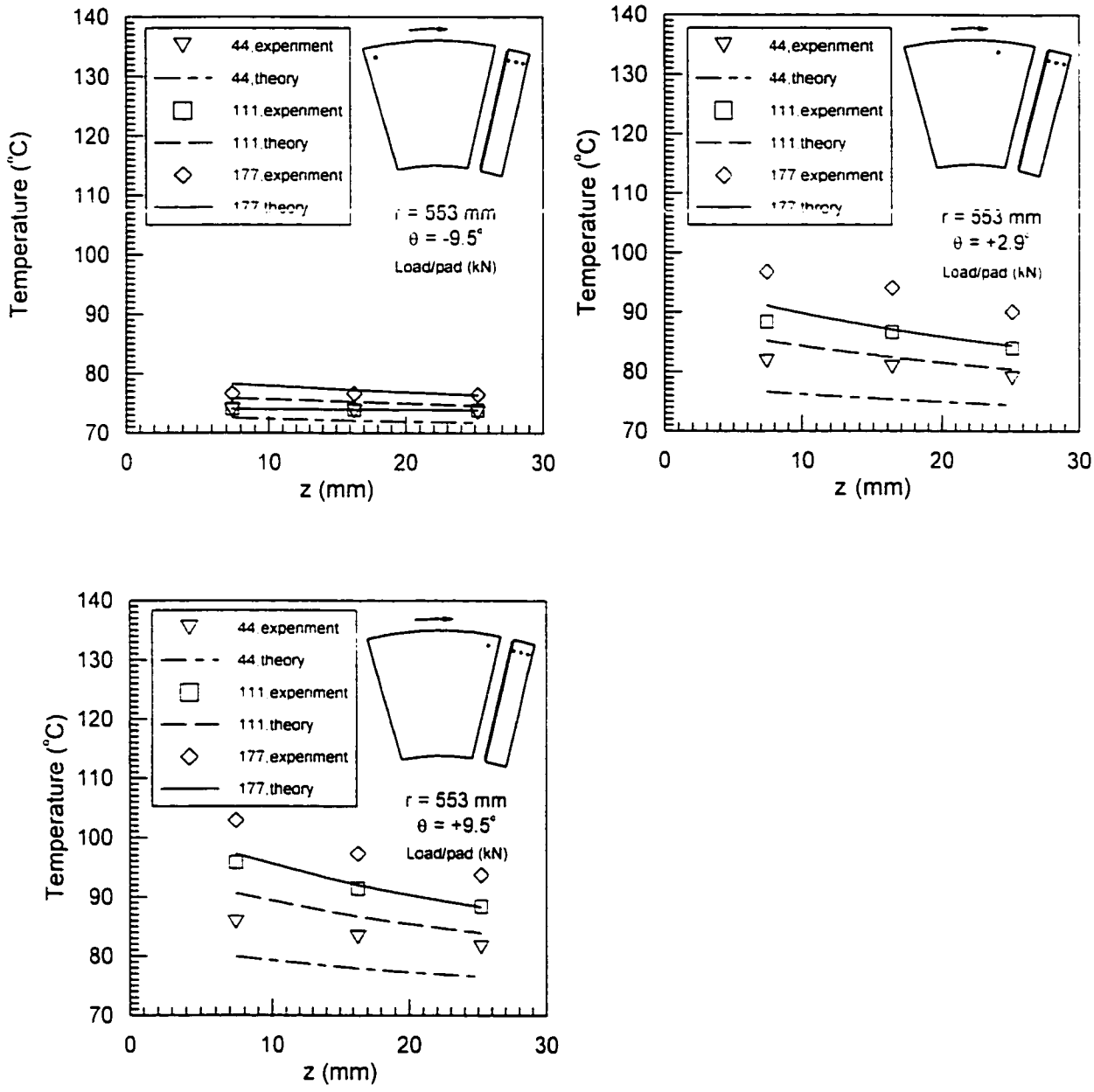

Figure 8.9bii. Temperature distribution for Group 8 (Cases 11, 20, 21) which had different load per pad

(Numbers in the caption box are load/pad in kN)

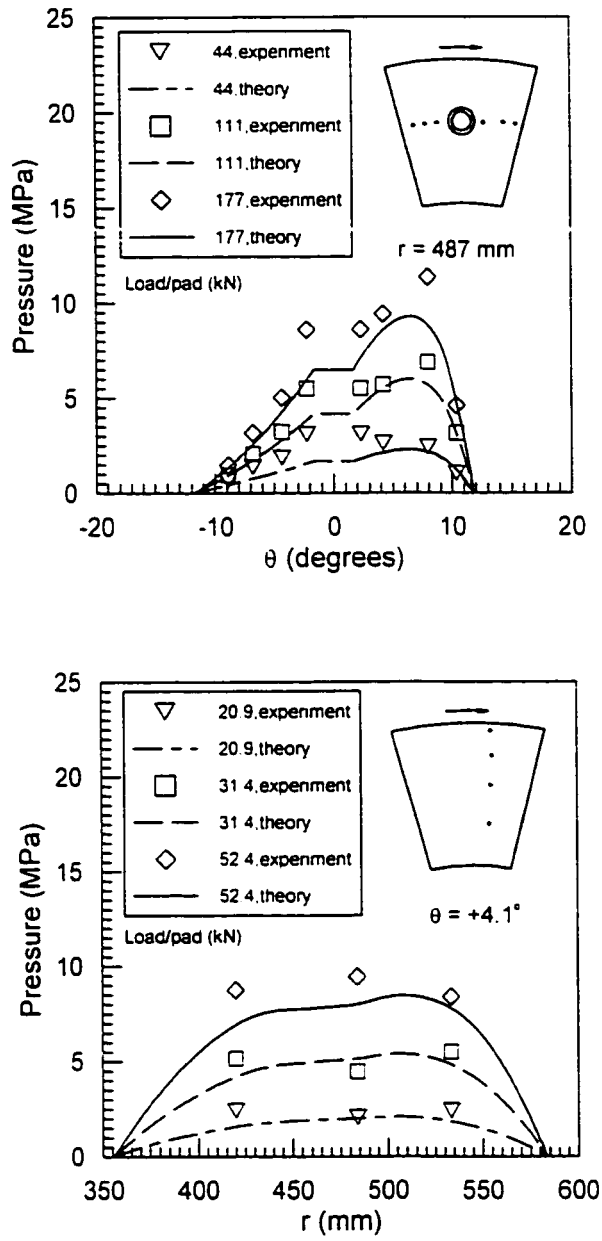

Figure 8.9c. Pressure distribution for Group 8 (Cases 11, 20, 21) which had different load per pad

(Numbers in the caption box are load/pad in kN)

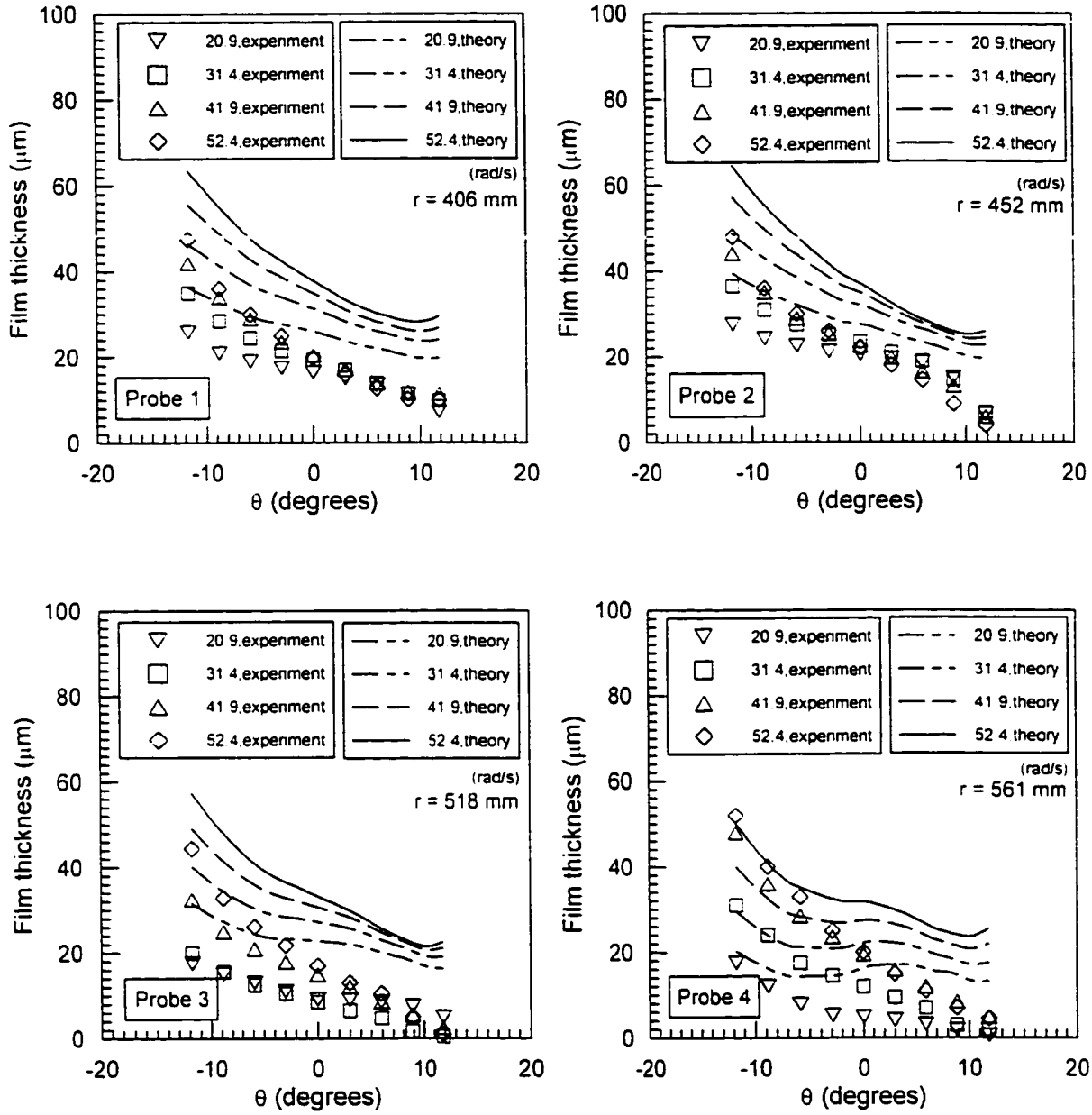

Figure 8.10a. Film thickness distribution for Group 9 (Cases 22, 6, 23, 1)

which had different rotational speeds

(Numbers in the caption box are rotational speed in rad/s)

(Probe positions as shown in Figure 8.1a)

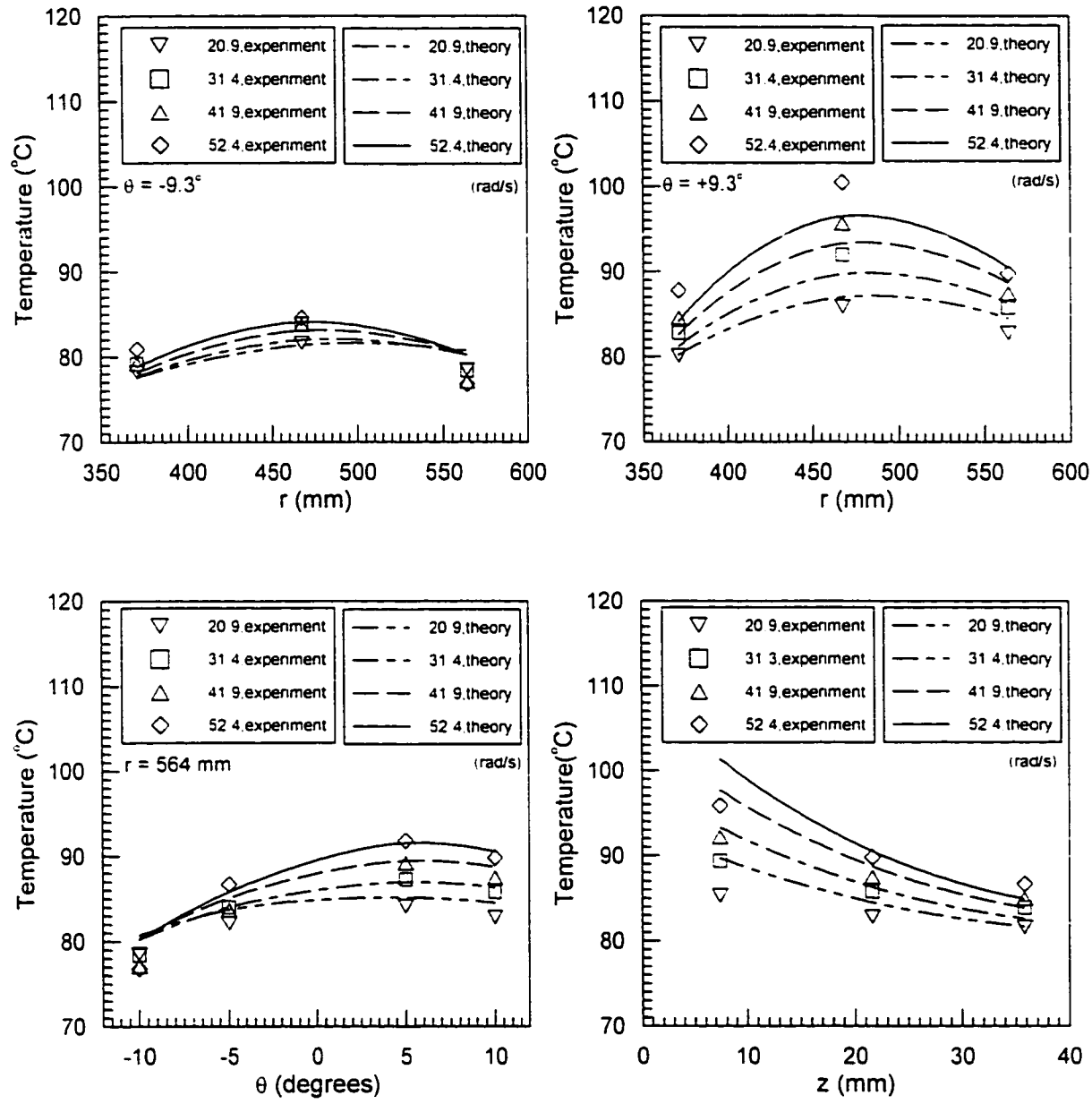

Figure 8.10b. Temperature distribution for Group 9 (Cases 22, 6, 23, 1)

which had different rotational speeds

(Numbers in the caption box are rotational speed in rad/s)

(Thermocouple positions as shown in Figure 8.1b)

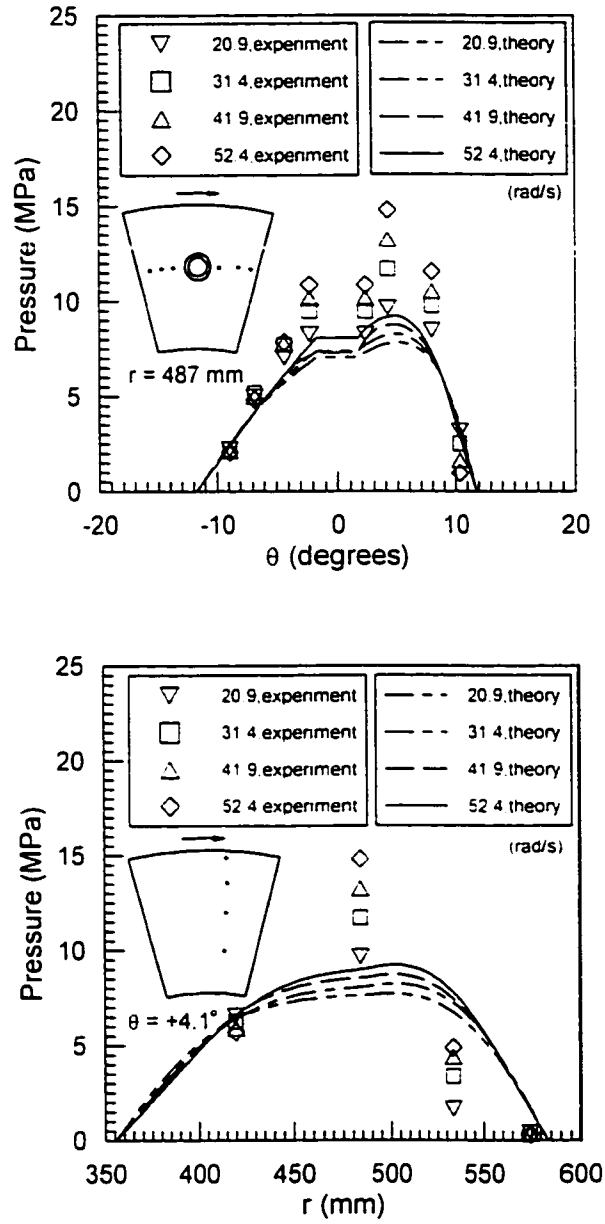

Figure 8.10c. Pressure distribution for Group 9 (Cases 22, 6, 23, 1)

which had different rotational speeds

(Numbers in the caption box are rotational speed in rad/s)

(Pressure probe positions as shown in Figure 8.1c)

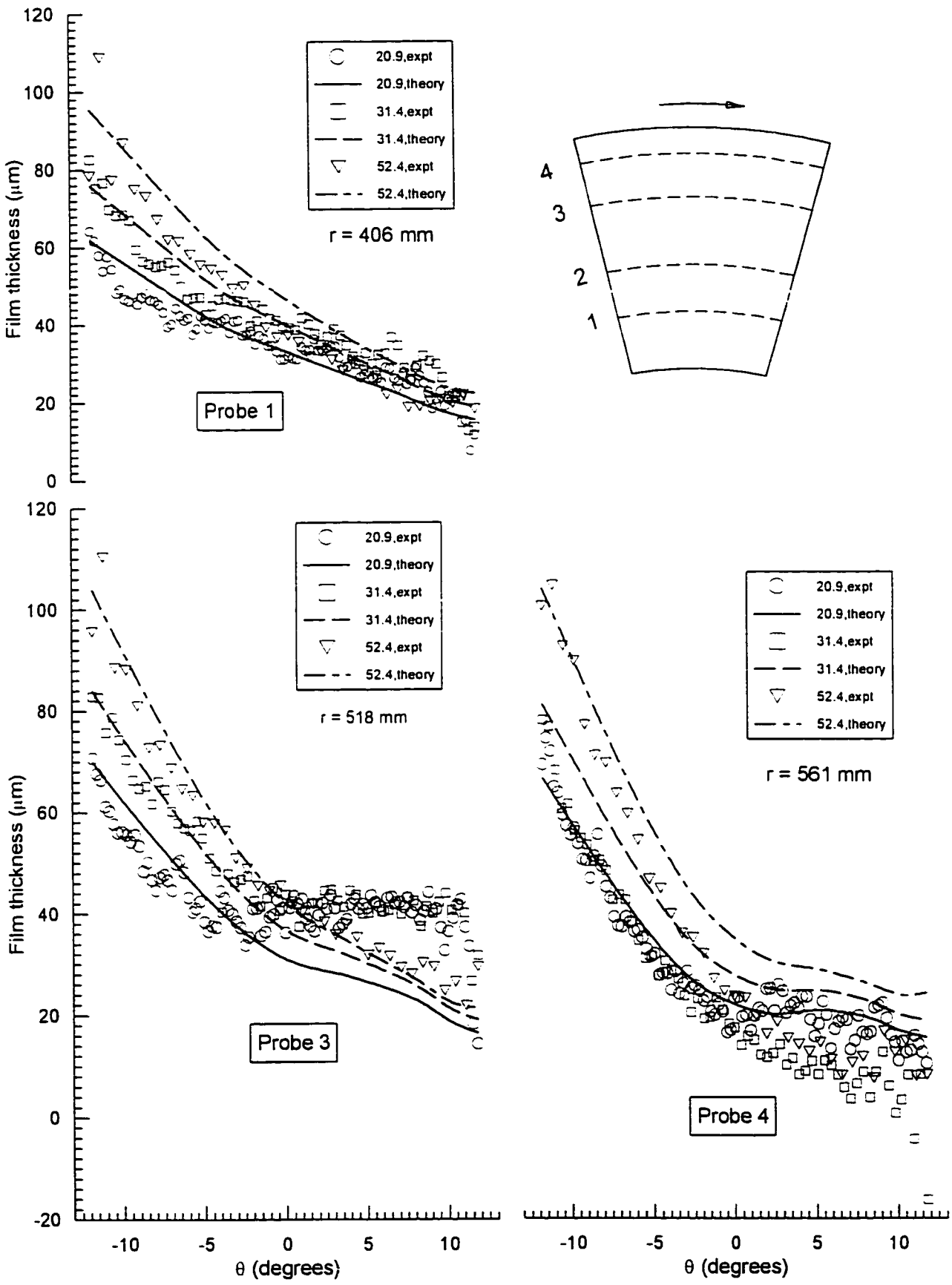

Figure 8.11a. Film thickness distribution for Group 10 (Cases 24, 2, 21) which had different rotational speeds

(Numbers in the caption box are rotational speed in rad/s)

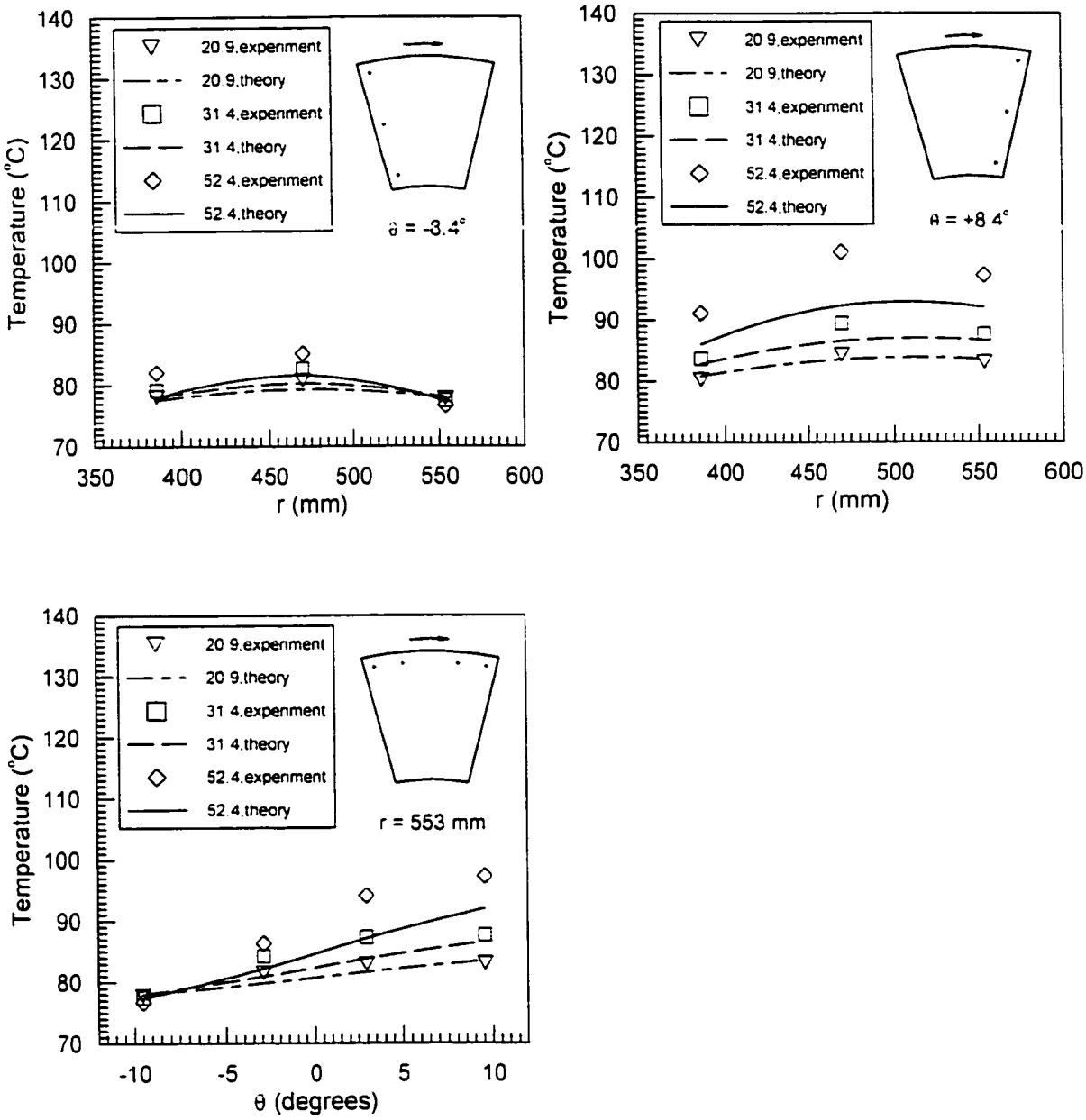

Figure 8.11bi. Temperature distribution for Group 10 (Cases 24, 2, 21) which had different rotational speeds (Numbers in the caption box are rotational speed in rad/s)

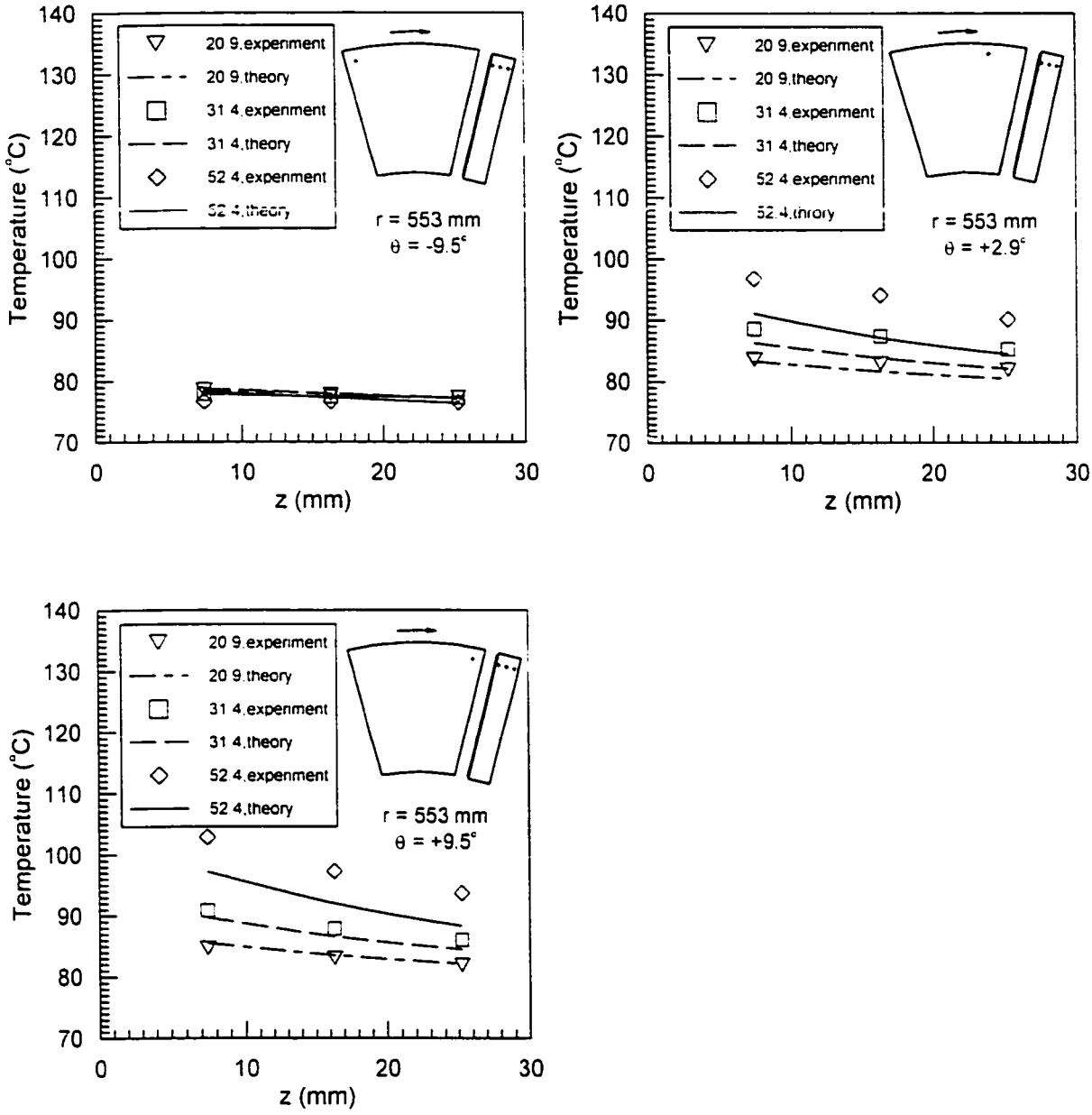

Figure 8.11bii. Temperature distribution for Group 10 (Cases 24, 2, 21) which had different rotational speeds (Numbers in the caption box are rotational speed in rad/s)

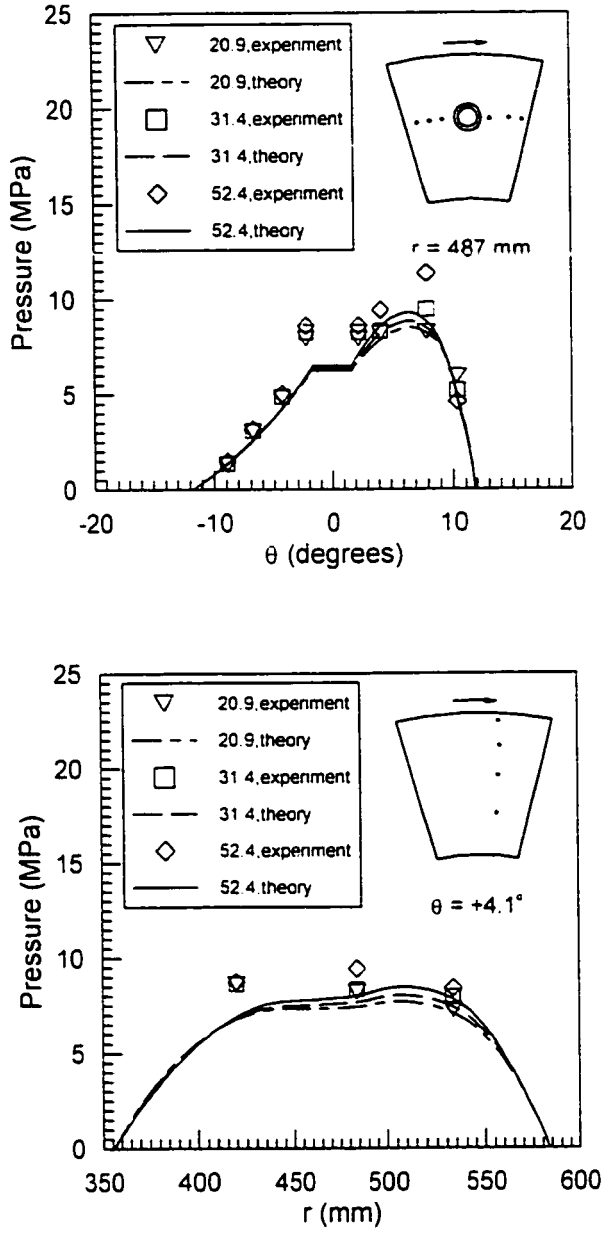

Figure 8.11c. Pressure distribution for Group 10 (Cases 24, 2, 21) which had different rotational speeds (Numbers in the caption box are rotational speed in rad/s)

Chapter 9

Conclusions and Recommendations

Spring-supported thrust bearings have been and will continue to be one of the major components in the reliable functioning of hydroelectric generators. In addition, the bearing performance affects the energy efficiency of the generator unit. The practical aim of the present research is to develop high performance spring-supported thrust bearings to generate power reliably, efficiently and economically.

9.1 Conclusions

1. The predicted pad deflections of the software package GENMAT for numerical analysis of spring-supported thrust bearings were compared with the predictions of the commercial finite element package ABAQUS with the same pressure and temperature distributions. For a single case, the agreement was not very close but without being able to include ABAQUS deflections in the iterative loops of GENMAT and compare the converged result with experimental data, it could not be ascertained which deflection model was more accurate.

2. The comparison of the numerical predictions of GENMAT and experimental data showed quite good agreement with pad temperatures and the pad shape. This agreement with pad shape suggested that the deflection modelling in GENMAT was adequate for the cases of the present thesis. The magnitude of the measured film thicknesses were usually less than GENMAT predictions but occasionally, when the *digital analyzer* was used rather than the analogue recorder for data acquisition, the measured values were quite close to the predictions. The measured pressures did not agree with GENMAT predictions. If rotor crown was arbitrarily adjusted, it was possible to obtain GENMAT predictions that agreed with the measured values. Since temperature and oil film thickness did not change much when rotor crown was varied, it seemed plausible to suggest that a model for rotor crowning would improve the accuracy of GENMAT.

3 When the comparisons of numerical predictions and experimental data were considered, a criterion for judging the accuracy of the GENMAT predictions of film thickness was developed. If the temperatures and pad shape showed good agreement, then the film thickness predictions were accepted as reliable.

4 The voltage-distance behaviour of the Eddy current displacement probes for measuring film thickness was examined in detail. It was found that their output voltage was not influenced by film pressure but the voltage-distance relationship became increasingly non-linear with increased temperatures and distances. This non-linearity was more pronounced when probes were in the rotor and the target surface was Babbitt. To improve the accuracy of the probes, it was considered necessary to place them a known distance below the surface, measure their temperature during operation and have specific calibration curves for each probe under various distances and temperatures. In the test facility measurements of bearing performance in the present thesis, a persistent thermal distortion of the rotor during the zero film thickness

measurement may also have contributed to the poor agreement between measured and predicted film thicknesses.

5. The numerical predictions of GENMAT were judged to be accurate for a thinner pad of similar shape to some found in the field. The thinner pad had lower film thickness and higher temperature but the pressure was more evenly distributed.

6. Removing springs from the leading edge of the pad produced larger fluid films in the inlet zone, lower temperatures throughout the pad but about the same minimum film thickness and a less uniform pressure distribution.

7. In the experiments of the present thesis, increasing the ISO grade of the lubricant had no significant effect on film thicknesses, pad temperatures or pressures. This supported the contention that a precise specification of lubricant viscosity-temperature behaviour was not essential in the analysis performed in the present thesis. The ISO grade and a typical behaviour of this grade of lubricant was found to be adequate.

8. Higher oil pot temperatures caused a small drop in the film thicknesses and higher temperatures throughout the pad.

9. When the load decreased, film thickness increased and both temperature and pressure decreased. The GENMAT numerical predictions were quite accurate for low loads even though some springs were loaded below their pre-load (non-linear springs were not represented in GENMAT).

10. Higher rotor speeds caused higher temperatures, higher inlet film thicknesses and higher pressures in the centre of the pad but the minimum film thickness was about the same. GENMAT accuracy was judged to decrease somewhat with increasing rotor speeds.

11 Enough experimental support was provided in the present thesis by temperature and pad shape measurements to suggest that GENMAT gave reasonably accuracy film thicknesses. Thus GENMAT can be used to predict the performance of bearings of similar size and imposed conditions to those of the experiments of the present thesis. For design and "trouble-shooting" problems with larger bearings in the field, it was considered likely, based on the agreements described in the present thesis, that GENMAT would provide fairly accurate predictions of temperature and film thickness distributions. The experimentally determined pressures were considered to be quite accurate (although not directly supported by GENMAT predictions) and they gave the designer some direct input for the bearings similar to those of the experiments of the present thesis.

Major accomplishments of the present thesis may be summarized as follows:

1. A rigorous experimental investigation has been performed on some large spring-supported thrust bearing configurations and the results provided a thorough understanding the thrust bearing physics and performance.

2. Numerical predictions were obtained through running software GENMAT. Extensive comparisons between experimental results and predictions from GENMAT have been performed and the ability of GENMAT to predict accurate temperature and film thickness distributions has been supported.

3. A new methodology has been suggested based on extensive laboratory experiments to measure oil film thickness using Eddy current displacement probes. By following this methodology, oil film thickness could be measured without interrupting the rotor motion.

4. A finite element numerical model (in ABAQUS) was developed to calculate the pad deflections considering both temperature and pressure distributions that act

on the pad. While comparisons of deflection data from both ABAQUS and GENMAT were inconclusive, the feasibility of developing and implementing a finite element analysis was supported.

9.2 Recommendations

1. Introducing a finite element deflection model as an option in GENMAT might improve accuracy in some cases and extend the applicability of GENMAT to complex pad design features.

2. The inclusion of a model for thermal crowning of the rotor in GENMAT was recommended to improve the prediction of the film pressures.

3. More experiments, including fluid film thickness measurements with better calibration procedures in particular, should be done and a closer agreement with numerical predictions sought. Once this is achieved, extensive design work could be done with GENMAT including study of the spring placement, inlet groove size, composite pads, "directed" lubrication (supplied in controlled quantities at the pad inlet) and synthetic lubricants. If such work proceeds without this improved agreement, some uncertainty must be accepted in the developed designs.

References

Ashour, N.M.E., Athre, K., Nath, Y. and Biswas, S. (1991), "Elastic Distortion of a Large Thrust Pad on an Elastic Support", *Tribology International*, pp.299-309

Baudry, R.A., Kuhn, E.C. and Wise, W.W. (1958), "Influence of Load and Thermal Distortion on the Design of Large Thrust Bearings", *Transaction of the ASME*, pp.807-818

Baudry, R.A.; Kuhn, E.C. and Cooper, G.D. (1959), "Performance of Large-Waterwheel-Generator Pivoted-Pad Thrust Bearing Determined by Tests Under Normal Operating" *Transaction of AIEE*, No. 12, **78**, pp.1300-1315

Brockett, T.S., Barrett, L.E. and Allaire, P.E. (1996) "Thermoelastohydrodynamic Analysis of Fixed Geometry Thrust Bearings Including Runner Deformation", *STLE, Tribology Transactions*, **39**, 3, pp. 555-562

Castelli,V. and Malanoski, S.B. (1969), "Method for Solution of Lubrication Problem with Temperature and Elasticity Effects: Application to Sector Tilting-Pad Bearings", *ASME, Journal of Lubrication Technology*, **91**, pp.634-640

Colynuck, A. and Medley, J.B, (1989), "Comparison of Two Finite Difference Methods for the Numerical Analysis of Thermohydrodynamic Lubrication", *Tribology Transactions*, No.3, **32**, pp.346-356

Dowson, D. and Hudson, D. (1963), "Thermo-Hydrodynamic Analysis of the Infinite Slider-Bearing: Part I, The Plate-Inclined Slider-Bearing", *Proceedings of the Lubrication and Wear Convention, I. Mech. E. London*, Paper 4, pp.31-41

El-Saie, Y.M.H. Ali and R.T. Fenner, (1988a), "Three-Dimensional Thermo-elastohydrodynamic Analysis of Pivoted Pad Thrust Bearings, Part 1: Treatment of Bearing Deflections and Fluid Film Flow and Heat Transfer", *Proc. Instn. Mech. Engrs.*, 11/88, IMechE, No.C1, **202**, pp.39-50

El-Saie, Y.M.H. Ali and R.T. Fenner, (1988b), "Three-Dimensional Thermo-elastohydrodynamic Analysis of Pivoted Pad Thrust Bearings, Part 2: Application of Theory and Comparison With Experiments", *Proc. Instn. Mech. Engrs.*, 12/88, IMechE, **202**, No.C1, pp.51-62

Elwell, R.C., Gustafson, R.E. and Reid, J.C. (1964), "Performance of Centrally Pivoted Sector Thrust Bearing Pads - Sea Trial Aboard USS Barry (DD 993)", *Transaction of the ASME, Journal of Basic Engineering*, pp.483-497

Ettles, C.M. (1976), "The Development of a Generalized Computer Analysis for Sector Shaped Tilting Pad Thrust Bearings", *ASLE Transactions*, **19**, pp.153-163

Ettles, C.M. (1980), "Size Effects in Tilting Pad Thrust Bearings", *Wear*, **59**, pp. 231-245

Ettles, C.M. (1989), "Analysis of the Thrust Bearing at the Churchill Falls Hydroelectric Plant", Technical Report, (For GE Canada)

Ettles, C.M. (1990), "Assessment of the 46" Shop Bearing for the Simulation of Full-Scale Hydroelectric Thrust Bearings and the Application of Boundary Layer Theory to Model Conditions Between Shoes", Technical Report, (For GE Canada)

Ettles, C.M. (1991), "Some Factors Affecting the Design of Spring Supported Thrust Bearing in Hydroelectric Generators", *ASME Journal of Tribology*, pp. 626-633

Ettles, C.M. (1994), "User's Manual for the Program GENMAT for the Computation of Spring Supported Thrust Bearing", Hatchbarn, London, UK

Ettles, C.M. and Advani, S. (1980), "The Control of Thermal and Elastic Effects in Thrust Bearings", *Proceedings of the 6th Leeds Lyon Symposium on Tribology"*, MEP Ltd., pp.105-116

Ettles, C.M. and Anderson, H.G. (1991), "Three-Dimensional Thermoplastic Solution of Thrust Bearings Using Code Marmac1", *Journal of Tribology, Transaction of the ASME*, No.2.**113**, pp.405-412

Ettles, C.M. and Cameron, A. (1968), "Considerations of Flow across a Bearing Groove", *Transaction of the ASME, Journal of lubrication Technology*, No.1, **90**, pp.312-319

Ferguson, J.H., Yuan, J.H., and Medley, J.B. (1998), "Spring-Supported Thrust Bearings for Hydroelectric Generators: Influence of Oil Viscosity on Power Loss", *Tribology for Energy Conservation*, Proceedings of the 24th Leeds-Lyon Symposium on Tribology, London, UK 4th-6th September, 1997, pp.187-193

Gero, L.R. and Ettles, C.M. (1988) "A Three Dimensional Thermohydrodynamic Finite Element scheme for Fluid Film Bearings" *STLE, Tribology Transactions*, Vol. 31, 2, pp.182-191

Grant, A. (1991), "Summary of Tests on Hydro Generator Thrust Bearing Rig", Technical Report, GE Document 91-AVG-01, General Electric Canada

Hahn, E.J. and Kettleborough, C.F. (1967), "Solution for the Pressure and Temperature in an Infinite Slider Bearing of Arbitrary Profile", *Journal of Lubrication Technology, Transaction of the ASME*, pp.445-452

Halling, J. (1975), "Principles of Tribology - Chapter 12", The Macmillan Press Ltd.

Hashimoto, H. and Wada, S. (1984), "Turbulent Lubrication of Tilting-Pad Thrust Bearings with Thermal and Elastic Deformations", ASME/ASLE Joint Lubrication Conference, San Diego, Calif., Paper No. 84-Trib-41

Heshmat, H. and Pinkus, O. (1986), "Mixing Inlet Temperatures in Hydrodynamic Bearings", *Journal of Tribology, Transaction of the ASME*, **108**, pp.231-248

Hibbitt, Karlsson & Sorensen, Inc. (1995), "ABAQUS User's Manual"

Huebner, K.H. (1974a), "A Three-Dimensional Thermohydrodynamic Analysis of Sector Thrust Bearings", *ASLE Transactions*, No.1, **17**, pp.62-73

Huebner, K.H. (1974b), "Application of Finite Element Methods to Thermohydrodynamic Lubrication", *International Journal Of Numerical Methods in Engineering*, pp.139-165

Huebner, K.H. (1974c), "Solution for the Pressure and Temperature in Thrust bearings Operating in the Thermohydrodynamic turbulent Regime", *ASME Journal of Lubrication Technology*, pp.58-68

Innes, G.E. and Leutheusser, H.J. (1991), "An Investigation into Laminar-to-Turbulent Transition in Tiling-Pad Bearings", *Journal of Tribology*, **113**, pp. 303-307

Kawaike, K., Okano, K. and Furukawa, Y. (1977), "Performance of a Large Thrust Bearing with Minimized Thermal Distortion", *ASLE Transaction*, **22**, 2, pp. 125-134

Kim, K.M., Tanaka, M. and Hori, Y. (1983), "A Three-Dimensional Analysis of Thermohydrodynamic Performance of Sector-Shaped, Tilting-Pad Thrust Bearings", *Transaction of the ASME, Journal of Lubrication Technology*, No.3, **115**, pp.406-413

Kline, S.J. and McClintock, F.A. (1953), "Describing Uncertainties in Single-Sample Experiments", *Mechanical Engineering*, 3-8.

Kumar, A. and Booker, J.F. (1994), "A Mass and Energy Conserving Finite Element Lubrication Algorithm", *Transaction of the ASME, Journal of Tribology*, **116**, pp.667-671

Launder, B.E. and Leschziner, M. (1978), "Flow in Finite-Width, Thrust Bearing Including Inertial Effects, I-Laminar Flow", *Journal of Lubrication Technology, Transaction of the ASME*, **100**, pp.330-338

Ma, Z. and Dong, Y. (1995) "Elastothermohydrodynamic Lubrication of Sector Thrust Bearings Using the Finite Element Method", *STLE, Tribology Transactions*, Vol. 38, 2, pp. 311-316

Mizgala, D. (1994), "Hydrogenerator Thrust Bearing Rig - Commissioning Loading Device", Technical Report, GE Document 94-DIM-01, General Electric Canada

Monk, T. (1991), " Summary of Tests on Hydrogenerator Thrust Bearing Rig", Technical Report, GE Document 91-TDM-01, General Electric Canada

Neal, P.B. (1979), "Some Factors Influencing the Operating Temperature of Pad Thrust Bearing", *Proceedings of 6th Leeds-Lyon Symposium on Tribology*, pp.137-142

Neal P.B. (1982), "Heat Transfer in Pad Thrust Bearings", *Proc. Instn. Mech. Engrs.* **196**, pp.217-228

Pinkus, O. and Wilcock, D.J. (1980), "Thermal Effects in Fluid Film Bearings", *Proceedings of 6th Leeds-Lyon Symposium on Tribology*, pp. 2-23

Patankar, S.V. (1980), "Numerical Heat Transfer and Fluid Flow", McGraw-Hill, New York

Qu, S., Wang, Y., Zhang, J. and Jiang, Z. (1993), "30 MN Thrust Bearing Test Stand", Presented at Symposium in China, pp.121-132, (Source: GE Canada)

Robinson, C.L. and Cameron, A. (1975), "Studies in Hydrodynamic Thrust Bearings", *Phil. Transactions Royal Society*, London, A, **278**, pp.351-395

Seyler, Jan Werner (1991), "Application of the Finite Element Method to Pad Deflection in Modelling the Lubrication Mechanics of Large Thrust Bearing", M.A.Sc. Thesis, Department of Mechanical Engineering, University of Waterloo

Sinha, A.N., Athre, K. and Biwas, S. (1993), "Spring-supported hydrodynamic Thrust Bearing with Special Reference to Elastic Distortion Analysis", *Tribology International*, **26**, pp.251-263

Sinha, A.N., Athre, K. and Biwas, S. (1994), "A nonlinear Approach to Solution of Reynolds Equation for Elastic Distortion Analysis of Spring-Supported Thrust Bearing", *Tribology Transaction*, **37**, pp.802-810

Sternlicht, B. et al, (1961a), "Adiabatic Analysis of Elastic, Centrally Pivoted, Sector Thrust Bearing Pads", *Journal of Applied Mechanics*, pp.179-187

Sternlicht, B.; Reid, J.C. and Arwas, E.B. (1961b), "Performance of Elastic, Centrally Pivoted, Sector Thrust Bearings Pads - Part I", *Transaction of the ASME, Journal of Basic Engineering*, Series D, **83**, pp.169-178

Tanaka, Masato; Hori, Yukio; Ebinuma, Ryuichi (1985), "Measurement of the Film Thickness and Temperature Profiles in a Tilting Pad Thrust Bearing", *Proceedings of the JSLE International Tribology Conference*, Tokyo, Japan, pp.553-558

Tieu, A.K. (1973), "Oil-Film Temperature Distribution in an Infinitely Wide Slider Bearing: An Application of the Finite Element Method", *J. Mech. Eng. Sci.*, No.4, **15**, pp.311-320

Vohr, J.H. (1981), "Prediction of the Operating Temperature of Thrust Bearings", *Journal of Lubrication Technology, Transaction of the ASME*, **103**, pp.97-106

Yuan, J.H. (1994a), "Probes Calibration for Oil Film Thickness Measurement", Technical Report, *GE Document 94-HY-04*, General Electric Canada

Yuan, J.H. (1994b), "Correlation with Preliminary Results from Test Rig", Technical Report, *GE Document 94-HY-02*, General Electric Canada (3.0)

Yuan, J.H. (1994c), "Influence of Spring Arrangement", Technical Report, *GE Document 94-HY-01*, General Electric Canada

Yuan, J.H. (1994d), "Influence of Thrust Bearing Pad Thickness", Technical Report, *GE Document 94-HY-06*, General Electric Canada

Yuan, J.H., Medley, J.B., and Ferguson, J.H., "Spring Supported Thrust Bearings Used in Hydroelectric Generators: Laboratory Test facility", *Tribology Transactions*, Volume 42 (1999), 1, pp126-135

Yuan, J.H., Medley, J.B., and Ferguson, J.H., "Spring Supported Thrust Bearings Used in Hydroelectric Generators: Comparisons of Experimental Results with Numerical Predictions of GENMAT", *Tribology Transactions* (in Press)